

Electrical Conductivity of Saturated Fine-Grained Soils: Modelling and Soil Classification Applications

MD FARHAD HASAN
Bachelor of Science

A thesis submitted in total fulfilment of the requirements for the
degree of Doctor of Philosophy

Department of Civil Engineering
School of Engineering and Mathematical Science
College of Science, Health and Engineering

La Trobe University
Bundoora, Victoria, 3086
Australia

October 6, 2020

Table of Contents

Table of Contents-----	3
List of Tables -----	11
List of Figures -----	13
Abstract -----	19
Statement of Authorship-----	20
List of Publications-----	21
Australian Postgraduate Research (APR) Internship-----	21
Acknowledgment-----	22
Chapter 1 -----	24
Introduction -----	24
1.1 Background -----	24
1.2 Problem Statement-----	25
1.3 Objectives of the Study -----	27
1.4 Outline of the Thesis -----	30
Chapter 2 -----	32
Literature Review -----	32
2.1 Introduction-----	32
2.2 Factors Influencing the Electrical Conductivity of Soils-----	33
2.2.1 Soil Porosity-----	33
2.2.2 Soil Moisture Content -----	34

2.2.3 Pore Water Salinity-----	36
2.2.4 Degree of Saturation -----	38
2.2.5 Soil Mineralogy-----	39
2.2.6 Liquid Limit and Plastic Limit -----	41
2.2.7 Clay Particle Orientation and Anisotropy-----	41
2.3 Effect of Temperature on Electrical Properties of Soils-----	43
2.3.1 DDL Properties of Clay Particles -----	43
2.3.2 Changes in Saline Water Conductivity-----	47
2.3.3 Overall Electrical Conductivity of Soil -----	48
2.4 Conceptual Understanding of Electrical Conductivity Models -----	49
2.4.1 Archie (1942) -----	50
2.4.2 Rhoades et al. (1976)-----	51
2.4.3 Rhoades et al. (1989)-----	52
2.4.4 Fukue et al. (1999) -----	53
2.4.5 Mojid et al. (2007)-----	55
2.4.6 Ellis et al. (2010) -----	56
2.5 Correlations between the Geotechnical Properties of Soil and its Electrical Conductivity -----	57
2.5.1 Determination of Moisture Content-----	58
2.5.2 Predicting Hydraulic Conductivity -----	59
2.5.3 Monitoring Soil Consolidation Properties -----	61
2.5.4 Estimation of Clay Content -----	62
2.5.5 Determining Liquid Limit and Plastic Limit -----	62
2.6 Review of Particle Size Distribution (PSD) Techniques-----	63
2.6.1 Sedimentation Methods-----	64

2.6.2 Sieve Analysis -----	70
2.6.3 Laser Diffraction (LD)-----	72
2.6.4 SediGraph Technique -----	76
2.6.5 Integrated Suspension Pressure Technique -----	79
2.6.6 Comprehensive Analysis of Current PSD Techniques-----	80
2.7 Discussion on the Available Liquid Limit Test Methods -----	86
2.7.1. Casagrande method-----	86
2.7.2. Cone penetration method -----	87
2.7.3. Limitations and drawbacks of the existing methods-----	88
2.8 Methods of Predicting Soil Plastic Limit-----	89
2.8.1 Atterberg Method (Thread Rolling) -----	90
2.8.2 Pfefferkorn Technique -----	91
2.8.3 Penetration and Indentation Method For Plastic Limit -----	93
2.8.4 Pros and Cons of Available Plastic Limit Methods -----	93
2.9 Concluding Remarks -----	95
2.9.1 Soil Electrical Conductivity Models-----	95
2.9.2 Conventional PSD Techniques -----	95
2.9.3 Liquid Limit Methods -----	96
2.9.4 Plastic Limit Measurements -----	96
Chapter 3 -----	98
Experimental Tools and Materials-----	98
3.1 Introduction-----	98
3.2 Tested Soils-----	98
3.2.1 Kaolin -----	98
3.2.2 Bentonite-----	100

3.2.3 Natural Soils-----	102
3.3 Experimental Devices and Apparatus-----	103
3.3.1 Electrical Conductivity Meter -----	103
3.3.1 Soil Resistivity Meter (Wenner Method) -----	104
3.3.2 Heat-Based Distilled Water Maker -----	106
3.3.3 Soil-water Suspension Mixer -----	107
3.3.4 Automatic Mortar Mixer -----	108
3.3.5 Standard Proctor -----	109
3.3.6 Optimised Temperature Controlling Water Bath -----	110
3.3.7 Hydrometer -----	111
3.3.8 Pipette -----	112
3.3.9 Laser Diffraction Particle Size Analyser-----	114
3.3.10 Casagrande Device for Determining the Liquid Limit (LL) of Soil -----	115
3.3.11 Cone Penetration Device for Liquid Limit -----	117
3.4 Summary -----	119
Chapter 4 -----	120
Electrical Properties of Clay Particles-----	120
4.1 Introduction-----	120
4.2 Effect of Pore Water Salinity and Temperature on DDL -----	120
4.3 Proposed Surface Conduction Parameters -----	122
4.3.1. Phase Relationship-----	122
4.4 Experimental Programmes -----	126
4.4.1 Testing soils -----	126
4.4.2 Determining Electrical Surface Conduction Parameters (σ_s and χ)-----	127

4.4.3 Modified free swelling index test -----	128
4.5 Results and Discussion-----	132
4.5.1. Effect of Pore Water Salinity on σ_s and χ -----	132
4.5.2 Coupled Thermo-chemical Effect on σ_s and χ -----	134
4.5.3 Effect of Temperature and Water Salinity on FSI -----	145
4.6 Summary -----	150
Chapter 5 -----	151
Series-Parallel Structure-Oriented Electrical Conductivity Model -----	151
of Saturated Clays -----	151
5.1 Introduction-----	151
5.2 Background-----	152
5.3 Proposed Model-----	153
5.3.1 Model Assumptions -----	153
5.3.2. Model Formulation -----	154
5.4 Laboratory Testing -----	158
5.4.1. Testing Materials and Experimental Programmes -----	158
5.4.2. Test Setup and Procedures -----	159
5.5 Results and Discussions -----	163
5.5.1. Model Parameters-----	163
5.5.2. Electrical conductivity measurements and model validation-----	166
5.6 Summary -----	171
Chapter 6 -----	172
Particle Size Distribution of Soils using the Electrical Conductivity Technique-----	172

6.1 Introduction-----	172
6.2 Proposed Theory -----	176
6.3 Experiments -----	177
6.3.1 Testing Materials and Tools -----	177
6.3.2 Role of Dispersion Agent -----	178
6.3.3 Acrylic-Brass Probe for Calibration and PSD test-----	179
6.3.4 Preparation of Suspension-----	183
6.3.5 Calibration Technique -----	187
6.4 Test Results and Discussion-----	192
6.4.1 Validation-----	193
6.4.2 Repeatability -----	195
6.5 Summary -----	197
Chapter 7 -----	198
A New Electrical Approach to Predict the Liquid Limit and Plastic Limit of Soils-----	198
7.1 Introduction-----	198
7.2 Background-----	198
7.3 Proposed Method and its Mathematical Formulation -----	201
7.4 Soil Samples-----	203
7.5 Determination of F_{LL} & F_{PL} using the Resampling Approach -----	205
7.6 Test Results and Discussions -----	206
7.6.1 Differences between the Casagrande and Cone Methods -----	206
7.6.2 Validation of EC Technique to Determine LL and PL-----	209
7.7 Summary -----	221

Chapter 8 -----	223
Conclusions and Recommendations -----	223
8.1 Summary -----	223
8.1.1 Findings After Literature Review -----	223
8.1.2 Electrical Surface Conduction of Solid Clay Particles -----	224
8.1.3 Series-Parallel, Structure-oriented EC Model of Saturated Clays -----	225
8.1.4 Particle Size Distribution of Soils -----	225
8.1.5 Liquid Limit and Plastic Limit of Soils -----	226
8.2 Recommendations for Future Studies -----	226
8.3 Concluding Remarks -----	227
List of References -----	230
Appendices -----	242
Appendix 1 -----	242
Derivation and Simplifications of the χ and σ_s -----	242
Appendix 2 -----	244
Mathematica Script of Determining χ and σ_s -----	244
Appendix 3 -----	245
Stokes' Law to Find Diameter of the Soil Particles -----	245
Appendix 4 -----	247
Viscosity (μ) of water at different temperature (T) (Arora, 1992) -----	247
Appendix 5 -----	248
Derivation of Percentage Finer (passing) -----	248
Appendix 6 -----	250
Determination of Effective Distance of Electrodes by Analysing Electric Field ---	250

List of Tables

Table 2.1: Level of anisotropy in electrical resistivity (Abu Hassanein et al., 1996).....	42
Table 2.2: Effect of temperature on the dielectric constant of water.	44
Table 2.3: Comparison among the existing series-parallel electrical conductivity models of clay.....	57
Table 2.4: Brief information on sedimentation methods	66
Table 2.5: Information on sieve analysis	71
Table 2.6: Summary of Laser Diffraction Analysis for PSD of Soils.	73
Table 2.7: Summarised information on SediGraph from the Literature.	77
Table 2.8: Basic information on the ISP technique	79
Table 2.9: Comprehensive comparisons of the different techniques to find the PSD of soils	85
Table 3.1: Properties of tested kaolin.....	99
Table 3.2: Composition of kaolin.	100
Table 3.3: Miscellaneous information on kaolin provided by the manufacturer.	100
Table 3.4: General properties of bentonite, provided by supplier.	101
Table 3.5: Composition of bentonite, as provided by supplier.	101
Table 3.6: Typical suspension properties of tested bentonite provided by the supplier. .	101
Table 4.1: Equations to determine σ_s of tested soils considered in this study.....	134
Table 4.2: Comprehensive experimental results for all types of tested soils in this study.	138
Table 4.3: Equations to determine χ of tested soils considered in this study.....	140
Table 4.4: Effect of temperature on the dielectric constant of water.	141
Table 5.1: Comparison of results for all three types of clay for both dry and wet of optimum water content tests	165

Table 6.1: Physical and chemical properties of three natural soils considered in this study.	
.....	178
Table 6.2: Properties of sodium hexametaphosphate.....	179
Table 6.3: Quantitative comparisons between laser diffraction, hydrometer, pipette, and the proposed approach for particle size analysis of kaolin.	195
Table 7.1: Soil Classification System (ASTM D2487-93; AS1726-1993). Only relevant soils are included in the chart.....	205
Table 7.2: Soils considered in this study for the sampling approach to predict LL and PL along with their geotechnical properties.	211
Table 7.3: Statistical resampling approach to validate the accuracy of F_{LL} prediction. ..	213
Table 7.4: Statistical resampling approach to assess the accuracy of F_{PL} prediction.	217

List of Figures

Figure 2.1 : The changes in electrical resistivity (ER) of soils at different water segments (Pozdnyakov, 2006).	34
Figure 2.2: Effect of changes in electrical conductivity of water (EC _p) on the electrical conductivity of soils (EC _a) and dielectric constant (D) (Bouksila et al., 2010).	37
Figure 2.3: SEM photographs of MX80 Bentonite soils mixed with (a) distilled water, and (b) 4M NaCl solution (Manca et al., 2016).	37
Figure 2.4: Different stages of the degree of saturation (terraGIS, UNSW).	38
Figure 2.5: Impact of degree of saturation on the electrical resistivity of (a) Ca-bentonite, (b) kaolin, (c) CL, and (d) CH (Kibria and Hossain, 2015).	39
Figure 2.6: Effect of the sand fraction on the electrical resistivity of compacted soils in different saline solutions (Lu et al., 2019).	40
Figure 2.7: Influence of CEC on the electrical resistivity of compacted soils (Kibria and Hossain, 2015).	40
Figure 2.8: Possible relationship between electrical resistivity and liquid limit, plasticity index of soils (Abu Hassanein et al., 1996).	41
Figure 2.9: Schematic of clay's DDL development (modified from Mitchell and Soga, 2005).	45
Figure 2.10: Effect of temperature on the electrical conductivity of lateritic soil (Bai et al., 2013).	48
Figure 2.11: The three possible electrical current pathways through saturated clay.	49
Figure 2.12: Schematic diagram of Rhoades et al. (1976) model.	51
Figure 2.13: Replication of Rhoades et al. (1989) model.	52
Figure 2.14: Model presentation of Fukue et al. (1999).	54
Figure 2.15: Mojid et al. (2007) model with the inclusion of DDL water.	55
Figure 2.16: A simplified diagram of Ellis et al. (2010) model.	56

Figure 2.17: Relationship between σ/σ_w and volumetric water content (θ). σ =overall EC of soils, and σ_w is the EC of free water (Kalinski and Kelly, 1993).	58
Figure 2.18: The relationship between soil electrical conductivity (EC) and hydraulic conductivity (Lu et al., 2019).....	61
Figure 2.19: Different methods of measuring the particle size distribution of soils considered in the literature review.	64
Figure 2.20: Settlement of clay particles in clay-water suspension, at the (a) beginning, and (b) after a while when the larger particles have reached the basement.....	66
Figure 2.21: Hydrometer for measuring density.....	69
Figure 2.22: Sieve analysis (911 metallurgist).	71
Figure 2.23: Laser diffraction technique (Kongas, 2003).....	74
Figure 2.24: Formation of a diffraction angle (source: Malvern).	74
Figure 2.25: Difference between Fraunhofer and Mie theory (Source: https://www.pharmaceutical-networking.com/laser-diffraction , accessed on June 21, 2019).	75
Figure 2.26: SediGraph method to measure PSD (source: Micromeritics).	78
Figure 2.27: Schematic presentation of the PSD measurement domain of ISP compared to pipette and hydrometer (Durner et al., 2017).....	79
Figure 2.28: Finding the liquid limit of a specific soil using the Casagrande method.	86
Figure 2.29: Finding W_c^{LL} of a specific soil using the cone penetration technique.	87
Figure 2.30: Atterberg's thread rolling test to determine the plastic limit (Arora, 2008)..	91
Figure 2.31: Pfefferkorn apparatus (Andrade et al., 2011).	92
Figure 2.32: Sample examples of deformation ratio (H_0/H_f) as a function of moisture content (Andrade et al., 2011).....	92
Figure 2.33: Clay indentation illustrating (a) lack of plasticity, and (b) excessive water (Modesto and Bernardini, 2008).	93

Figure 3.1: Particle size distribution of tested kaolin.	99
Figure 3.2: Particle size distribution of bentonite considered in this study.	102
Figure 3.3: Electrical conductivity meter used to measure soil-water suspension conductivity: a) complete set up of the device, b) brief information on meter display, c) a sample experiment process, and d) solutions with known EC values for the calibration purpose.	103
Figure 3.4: Soil resistivity meter and its specifications: a) complete set up, b) four pins representing four electrodes, c) range selector for resistance, d) a sample experiment, and e) information on the formulae for the conversion purpose.	106
Figure 3.5: Heat-based distilled water maker.	107
Figure 3.6: Soil-water suspension mixer used in this study: a) information on the parts of the device, and b) a sample mixing process ongoing.....	108
Figure 3.7: Automatic mortar mixer used in this study to mix dry soil samples at different moisture contents.	109
Figure 3.8: Sample diagram of the standard proctor compaction test for soils.	110
Figure 3.9: The optimised temperature controlling water bath used in this study: a) front set up of the device before starting the experiment, b) beakers are merged into the water to reach the targeted temperature, and c) display of keypad to enter the desired temperature input.	111
Figure 3.10: Hydrometer used to determine the particle size distribution of soil (AS 1289.3.6.3-2003).	112
Figure 3.11: Sample pipette analysis for particle size distribution of soils: a) complete set up, and b) sample collection procedure.	113
Figure 3.12: Malvern Mastersizer 3000 Laser Diffraction Particle Size Analyser setup.	114
Figure 3.13: Sample Casagrande test to determine LL: a) groove creation before the actual test begins, and b) different parts of the Casagrande device.	116

Figure 3.14: Cone penetration method for soil.	118
Figure 4.1: Postulation on effective clay particle/effective solid formation with DDL water.....	123
Figure 4.2: Representation of diluted clay-water system.....	125
Figure 4.3: Flowchart depicting the major steps of the experimental programmes.....	126
Figure 4.4: Particle size distribution of dermosol and chromosol, obtained by laser diffraction technique.	127
Figure 4.5: Free swelling test (Gibbs and Holtz, 1956).	129
Figure 4.6: Soil suspensions inside the oven.	131
Figure 4.7: Soil samples after being subjected to a constant temperature for 24 hours...	131
Figure 4.8: Effect of saline water on electrical conductivity for different clay particles.	133
Figure 4.9: Effect of saline water on different values of χ for different clay particles. ...	133
Figure 4.10: Evolution of σ_s as a function of T and σ_{FW} for a) bentonite, b) kaolin, c) chromosol, and d) dermosol.....	134
Figure 4.11: Changes in σ_s as T varies in different salt concentrations in water in (a) bentonite, (b) kaolin, (c) dermosol, and (d) chromosol.	136
Figure 4.12: Behavioural changes in χ as T and σ_{FW} vary.....	140
Figure 4.12: Effect of T on χ as the salinity of water changes for (a) bentonite, (b) kaolin, (c) dermosol, and (d) chromosol.	143
Figure 4.13: Schematic diagrams explaining DDL development and reduction in free swelling and DDL size due to temperature.....	145
Figure 4.14: Effect of temperature on the FSI of soils.....	148
Figure 5.1: Series and parallel configurations of electrical conductivity of clay.	155
Figure 5.2: Proposed series-parallel electrical conductivity model for clays in this study.	157

Figure 5.3: Dry density curve against different moisture contents for (a) kaolin, and (b) bentonite.....	160
Figure 5.4: Assumption of particle orientation of clay fabric.....	161
Figure 5.5: A sample procedure of mixing clay with water at a targeted moisture content: (a) spraying water to reach targeted moisture content, (b) mixing procedure of water with clay, (c) further mixing with mortar mixer, (d) some fractions of clay being transferred to sealed bag to ensure moisture equilibrium.....	162
Figure 5.6: Saturation process inside a CBR soaking tank.....	164
Figure 5.7: Arrangement for measuring electrical conductivity of saturated clays (σ^{vl} : principal axis orientated parallel to the compaction direction; σ^{hl} : principal axis orientated perpendicular to the compaction direction).	164
Figure 5.8: Variation of σ^{vl} at different porosities (n).....	167
Figure 5.9: Variation of σ^{hl} at different porosities (n) for (a) isotropic, and (b) anisotropic condition.	168
Figure 5.10: Agreement between predicted and measured values of σ^{vl} for (a) isotropic, and (b) anisotropic conditions (the straight line is the identity line).	169
Figure 5.11: Agreement between predicted and measured values of σ^{hl} for (a) isotropic, and (b) anisotropic conditions (the straight line is the identity line).	170
Figure 6.1: Particle size analysis by (a) Histogram of colloidal gold nanoparticles (Link and.....	173
Figure 6.2: Different parts of the probe considered in this research: (a) acrylic tube with grooves, (b) width of each groove, (c) inner and outer diameter of the tube, (d) dimension of the brass electrodes, (e) assembly of electrodes and insulation, (f) approximate height (position) of each pair of electrodes submerged into the soil-water suspension, and (g) complete tool after the setup.	183
Figure 6.3: Oven-dried soil sample for PSD test.	184

Figure 6.4: Steps of removing organic carbon from soil: (a) mixing H_2O_2 , and (b) reaction process.....	185
Figure 6.5: Methods of removing calcium compounds by HCl: (a) pouring HCl into the soil sample, and (b) after the reaction.	185
Figure 6.6: The EC setup before the commencement of the PSD test.....	187
Figure 6.7: Snippets of the experimental procedures as part of the calibration and PSD analysis: (a) a sample test for kaolin, and (b) resistivity reading from the SR-2 meter...	188
Figure 6.8: Comparison between direct calibration and 3-point calibration of (a) kaolin, and (b) vertosol.	189
Figure 6.9: A complete overview of the PSD analysis of soils using the EC technique.	191
Figure 6.10: PSD curves from the EC approach of (a) laboratory clays, and (b) natural soils.	193
Figure 6.11: Accuracy analysis of the proposed method to find the PSD (kaolin).....	194
Figure 6.12: Reproducibility of (a) hydrometer, and (b) EC approach for the PSD tests for kaolin.....	196
Figure 7.1: Different stages of Atterberg Limits.....	199
Figure 7.2: Plasticity range for the ASTM soil classification system (ASTM D2487-93; AS1726-1993).....	204
Figure 7.3: Non-linear surface analyses to observe behaviours of (a) F_{LL} and (b) F_{PL} , as functions of σ_n and χ	207
Figure 7.4: Agreement of values obtained from the Casagrande and cone technique at low LL (the straight line is the identity line).	208
Figure 7.5: Agreement between the liquid limit values of soils obtained from the cone and EC techniques.	209
Figure 7.6: Agreement between the thread-rolling test and the EC technique to determine the plastic limit of soils.	221

Abstract

The electrical conductivity of soils has become an important topic in geotechnical engineering as it provides essential information on a specific soil sample from a broader perspective. Soil electrical conductivity is a function of soil mineralogy, pore water salinity, pore connectivity, particle size distribution, temperature, degree of saturation, and water content. Therefore, in-depth research on soil electrical conductivity can guide geotechnical engineers or soil scientists to a new pathway in determining the geotechnical properties of soils. Although numerous research studies have been conducted over the past decades to develop methods for the geotechnical testing of soils, there are still limitations in these methods in terms of timing, accuracy, reproducibility, and technicality. Therefore, it is necessary to identify alternative and appropriate methods to address these limitations in the geotechnical research of soils. The aim of this research is to understand the electrical conductivity of soils and its application. Hence, at the commencement of this study, electrical conductivity of clay ingredients is studied. Based on the electrical properties of clay materials, a new series-parallel structure-oriented model is developed to determine the electrical conductivity of soils. Later, the new concepts of the aforementioned model are applied to extend the research and new methods are introduced to determine some of the basic properties of soils, such as particle size distribution, liquid limit, and plastic limit. In terms of accuracy and usefulness, it is found that studying the electrical conductivity of soils is a useful alternative to conventional geotechnical testing methods. The results obtained from the newly introduced methods are validated through comparisons with the results achieved by the conventional methods. It is found that it is possible to predict particle size distribution, liquid limit, and plastic limit of soils by establishing the connection with the electrical conductivity of the tested specimens.

Statement of Authorship

This thesis includes work by the author that has been published or accepted for publication as described in the text. Except where reference is made in the text of the thesis, this thesis contains no other material published elsewhere or extracted in whole or in part from a thesis accepted for the award of any other degree or diploma. No other person's work has been used without due acknowledgment in the main text of the thesis. This thesis has not been submitted for the award of any degree or diploma in any other tertiary institution.

The details of any publications reproduced in the thesis, including content reproduced from a book; and the title, nature and details of any practice-based work (including its public performance, presentation or exhibition or publication).

A handwritten signature in black ink, appearing to read 'Md Farhad Hasan', written in a cursive style.

Md Farhad Hasan

Date: October 6, 2020

List of Publications

1. **Hasan, M.F.**, Abuel-Naga, H., Broadbridge, P. and Leong, E.C., 2018. Series-parallel structure-oriented electrical conductivity model of saturated clays. *Applied Clay Science*, 162, pp.239-251.
2. Lu, Y., Abuel-Naga, H., Al Rashid, Q. and **Hasan, M.F.**, 2019. Effect of Pore-Water Salinity on the Electrical Resistivity of Partially Saturated Compacted Clay Liners. *Advances in Materials Science and Engineering*.
3. **Hasan, M.F.**, Abuel-Naga, H. Role of Distribution and Diffusion Coefficients of Compacted Clay Liner and Geomembrane in Landfills, 2019. *Research and Development in Material Science* 11(5), pp.1234-1240.

Australian Postgraduate Research (APR) Internship

Organisation: Environment Protection Authority (EPA) Victoria.

Collaboration: La Trobe University

Finance: Funded by Australian Government's Department of Education and Training.

Project Title: Contaminant Mobility Tracking by Diffusion Modelling Through Victorian Landfills.

Duration: April 2019-July 2019

Acknowledgment

I wish to convey my deep gratitude to my thesis supervisors Associate Professor Dr Hossam Abuel-Naga and Emeritus Professor Philip Broadbridge. Dr Abuel-Naga provided valuable training in research methods and continually guided me to overcome any problems I encountered in relation to this research. He also gave me indispensable advice on conducting the experiments and completing the technical writing. Professor Broadbridge helped me understand how to apply mathematics in engineering applications. The combined skills of my esteemed supervisors ensured that I had the best possible PhD supervision, for which I am extremely grateful.

I would also like to thank La Trobe University for providing financial support through a La Trobe University Postgraduate Research Scholarship (LTUPRS) and a La Trobe University Full-Fee Scholarship (LTUFFS). These scholarships certainly made my life in Melbourne easier.

The considerate support from the technical team of the Department of Engineering and Physical Sciences cannot be overlooked. Words are not enough to thank Mr Peter Stewart, Mr Adam Console, Mr Jack Zyhalak, Mr Eric Huwald, Mr Habib Rahman, and last but not least, Mr Mark Gentile for both their technical and friendly advice and support. My frequent chats with Mr Gentile helped me settle quickly at the beginning of my PhD candidature. I would also like to thank Professor Tang and his Agri Bio team and Dr Shahidul Islam of La Trobe University for providing materials for further research. I'm also grateful to my research collaborators, Professor EC Leong, Dr Yi Lu, and Mr Qais Al Rashid for their assistance with the high-quality publications. A special thanks to my friends, Dr Son Thai and Dr Dilruk Gallage for keeping an eye on me during the difficult times.

I'm also grateful to LTU GRS, APR.Intern and the Environment Protection Authority (EPA) Victoria for allowing me to complete an internship during my PhD tenure. The industrial experience I received from EPA Victoria has developed my research knowledge. Special thanks to Dr Mathew Watts for training me on Victorian landfill and diffusion modelling. I also remain grateful to my undergraduate thesis advisor Professor Md Mamun Molla who sowed the seeds which grew my love of research.

I sincerely thank my parents, in-laws, and siblings for their unconditional trust, and timely encouragement. I would also like to mention the significant role played by my late grandmother who passed away in 2019. When I was a child, she took me to school every day and any success I may achieve, I owe to her.

Finally, I lovingly thank my wife for being my best friend and for her continuous support throughout my PhD candidature. It would have been an arduous task to finish this research on time without her continuous encouragement. I dedicate this work to her.

Chapter 1

Introduction

1.1 Background

Interest in studying the electrical properties of geo-materials dates back to 1912 when Schlumberger introduced the idea of using electrical resistivity measurements to investigate the properties of the subsurface ground to understand the soil characteristics ([Herman, 2001](#); [Samouelian et al., 2005](#)). Other areas where an understanding is required of the electrical properties of soils are: (i) earthing of electrical installations ([Laver and Griffiths, 2001](#); [Lim et al., 2013](#)), (ii) measuring moisture content for agriculture applications ([Rhoades et al., 1976](#); [Tabbagh et al., 2002](#); [Brillante et al., 2015](#)), and (iii) electro-osmosis consolidation and drainage of soils ([Casagrande, 1949](#); [Jones et al., 2011](#)). Electrical conductivity is a fundamental property of a material which quantifies how strongly it can conduct electrical current. This is actually the opposite of electrical resistivity, which shows a material's property to resist the electrical current. Considering the broader applications of the electrical properties of soils, further research should be conducted to investigate soil classification applications using the electrical conductivity. The implementation of electrical conductivity is non-destructive and sensitive and therefore, it offers an attractive alternative in soil science and agriculture, as well as in geotechnical engineering.

Several studies have indicated that the electrical conductivity of soils is controlled by soil mineralogy, particle size distribution, void ratio, pore size distribution, pore connectivity, degree of water saturation, pore water salinity, and temperature ([Kalinski and Kelly, 1993](#); [Abu-Hassanein et al., 1996](#); [Saarenketo, 1998](#); [Samouelian et al., 2005](#); [Kim et al., 2011](#); [Long et al., 2012](#); [Al Rashid et al., 2018](#); [Ondruška et al., 2018](#)). Nevertheless, in the last few decades, research dedicated to the applications of electrical conductivity/resistivity of

soils to investigate soil properties has been limited to the investigation of soil-water moisture content, pore water salinity, and hydraulic conductivity (Rhoades et al., 1976; Kalinski and Kelly, 1993; Saarenketo, 1998; Brunet et al., 2010; Gunn et al., 2015; Merritt et al., 2016). Therefore, it is practical to believe that the electrical conductivity of soils can be utilised to replace the conventional soil classification applications required in Geotechnical Engineering. However, before extending the application of electrical conductivity of soil to geotechnical engineering, a precise electrical conductivity model has to be developed which considers all the influential attributes. The following section provides a detailed justification for the requirement of such modelling.

1.2 Problem Statement

Soil is a complex material. Researchers have tried for decades to understand the physico-chemical properties of clay such as clay surface conductivity, the role of a diffuse double layer (DDL) and how these interact with the changes under different influential circumstances such as pore water salinity, temperature, and mineralogy, to name a few. In general, DDL is an ionic structure that demonstrates changes in electric potential near a charged clay surface (Mojid et al., 2007). Clay particles are surface-active and their physico-chemical properties mostly depend on surface phenomena. Therefore, a proper understanding of the DDL and clay surface conduction is required before including its effect in the soil electrical conductivity model.

The effect of temperature on the electrical conductivity of soils has been discussed extensively in the literature (Brevik et al., 2004; Robinson et al., 2004); however, the possible impact of temperature on the DDL has been barely investigated. On the other hand, there have been several attempts to introduce simpler and easier soil conductivity models. To implement such requirements, one of the widely accepted approaches is to consider soil as a multi-phase material comprising solid (soil), water, and in some case the DDL

(Waxman and Smits, 1968; Rhoades et al., 1976; Rhoades et al., 1989; Fukue et al., 1999; Mojid et al., 2007; Ellis et al., 2010; Ming et al., 2019). The models were presented by considering a soil resistivity element comprising soil, water and sometimes the DDL either in series-parallel or just parallel connectivity, with at least one conducting phase (water). By analysing all the models, it was found that there is still a need to answer some of the concerns which have been identified but not yet resolved.

Application of the electrical conductivity method in the geotechnical field requires modelling a soil conductivity model that includes all the important parameters that can influence the electrical properties of soils. Although there are several types of research available in the literature which focus on understanding soil resistivity/conductivity models by considering soil as a multi-phase material, there are still some discrepancies surrounding some other physical properties of soils such as behaviour of DDL, possible involvement of empirical parameters which are needed to be defined with physical meaning, inclusion of equivalent conductive solid, to name a few. Despite its shortcomings, this approach has been widely utilised due to its simpler geometry and easier mathematical formulations. Most of the soil conductivity models between 1960 to 2010 considered solid soil particles to be insulators and the pathway for the electrical current flow was restricted through free water only (Waxman and Smits, 1968; Rhoades et al., 1976; Rhoades et al., 1989; Fukue et al., 1999). The intriguing inclusion of the DDL was ignored entirely. Later, the consideration of DDL water was involved in some of the parallel models (Mojid and Cho, 2006; Mojid et al., 2007). Nevertheless, the solid soil particles were still considered to be non-conductive. In addition, it has been reported that the orientation of the soil fabric can heavily influence soil conductivity (Abu-Hassanein et al., 1996) and therefore, by studying the level of anisotropy, it is also conceivable that conductivity can be modelled more accurately. Furthermore, the models in the literature mostly involve some empirical parameters which do not have any physical meaning and these models rarely consider the

effect of surface conduction and size/thickness of the DDL. In some of the literature, the experimental programmes are unclear, and insufficient validation techniques are proposed. Therefore, the proper modelling of the electrical conductivity model of clay soils is still required.

Meanwhile, the existing models in the literature rarely discuss the possibility of extending the study to determine the geotechnical properties of soils which limits the value of these models. If the soil electrical conductivity model and its relevant parameters can be utilised in applications of geotechnical engineering, the research outcomes should withstand a higher level of scrutiny. It should be mentioned here that some of the conventional techniques to determine soil properties are still considered to be tedious, time-consuming, and less reliable, in short, obsolete. For example, the particle size distribution, liquid limit, and plastic limit of soils can be determined using several techniques that vary based on the type of standards. Each technique has its own advantages and disadvantages per se, but the outputs for the identical specimens are not consistent. In addition, some of the modern devices for determining particle size distribution are delicate, expensive, and not user-friendly. Therefore, this research concentrates on developing an accurate electrical conductivity model in such a way that it takes all the essential parameters into account, and proposes new and simple electrical conductivity test methods that can be used to determine geotechnical properties of clayey soils.

1.3 Objectives of the Study

The proposed research covers the following objectives:

- Conduct an intensive literature review to assess the robustness of the available electrical conductivity models of soils and identifying their limitations. The process includes presenting the existing electrical conductivity models from the literature with simplified visual representations and mathematical as well as conceptual

background. After the comprehensive comparisons, the advantages and disadvantages would be analysed. This part of the analysis would be utilised for the new electrical conductivity models of soils. Later, the existing soil classification applications would be analysed for the purpose of application of electrical conductivity to determine geotechnical properties of soils. The literature review on the existing methods would provide information on the disadvantages and shortcomings, which would be solved by the electrical conductivity method.

- Develop a simple laboratory test method to assess quantitatively the surface electrical conduction of fine-grained particles and the factors controlling it (pore water salinity, and temperature). In order to introduce a simple electrical conductivity model for saturated soils, two new electrical surface conduction parameters would be introduced namely, electrical conductivity of solid (soil), and thickness/size of diffuse double layer (DDL) of soils. Later, a proper explanation on the physical meaning and characteristics of those parameters would be provided. For the purpose of sensitivity test, the effect of pore water salinity, and temperature would be investigated.
- Propose a novel series-parallel structure-oriented electrical conductivity model for fully saturated organic-free clays by considering the following:
 - i. The effect of surface conduction on the electrical conductivity of saturated clay soils. Experimental programmes would be designed and mathematical formulation would be provided in order to determine the parameter, subject to the sensitivity tests as mentioned above.
 - ii. The role of the diffuse double layer (DDL) to form effective clay particles as a single unit.
 - iii. The inclusion of anisotropy in the apparent electrical conductivity of clays. It has been found in the literature that the particle orientation of the clays controls the

electrical conductivity of clays, however, it was seldom investigated in detail. The present electrical conductivity model of saturated soils also considers the level anisotropy along with other key factors such as pore water salinity, dry density, moisture contents, to name a few.

- Introduce and validate new alternative fine-grained soil classification test methods that make use of electrical conductivity measurements to determine the following geotechnical properties of soils:
 - i. **Particle size distributions:** It has been found that the existing methods to determine particle size distributions (PSD) have several shortcomings such as inaccuracy in the results, timescale of the experiments, and cost of the modern equipment. The present study aims to introduce a novel approach to determine PSD of soils by EC technique, which can be completed within 1-2 hours, is repeatable and cost effective (less than \$100 for the materials). The PSD curves obtained from the EC technique would be compared with the existing methods to assess the level of accuracy.
 - ii. **Liquid and Plastic limits:** The methods to determine Liquid Limit (LL) of soils have been subject to criticism for decades due to not being able to provide an accurate, repeatable results. The two of the popular methods to determine LL of soils are Casagrande and Cone techniques, which produce inconsistent results for the identical soil samples. Therefore, it's still not confirmed which test is actually providing the accurate results. On the other hand, the conventional thread-rolling technique to determine Plastic Limit (PL) of soils has been labelled as “unscientific” and time-consuming. The consistency of the results as well as the chances of “human errors” have been mentioned in the literature too. Therefore, the EC technique introduced in this study to determine LL and PL of soils would be able to solve most of the

concerns mentioned above. While it takes 24 hours to get the LL and PL of soils from the conventional techniques, EC technique would be able to provide the same within 1 minute with just one experiment. The obtained results were compared with the conventional techniques and excellent agreement was observed.

1.4 Outline of the Thesis

- In Chapter 2, the information from the literature regarding the soil conductivity models considering all the possible effects is reviewed. After this, conventional methods of determining particle size distribution, liquid limit, and plastic limit are discussed in light of the advantages and disadvantages.
- In Chapter 3, the research methods and relevant materials/equipment are discussed in brief.
- In Chapter 4, a new laboratory method to assess the electrical surface conduction of fine-grained particles is presented. The effect of temperature and water salinity on clay surface conduction is discussed.
- In Chapter 5, the newly developed electrical conductivity model for fully saturated clay is introduced and phase relations are discussed, followed by the assumptions considered in this study. The model is then validated with experimental programs and by analysing the level of anisotropy. Then, the effects of pore water salinity on the surface conduction parameter and the size of the DDL are presented based on the test results.
- In Chapter 6, a new approach to determine the particle size distribution of soils is introduced by the electrical conductivity method. After a short discussion on the theory of sedimentation, the proposed method is discussed. The results are validated with the conventional hydrometer and pipette methods and laser diffraction

analysis. Good agreement is observed between all the approaches for an identical soil sample.

- In Chapter 7, predicting the liquid limit and plastic limit of soils using the electrical conductivity technique is discussed. The dimensionless parameters are introduced with a brief explanation and the new methodology of determining the liquid limit and plastic limit is introduced. Comparisons with conventional methods are presented for validation purposes. Comprehensive comparison and research data are presented in tabular format for better clarification.
- In Chapter 8, a summary of the preceding chapters is presented. Lastly, recommendations for possible improvement and further research in this area are discussed.

Chapter 2

Literature Review

2.1 Introduction

In the last four decades, research into the electrical properties of soils has seen remarkable improvements. Although progress in the research outcomes has been promising, most of the works were not able to establish a compelling belief in the accuracy of the approach. While some models were remarkably better in predicting soil electrical resistivity, the implementation of the proposed models was quite limited. In addition, the inclusion of some empirical parameters was observed in the literature without any prior explanation of the formulation or physical properties. Although the limitations of these models were discussed in the literature, nevertheless, the possibility of expanding their use for practical engineering applications was seldom mentioned. In fact, before applying electrical conductivity techniques to determine the geotechnical properties of soils, it is essential to acquire adequate knowledge and an understanding of the electrical conductivity of soils including the effect of temperature on clay ingredients. In the following, a literature review of the existing electrical conductivity models and the available methods to determine soil classification applications is presented. The review discusses the following points:

- factors influencing electrical resistivity/conductivity of soils
- several relevant soil resistivity/conductivity models in the literature and their advantages/disadvantages
- available soil classification methods and their limitations

2.2 Factors Influencing the Electrical Conductivity of Soils

The electrical conductivity of soils can be influenced by several factors depending on the type of changes. Several studies have shown that changes in the pore water salinity lead to an increased amount of ions, which conduct electricity. Therefore, as pore water salinity increases, the soil electrical conductivity should increase. The similar statement could be mentioned about moisture content and degree of saturation of the soil as well as more percentage of water ensures the pores of the soils contain free water, which increase the EC of soils. Furthermore, it has been found also reported that changes in the soil mineralogy influence the EC of the soils. The ratio of fine and coarse materials in the soil samples will largely affect the EC of soils. Some of the factors affecting the soil mineralogy were found to be cation exchange capacity (CEC) and the inclusion of sand fraction. In addition, clay particles' orientation in a sample also influences the EC of soils due to the level of anisotropy. A detailed analysis has been provided in the later section.

2.2.1 Soil Porosity

Porosity is one of the most important indices of soils. Porosity is determined by the ratio of the volume of the void and the total volume. On the other hand, dry density refers to the ratio of the mass of the soil and total volume. An increment in dry density or a decrease in porosity improves the contact between soil particles which leads to enhanced electrical current flow through the moist soil. Each soil can be prepared at different porosities or dry densities by either dynamic or static compaction. In dynamic compaction, soils of identical moisture content will exhibit different porosities if compaction blows are varied ([ASTM D698; AS 1289.5.1.1:2017](#)).

2.2.2 Soil Moisture Content

The moisture content is determined either in terms of weight or volume. The moisture content by weight is calculated as a ratio of water present in the solid soil voids, whereas the volumetric water content is determined in the light of the ratio of water volume present in the soil and total volume.

In general, the electrical conductivity of clays increases as soil moisture content and dry density increase (Rashid et al., 2018). As the moisture content increases, the absorbed ions present in the soil particles are diffused in the pore water. As the soil particles come in contact with the pore water, they become hydrated. Therefore, it increases soil particle's electrical surface activity due to the moisture content. If the moisture content is increased, soil particle's electrical surface conduction will increase, leading to an increase in electrical conductivity of the soil.

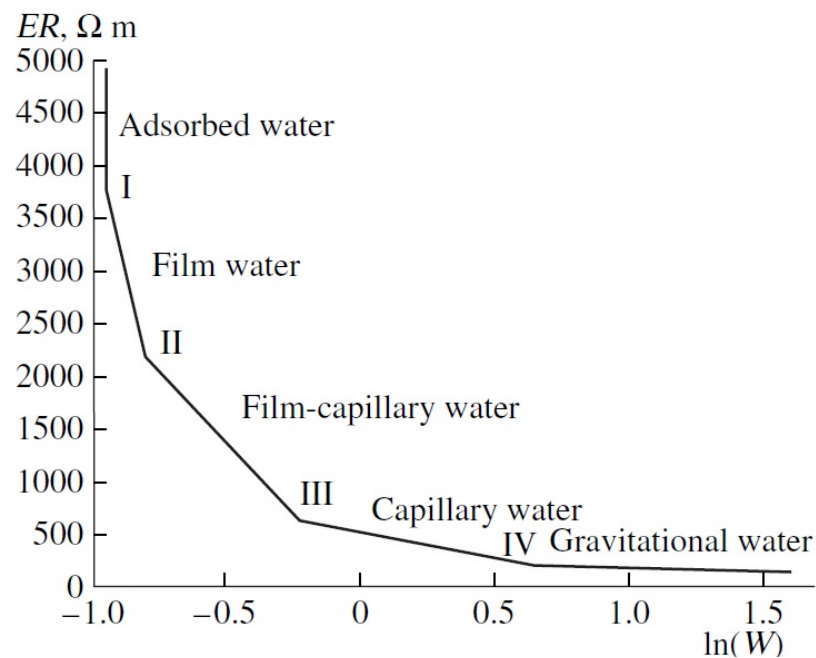


Figure 2.1 : The changes in electrical resistivity (ER) of soils at different water segments (Pozdnyakov, 2006).

[Mojid and Cho \(2006\)](#) reported that the electrical conductivity of soils depends on the moisture content-based phenomena, however, the inclusion of the DDL also has to be taken into account. Their experimental results show that as moisture content increases, soil conductivity continued to increase to a certain value and then decreased, regardless of the high moisture content values. This behaviour was explained in terms of the DDL development of soils, which is associated with the moisture content and cations of soils. At low water content, some of the cations form a precipitate on the clay surface. However, the size of the DDL remains thin due to the lack of moisture. Therefore, when the moisture content is increased, the DDL becomes larger and it increases soil conductivity until DDL formation reaches its threshold values for that specific soil. After a while, when further water is added to the clay, the DDLs begin to lose connectivity with each other and therefore, the soil conductivity of soil remains almost unchanged, and with the further inclusion of water, conductivity starts to decrease due to the dissociation of the DDL. This is supported by [Pozdnyakov \(2006\)](#), who sub-categorised the type of water present in the soil pore namely, absorbed, film, film capillary, capillary, and gravitational, as shown in [Fig.2.1](#). It is noted that with an increase in moisture content, soil conductivity increases concurrently at the absorbed water zone. Although the water molecules are considered to be static in this zone, the water dipole plays a pivotal role in developing the conductive pathway for the electrical current. Therefore, soil conductivity increases. In the next stage (film water), soil conductivity also increases, but the rate of increment is less than that of the absorbed zone due to the increase in the Van der Waals force, which is associated with the attraction and repulsion between atoms, molecules, and the clay surfaces ([Anandarajah and Chen, 1997](#)). On the other hand, the molecular attraction force is greater than the capillary force in the film capillary water area, and as a consequence, the electrical conductivity of soils increases at a much slower rate at film-capillary and capillary water areas than the previous segments. Finally, the gravitational water zone contains mobile

electrical charges which are independent of water ion movement and therefore, the electrical conductivity remains unchanged despite the increment in the moisture content.

2.2.3 Pore Water Salinity

The term pore water in soil refers to the existence of the water among the gaps in soil particles, and pore water salinity means the presence of salt concentration in the pore water. The electrical conductivity of soil is also a function of the salinity of pore water. Pore water salinity depends on the concentration of the total dissolved salt in water. Therefore, the presence of different concentrations of salt in the water directly influences the electrical conductivity of water. Salt dissolves into positively charged and negatively charged ions which conduct electricity. Therefore, increasing pore water salinity increases pore water electrical conductivity. Once the saline solutions are mixed with soil samples, it increases the electrical conductivity of clay soils ([Mojid et al., 2007](#)). [Figure 2.2](#) represents the increase in soil electrical conductivity at different pore water salinity, where soil mixed with the salt-water solution with the highest electrical conductivity exhibited the most increase in the dielectric constant (D), which indirectly represents the increase in the overall electrical conductivity of soils ([Bouksila et al., 2010](#)).

However, it has been also found in the literature that the influence of pore water salinity on soil conductivity goes beyond the direct effect. For example, clay surface conduction is a function of clay plasticity and pore water salinity. As the pore water salinity increases, the electrical conductivity of pore water increases, and at the same time, the surface conduction increases. Therefore, only determining pore water salinity won't provide a clear insight into some of major the electrical properties of soils such as information on size of DDL, and surface conductivity.

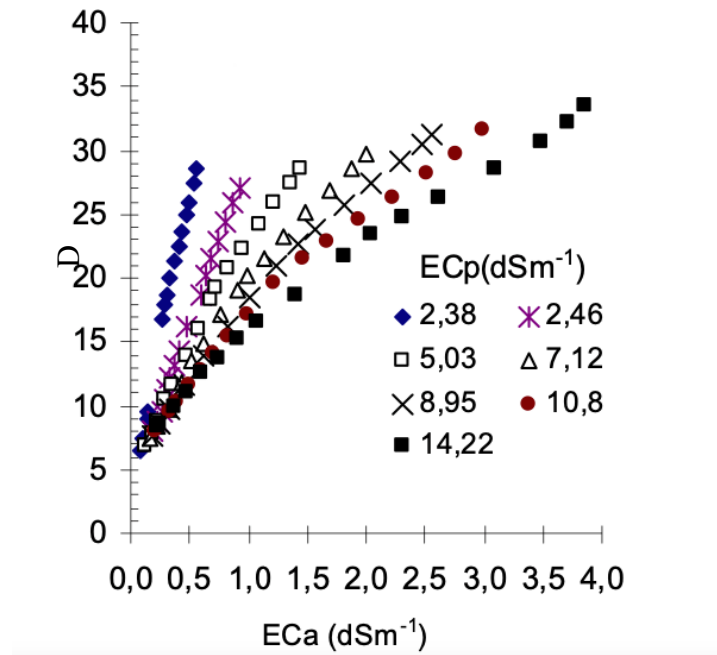


Figure 2.2: Effect of changes in electrical conductivity of water (EC_p) on the electrical conductivity of soils (EC_a) and dielectric constant (D) (Bouksila et al., 2010).

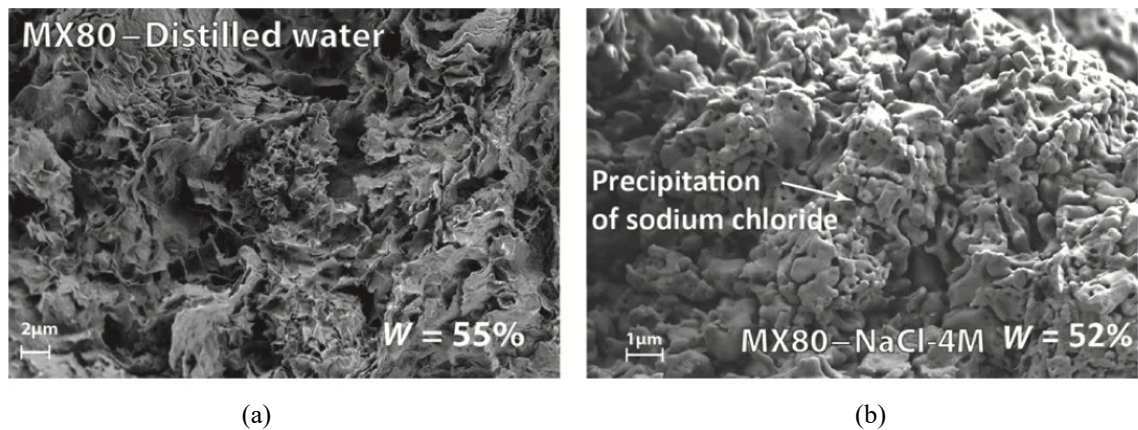


Figure 2.3: SEM photographs of MX80 Bentonite soils mixed with (a) distilled water, and (b) 4M NaCl solution (Manca et al., 2016).

The salinity of pore water can also affect the microstructure configuration of compacted clays which is controlled by the magnitude of developed interparticle repulsive forces during clay particles' hydration period (Cui et al., 2002; Wang et al., 2014; Lu et al., 2018). Therefore, a different pore size distribution is expected for soils with a similar dry density but mixed with water of different salinities. Several researchers showed that reconstituting clay specimens with distilled water could produce a monomodal pore size microstructure, whereas aggregated microstructure (bimodal pore size) is expected as the pore water

salinity increases (Manca et al., 2016; Lu et al., 2018). Figure 2.3 represents SEM photographs described by Manca et al. (2016), where aggregated microstructure of MX80 Bentonite soil particles could be observed. Therefore, clay specimens prepared at different water salinity levels will have distinctive interparticle contacts. As a result, the electrical conductivity of soils will be affected.

2.2.4 Degree of Saturation

It has been mentioned that soil can be represented as a multi-phase complex material (Rashid et al., 2018). According to phase relation, the combined impact of water content and dry density can be evaluated by observing changes in the electrical resistivity of soils

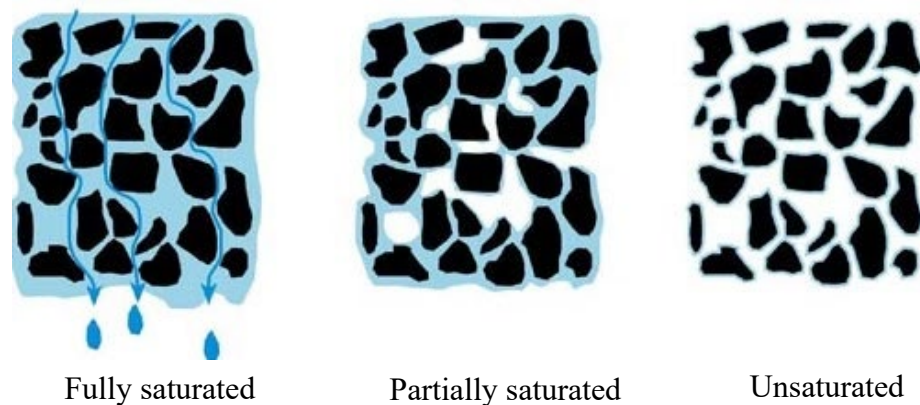


Figure 2.4: Different stages of the degree of saturation (terraGIS, UNSW).

against the degree of saturation. For fully saturated soils, the degree of saturation is 100%, which means all the voids among the pores have been completely filled by water, as shown in Fig.2.4. As a consequence, moisture bridging increases the electrical current flow through the soil mass and results in low electrical resistivity as the degree of saturation increases (Rashid et al., 2018).

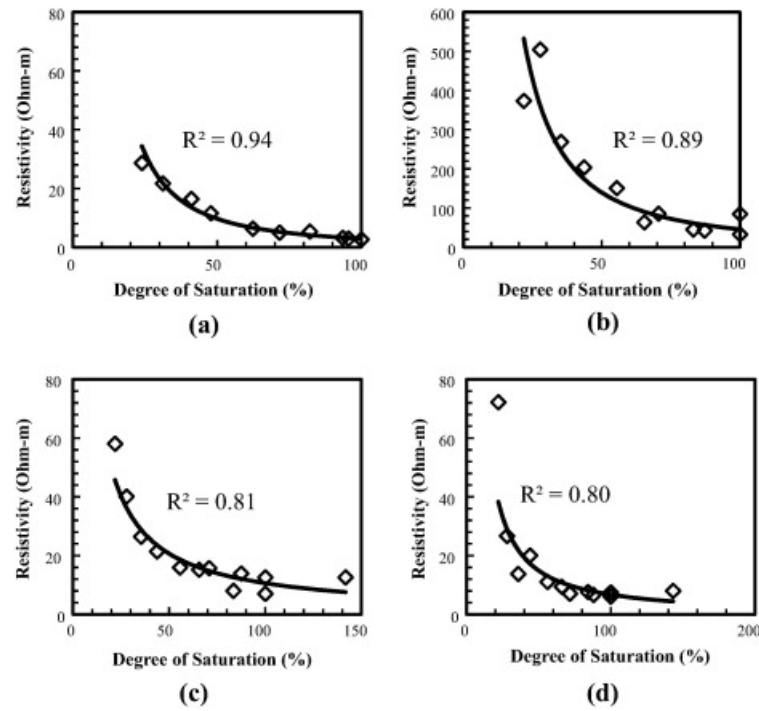


Figure 2.5: Impact of degree of saturation on the electrical resistivity of (a) Ca-bentonite, (b) kaolin, (c) CL, and (d) CH (Kibria and Hossain, 2015).

Kibria and Hossain (2015) reported that the variations in electrical resistivity of compacted clay specimens can decrease approximately 11 times the initial value with an increment in the degree of saturation from 23% to 100%, as illustrated in Fig.2.5, for different types of materials.

2.2.5 Soil Mineralogy

Soil electrical resistivity is also influenced by fine fraction and surface activity, which is controlled by soil mineralogy (Friedman, 2005; Kibria and Hossain, 2015). Lu et al. (2019) conducted an extensive study comprising seven different fractions of fine and coarse contents in the soil samples and the electrical resistivity values were recorded accordingly, as shown in Fig. 2.7. As the percentage of sand fraction increases in any soil sample, soil resistivity is expected to increase since sand acts as insulation.

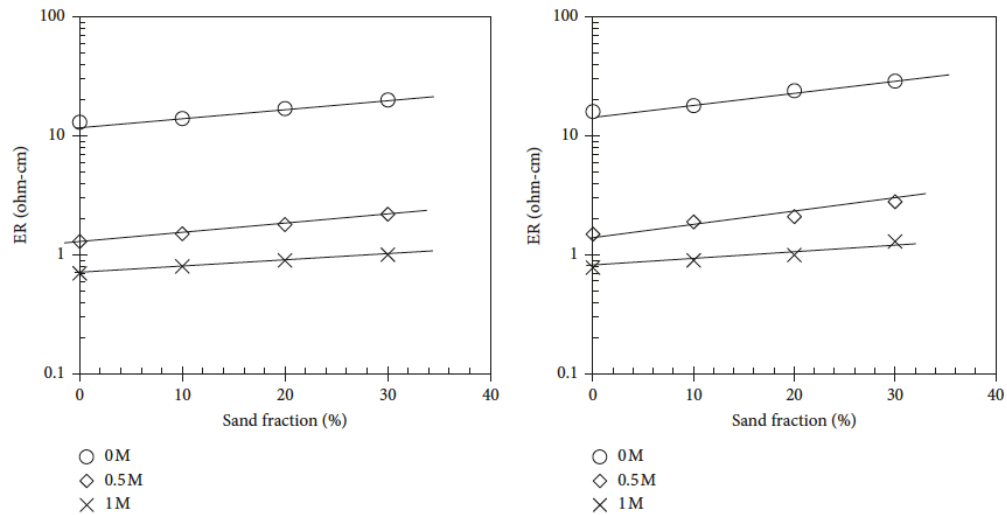


Figure 2.6: Effect of the sand fraction on the electrical resistivity of compacted soils in different saline solutions (Lu et al., 2019).

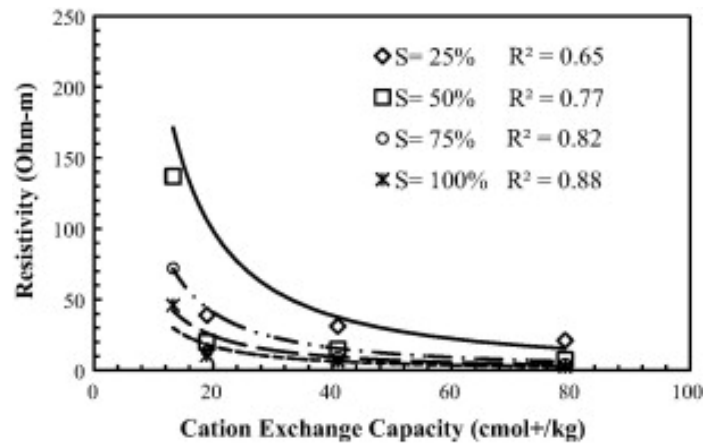


Figure 2.7: Influence of CEC on the electrical resistivity of compacted soils (Kibria and Hossain, 2015).

Shah and Singh (2005) showed that clay fraction can be linearly correlated with the cation exchange capacity (CEC) of soils, a comprehensive discussion of which was validated by Kibria and Hossain (2015) by presenting the relation among pore water properties, CEC, and clay mineral. Soil electrical conductivity can increase due to increasing moveable ions in the pore water. Since both kaolin and bentonite minerals possess exchangeable ions, the effect of clay properties in soil conductivity can be presented by CEC concurrently. Fig. 2.8 demonstrates one such example, presented by Kibria and Hossain (2015).

2.2.6 Liquid Limit and Plastic Limit

The first approach to establish a connection between the electrical conductivity/resistivity of soils was introduced by [Abu Hassanein et al. \(1996\)](#). The experimental results imply that soil which has a higher liquid limit (LL) ($>70\%$) and plasticity index (PI) (>35) usually

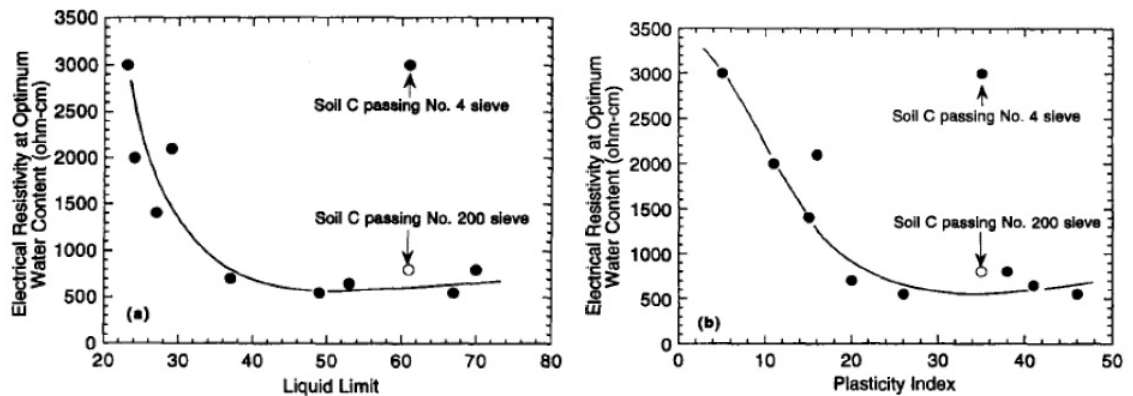


Figure 2.8: Possible relationship between electrical resistivity and liquid limit, plasticity index of soils ([Abu Hassanein et al., 1996](#)).

exhibits higher electrical conductivity, as shown in [Fig.2.8](#). [Abu Hassanein et al. \(1996\)](#) also explained the variations in LL and PI values in terms of mineralogy. The clays with montmorillonite or smectite were found to have higher LL and also had higher surface conductivity.

2.2.7 Clay Particle Orientation and Anisotropy

As previously discussed, clay specimens of different porosities are prepared by varying the number of compactions per layer. Clay specimens are compacted perpendicular to the orientation. Consequently, clay pore structure and particle orientation can exhibit preferential orientation ([Benson and Daniel, 1994](#); [Abu Hassanein et al., 1996](#)). As a result, a situation called anisotropy can develop in terms of soil conductivity. Therefore, the soil conductivity model should assess the degree of anisotropy since the orientation of the clay fabric influences the conductivity reading which involves Wenner arrays or electromagnetic methods ([Abu Hassanein et al., 1996](#)).

[Abu Hassanein et al. \(1996\)](#) experimentally showed how anisotropy can change soil resistivity. They compacted four different soil specimens prepared at the optimum moisture content using the standard proctor. The compacted specimens were trimmed into cylinders with their principal axes oriented at 45^0 and 90^0 (horizontal position). Then, the electrical resistivity of each specimen was measured and the effect of anisotropy was evaluated, as shown in [Table 2.1](#).

Table 2.1: Level of anisotropy in electrical resistivity ([Abu Hassanein et al., 1996](#)).

Soil	Vertical electrical resistivity (Ω -cm)	Horizontal electrical resistivity (Ω -cm)	Difference
A	620	533	14%
B	550	467	15%
C	3003	2462	18%
D	2010	1688	16%

According to [Table 2.1](#), the electrical resistivity measured from vertical and horizontal directions varied by almost 16% on average. An isotropic soil specimen should have identical vertical and horizontal electrical resistivity; however, it is a difficult task to achieve this as far as experimental research is concerned. Furthermore, [Abu Hassanein et al. \(1996\)](#) added that the soils compacted at the dry side of the compaction displayed less anisotropy in terms of soil conductivity than the soil compacted at the wet side. Therefore, the role of anisotropy should not be neglected in the soil conductivity model. A carefully developed soil conductivity model should be able to establish a connection between the conductance of the soil and the anisotropy, which is one of the major objectives of this study.

2.3 Effect of Temperature on Electrical Properties of Soils

2.3.1 DDL Properties of Clay Particles

Temperature is one of the important factors influencing soil electrical conductivity (Brevik et al., 2004; Robinson et al., 2004). In this part of the review, the clay ingredients associated with the DDL are discussed in terms of the temperature effect. Although several research works have proven the effect of pore water salinity or electrolytes on the development of the DDL, most of the research does not provide experimental data regarding the influence of temperature on the DDL of clay particles. Fig. 2.10 illustrates the DDL development in clay, where the negatively charged clay particle (anion) is surrounded by the cations to form a unit of charged particles. Stern layer refers to the first internal layer of the DDL, and is immobile relative to the surface. The slipping plane shown in Fig 2.10 works as an interface which keeps mobile and immobile surfaces separate, and the electrical potential at the slipping plane is defined as the Zeta Potential.

The DDL theory provides a basic understanding of the physico-chemical behaviour of fine-grained soils. Mitchell and Soga (2005) described the DDL of soils by demonstrating the role of ion concentration and potential distributions near the charged surfaces. Both of these are influenced by several parameters, namely surface charge density (c), surface potential (Ψ_0), electrolyte concentration (n_0), cation valence (v), the dielectric constant of the medium (D), and temperature (T). The approximate calculation of the effects of n_0 , v , D , and T are determined by the Debye length or thickness of the DDL ($1/K$), which can be written as follows (Mitchell and Soga, 2005):

$$\frac{1}{K} = \left(\frac{\epsilon_0 D k T}{2 n_0 e^2 v^2} \right)^{1/2} \quad (2.1)$$

where ϵ_0 is the permittivity of the free space, k is the Boltzmann's constant ($1.38 \times 10^{-23} \text{m}^2\text{kgs}^{-2}\text{K}^{-1}$), e is the charge of an electron ($1.6 \times 10^{-19} \text{C}$).

According to [Eq.2.1](#), if T increases, the DDL thickness increases. Based on this relation, [Hammel et al. \(1983\)](#) and [Mitchell and Soga \(2005\)](#) demonstrated that with an increase in temperature, the DDL thickness increases since the dielectric constant decreases, whereas for the constant surface charge, the surface potential increases as the dielectric constant decreases. Therefore, considering both characteristics, changes in DDL thickness have a negligible impact on temperature. The effect of temperature of the dielectric constant of water is shown in Table 2.2 ([Mitchell and Soga, 2005](#)):

Table 2.2: Effect of temperature on the dielectric constant of water.

T (°C)	T (K)	D	DT
0	273	88	2.40×10^4
20	293	80	2.34×10^4
25	298	78.5	2.34×10^4
60	333	66	2.20×10^4

The small variations in DT values provide the basis of the statement for [Mitchell and Soga \(2005\)](#). [Table 2.2](#) presents the D values based on several assumptions. [Sposito \(1989\)](#) showed that D of water in soil could be between 2 and 50, which makes the assumption of [Mitchell and Soga \(2005\)](#) doubtful. Furthermore, it is observed that the dielectric constant (D) of a substance (for example, water) decreases as the temperature increases. However, for soil, the dependency of D on the temperature is more complicated due to the existence of surrounding or bound water. As the temperature increases, the molecular vibrations of the water and cations attracted to the soil particles affect the dipole. In practical applications, the effect of temperature on D is highly dependent on the type of soils. According to [Seyfried and Murdock \(2001\)](#) and [Seyfried \(2004\)](#), D can either increase or decrease significantly as the temperature increases, but the impact is not negligible. In

addition, Eq.2.1 was derived considering the Gouy-Chapman model for the DDL (Gouy, 1910; Chapman 1913).

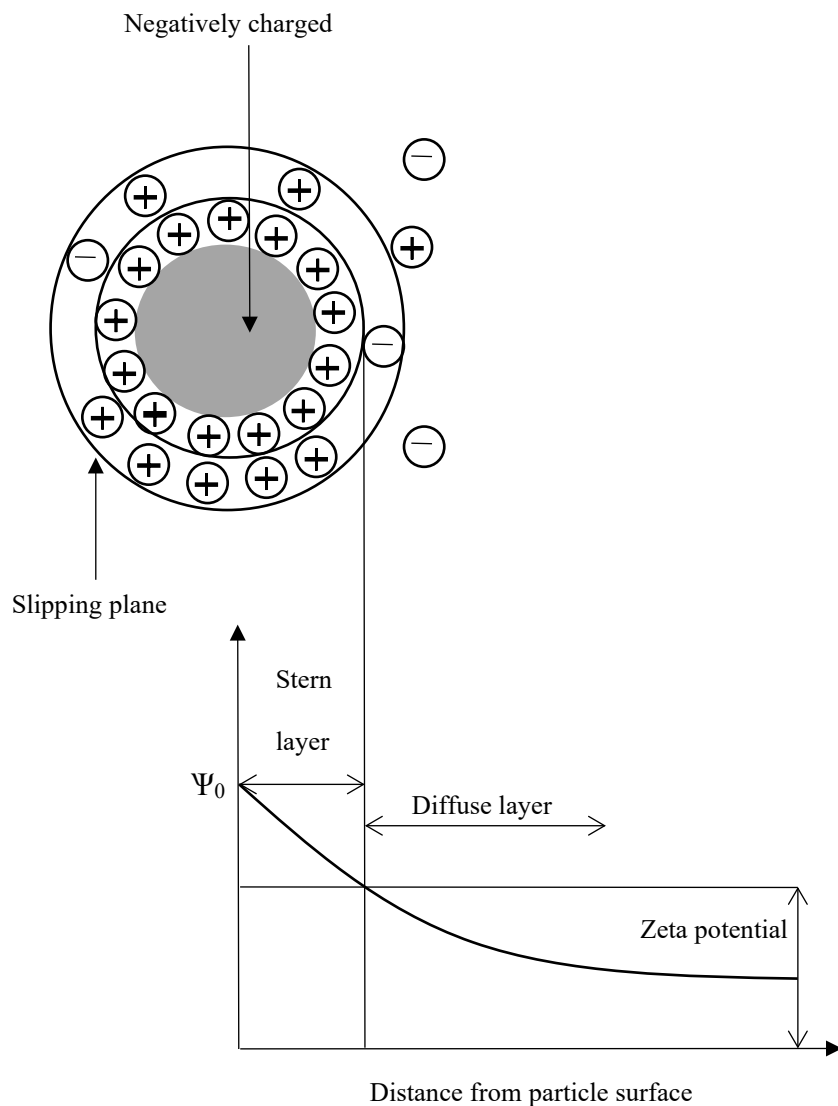


Figure 2.9: Schematic of clay's DDL development (modified from Mitchell and Soga, 2005).

The Gouy-Chapman theory for DDL has numerous limitations which do not consider the interaction between clay particles, the electrical properties of water, the hydration properties of clay, and the interactive attractive forces (Sogami and Ise, 1984; Guven, 1992; Bharat et al., 2013), which were discussed in Chapter 1. Furthermore, the properties of free water and DDL water are different. Therefore, the concept regarding DDL thickness,

presented with Gouy-Chapman theory should be revised, which will possibly introduce a concept of including the dielectric constant of DDL water.

The statement by [Mitchell and Soga \(2005\)](#) also contradicts the report provided by [Zhang et al. \(2004\)](#) who explained the changes in the thickness of the DDL by linking it with Atterberg limits (liquid limit and plastic limit). They stated that with an increase in temperature, the soil starts to dry out and goes through mechanical, physico-chemical and chemical transitions. One of the changes in the physico-chemical process involves the loss of the DDL layer, which also affects the Atterberg limits. Therefore, the thickness of the DDL should decrease with an increase in the temperature. Dehydrated soils generally possess strong bonds between the clay particles and restrict themselves from water penetration ([Fookes, 1997](#)). The process cannot be reversed by rewetting since dehydration causes a significant increase in particle size, and at the same time, the plasticity of soil decreases ([Fookes, 1997](#)). The term “increase in particle size” can be explained in light of the effect of an increase in temperature on clay particles which results in clay soil particles being pasted to each other, forming bigger agglomerates ([Blight, 1997; Fookes, 1997](#)).

[Estabragh et al. \(2017\)](#) contributed to the research on the formation of bigger clay particles by conducting experiments to determine the free swelling and swelling potential of clays, particularly bentonite. Tests were conducted on the dry, optimum, and wet side of the compaction of bentonite to observe the changes in the swelling behaviour of bentonite. Although the experiment results did not directly indicate changes in the thickness of the DDL, it suggested there is a link between temperature, free swelling of clay, and DDL thickness. [Estabragh et al. \(2017\)](#) found that soil at the wet side of the compaction possesses thicker DDL than that on the dry or optimum side. This behaviour can be attributed to the fact that as soils are in contact with water, the dry and optimum side of the compaction soils require more water to be fully saturated and therefore leads to a greater amount of swelling

due to the higher suction and over consolidation ratio. The experiment results were subject to different temperatures, with the highest temperature being 200°C. The results demonstrate that both swelling potential and swelling pressure decreases with an increase in temperature. Noting these behavioural changes in bentonite, [Estabragh et al.](#) described this physical change by considering the role of the interaction of clay particles, which leads to Van der Waals and attractive forces within the adsorbed water layer. The DDL is formed on the surface of the external clay particles. The DDL can be developed both for an individual unit layer and clay platelets, and the DDLs of the neighbouring unit layers and clay platelets interact with each other, which results in a net repulsive force. On the other hand, the attractive molecular forces can be developed between two double layers if they are located extremely close to each other ([Anandarajah, 1990](#)). The effect on interparticle attractive and repulsive forces at a variable temperature was previously discussed by [Evans \(1991\)](#) and [Yong et al. \(1992\)](#), who noted the changes in these two types of forces at elevated temperatures. It was also reported that an increase in temperature induces ion exchange inside the clay's DDL and as a result, it might change the DDL thickness as well as changing particle orientation.

2.3.2 Changes in Saline Water Conductivity

Temperature also affects the electrical conductivity of saline water. Both the ion mobility and the electrical conductivity of saline water increases with an increase in temperature, and the following empirical equation can be utilised to predict changes in conductivity ([Keller and Frischknecht, 1966](#)):

$$\sigma_w = [1 + \beta_T(T - 18)]\sigma_{w-18} \quad (2.2)$$

where $\beta_T \approx 0.025/^\circ\text{C}$, T is the room temperature in $^\circ\text{C}$ ($T < 150^\circ\text{C}$), and σ_{w-18} is the water conductivity at 18°C .

2.3.3 Overall Electrical Conductivity of Soil

According to [Corwin and Lesch \(2005\)](#), the electrical conductivity of soil can rise by approximately 1.9% per °C increment in the temperature due to the agitation of ions present in the soil. [Bai et al. \(2013\)](#) found that the electrical conductivity of soil can increase non-linearly with temperature and the rate of conductivity increases abruptly once the temperature is more than 30°C, as shown in [Fig. 2.11](#).

Soil conductivity is considered to be standard at 25°C. Therefore, the conductivity reading has to be adjusted if the temperature is not standard room temperature using the following equation ([US Salinity Laboratory Staff, 1954](#)):

$$EC_{25} = f_T EC_T \quad (2.3)$$

where f_T is the temperature correction factor. The values of f_T are listed in the table provided by [US Salinity Laboratory Staff \(1954\)](#).

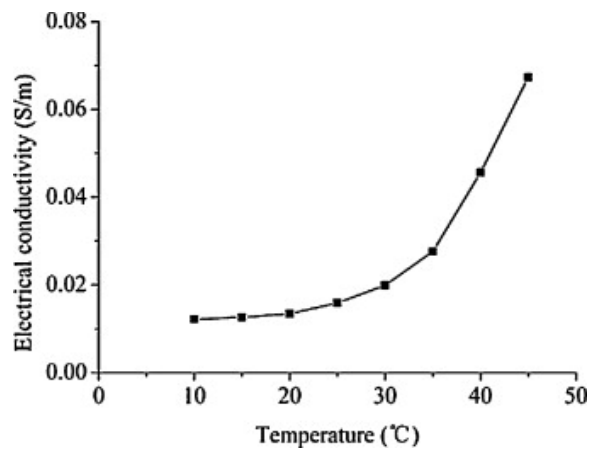


Figure 2.10: Effect of temperature on the electrical conductivity of lateritic soil ([Bai et al., 2013](#)).

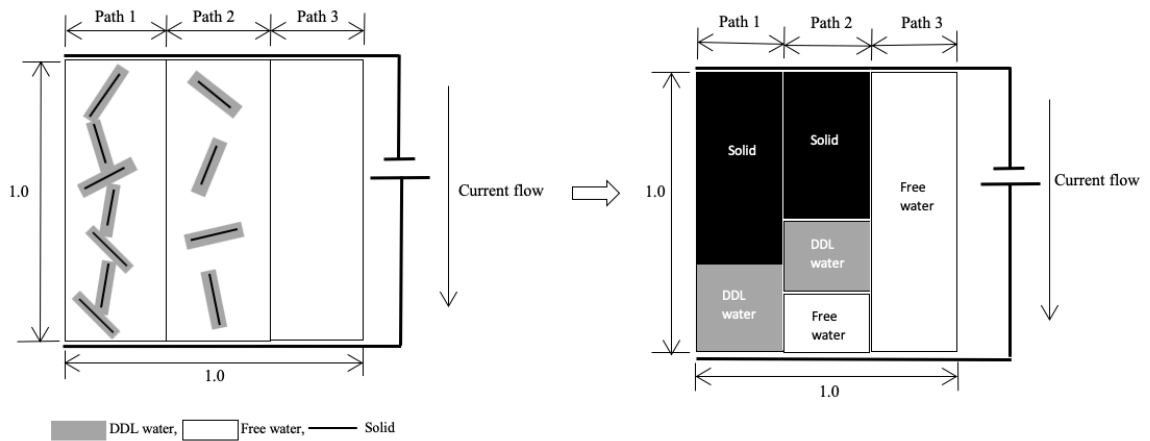


Figure 2.11: The three possible electrical current pathways through saturated clay.

Soil electrical conductivity is a sensitive measurement. During the experiments, the temperature of the saline water, suspension or compacted specimens should always be checked to ensure precise measurement.

2.4 Conceptual Understanding of Electrical Conductivity Models

At the microscopic level, three electrical current pathways through the saturated clays can be identified as follows (Fig. 2.12):

- Conductance through the solid particle contact points. However, as the clay particles are surrounded by DDL water, direct solid particle contact is not possible. Therefore, the conductance at the solid particle contact points occurs through the contact points of DDL water (path 1).
- Conductance through alternating layers of solid particles, DDL water, and free pore water (path 2).
- Conductance through continuous free pore water (path 3).

To predict/model the electrical conductivity of saturated clays successfully, the proposed model includes an accurate representation of the role of the three aforementioned electrical

current paths in terms of their contributions which are the functions of the volume, the electrical conductivity of each phase and the geometrical relationship between the phases (fabric). In light of the aforementioned requirements for developing an accurate electrical conductivity model for saturated clays, the suitability of the available electrical conductivity models in the literature can be assessed.

2.4.1 Archie (1942)

Archie's power-law relation to determine electrical conductivity is still widely utilised, and can be expressed as follows (Archie, 1942):

$$\sigma = \sigma_w \frac{n^b}{a} \quad (2.4)$$

where n is the porosity, a is the tortuosity factor, and b is the cementation exponent.

Although Archie's law was found to be accurate in terms of determining the electrical conductivity of water-saturated soils and rocks, it has been subjected to severe criticisms as it does not consider the possible effect of surface conduction (σ_s) (Klein and Santamarina, 2003). Therefore, Archie's law only considers path 3, ignoring the surface conductivity of the soil, and as a consequence, Archie's law is not valid for fine-grained clays. Furthermore, Archie's law considers two additional parameters namely, tortuosity factor and cementation exponent, which could also be affected by the surface conductivity of soils and pore water salinity (Klein and Santamarina, 2003; Oh et al., 2014). In fact, both Archie's parameters have been criticised for failing to carry distinctive identities particularly in multi-phase soil elements (Glover, 2010). Nevertheless, a few researchers have attempted to upgrade Archie's model to fit the electrical behaviour of fine-grained soils and proposed a modified Archie's model (Atkins and Smith, 1961; Salem and Chilingarian, 1999; Glover, 2010). However, these modified models were not established based on a robust theoretical background. Most of the modified Archie's models are case-

dependent, and therefore require a large volume of experimental tests to determine its parameters.

2.4.2 Rhoades et al. (1976)

The electrical conductivity model of Rhoades et al. (1976) only considers the first and the third pathway in a parallel configuration as follows (Fig. 2.13):

$$\sigma = T\theta\sigma_w + \sigma_s \quad (2.5)$$

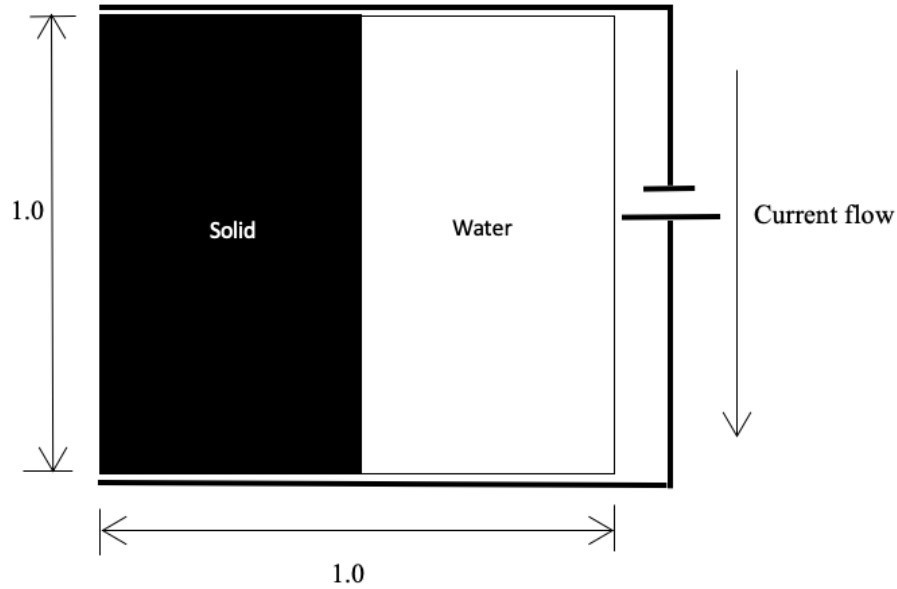


Figure 2.12: Schematic diagram of Rhoades et al. (1976) model.

where σ , σ_w , and σ_s are the electrical conductivity of soil, free pore water, and solid particles, respectively. The symbols θ and T denote the volumetric water content and transmission coefficient (≤ 1.0) to account for the tortuosity effect. This model ignores the possibility of the second pathway. Furthermore, the possible effect of DDL water is implied indirectly in the value of σ_s , whereas the volume of DDL water is not considered. The

model also assumes that σ_s is independent of σ_w , which is not correct when $\sigma_w < 4$ deci Siemens per meter (dS/m) (Nadler and Frenkel, 1980; Shainberg et al., 1980; Mojidi et al., 2007).

2.4.3 Rhoades et al. (1989)

To overcome the limitations in the aforementioned model, Rhoades et al. (1989) introduced a revised model that uses the concept of series-parallel models proposed by Sauer et al. (1955) and Shainberg et al. (1980) for saturated media. The Rhoades et al. (1989) model includes the second and third pathways. The series pathway of this model comprises the solid particles and part of the soil water, whereas the remaining soil water constitutes the parallel pathway as demonstrated in Fig. 2.14. The model is expressed as follows:

$$\sigma = \frac{(\theta_s + \theta_{ws})^2 \sigma_{ws} \sigma_s}{\theta_s \sigma_{ws} + \theta_{ws} \sigma_s} + (\theta - \theta_{ws}) \sigma_{wc} \quad (2.6)$$

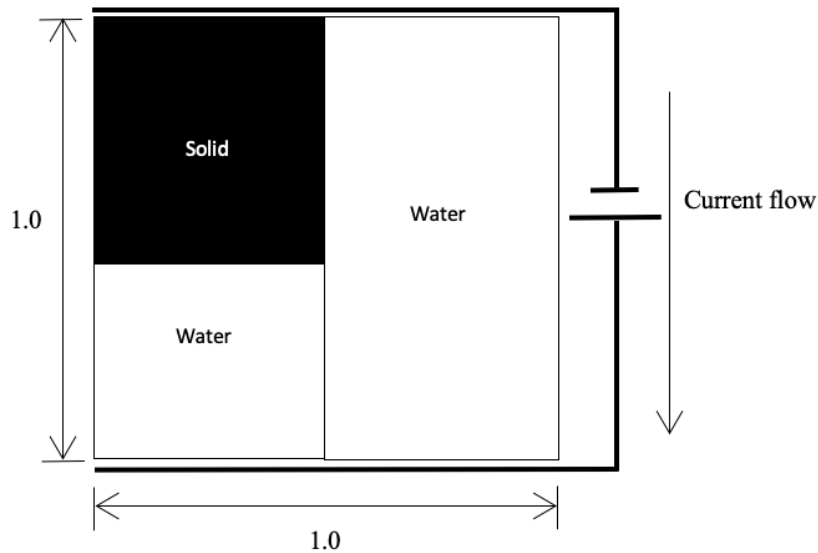


Figure 2.13: Replication of Rhoades et al. (1989) model.

where θ_s is the volumetric fraction of the solid phase and $\theta_s = 1 - n$, where n is the porosity; $\theta - \theta_{ws}$ is the volumetric fraction of the water in the parallel configuration, θ_{ws}

is the volumetric water content in the series configuration; σ_s , σ_{ws} , and σ_{wc} are the electrical conductivity of the solid phase, soil water in the series and parallel configuration, respectively. Rhoades et al. (1989) assumed that $\sigma_{ws} = \sigma_{wc}$. Although the revised model by Rhoades et al. (1989) incorporates the dependent relationship between the electrical conductivity of the solid particles and free pore water, it inherited the limitations of the earlier Rhoades et al. (1976) model in terms of representing the role of DDL water. Furthermore, the omission of the possible role of the first pathway leads to the overestimation of θ_{ws} to match the soil electrical conductivity measurements (Rhoades et al., 1989).

2.4.4 Fukue et al. (1999)

Fukue et al. (1999) proposed a micro-structure electrical conductivity model for clays. The model treats the soil phases as being arranged in a series and parallel configuration where a structural coefficient F was introduced to determine the share of the series configuration in the proposed series-parallel soil system (Eq.2.6). For saturated clay, the series part includes part of the solid and soil water phases, whereas the remaining solid and water phases were arranged in a parallel configuration, as shown in Fig. 2.15. The equation proposed by Fukue et al. (1999) is expressed as follows:

$$\sigma = \frac{\pi r}{\left(\frac{w}{100}\right)G_s\left(1-\frac{n}{100}\right)(1-F)} \frac{\sigma_w}{(1-F)} \quad (2.7)$$

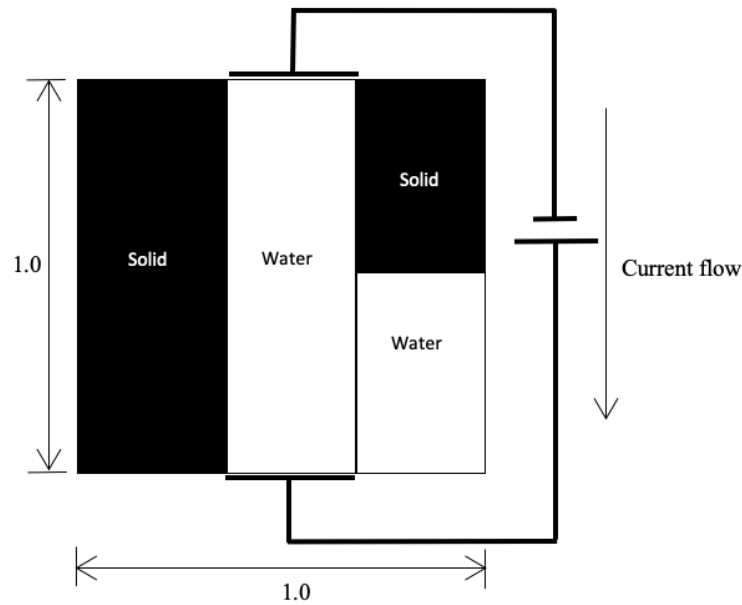


Figure 2.14: Model presentation of Fukue et al. (1999).

where r is the radius of the prepared clay specimen, G_s is the specific gravity, and n is the porosity.

The structural coefficient F in the model by Fukue et al. (1999) is related to the preferred orientation of the soil particles. The Fukue et al. (1999) model considers the solid phase as an electrical insulator, hence the electrical current flow through the series part and the parallel solid phase are neglected and only the parallel soil water phase is considered responsible for conducting the electrical current through the soil (third pathway). Therefore, the Fukue et al. (1999) model ignores the possible electrical current flow through the first and the second pathways. Furthermore, the possible effect of DDL water is not represented in the model formulation. Therefore, as this model does not capture some of the main features of the expected electrical current flow behaviour through saturated clays, the evaluation of the anisotropy behaviour of the electrical conductivity of soil using the proposed structural coefficient F is doubtful.

2.4.5 Mojid et al. (2007)

Mojid et al. (2007) proposed an electrical conductivity model for soils that incorporates the possible effect of DDL water. In this model, the volumetric soil water content is divided into free water, θ_w , and DDL water, θ_{DDL} , which are arranged in a parallel configuration as presented in Fig. 2.16. The soil electrical conductivity, σ , is expressed in this model as follows, where σ_w and σ_{DDL} are the electrical conductivity of free water and DDL water, respectively, and T is a transmission coefficient:

$$\sigma = T(\theta_w \sigma_w + \theta_{DDL} \sigma_{DDL}) \quad (2.8)$$

The model of Mojid et al. (2007) ignores the possible electrical current flow through a series configuration (second pathway). In general, the Mojid et al. (2007) model can be seen as a modification of the Rhoades et al. (1976) model as the volume of the free water in the Mojid et al. (2007) model is adjusted to replace the parallel solid phase in the Rhoades et al. (1976) model by a parallel DDL water phase.

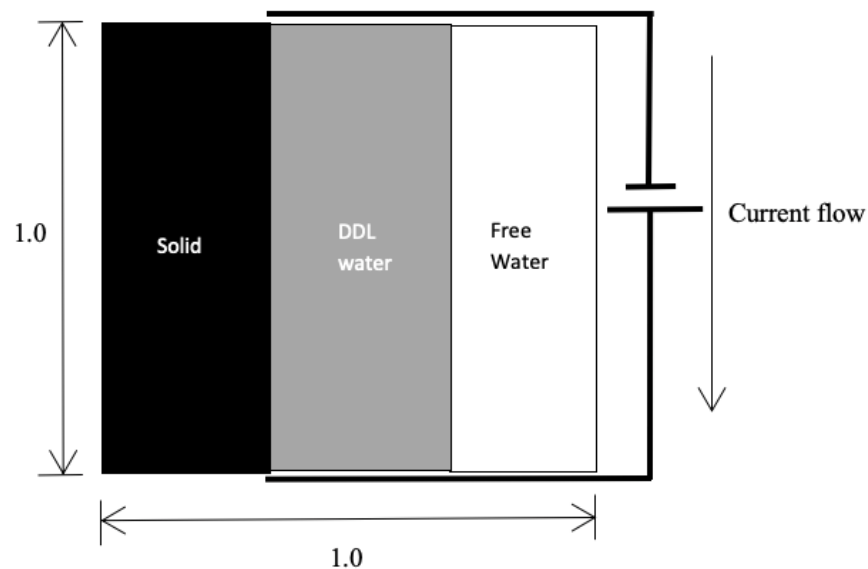


Figure 2.15: Mojid et al. (2007) model with the inclusion of DDL water.

2.4.6 Ellis et al. (2010)

Ellis et al. (2010) modified the model of Hashin and Shtrikman (1962) by adding a geometric factor that can express the possible anisotropy behaviour of the electrical conductivity of soils. This model considers that soil water is totally interconnected and the solid phase occurs as totally isolated inclusions. Furthermore, the effect of DDL water is not incorporated into the model. Therefore, the model considers the second and the third pathway, whereas the first pathway is ignored, as shown in Fig. 2.17. The proposed geometric factor by Ellis et al. (2010) is mainly a function of the soil particle aspect ratio. However, as plate-shaped soil particles in clay exhibit isotropic electrical conductivity behaviour, the geometric factor by Ellis et al. (2010) cannot be used to assess the anisotropic behaviour of the electrical conductivity of soil.

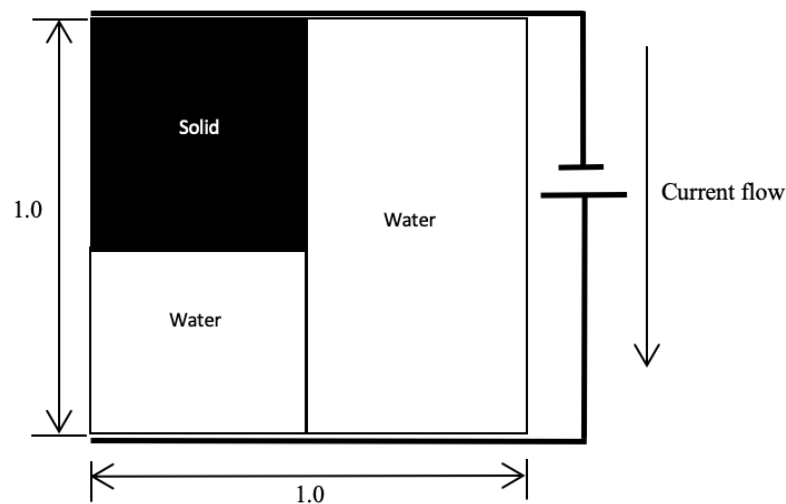


Figure 2.16: A simplified diagram of Ellis et al. (2010) model.

For the purpose of better understanding, a comprehensive comparison has been added in Table 2.3.

Table 2.3: Comparison among the existing series-parallel electrical conductivity models of clay.

Model Name	Advantages	Disadvantages
Archie (1942)	One of the pioneers of parallel conductivity model for soil	Ignores surface conduction of clay, not valid for fine-grained clay
Rhoades et al. (1976)	Opens the pathway for series-parallel modelling	Only considered parallel conduction, and considered pathway through free water only
Rhoades et al. (1989)	Improved version of Rhoades et al. (1976)	Considers conductive path through free water only
Fukue et al. (1999)	Considers series-parallel connection	Considers electrical current flow through free water only
Mojid et al. (2007)	Considers DDL	Only considered parallel connection
Ellis et al. (2010)	Considers series-parallel option	No inclusion of DDL

2.5 Correlations between the Geotechnical Properties of Soil and its Electrical Conductivity

The factors influencing the electrical conductivity of soils were discussed in the previous section. Based on this discussion, it is clear that soil conductivity monitoring can lead to the evaluation of the geotechnical properties of soils, which is one of the important aims of this study. Several researchers have already utilised the soil resistivity method or imaging with a view to determining moisture content ([Kalinski and Kelly, 1993](#); [Goyal et al., 1996](#); [Ozcep et al., 2009](#); [Brunet et al., 2010](#)), compaction condition ([Abu Hassanein et al., 1996](#); [Rinaldi and Cuestas, 2002](#)), hydraulic conductivity ([Arulanandan, 1968](#); [Sadek, 1993](#); [Bryson, 2005](#)), soil consolidation ([McCarter and Desmazes, 1997](#)), clay and mineral content ([Abu Hassanein et al., 1996](#)). Therefore, considering the wide range of applications of the electrical properties of soils, this study is hugely motivated by some of the established applications of the electrical conductivity of soils. In order to provide a short introduction to the applicability of soil conductivity, several examples from the literature will be discussed next.

2.5.1 Determination of Moisture Content

It is undoubtedly true that determining moisture content using conventional method is a better approach as far as user-friendliness and simplicity are concerned. However, the overnight drying method is somewhat a bit time consuming to some extent. On the other hand, when it comes to finding the moisture content of the representative subsurface moisture profile, researchers have faced certain difficulties due to the lack of homogeneity as well as the complex hydro-geological structure of soils. Several methods are available to determine the moisture content of soils, such as time domain reflectometry (TDR), neutron probes, gypsum blocks, gravimetric scaling, to name a few. However, most of these methods require skilled operators and these devices are expensive. Therefore, a simple and direct soil resistivity measurement could be a good alternative since moisture content affects the electrical properties of soils.

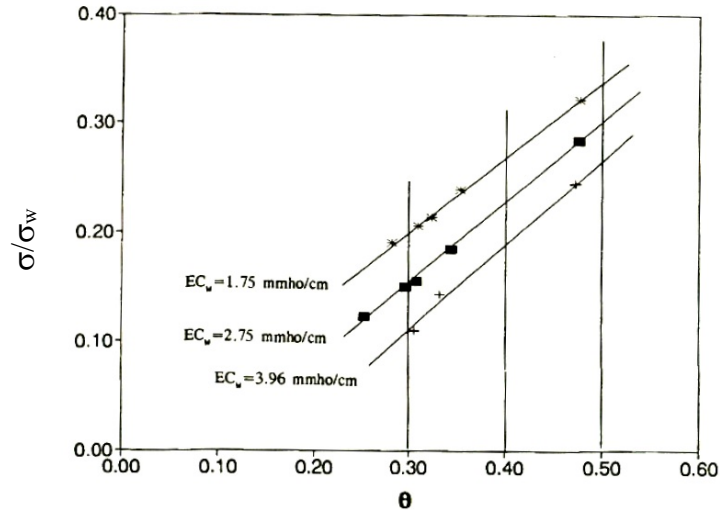


Figure 2.17: Relationship between σ/σ_w and volumetric water content (θ). σ =overall EC of soils, and σ_w is the EC of free water (Kalinski and Kelly, 1993).

The experimental investigation by Kalinski and Kelly (1993) with the four-probe circular cell found that the electrical conductivity ratio of soil and water produces a regression equation which can be utilised to infer the moisture content of soil. However, one major concern about their analysis is the assumption of the σ_s values, which was considered to be

0.24 S/cm for each and every segment. The curves obtained from the analysis serves the basic purpose of the researchers, as shown in [Fig. 2.18](#), but the assumption of surface conductivity makes the approach doubtful. Based on the regression analysis, the following equations were proposed ([Kalinski and Kelly, 1993](#)):

$$\sigma = \sigma_s + \sigma_w \theta (1.04\theta - 0.09) \quad (2.9)$$

[Ozcep et al. \(2009\)](#) suggested two different exponential equations for two different types of samples using the soil resistivity method, however coefficient correlations were found to be between 0.75-0.76 which makes the equations questionable. Later, [Schwartz et al. \(2008\)](#) and [Brunet et al. \(2010\)](#) opted for Archie's empirical parameters with a view to establishing the connection between soil resistivity and soil moisture content. Both were able to validate their experimental results using conventional soil moisture content techniques, however the possible implications of Time Domain Reflectometry (TDR) ([Schwartz et al., 2008](#)) and Electrical Resistivity Tomography (ERT) ([Brunet et al., 2010](#)) made the process complicated hence these haven't been discussed in this study. However, the discussion on the aforementioned literature offers an insight that soil conductivity monitoring provides a pathway by which to find other geotechnical properties of soils.

2.5.2 Predicting Hydraulic Conductivity

Hydraulic conductivity also depends on the porosity, degree of saturation, soil microstructure, and tortuosity of the soils ([Abu Hassanein, 1996](#); [Bryson, 2005](#)). Since soil conductivity is also dependent on these attributes, it is generally possible to establish a correlation between hydraulic conductivity and electrical conductivity ([Sadek, 1993](#); [Abu Hassanein, 1996](#)).

[Farzamian et al. \(2015\)](#) considered ERT to establish a link between soil resistivity and the hydraulic conductivity of saturated soils. The research was conducted in light of the

relationships between soil resistivity and degree of saturation using an in-site investigation. It was found that the predicted hydraulic conductivity from the soil resistivity readings had less than 10% error when the results were compared with the measured hydraulic conductivity of the saturated soils.

The statistical model by [Niu et al. \(2015\)](#) considered the tortuosity factor as well as the correlations between water flow and electrical current flow through a porous medium. In fact, the model focused entirely on the estimation of unsaturated soil hydraulic conductivity from electrical conductivity values. In the end, their predicted results had good agreement with the experimental values with coefficient correlation $R^2=0.97$.

The latest research presented by [Lu et al. \(2019\)](#) considered all the missing attributes discussed in the preceding paragraph. The model by [Lu et al. \(2019\)](#) was validated in the light of the type of compaction (dense or slightly dense), pore size distribution as well as pore water salinity by conducting 54 experimental tests, the graphical representations of which are shown in [Fig. 2.19](#). Although the model was able to show good comparison compared well to the existing models, by eliminating complicated equations from the literature, the introduction of several empirical parameters with ambiguous meanings is one of the major disadvantages.

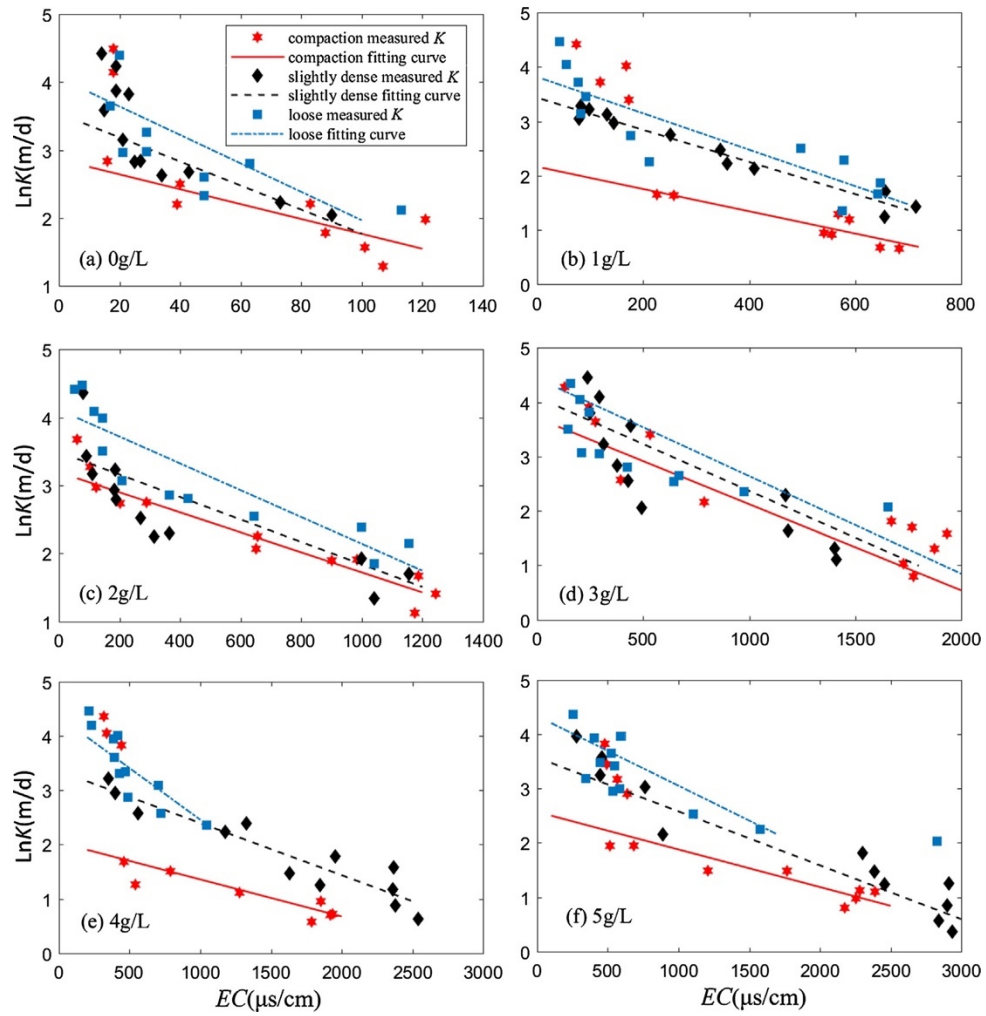


Figure 2.18: The relationship between soil electrical conductivity (EC) and hydraulic conductivity (Lu et al., 2019).

2.5.3 Monitoring Soil Consolidation Properties

Soil consolidation is considered to be dependent on the interpenetration of pore water, reduction in the void ratio, and changes in soil fabric (Hong et al., 2011; Horpibulsuk et al., 2012; Zhou and Zhao, 2013). Therefore, the electrical conductivity of soils could be linked to soil consolidation properties. McCarter and Desmazes (1997) developed a modified consolidation cell to monitor the changes in saturated soil electrical conductivity along with the void ratio. They considered both σ^{vl} and σ^{hl} values by altering effective stress. At the end of their study, it was deduced that since soil consolidation and soil electrical

conductivity both are influenced by several similar parameters, it is possible to find a correlation between them; however, the effect of soil anisotropy was not properly analysed. Later, [McCarter et al. \(2005\)](#) further developed the consolidation cell to study soil fabric changes simultaneously and recorded the soil electrical conductivity measurements. The results obtained were further improvements to the approach in 1997 since the latter considered the formation factor of Archie's law as well as the anisotropy condition of soils.

On the other hand, [Kibria et al. \(2018\)](#) observed changes in the electrical conductivity of soils at different consolidation stages. For each specimen, the scanning electron microscope (SEM) analyses were described in the light of changes in soil fabric, which also provided information on the soil anisotropy. It was reported that soil conductivity decreases with an increase in pressure. Based on their study, the coefficient of soil consolidation and 1D strain were estimated using the electrical conductivity of soils.

2.5.4 Estimation of Clay Content

[Shevinin et al. \(2007\)](#) studied the estimation of the clay content in soils by monitoring electrical resistivity, considering the electro-chemical properties of soil at the microscopic level. The experimental programs were conducted on saturated soil samples at different pore water salinity. Based on the database established by the experimental values, the attempt to predict the clay content from a sand-clay mixture had less than 20% error. Although the variations in the soil samples were not abundant, it still provided a different application of electrical resistivity, which could be further extended in the future.

2.5.5 Determining Liquid Limit and Plastic Limit

Surface conductivity is considered to be an influential factor in the soil's liquid limit (LL) and plastic limit, as reported by [Bryson \(2005\)](#). Based on the conceptual understanding, the

equations correlating electrical conductivity with LL and plasticity index (PI) are as follows (Bryson, 2005):

$$LL = (\sigma_s)^{\varphi^1} \alpha_1 \quad (2.10)$$

$$PI = (\sigma_s)^{\varphi^2} \alpha_2 \quad (2.11)$$

where, α and φ are empirical parameters which are functions of clay mineralogy.

Although Bryson (2005) introduced a new approach to estimate the LL and PI of soils, the empirical parameters in the equations do not have any physical meaning. In fact, at the LL, distilled water was used, which has very low electrical conductivity. Therefore, the possible inclusion of the size of the DDL is missing from Eqs. (2.10 and 2.11), which is distinctive for different types of soils. Chapter 7 of this study addresses this issue, which considers both σ_s and χ .

2.6 Review of Particle Size Distribution (PSD) Techniques

Determining the PSD of soil samples is not a trivial task due to the heterogeneity of the shape and particle density. The techniques to find PSD are generally categorised into two sections, namely classical and modern. The classical methods are sub-categorised into two parts: (i) sieve analysis, and (ii) sedimentation. The sedimentation-based technique generally comprises hydrometer and pipette analysis, which are two of the most commonly researched. On the other hand, some of the modern techniques also take the sedimentation theory into account, but the process of analysis is multifarious. For the ease of discussion, a flow chart is presented in Fig. 2.20 and the analysis is conducted from different perspectives.

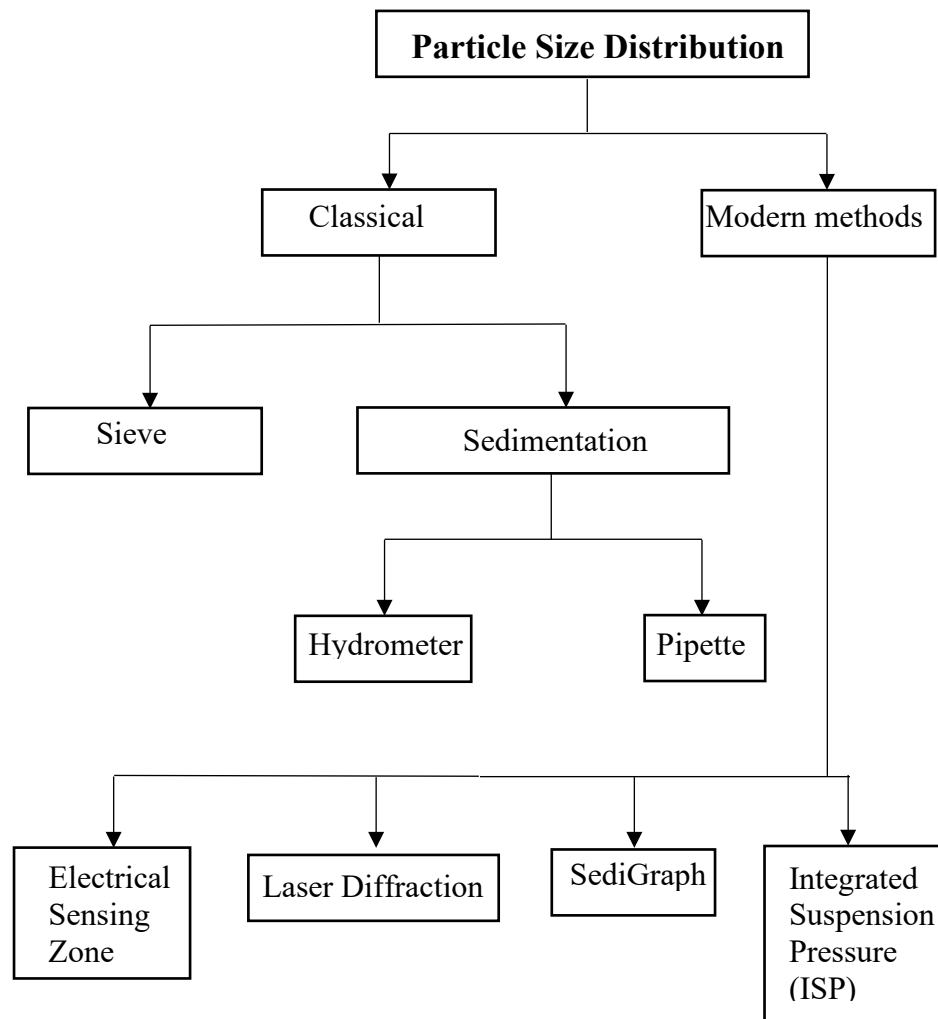


Figure 2.19: Different methods of measuring the particle size distribution of soils considered in the literature review.

2.6.1 Sedimentation Methods

Sedimentation refers to the settling of particles under the effect of gravitational or centrifugal forces. Devices based on gravitational sedimentation measure the velocity of settling particles due to the gravitational forces acting on the particles against the buoyancy of the fluid as well as other drag forces against the setting of the particles. The mathematical relationship is expressed by classical Stokes' law, which is valid only for particles settling under terminal velocity and non-turbulent flow (Day, 1950). The terminal velocity (v) can be expressed as follows:

$$v = \frac{d^2(G_s - \rho_L)g}{18\mu} \quad (2.12)$$

where d is the particle diameter, g is the acceleration due to gravity, μ is the fluid viscosity, G_s and ρ_L are the specific gravity of soils and fluid density, respectively. The derivation of Stokes' law is included in [Appendix 1](#). A chart of viscosity of water at different temperature is presented in [Appendix 2](#), based on [Arora \(2008\)](#).

From [Eq. \(2.12\)](#), it is possible to find the diameter of the clay particles passing at a specific time in a column of height h . Therefore, [Eq. \(2.12\)](#) can be re-written as:

$$d = \sqrt{\frac{18\mu h}{g(G_s - \rho_L)t}} \quad (2.13)$$

In most cases, the velocity of particles depends on its position in the suspension as well as the size (diameter) of the particle. In addition, due to the increased sensitivity, it is important that there is a significant difference between the particle density and suspension density.

[Figure 2.21](#) illustrates the theory of sedimentation. Let us assume a soil sample is composed of particles of only three sizes which have the terminal velocity ratio of 1:2:3. The three types of soil particles are arranged in three columns and each level contains a pair of particles as shown in [Fig 2.21](#). At the commencement of particle sedimentation, the concentration of particles is the same at all depths, as shown in [Fig. 2.21 \(a\)](#). After a while, the larger particles settle at the bottom (level E) and the smaller ones settle at a certain depth, as shown in [Fig. 2.21 \(b\)](#). For example, at level B, at the beginning, the concentration is uniform, but after a certain time period, particle 4 of that particular level settled at level C. The size of particle D can be calculated from Stokes' law as described in [Eq. 2.13](#), and the passing of the soil particles is calculated from the following equation ([Arora, 2008](#)):

$$N = \left(\frac{G_s}{G_s - 1} \right) \cdot \frac{\rho_s - \rho_f}{M_s} \times 100 \quad (2.14)$$

Table 2.4: Brief information on sedimentation methods

Particles range	5-150 μm
Standard sample amount	10 g-20 g (pipette), 50 g (hydrometer)
Analysis time	2-24 hours
General cost	\$50-\$100
Advantages	i) Rapid analysis under the particle range, ii) Well suited for industrial environment, iii) Inexpensive instrumentation, iv) Highly skilled operators are not needed.
Disadvantages	i) Long analysis time, ii) Accuracy can be affected by certain physical factors such as particle-particle interaction, Brownian motion etc, iii) Selection of dispersing agent could be difficult, iv) Requires a quick start of the experiment once the sample is prepared.

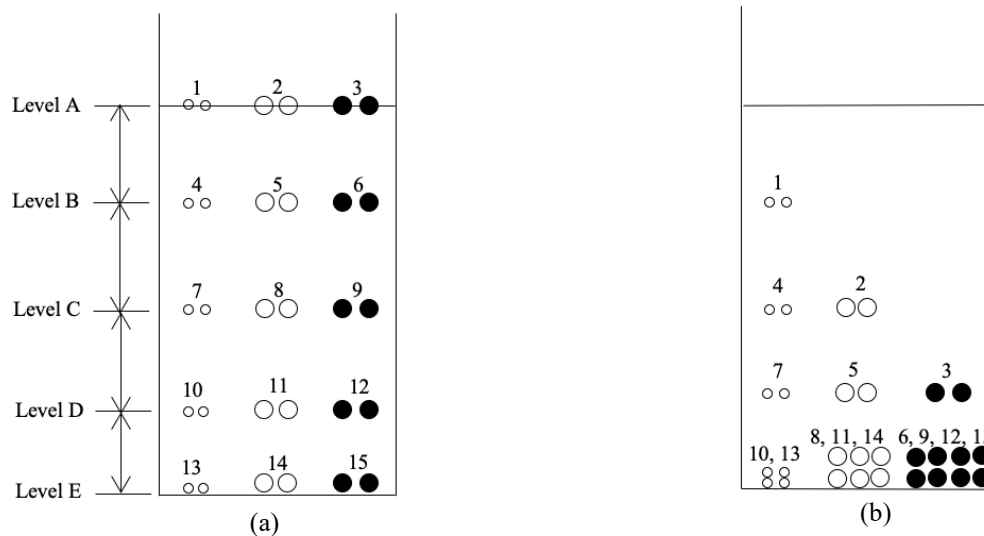


Figure 2.20: Settlement of clay particles in clay-water suspension, at the (a) beginning, and (b) after a while when the larger particles have reached the basement.

where ρ_s is the density of the solid, M_s is the mass of the soil, and $G_s (= \frac{\text{unit weight of solids}}{\text{unit weight of water}})$

is the specific gravity, which is considered to be 2.58 for kaolin and 2.68 for bentonite, as confirmed by the supplier. The detailed derivation of Eq.2.14 is presented in [Appendix 3](#).

The sedimentation techniques for PSD can be classified into two categories, namely (i) incremental, and (ii) cumulative measurements. In the incremental technique, the particle concentration in the suspension is calculated at a given height (h) and time (t). On the other hand, the cumulative measurements represent the rate at which the particles settle out of the suspension.

Information regarding configurations and advantages/disadvantages of the sedimentation methods is given in [Table 2.4](#). The errors and discrepancies in the reproducibility of the sedimentation methods may occur at various stages of the experiment. The issues can be attributed to different cases like the sensitivity of the specimens or the pre-treatment of the suspension. In addition, since classical methods require the heavy involvement of an operator, human-made errors can also take place. Some of the commonly encountered errors or limitations are discussed here in brief.

Theoretically, Stokes' law is applicable to spherical particles only. For non-spherical particles, the sedimentation-based PSD method largely depends on the particle shape and alignment of a particle to the direction of the flow ([Kissa, 2017](#)). Moreover, if sedimentation is considered for particle sizing between 0.1 to 100 μm , the particle shape has to be valued. An extension of Stokes' law for non-spherical particles yields the Stokes diameter, which is classified as the effective particle size corresponding to the size of a sphere that settles at the same velocity. The concept of non-spherical particles is still not clear to researchers, and hence most of the PSD analysers assume samples to be spheres.

On the other hand, the sedimentation-based techniques significantly depend on the settling rate which is largely influenced by the surface conditions of particles as the latter is dependent on particle density. Therefore, the particle size value calculated from the sedimentation rate depends on the porosity of the particles (n). If this correction is not made,

the particle size will be undervalued by a factor of $\sqrt{1-n}$ (Hietala and Smith, 1989). As a result, the PSD analysis will not be error-free.

Furthermore, the analysis of clay particles finer than 0.5 μm can be largely influenced by Brownian motion (Arora, 1992; Allen, 2013). Brownian motion is a random movement of particles created by collisions with molecules of the liquid phase. The impact of Brownian motion is higher on particles with lower density, and due to its interference, the settling time of particles with lower density increases. However, the impact of Brownian motion is negligible if the amount of soil samples is ($\leq 50 \text{ g/L}$) (Arora, 1992).

Several researchers raised concerns regarding the sensitivity of the samples. The involvement of the dispersing agent means the PSD based on sedimentation has to commence as soon as possible since delays may change the sample properties due to several chemical and surface phenomena including dissolution, leaching, and re-precipitation (Jillavenkatesa et al., 2001).

In addition to the general advantages and concerns of the sedimentation techniques, two well-known methods namely, (i) pipette, and (ii) hydrometer, are discussed here.

2.6.1.1 Pipette method

The pipette method, first introduced by Andreasen in 1928, is a sedimentation-based procedure which utilises direct pipette sampling at different controlled depths and times. In other words, the analysis relies on the concept that sedimentation is eliminated from a depth h in a time t , and all particles in the suspension have terminal velocities greater than h/t (Jillavenkatesa et al., 2001), as seen in Eq. (2.12). The details on the pre-treatment, calibration and calculation techniques can be found in the literature (Day, 1965; Arora, 1992; Jillavenkatesa et al., 2001).

Although the pipette method has the advantage of being a comparatively simple and inexpensive instrument and clarifies the results upfront, it is an invasive method and requires a long time-scale to complete the task. Therefore, it was found to be less effective for investigating samples with faster settling rates (Kissa, 2017). In addition, the pipette method requires at least 10-20 g of samples (Eshel et al., 2004), which could be an issue if the availability of a particular soil sample is less than the minimum range.

2.6.1.2 Hydrometer method

The hydrometer measures the density of a settling suspension or dispersion at a known depth. The method is fairly simple and the instrument is quite cheap. The hydrometer method was able to produce results identical to the pipette technique. However, similar to the pipette method, calculating the PSD of the soil samples using a hydrometer is also time-consuming.

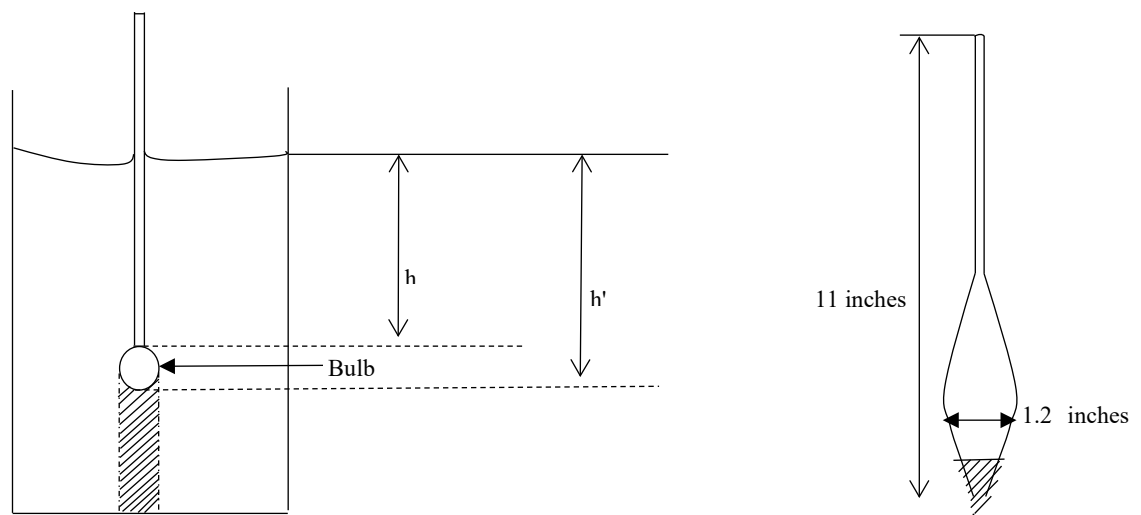


Figure 2.21: Hydrometer for measuring density.

Two common disadvantages should be discussed here. First, if the hydrometer is kept in the suspension all the time, then the bulb covers the underneath area, and therefore, particles cannot enter this region from the top. Secondly, every time the hydrometer is inserted into

the 1000 ml cylindrical glass container, the settling particles are interrupted, the height of the suspension rises from h' to h (Fig. 2.22), and it sometimes becomes difficult to decide when the hydrometer will attain equilibrium with the surrounding suspension.

On the other hand, though the calibration of the suspension is relatively easier compared to other procedures, it may still create concerns regarding the concentration of the suspension since at high concentrations, particle-particle interactions can be observed. As a consequence, based on the surface chemistry of the sample powder, high solid concentrations can hinder the settling of particles, causing a decrease in the settling velocity. This reduction in the settling velocity may provide erroneous values in the PSD and produce an effect that shows a greater concentration of fines than what is actually present in the suspension.

2.6.2 Sieve Analysis

Sieving is one of the oldest techniques for PSD. The preponderance of this method can be attributed to the relative simplicity of the technique, the low involvement of capital, high reliability, and low level of technical expertise requirements. Although there are different opinions on the size range which is covered by this technique, it is safe to say the method is useful within a size range of 2000-50 μm (Eshel et al., 2004), with more details on the advantages and disadvantages described in Table 2.5. A test sieve is a device that retains particles larger than the designated size and it allows smaller particles to pass through, as shown in Fig. 2.23. Sieve analysis can be performed either for free-flowing powders and some precisely prepared slurries, if applicable. In general, the method consists of agitating the sample through a fixed series of sieves with decreasing mesh size (from top to bottom). PSD is reported as the mass of the material retained on a mesh of a given size. However, the distribution can also be reported as the cumulative mass retained on all sieves above a particular mesh size or the cumulative mass fraction above a specified mesh size. Details

on the procedures have been reported in the literature ([Leschonski, 1979](#)) so are not discussed in depth here.

Table 2.5: Information on sieve analysis

Particles range	2000 μm to 50 μm
Standard sample amount	Approximately 100 gm (depends on the size of the sieves)
Analysis time	Depends on the size range, can be done within 10 minutes, or it may 2-3 hours.
General cost	\$21-\$100 (manual shaker), \$1,300-\$4,000 (mechanical shaker)
Advantages / Strengths	i) Broad size range, ii) Does not require highly-skilled operators, iii) A relatively low-cost instrument, iv) Easier sample preparation.
Disadvantages/ Limitations	i) Long analysis time, ii) Lacks automated task, hence more chance of human-made errors, iii) Repeatability and reproducibility have been questioned due to the impact of mechanical motion.

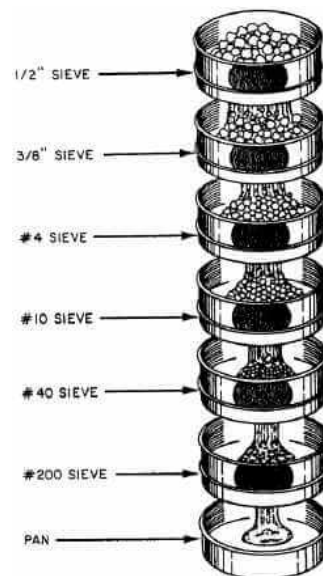


Figure 2.22: Sieve analysis ([911 metallurgist](#)).

The amount of time needed to complete the analysis can cause a major concern if the operational technique is not designed properly. Since the aperture openings become smaller

from top to bottom, the analysis time becomes longer. Therefore, it is important to study the powder size range and size resolution and fix the size of the sieve in the stack before starting the experiment, which increases the time of the pre-treatment procedure.

Another major and well-known limitation of sieve analysis relates to the size range it covers. A particle size of less than 50 μm cannot be sieved through the procedure. Although computerised tools are not generally required, there is a chance of human-made errors impacting the results. In some cases, there is a possibility that agitation may affect the repeatability and reproducibility of the result. In general, a mechanical shaker maintains the consistency during the agitation time, but the same confidence cannot be guaranteed for manual shakers. Therefore, there could be discrepancies in the results.

2.6.3 Laser Diffraction (LD)

LD can provide PSD in a range from approximately 2-300 μm with adequate precision. This method does not disturb the sample by probing unless it is necessary to dilute the sample. The optical fundamentals were introduced by Fraunhofer over 100 years ago but the mathematical calculations for the analysis of the laser diffraction pattern were considered to be complicated (Kissa, 2017). It became much simpler when computers were included in the setup. Summary of LD analysis for soil PSD has been mentioned in [Table 2.6](#).

The LD method provides an average diameter over all orientations of the particles as particles with random orientation pass through the light beam. A collimated and vertically polarised laser beam illumines a particle dispersion and creates a diffraction pattern with the non-diffracted light beam at the centre (Eshel et al., 2004; Kongas, 2003; Blott and Pye, 2006), as shown in [Fig. 2.24](#). The energy distribution of the diffracted light is provided by

Table 2.6: Summary of Laser Diffraction Analysis for PSD of Soils.

Particles range	2-300 μm (effective range), may cover 0.04 μm -8000 μm with less accuracy
Standard sample amount	1 g-5 g
Analysis time	5-10 minutes
General cost of equipment	\$60,000-\$120,000
Advantages	<ul style="list-style-type: none"> i) Quick analysis, ii) Dispersion/extra pre-cautionary approach regarding specimen preparation is generally not required, iii) Calibration is not needed if the particle size is within the device range, iv) Excellent reproducibility, v) Fully computerised calculation/algorithm. Rare chance of human-made errors.
Disadvantages	<ul style="list-style-type: none"> i) Particles smaller than the range of theory are treated as “ghost” particles (Fraunhofer), ii) Computer algorithms are yet to be known completely to the users, iii) Density for all particles must be exactly the same, iv) Knowledge of optical properties of the sample is required, v) Expensive instruments, vi) Highly sensitive, therefore, maintenance cost is quite high.

a detector with light-sensitive concentric circles, separated by isolating circles of identical width. The increase in the diffraction angle, created inside, is inversely proportional to the particle size of the sample. The intensity distribution, which is dependent on the diffraction angle (Fig. 2.25) is converted by Fourier optics into a spatial intensity distribution, which is the sum of the Fourier transformed projections of the sample's particles. Later, the spatial intensity is converted into a set of photocurrents, and the PSD is measured by the computer.

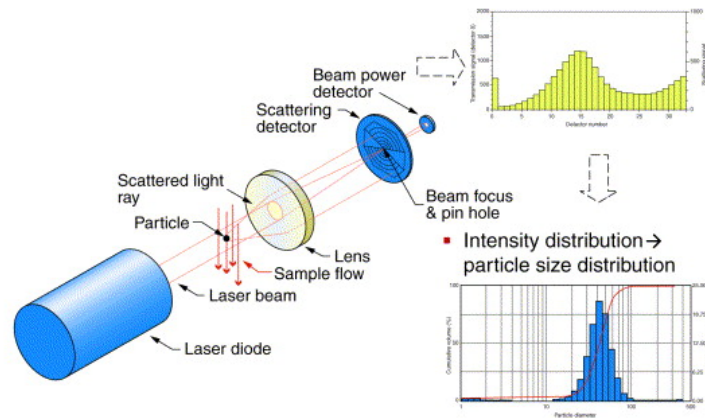


Figure 2.23: Laser diffraction technique (Kongas, 2003).

One advantage of LD based on Fraunhofer theory is that if the particle size of the sample is within the range of the theory, then calibration is not required. However, it is not possible to know the range of the particle size of a sample without prior experimentation, which puts the practicality of Fraunhofer theory into question.

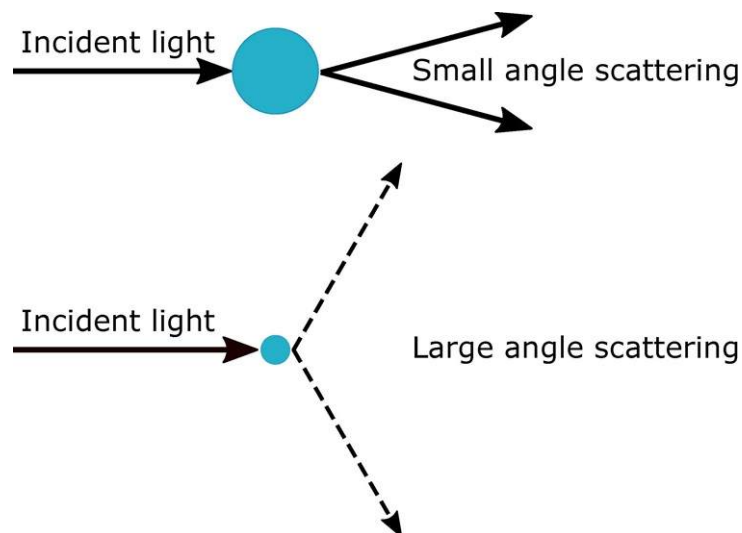


Figure 2.24: Formation of a diffraction angle (source: Malvern).

In addition, the LD technique based on Fraunhofer theory is not valid for particles whose diameter is much larger than the wavelength (λ) of illumination. In general, a He/Ne laser

is used with $\lambda=632.8$ nm (Kissa, 2017) for particle size within the 2-120 μm range. According to the optical properties of sphere-shaped particles, the diameter of these should be at least four times the λ , therefore the accuracy of the instrument based on Fraunhofer theory is questioned severely for dispersion containing a large fraction of particles in the <10 μm range (Sperazza et al., 2004). The particle size range can be broadened if a He-Cd laser is used, which has $\lambda=325.8$ nm, but this would be expensive. For small particles (<10 μm in diameter), a different theory called the Mie theory is applied, which is found to be more accurate than the Fraunhofer theory (Kissa, 2017). Mie theory is not entirely based on the diffraction phenomena, rather it considers Maxwell's equations in the electromagnetic field when the interaction between the particle and laser takes place. One of the disadvantages of Mie theory is that it considers transmission through the particle (Fig. 2.26), therefore it will require extra knowledge on the refractive index of the sample (Eshel et al., 2004).

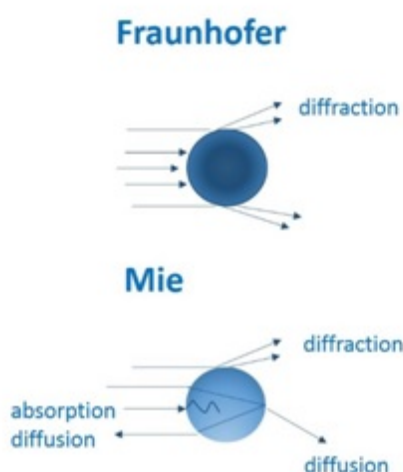


Figure 2.25: Difference between Fraunhofer and Mie theory (Source: <https://www.pharmaceutical-networking.com/laser-diffraction>, accessed on June 21, 2019).

On the other hand, diffraction patterns are affected significantly by the dispersion medium and particle shape. Similar to the classical methods, LD techniques also assume all particles

are spheres (Kissa, 2017). There are real dispersions which contain irregular-shaped particles, and therefore, the differences in the shape of a geometrical particle dimension and the measured equivalent particle diameter must be recognised. There have been attempts to consider non-spherical particles in the laser diffraction method. For example, Gabas et al. (1994) analysed the PSD of non-spherical particles using laser diffraction and concluded that the mean surface area of anisometric particles could not be calculated using this technique. Therefore, obtaining meaningful data regarding the PSD of clay soils is still a challenging task. In addition, at moderate and high particle concentrations, particles do not scatter light independent of each other. Therefore, an accurate calculation of particle size in a certain dispersion is required before starting the PSD task. Furthermore, the surrounding environment has to be considered as well. A delicate device, which is used very carefully inside a laboratory, may not survive at a plant site.

2.6.4 SediGraph Technique

The SediGraph method is also established based on the settling theory (Stokes' law). Therefore, a precise measure of the cumulative size distribution of the sediments in the suspension can be achieved by observing both the particles' settling rate and monitored volume. The latter monitoring involves the rate at which the particles settle below a certain depth in the sedimentation column. Further information has been added in Table 2.7 for better understanding.

The procedure is illustrated in Fig. 2.27. It requires the use of a collimated beam of x-rays which sense the change in the concentration of fine sediments settling in a suspension with time. Compared with the other procedures discussed in the literature, this process does not disturb or create obstacles for particles. The quality of the suspension remains consistent as well. Being an entirely computerised technique, there is minimal chance of operator error or human-made error which is possible with the classical techniques. In addition, the

involvement of the closed sensor-housing chamber, which is mandatory before using an x-ray beam for safety reasons, isolates the soil sample from certain surrounding effects such as temperature fluctuations, physical disturbance from any external source, and contamination, thus increasing the efficacy of the method.

Table 2.7: Summarised information on SediGraph from the Literature.

Particles range	100-0.1 μm
Standard sample amount	$\leq 3 \text{ g}$
Analysis time	Maximum 10 minutes
General cost of equipment	\$60,000 (AUD)
Advantages	i) A quick analysis with no loss of accuracy, ii) Automated operation, iii) Small size of sample required, iv) Isolation from the surrounding influence, v) Adaptability with computerised data processing.
Disadvantages	i) Erroneous results for particles with high absorption rate, ii) Size of hose/pump of the reservoir has to be exactly accurate, iii) Suspension has to be very dilute. iv) A sensitive device requires continuous maintenance.

The device has the capability of generating results within a short period as it functions through an organised downward movement of the sedimentation cell with time and this constantly minimises the depth of the x-ray sensor below the cell surface. Therefore, the effective settling depth decreases with an increase in time. As a consequence, the analysis can be completed within 10 minutes measuring particle size down to 0.1 μm , and the diameter of the soil particles is calculated from Stokes' law. The technique provides accurate data even for a small sample size such as 3g or less.

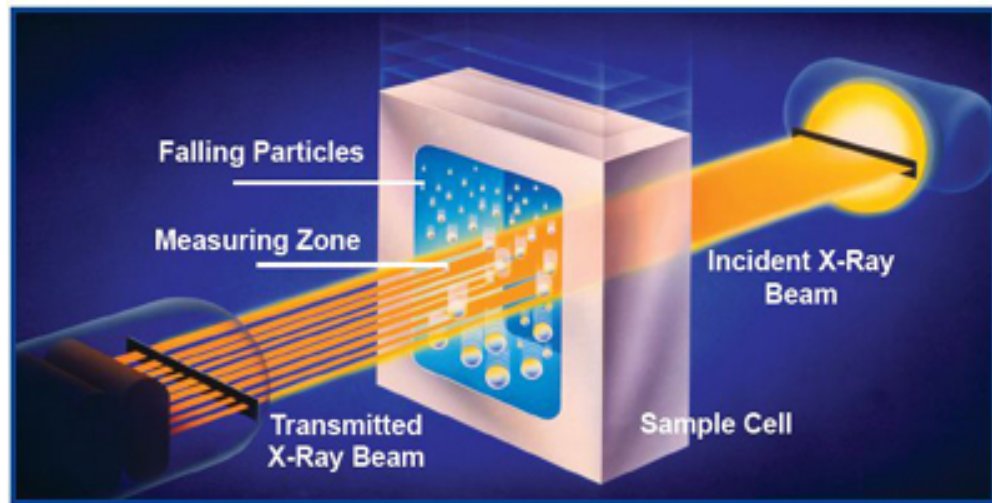


Figure 2.26: SediGraph method to measure PSD (source: Micromeritics).

However, the SediGraph technique faces criticism when it comes to linking absorption effects. The instrument assumes uniform x-ray absorption by all particles in a certain suspension. But in practical life, this is not always the case. Some of the x-rays produced by the primary beam can be absorbed due to inter-atom contacts of different elements in the sample, thus reducing the intensity of the x-ray radiation (Goldstein, 1986; Syvitski, 2007). Samples containing a significant amount of Mg, Fe, and Ti have a very high absorption coefficient. It is possible that particles with a high absorption rate can literally blind the device, and hence the accuracy of the particle analysis will be doubtful (Jones et al., 1988). Moreover, similar to Mie theory of LD, SediGraph may require the operators to know the refractive index (RI) of a particle, but for particle size less than $2\text{ }\mu\text{m}$, RI has to be assumed (Jillavenkatesa et al., 2001). This assumption is made based on the optical properties of the particle and a wrong assumption will lead to a significant error in the measurement.

In addition, the relatively high cost (approximately \$60,000 AUD) is a substantial financial expenditure for all but the larger research laboratories.

2.6.5 Integrated Suspension Pressure Technique

The integral suspension pressure (ISP) method considers the temporal change of suspension pressure determined precisely at a certain depth such as hydrometer or pipette analysis, as shown in Fig.2.28. The pressure integrates the spatially changing particle density in the suspension above a certain depth (Durner et al., 2017). Basic information on the ISP technique could be found in Table 2.8.

Table 2.8: Basic information on the ISP technique

Particles range	630-0.63 μm
Standard sample amount	40 g
Analysis time	30 minutes to 6 hours
General cost	\$1500 (USD)
Advantages	i) Automated analysis, ii) No suspension disturbance, iii) Relatively cheaper than other computer-based devices, iv) Good repeatability (almost 95% accurate), if conducted in 6 hours.
Disadvantages	i) Random or systematic errors lead to severe PSD errors, ii) Experimental results obtained at 30 minutes are mostly erroneous at the beginning, iii) Complicated mathematical formulation, iv) A sensitive device, and requires completely secured surrounding to avoid noise in the system.

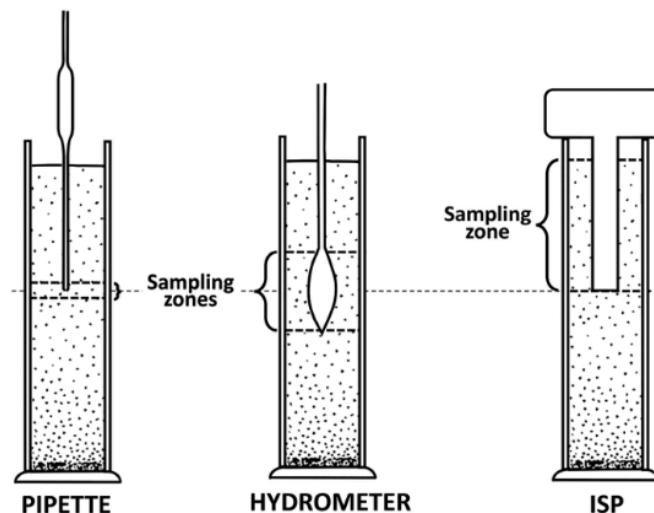


Figure 2.27: Schematic presentation of the PSD measurement domain of ISP compared to pipette and hydrometer (Durner et al., 2017).

The determination of the time scale of the suspension pressure is based on a combination of a mathematics and statistics model, where the PSD of each sample is calculated by fitting the simulated time series of the observed pressure by inverse modelling by global optimisation. Although the technique is also based on the sedimentation theory, the device doesn't create interference in the suspension which occurs with pipette and hydrometer. In addition, since the sensor is fixed at a certain depth and the results are recorded automatically onto a computer, there is no chance of a manual operating error. Considering the automated procedure and easy-to-use software, the device is cheaper compared to other automated equipment such as laser diffraction or SediGraph.

It should be mentioned here that the ISP method is considered to be very sensitive by the inventors themselves who stating that it was not possible for them to obtain complete error-free data for any soil ([Durner et al., 2017](#)). One of the reasons for this can be explained in terms of the surrounding noise which creates systematic or random errors where the latter lead to stochastic errors. Another reason was observed in terms of the duration of the experiment. It is a well-known fact that particle settlement is a quicker process at the beginning after which it slows, therefore fast-forwarding the procedure leads to severe errors in the measurement at the initial stage, as reported by [Durner et al. \(2017\)](#). Therefore, the ISP method requires more or less six hours to completely obtain the PSD curve for a soil sample. In general, automated devices like laser diffraction or SediGraph do not require more than 10 minutes to display the full PSD curves. As a result, the ISP method-based PSD analyser device still falls behind in relation to the duration of the experiment.

2.6.6 Comprehensive Analysis of Current PSD Techniques

Most of the classical methods have been criticised for being unable to provide the PSD of a narrow particle diameter range. For example, sieve analysis is only useful if the soil particle diameters are within the range of 50 μm to 2000 μm (coarse-grained) ([Gee and](#)

[Bauder, 1979](#)). On the other hand, concerns regarding the particles' diameter range can be reduced to some extent by using both the hydrometer and pipette methods as they generally cover from 5 μm -150 μm (fine-grained) ([Allen, 2013](#)). Nevertheless, the ability of these two sedimentation-based techniques has produced inconsistent results for particles smaller than 1 μm due to the existence of Brownian motion and its influence on the rate of sedimentation ([Eshel et al., 2004](#); [Allen, 2013](#)). Furthermore, some researchers were not satisfied with the amount of samples required for PSD analysis based on classical methods. Sieve analysis, for instance, may require 100 g of soil samples based on the size of the sieve. Although the amount is reduced for the hydrometer (20g-30 g) and pipette (10g-20g), sometimes the unavailability of certain soil samples in these amounts creates a perplexing situation for researchers. In addition, sedimentation-based techniques are time-consuming, depending on the particle size range. Conducting standard PSD analysis using a hydrometer may take 24 hrs to finalise. Classical methods also suffer from the disadvantage of creating a possible disruption during the settlement of the particles. It is a well-known fact that pipette and hydrometer techniques require operators to interrupt particle settlement. The pipette technique requires operators to collect a sample after a certain time-scale from a certain depth, however a hydrometer has to be submerged in the suspension freely to record the density readings. Meanwhile, the calibration techniques of these methods are tedious to some extent. For instance, a hydrometer has to be calibrated to find the effective depth, at which the specific gravity is measured ([Arora, 1992](#)). The calibration for the pipette requires a sensitive balance and skills to operate quickly. Therefore, there is a greater likelihood of human error since none of the classical methods are automated or controlled by a computer.

In addition, Stokes' law considers the particle's shape to be a sphere for the ease of measurement, which is one of the major limitations of sedimentation theory. In sieve analysis, the likelihood of a non-spherical solid particle passing through depends on the

sieve size and the time allowed for the operation. Nevertheless, such an orientation exists when particles with the smallest cross-section can easily pass through the sieve's aperture. Exceptions may occur if there are very flat disk-shaped particles in the sample. Therefore, that specific soil particle will be retained by the sieve. In the sedimentation-based technique, a settling non-spherical particle is considered to have the most stable position when it has the maximum cross-sectional area orthogonal to the direction of the fluid motion ([Eshel et al., 2004](#)). This stable position is the factor behind the augmented particle drag force, which in return, decreases the settling velocity. Therefore, the PSD analysis is mostly overestimated. As a result, when using sedimentation-based techniques, PSD analysis contains discrepancies in the results generated by modern equipment.

To solve most of the drawbacks of the sedimentation-based techniques, SediGraph has gained popularity recently as it is able to produce a PSD curve in just 10 minutes. The procedure takes Stokes' law into account, therefore the limitation regarding the particle shape remains, but the other disadvantages of the classical methods can be avoided. Although the whole procedure is automated, it still requires skilled operators to conduct the analysis. Prior to this, the calibration technique of SediGraph is considered to be complicated and time-consuming ([Allen, 2013](#)). Furthermore, a delicate device that is worth \$60,000 (AUD) also needs extra attention in terms of maintenance, whereas the whole hydrometer or pipette setup may cost only \$50-\$100 (AUD) and sieves are even cheaper. To summarise, SediGraph is able to solve the disadvantages of the classical methods regarding particle diameter range, time constraints, precision of the results, reproducibility, the required amount of samples, but it increases the cost of maintenance, sensitivity, and most importantly the calibration technique remains a lengthy part of the experimental program.

The introduction of LD in PSD analysis solves most of the problems from the past. Built on the concept of the diffraction of lights, the LD device is able to cover a wide range of particle diameters between 0.04 μm -8000 μm (Pye and Blott, 2004; Ryzak and Magdalena, 2011), which is better than the hydrometer, pipette or SediGraph. LD is also able to complete the analysis within 10 minutes, utilising only 1g-5g of soil samples. The device is credited to have excellent repeatability in terms of both natural and laboratory-based soil samples. Nevertheless, the device prefers dry samples, and hence the use of a dispersing agent can be avoided. In most cases, calibration is not required if a soil sample has particles within the preferred range. Therefore, it possesses a significant advantage over the SediGraph technique. However, it was found in the literature that the laser diffraction approach underestimates the PSD values of soils particularly in clay fraction (Konert and Vandenberghe, 1997; Taubner et al., 2009). It was observed that a pipette fraction $<2 \mu\text{m}$ corresponds to $<8 \mu\text{m}$ for laser diffraction, which is one of the major technical disadvantages of the LD method. In addition, the LD device is also one of the most expensive in the current market, being worth \$120,000 (AUD) based on functionality and versatility. As a consequence, purchasing LD equipment is a substantial financial expenditure for all but the larger research laboratories.

It is evident from the current research that there are multiple alternatives available to any application. The ISP method is one of the alternatives to LD or SediGraph, which surprisingly reduces the expenditure to only \$1500 (AUD) including the commercial software for data logging purposes. Introduced by Durner et al. (2007), the ISP method considers the chronological change in pressure measured with precise accuracy at a certain depth in the soil-water suspension to find the PSD. Although the device is considered to be user-friendly, the analysis time is a concern (6hrs-8hrs), which is again the problem researchers wanted to avoid in the past regarding the classical methods. Furthermore, the principle of the device is highly statistical, and the inventors reported the existence of

stochastic errors in the mathematical analysis. A comprehensive comparison of the aforementioned techniques is presented in **Table 2.9**.

Based on the brief discussion above, it is clear that both classical and modern techniques have advantages and disadvantages to some extent. It is highly unlikely that an automated and human-operated manual device will provide identical results for a specific soil sample. Therefore, no technique serves as a universal yardstick because of the existence of inherent flaws. The choice of instrument or technique depends on the specification and budget available.

Table 2.9: Comprehensive comparisons of the different techniques to find the PSD of soils

Methods	Particles range (µm)	Samples required (g)	Analysis time	Remark on calibration process	Reproducibility	Cost (AUD)
1. Sieve analysis	50-2000	100	10 mins-3 hrs	N/A	Low	\$20-\$50
2. Hydrometer/pipette	5-150	10g-20g (pipette), 20g-30g (hydrometer)	2 hrs-24 hrs (pipette) 24 hrs (hydrometer)	Tedious and lengthy	Low	\$50-\$100
3. SediGraph	0.1-250	1g-5g	5 mins-10 mins	Lengthy and complicated	High	\$60,000
4. Laser Diffraction	0.04-8000	1g-5g	5 mins-10 mins	Not needed if the particle diameter is within the range	Very high	\$120,000
5. ISP	3-300	40g	30 mins-6hrs	Complicated and error-prone	Moderate	\$1500

2.7 Discussion on the Available Liquid Limit Test Methods

2.7.1. Casagrande method

The Casagrande method is widely used in geotechnical industries to determine the liquid limit (LL) of soils. The most challenging part is to predict the water content at which 25 blows will accomplish the task. Therefore, the test is conducted using a different number of blows ranging from 10 to 40. Water is added to the sample randomly as it is not feasible to add the targeted water content. At each step, more water is added, therefore it is expected that the water content reading will be larger than the previous reading.

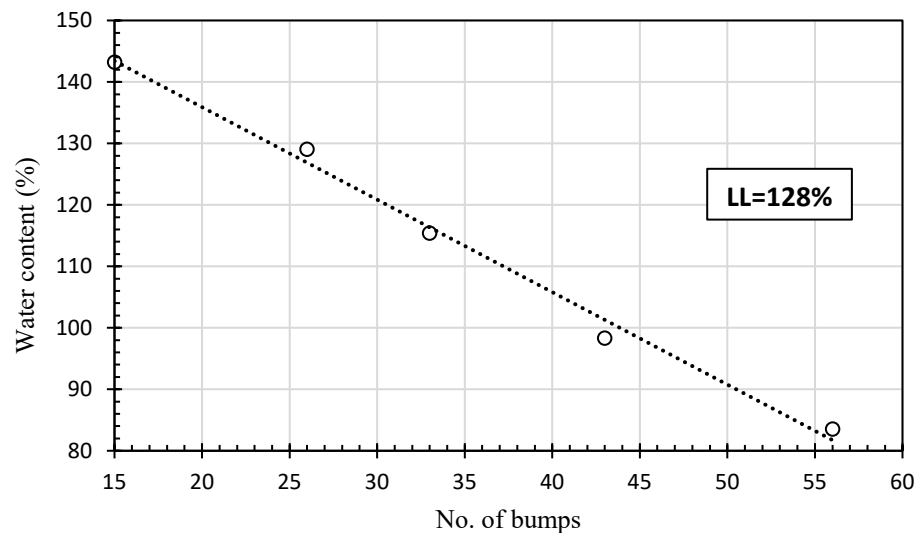


Figure 2.28: Finding the liquid limit of a specific soil using the Casagrande method.

Once 4-5 readings have been recorded, a plot known as a flow curve is generated with the water content shown on the vertical axis and the blow numbers shown on the horizontal axis. A line is drawn which connects all the points and the LL is determined from the curve corresponding to 25 blows (Fig.2.29). Due to the continuous rapping in the Casagrande device, the sample faces small shear stresses. It is reported that a soil sample can withstand

these stresses if induced in 25 blows (Arora, 2008). The accuracy of this concept is, however, not welcomed by everyone.

2.7.2. Cone penetration method

The cone test originated in Scandinavia to determine the strength of remoulded cohesive soils and later became a technique to predict the LL of soils (Koumoto and Houlsby, 2001). However, the standard cone penetration test was first developed in France by the Laboratoire Central des Ponts et Chaussees in 1966, as described by Sherwood et al. (1970).

The flow curve is plotted with water content shown on the horizontal axis and penetration (mm) shown on the vertical axis. The LL is specified at a penetration of 20 mm, as illustrated in Fig. 2.30. The cone penetration method has also received severe criticism such as a longer time-scale to complete the task for one sample, inaccurate and inconsistent results for soils with low plasticity, and so on, which is discussed in the following section.

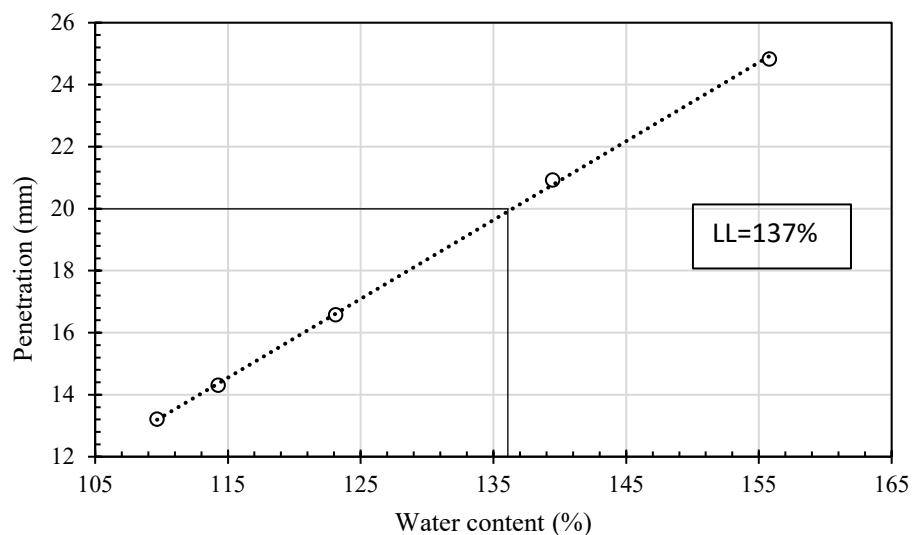


Figure 2.29: Finding W_c^{LL} of a specific soil using the cone penetration technique.

2.7.3. Limitations and drawbacks of the existing methods

Although the Casagrande and cone penetration methods are preferred by different researchers, none fully satisfy the standard requirements based on accuracy, repeatability, and suitability. The Casagrande device, for example, has been criticised for failing to produce identical results for similar soil samples (Haigh, 2012). In fact, Casagrande (1958) himself postulated that his proposed method was established on the fact that the LL test was actually a dynamic shear test. The statement highlights the major drawback of the Casagrande technique, this being that it does not provide a clear insight into determining the LL of fine-grained soils such as kaolin or bentonite, which exhibit different reactions when they are subjected to a different number of blows. In addition, researchers have reported the difficulties they faced while cutting the groove in some sandy soils. In other cases, some of the soils with low LL were reported to slide into the cup or became further liquefied with blows instead of flowing as plastic (Sherwood et al., 1970). The Casagrande cup and test method has undergone significant changes since it was proposed in 1932, such as changes to the type of base or resilience of the cup. Casagrande (1958) also found that the flexibility or type of base influences the LL values. Further research was carried out by Norman (1958) to test the impact of the base on the LL. His experiments were conducted in two stages, one with the soft base and the other with the hard base. The findings show there is approximately a 7% difference in LLs when the base was changed from soft to hard. On the other hand, the durability of the Casagrande cup sometimes varied based on the geographic locations (Powell et al., 2015) and therefore could also affect the LLs of identical samples. Several literature reviews criticise the Casagrande technique for being a time-consuming method without a procedure to speed up the progress (Sowers et al., 1960; Hanks, 1981).

The cone penetration method, on the other hand, is able to solve most of the drawbacks of the Casagrande method. The cone test is easier to conduct and the accuracy of its results

has been proved in the literature. However, the issue of soils being liquefied has not been completely overcome by the cone technique (Sherwood et al., 1970). In terms of repeatability, cone penetration was reported to have errors of around 0.7%, whereas this is around 1%-3% for the Casagrande method (Sherwood et al., 1970).

Many researchers have tried to explain why the Casagrande and cone methods do not produce identical LL values for the same sample (Budhu, 1985; Sivapullaiah and Sridharan, 1985; Wasti and Bezirci, 1986). For instance, the cone penetration method often produces a higher LL value than the Casagrande method if the soil has low plasticity. On the other hand, Casagrande has been criticised for overestimating the LL values if any soil has a high LL (Mishra et al., 2011). This difference could be attributed to the impact of the clay content in the soil sample, where the deformation of clay is not the same in both devices (Budhu, 1985). In addition, the shear strength of any soil at LL consists of two types of shear resistance namely, viscous and frictional. Therefore, it is not possible for a device to determine both types simultaneously (Mishra et al., 2011). Based on this conceptual understanding, LL by the Casagrande method is focused primarily on the predominant viscous shear resistance (number of blows), whereas the cone is based mainly on frictional shear resistance. As a result, it is clear that Casagrande is better suited to soils that have high LLs, and the cone method is better suited to soils that have lower LLs (Sridharan and Prakash, 2000).

2.8 Methods of Predicting Soil Plastic Limit

The characterisation or prediction of soil plastic limit is mostly operator-dependent, hence the inconsistency in the results for identical samples. The Atterberg method is widely used in the geotechnical field to determine the plastic limit of soils, however there are alternative methods such as Pfefferkorn, stress/strain curves, and indentation measurements (Van der

Velden, 1979; Bekker, 1981; Ribeiro et al., 2005; Vaillant, 2008; Sharma and Sridharan, 2018).

In general, the Atterberg and Pfefferkorn techniques are based on determining water content at which the soil sample exhibits some randomly defined uniformity. The higher the water content, the higher the plasticity and vice versa. On the other hand, stress/strain curves and indentation measurements evaluate the relationship between the applied force and the resulting deformation (Andrade et al., 2011). However, these methods are comparatively expensive and may require expert operators.

2.8.1 Atterberg Method (Thread Rolling)

Calculating the plastic limit using the Atterberg method has been criticised in the field of geotechnics. Although the method has been considered “unscientific”, this is one of the most commonly used methods to determine the plastic limit. According to Atterberg, there is a unique amount of water at which a clay specimen will be easily mouldable or rolled like a thread (Fig. 2.31). With lower water content, the soil body will crack. The Atterberg method determines the plastic limit at the lowest water content at which the soil specimen can be rolled into threads without any cracking or breaking (Bergaya et al., 2006, Haigh et al., 2013; Barnes, 2013; Shimobe and Spagnoli, 2019).

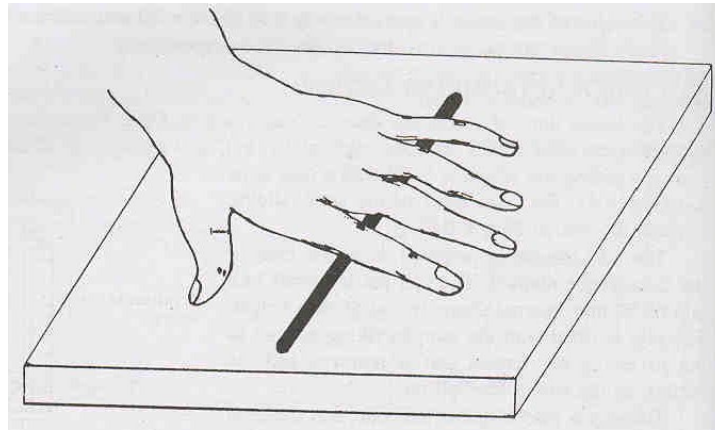


Figure 2.30: Atterberg's thread rolling test to determine the plastic limit (Arora, 2008).

However, Wintermeyer (1926) and Terzaghi (1926) separately modified the Atterberg test to measure soil plasticity, which is now defined as BS 1377-2:1990. They argued that thread rolling should be continued until the thread itself shears both longitudinally and transversely up to 3mm in diameter, as gauged by a standard rod with known thickness. While rolling the thread, it is advised not to gather the broken pieces together after they have crumbled to reform a thread and continue rolling, since the first crumbling point is the corresponding soil's plastic limit. It should be mentioned here that even though Casagrande (1932) supported the 3 mm diameter of the thread rolling test, there was no precise evidence to support the claim. In fact, Prakash et al. (2009) reported that there is no mathematically or statistically proven theory to support the relation between the varying moisture content with the thread diameter at the breakdown stage.

2.8.2 Pfefferkorn Technique

This method finds the amount of water needed to obtain a 30% contraction in relation to the initial height of a tested specimen under the action of a standard mass (Pfefferkorn, 1924; Modesto and Bernardin, 2008; Andrade et al., 2011).

Using the Pfefferkom technique to determine the plastic limit is dependent on the concept of impact deformation and a sample apparatus setup is shown in Fig. 2.32. For experimental purposes, the soil sample is reconstituted with a diameter of 33 mm and an initial height of 40 mm. The height can be adjusted by extrusion or manual compression using a free-falling metal plate with a mass of 1.192 kg (Modesto and Bernardin, 2008; Andrade et al., 2011). The initial height adjustment is related to the impact deformation height and the ratio of these two heights yields a deformation ratio. At multifarious water content, the deformation ratio is plotted (Fig. 2.33). The steeper the curve, the more intensely the soil reacts to water content variations.



Figure 2.31: Pfefferkorn apparatus (Andrade et al., 2011).

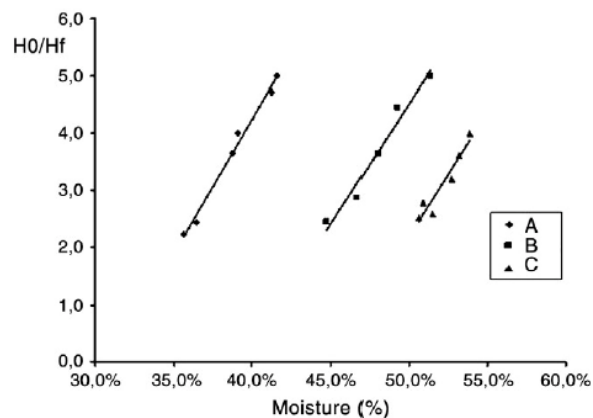


Figure 2.32: Sample examples of deformation ratio (H_0/H_f) as a function of moisture content (Andrade et al., 2011).

2.8.3 Penetration and Indentation Method For Plastic Limit

The fall cone penetration method is similar to the test to determine soil liquid limit, as discussed in [section 2.7.2](#). The plastic limit is determined by the same cone, but for the liquid limit, the amount of soil was roughly between 80g to 85g, whereas at least 240g of soil specimen is required to determine the plastic limit by cone penetration ([Campbell, 1976](#); [Harison, 1988](#); [Feng, 2000](#); [Sharma and Sridharan, 2018](#)).

[Modesto and Bernardini \(2008\)](#) used indentation equipment to show that as penetration occurs, cracks surrounding the penetration indicate a lack of plasticity or low water content. The threshold value corresponds to the soil plastic limit. Adequate plasticity implies that there should not be any crack or inconsistency in the soil texture, as shown in [Fig. 2.34](#).

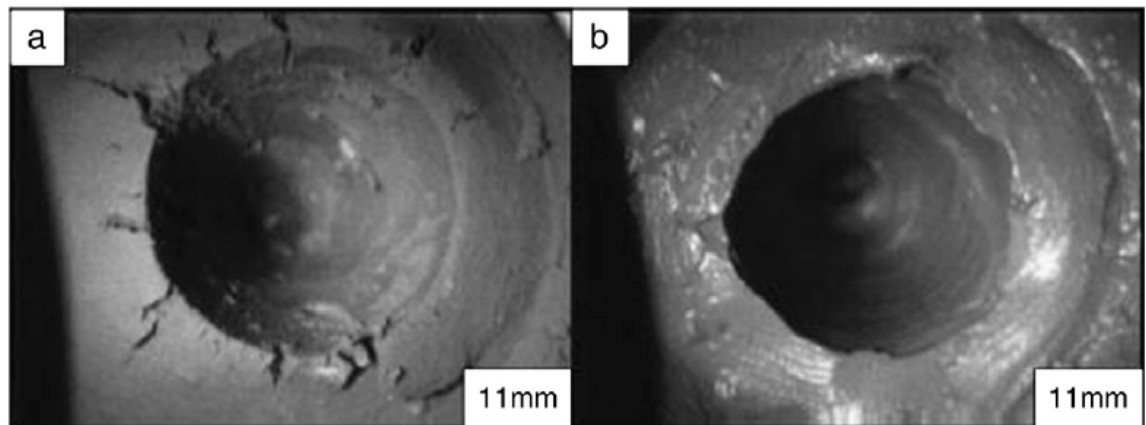


Figure 2.33: Clay indentation illustrating (a) lack of plasticity, and (b) excessive water ([Modesto and Bernardini, 2008](#)).

2.8.4 Pros and Cons of Available Plastic Limit Methods

As previously discussed, the Atterberg method is comparatively cost-efficient and easier to perform, however the calculation of plasticity may not be accurate for organic or marine soils ([Andrade et al., 2011](#)). Due to the fact that the one-point method requires the operator

to judge the plastic limit, it may not be a suitable method for inexperienced users. Furthermore, as the specimen has to be homogeneously mixed with water, it requires careful attention to avoid erroneous results. Another source of error could be an incorrect final thread diameter or stopping the rolling procedure earlier than expected. The premature breakdown of soil was explained by [Schofield and Wroth \(1968\)](#), who showed that tensile failure could be the primary reason behind this since the mechanical processes while rolling the thread are not mathematically understood. Therefore, discrepancies in the plasticity of the identical sample may exist depending on the operator's judgement. [Sherwood \(1970\)](#) found that the results of tests conducted by 45 independent UK soil-testing labs differed by around 3% for the plastic limit measurement of identical soil samples.

The Pfefferkorn method avoids the need to conduct the tedious thread rolling task, however, as discussed in the literature, the Pfefferkorn method is not appropriate for stiffer soil specimens ([Andrade et al., 2011](#)). In addition, similar to the thread rolling test, the Pfefferkorn technique is also time-consuming since it requires the operator to continuously add small amounts of water concurrently until a contraction of 30% has been reached. As a result, the reproducibility of the results may not be easily attained, as reported in the literature ([Andrade et al., 2011](#)).

The penetration tool was found to be more precise in terms of repeatability and less operator-dependent ([Domenech et al., 1994](#); [Feng, 2004](#)). However, [Benbow and Bridgwater \(1993\)](#) focused on bridging the gap between the accuracy of the plastic limit and the depth of penetration by saying that if penetration is comparatively smaller, the results will not always be precise. If the sample is predominantly viscous rather than plastic, the time of penetration will determine the penetration of the sample. Moreover, the small force due to the deceleration of the cone is never taken into account in the penetration tool, which might alter the soil texture to some extent ([Haigh et al., 2013](#)).

2.9 Concluding Remarks

After the thorough discussion in the literature concerning the existing electrical conductivity/resistivity models of saturated soils and the applications of electrical conductivity in geotechnical engineering, the following crucial points should be mentioned:

2.9.1 Soil Electrical Conductivity Models

- Most of the relevant electrical conductivity/resistivity models consider only connections between water, solids, and sometimes diffuse double layer of soils ([Mojid et al., 2007](#)). In these models, a solid is considered to be non-conductive and the electrical conductivity through the water was the only pathway for the electrical current flow. The possibility of combining a solid with DDL to form an equivalent conductive material was not considered in any of the existing literature.
- Apart from the work of [Abu Hassanein et al. \(1996\)](#), none of the models considers the effect of clay fabric on electrical conductivity. Therefore, further improvement is required to connect the missing dots.
- Most of the soil conductivity models have empirical parameters which do not have any physical meaning. In addition, some of the models attempt to establish a connection with Archie's power-law equation. However, there is no consistent discussion on the impact of Archie's elusive parameters on soil conductivity.

2.9.2 Conventional PSD Techniques

- Conventional methods (hydrometer, pipette, sieve) of determining the PSD of soils are cheaper and easier to operate, but they are time-consuming and operator-related errors are likely to occur. In addition, the repeatability of these methods has been questioned for the same reason.

- Modern devices (laser diffraction, SediGraph, ISP) are generally quicker than conventional ones but these delicate devices are very expensive and are not suitable for inexperienced operators. Although all of these tools are run by computerised programs, operators must input the required settings for flawless operation. In addition, since laser and SediGraph are based on the optical properties of soil particles, civil and geotechnical engineers require some basic knowledge in this field, should any discrepancy arise or if the results require analysis.

2.9.3 Liquid Limit Methods

- The most commonly used Casagrande or cone penetration methods display inconsistent results for identical samples, particularly at higher liquid limits. Although it is unlikely that natural soils will have a liquid limit higher than 100%, none of these techniques have been reported to be reliable for all types of soils.
- Both techniques are mostly operator-based, therefore, a small error in the homogeneity of soils will lead to erroneous results. Mixing the soil with water, which is a tedious job, requires quick judgement to avoid moisture loss during the test.
- None of the aforementioned techniques can be finished in a day. The sample has to be kept inside the drying oven for at least 24 hours. Therefore, researchers have to wait 24 hours before finalising the test.

2.9.4 Plastic Limit Measurements

- The thread rolling tests are considered to be non-scientific and are entirely dependent on the operator's call. In addition, the technique is also time-consuming and has been criticised for being a less efficient method.

- The inclusion of any device, rather than thread rolling by hand, will not necessarily solve the inaccuracy in determining the plastic limit. For example, the cone is widely used for both liquid limit and plastic limit measurements, however the penetration of each soil will not be the same, and as discussed in the literature, soils with smaller penetration are not suitable for the cone test.
- Alternative tests like Pfefferkorn or soil compression require further validation to improve their suitability for all types of soils. Thread rolling is still the most used technique due to the ability to produce a result for all types of soils, whereas the other techniques have some restrictions as far as the classification of the soils is concerned.

Chapter 3

Experimental Tools and Materials

3.1 Introduction

In this study, the electrical properties of soil ingredients at different temperatures were experimentally measured. Then, a new clay electrical conductivity model for fully saturated fine-grained clays was proposed and validated experimentally. The experimental validation program includes reconstituting different types of soil specimens at different dry densities, degree of saturation, and pore water salinity levels. After this, new electrical testing methods were proposed in this study to determine the particle size distribution and consistency limits of fine-grained soils. Therefore, this chapter includes basic properties on the tested soil materials, followed by a discussion of the experimental equipment.

3.2 Tested Soils

Although this study contains experimental results using different types of soils, only kaolin and bentonite were consistently used in all the applications. The other soils played different roles based on the requirements and purpose of the tests. Therefore, in the following section, only the properties of kaolin and bentonite are discussed.

3.2.1 Kaolin

The laboratory-based kaolin used in this research is chemically known as hydrous aluminium silicate, purchased from BASF Australia. In general, this type of kaolin is chemically inert and highly pulverised for better dispersion. The relevant geotechnical properties are listed in [Table 3.1](#), followed by the composition of kaolin in [Table 3.2](#). Distinctive information is available on the tested kaolin, provided by the manufacturer, as

listed in Table 3.3. The particle size distribution obtained by laser diffraction (Taubner et al., 2009) is shown in Fig.3.1.

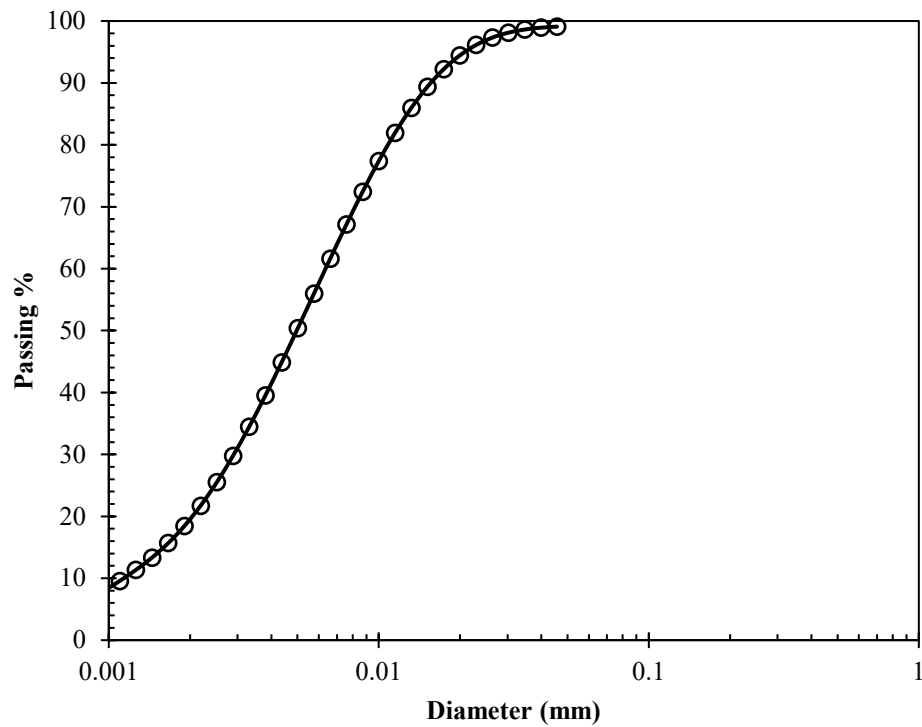


Figure 3.34: Particle size distribution of tested kaolin.

Table 3.10: Properties of tested kaolin.

Properties	Values
Liquid limit (%)	74
Plastic limit (%)	32
G_s	2.58
Cation exchange capacity (meq/100g)	0.075
Total surface area (m^2/g)	20
Surface charge density ($\mu C/m^2$)	0.36
Optimum moisture content (%)	29

Table 3.11: Composition of kaolin.

Composition of Kaolin	Weight%
SiO ₂	45.2
Al ₂ O ₃	38.8
NaO ₂	0.05-0.3
TiO ₂	0.6-1.7
CaO	0.02

Table 3.12: Miscellaneous information on kaolin provided by the manufacturer.

Form	Powder
Special Modification	None
Brightness (%)	87
pH	7
Oil Absorption	40

3.2.2 Bentonite

Bentonite is an expansive soil with low permeability, high plasticity and swelling potential. These attributes make this type of soil well-suited to be used as a buffer and sealing material as the clay liner as well as the cover of landfill.

Sodium bentonite from Sibelco's Trugel 100 was used in different experiments in this study. The clay contains a large ratio of active minerals such as montmorillonite, as presented in [Table 3.4](#), followed by the composition of bentonite in [Table 3.5](#), and suspension properties in [Table 3.6](#). The particle size distribution was obtained from the laser diffraction method ([Taubner et al., 2009](#)), as shown in [Fig.3.2](#).

Table 3.13: General properties of bentonite, provided by supplier.

Properties	Values
Natural Moisture Content (%)	10
Liquid limit (%)	504
Plastic limit (%)	53
G_s	2.68
Cation exchange capacity (meq/100g)	80
Total surface area (m^2/g)	750
Surface charge density ($\mu C/m^2$)	10.24
Optimum moisture content (%)	23
Swelling Index (ml/2g)	32

Table 3.14: Composition of bentonite, as provided by supplier.

Composition of Bentonite	Weight %
SiO_2	63.8
Al_2O_3	13.6
TiO_2	0.3
Fe_2O_3	2.8
CaO	0.2
Na_2O	2.3
MgO	2.0
K_2O	0.2

Table 3.15: Typical suspension properties of tested bentonite provided by the supplier.

Suspension Properties (kg/m^3)	40	50	60
Form	Powder		
Apparent viscosity (cP)	12	17	23
Plastic Viscosity (cP)	7	9	12
Yield Point (lb/100ft ²)	5	8	11
Gel - 10 sec (lb/100ft ²)	2	4	6
Gel - 10 min (lb/100ft ²)	4	8	12
Marsh Funnel (sec/l)	37	43	60
pH	9.5	9.5	9.5

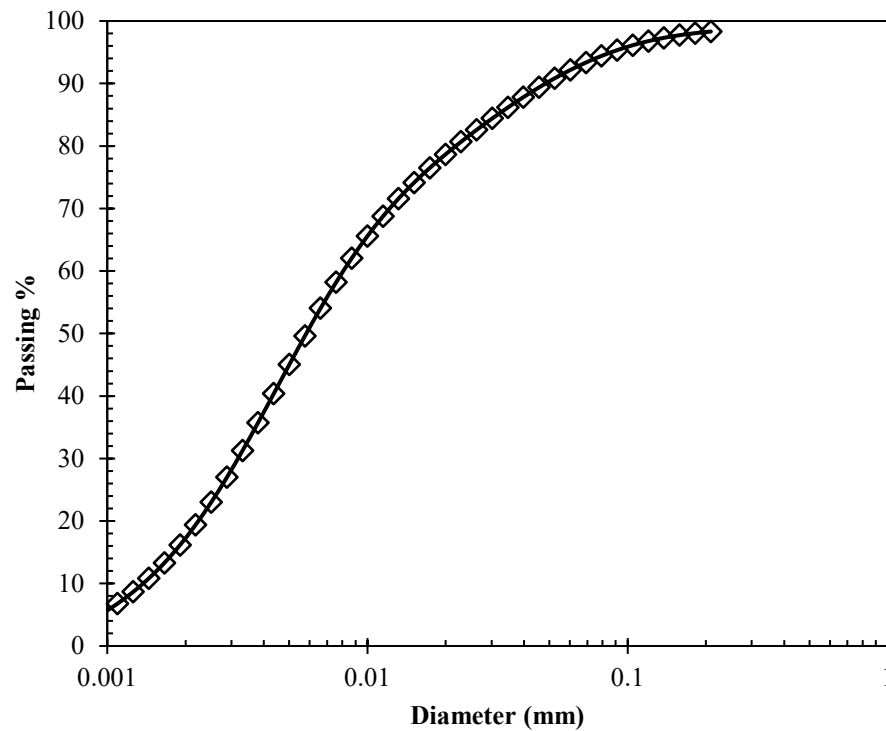


Figure 35: Particle size distribution of bentonite considered in this study.

3.2.3 Natural Soils

Most of the natural soils were utilised to assess the suitability and accuracy of the newly-proposed techniques to determine particle size distribution, liquid limit, and plastic limit, introduced in this study. Information on the used natural soils has been included in the relevant chapters since these soils were not used in all the experiments. Most of the basic properties of natural soils were collected from the supplier. However, some of the electrical properties of these soils were determined from the approach introduced in this study ([Chapter 4](#) and [Chapter 5](#)).

3.3 Experimental Devices and Apparatus

3.3.1 Electrical Conductivity Meter

In order to develop an electrical conductivity model of saturated soils, it is essential to find the electrical conductivity of soil-water suspension. This experiment was carried out using an electrical conductivity meter (Horiba Scientific LAQUA-PC1100), as shown in Fig.3.3.

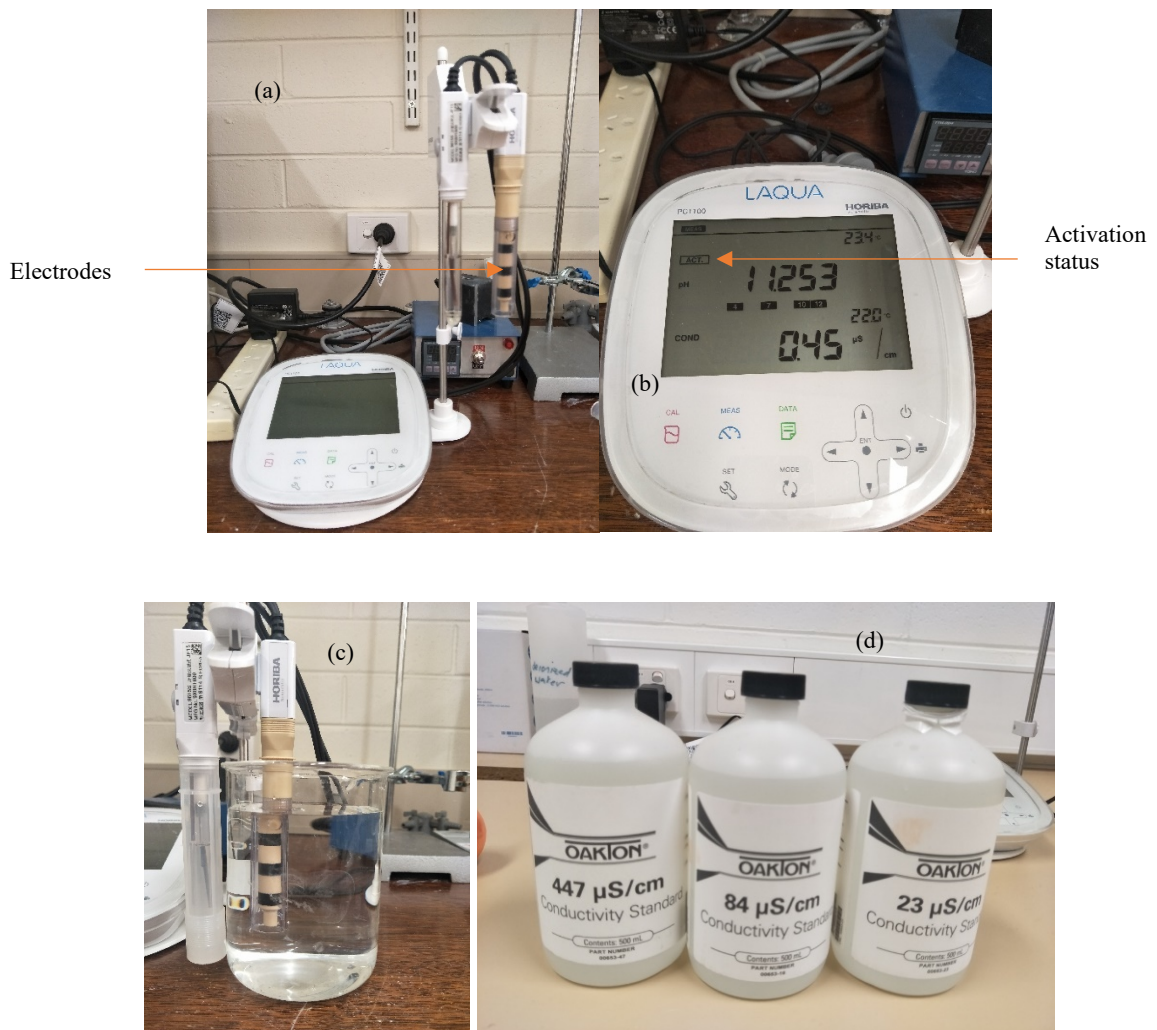


Figure 36: Electrical conductivity meter used to measure soil-water suspension conductivity: a) complete set up of the device, b) brief information on meter display, c) a sample experiment process, and d) solutions with known EC values for the calibration purpose.

The unit consists of one display unit with function keys for calibration, measurement, and settings. The device is connected to two different probes to determine pH and electrical conductivity, as shown in Fig.3.3a. Before each operation, probes should be washed

carefully with de-ionised water, without touching the probes. Next, the probes are wiped smoothly with filter paper or tissues. Before starting the test, the respective probe has to be activated and “ACT” should be displayed on top of the respective function, as shown in [Fig.3.3b](#) (pH probe is activated). Once the probe is activated, it is immersed inside a glass beaker to measure the electrical conductivity/pH of the liquid at a specific temperature displayed at the right corner of each respective operation. For the conductivity measurement, three black electrodes must be submerged together, leaving no electrode outside the liquid in order to obtain a precise measurement, as shown in [Fig.3.3c](#). The device provides the average electrical conductivity (EC) measurement coming from each electrode at a different distance. The pH probe doesn't have any special instructions; however, the probe has to be submerged at least 3 cm into the solution from the tip. Each probe is also able to provide the temperature of the solution, and therefore careful attention must be paid to the temperature exhibited by the active probe only.

However, before the commencement of any test, the device is calibrated (CAL tab) at standard room temperature with three different conductive solutions with known EC and pH, as shown in [Fig.3.3d](#).

3.3.1 Soil Resistivity Meter (Wenner Method)

The soil resistivity (SR) meter used in this research considers the Wenner four-electrode method ([Wenner, 1915](#); [Sangray and Mitchell, 1976](#)), as shown in [Fig. 3.4](#). For this purpose, a modified plastic cap containing four copper electrodes (two outer and two inner electrodes, each 0.8 mm in diameter) was used, as shown in [Fig. 3.4b](#). As per the configuration, the electrical current flows through the two outer electrodes and the voltage drop is monitored by the inner electrodes. It has been reported in the literature that a four-terminal pair configuration deals with perturbation better than a two-electrode method, as

the former is capable of reducing electrical interference and electrode polarisation (Wenner, 1915).

To measure soil resistivity, the plastic probe has to be placed through the soil specimen. The specimen has to be placed inside a plastic or glass or any non-conductive container to ensure consistency in the reading. Once the set up is ready, the “push test” button is pressed and the reading is taken after 3 seconds. If the device shows an error or 1, the range of the resistor has to be adjusted by tuning the black regulator, as shown in Fig.3.4c. If the resistance range is higher than 1, the value has to be included in the calculation. Each test has to be repeated at least three times and the average should be recorded. The display provides the reading, which is also shown in Fig.3.4d. Later, electrical resistivity is calculated by utilising the same equation. The conversion formulae are also available on the device, as seen in Fig.3.4e.

The Wenner four-electrode method provides an average ER of a hemisphere of space within the test specimen where the radius of the hemisphere space is approximately proportional to the electrode spacing and the term $2\pi a$ is a geometric factor defined based on a semi-infinite boundary condition (half space). The impact of geometric factors is decisive to confirm the precise measurement of ER. To calibrate the experimental setup used in this study, the test cell was filled at different heights with two reference salt concentrated water solutions of known ER. A similar approach has previously been used by several researchers (Wenner, 1915; Al Rashid et al., 2018).



Figure 37: Soil resistivity meter and its specifications: a) complete set up, b) four pins representing four electrodes, c) range selector for resistance, d) a sample experiment, and e) information on the formulae for the conversion purpose.

3.3.2 Heat-Based Distilled Water Maker

Distilled water is prepared by the heat-based distilled water maker, as shown in Fig.3.5.

The device is connected to a nearby tap, from where the water goes into the reservoir. The black tube at the right supplies the distilled water, which is collected in a glass beaker. A safe distance should be maintained between the user and the unit since the device works with a heating system. The collection beaker shouldn't be touched without heat-protective thick gloves (latex gloves should not be worn). In addition, it is also mandatory that no parts of the unit are touched or dismantled while an operation is being performed.

Distilled water is used exclusively in almost all the major experiments of this study. For example, distilled water is required for the free swelling test described in [Chapter 4](#). In the experiments described in [Chapter 5](#), distilled water is prepared first and allowed one day to cool down. Once the temperature reaches 25⁰C, different amounts of NaCl are mixed to form different salt concentrations in the water to vary water salinity as well as the electrical conductivity of the water. A similar approach is followed to prepare the particle size distribution's soil-water homogeneous suspension, described in [Chapter 6](#). The conventional liquid limit and plastic limit have always necessitated the use of distilled water at room temperature, as well as the newly introduced approach ([Chapter 7](#)).



Figure 38: Heat-based distilled water maker.

3.3.3 Soil-water Suspension Mixer

The MATEST suspension mixer is used extensively in this study mostly to make the homogeneous suspension described in [Chapter 5](#) or the suspension for particle size distribution detailed in [Chapter 6](#). The unit has a rotary blade that spins through the suspension to ensure homogeneity, as shown in [Fig.3.6](#). The standard container is made of

aluminium and has to be adjusted and aligned properly with the black holder (Fig.3.6a), otherwise the blade won't rotate despite pressing the start button. The time-scale to mix the suspension with the mixer depends on the amount of sample present in the water, however, before re-using the unit for another sample, the metal rod and blades are washed with de-ionised water to avoid contamination. One sample of mixing is demonstrated in Fig.3.6b for a clear view.



Figure 39: Soil-water suspension mixer used in this study: a) information on the parts of the device, and b) a sample mixing process ongoing.

3.3.4 Automatic Mortar Mixer

In order to mix soil specimens at a targeted water content in the soil electrical conductivity tests, the automatic mortar mixer is utilised. The device comprises a lightweight aluminium construction and comes with a stainless steel/plastic stirrer and a mixing bowl, as shown in Fig.3.7. Once the soil is completely mixed with water, the soil specimens are transferred to a sealed plastic bag for moisture equilibrium.



Figure 40: Automatic mortar mixer used in this study to mix dry soil samples at different moisture contents.

3.3.5 Standard Proctor

The standard proctor compaction test ([ASTM D698](#); [AS 1289.5.1.1:2017](#)) is used to reconstitute soil specimens at a targeted water content in a standard compaction mould using standard compaction energy. The mould's diameter is 4 inches and a 2.7 kg hammer is used for compacting clays in 3 separate layers ([Fig.3.8](#)). In addition, the compaction energy is approximately 591.3 kN-m/m^3 for 25 blows per layer.



Figure 41: Sample diagram of the standard proctor compaction test for soils.

3.3.6 Optimised Temperature Controlling Water Bath

The temperature controlling water bath from Thermo Scientific ([Fig.3.9a](#)) is used for the free swelling test of soils at different temperatures ranging from 15°C to 35°C ([Chapter 4](#)). The water bath has a reservoir inside where the beaker or container with soil-water suspension is placed, as shown in [Fig.3.9b](#). The power touchscreen works both as the display unit as well as the operation indicator. Once the container or beaker is placed inside the water bath, the top lid is closed and the targeted temperature is entered ([Fig.3.9c](#)). Since the inner temperature varies, it takes a while to reach the desired temperature. However, after the device confirms the inside temperature, a further assessment is conducted to check the consistency of the temperature of the beaker's fluid as well, where the free swelling of soils takes place.



Figure 3.42: The optimised temperature controlling water bath used in this study: a) front set up of the device before starting the experiment, b) beakers are merged into the water to reach the targeted temperature, and c) display of keypad to enter the desired temperature input.

3.3.7 Hydrometer

A hydrometer comprises a bulb and a graduate stem. It is designed with sloping sides which are able to decrease the settling of the particles on the hydrometer. The hydrometer is left in the suspension for a while so the density reading can be taken. After the reading is recorded, the hydrometer is withdrawn from the suspension and inserted later to take the next reading.

In order to determine the particle size distribution, the hydrometer needs to be inserted into the suspension when the density needs to be recorded. Once the density is recorded at a specific time, the hydrometer is later submerged into another 1000 ml cylindrical beaker filled with distilled water, as shown in [Fig.3.10](#).

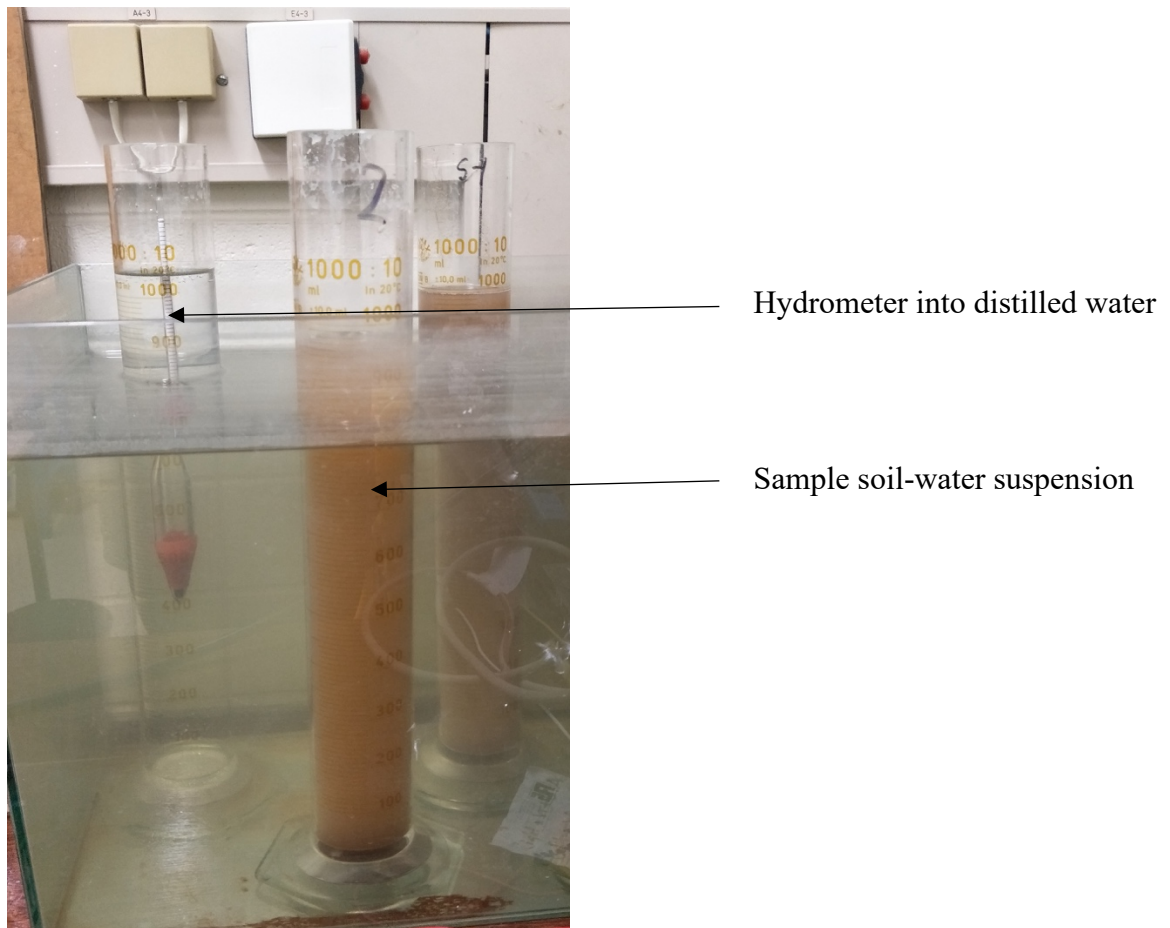


Figure 3.43: Hydrometer used to determine the particle size distribution of soil (AS 1289.3.6.3-2003).

3.3.8 Pipette

The pipette technique is another way to determine the particle size distribution of soil. A volumetric pipette made of borosilicate glass is used only for validation purposes in relation to the technique introduced in this study in [Chapter 6](#).

For PSD analysis, a pipette was fixed at a specific height by a clamper ([Fig.3.11a](#)) and a fraction of the suspension was collected at a specific timeframe. During the test, at the time of sample collection, the spherical-shaped black rubber suction bulb shown in [Fig.3.11a](#) is pressed gently to avoid air going in or out and knob A at the top is slowly pressed using the index finger and thumb at the same time. When pressure is applied to knob A, the sample

slowly goes into the pipette. This task has to be done at one go with minimum disruption to the particle settlement.

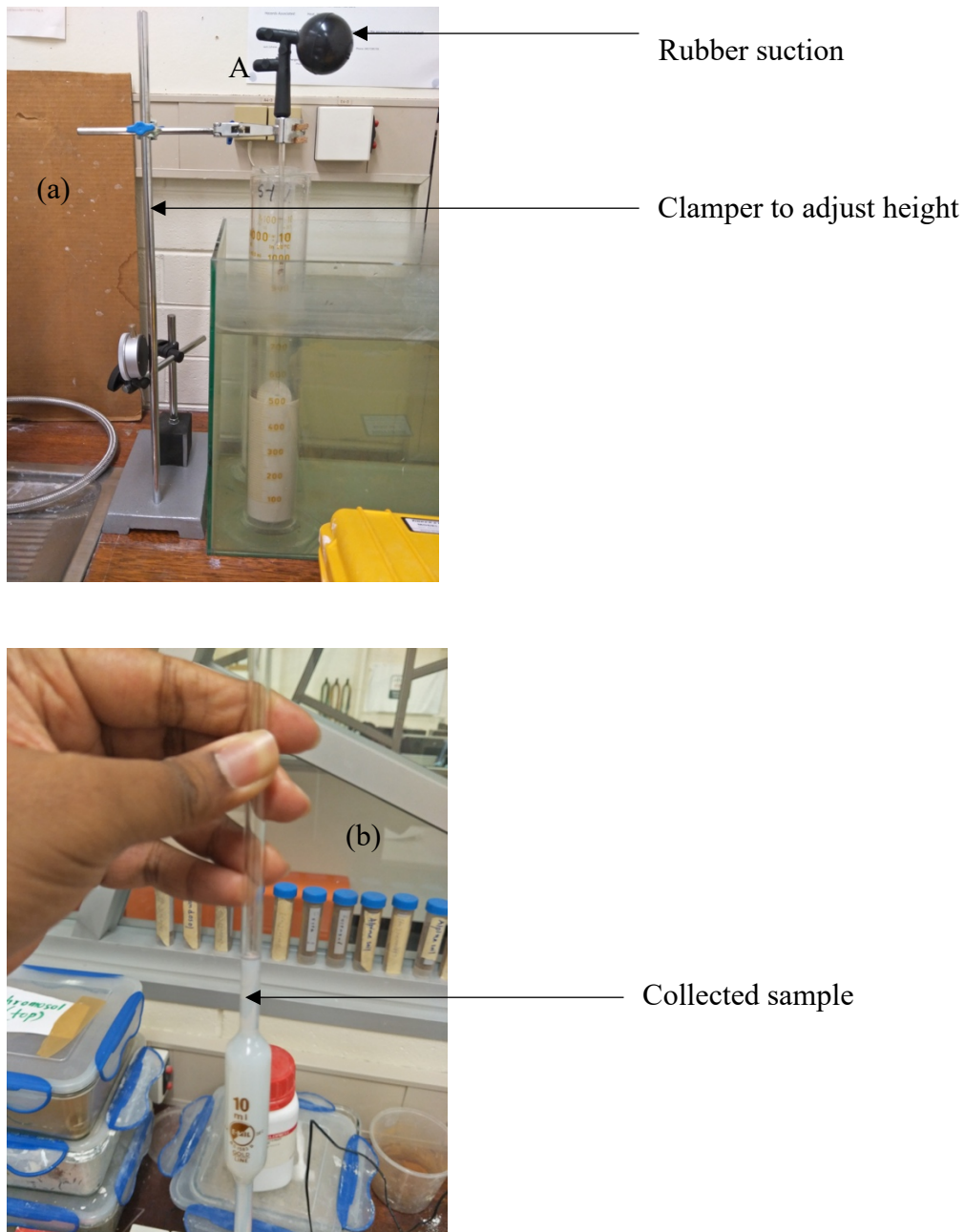


Figure 3.44: Sample pipette analysis for particle size distribution of soils: a) complete set up, and b) sample collection procedure.

Before the test, the thoroughly mixed suspension is poured into a graduated cylinder and after 2 hours and then 24 hours, approximately 1 ml of sample is withdrawn from 5 cm below the surface of the cylinder (Fig.3.11b) and the mass of the dry solid matter is calculated after drying out the suspension inside the oven overnight.

3.3.9 Laser Diffraction Particle Size Analyser

Laser diffraction (LD), one of the modern techniques, uses the optical properties of particles and light to find the PSD of soil particles. The basic theory of any light scattering method significantly depends on the interaction between a particle and light incident upon that particle. This interaction creates four different but inherently related scattering patterns, namely diffraction, refraction, reflection, and absorption of the incident beam. The magnitude of each aforementioned phenomenon varies based on nature, size of the particle and wavelength of the light beam. One of the recent techniques involves using the LD of the particle to find the PSD.

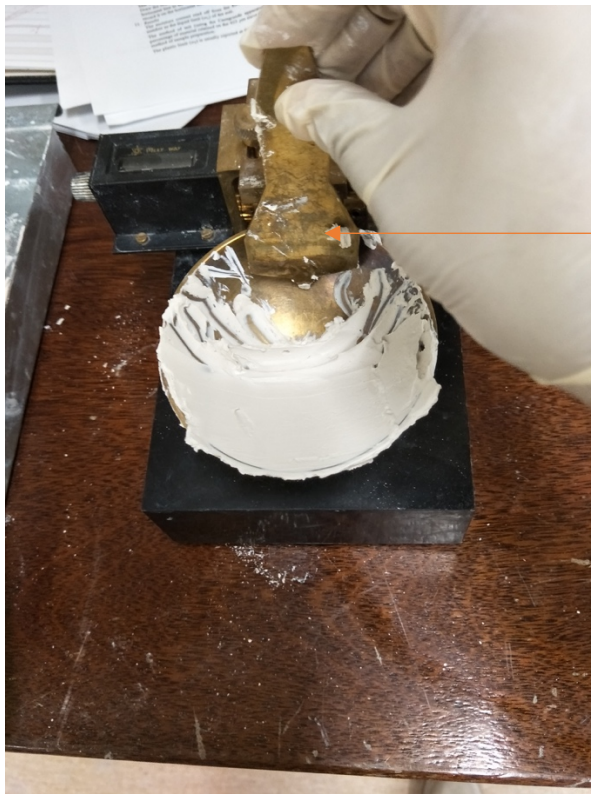


Figure 3.45: Malvern Mastersizer 3000 Laser Diffraction Particle Size Analyser setup.

The Malvern Mastersizer 3000 device was used to determine the particle size distribution of soils to assess the accuracy of the proposed method introduced in [Chapter 6](#). The device disperses soil samples in the liquid, as shown in [Fig.3.12](#). A laser beam is passed through the cell and the soil particles scatter the light to create scattering patterns. The automated device's optics determine the angles and intensity of the light, scattered by the particles and the PSD curve is generated within 5-10 minutes.

3.3.10 Casagrande Device for Determining the Liquid Limit (LL) of Soil

The Casagrande technique requires a brass cup that drops from a pre-determined height on a flat, hard base when operated by the handle ([Fig. 3.13](#)). The height of the cup is adjusted by tightening the screw by hand. Then, the device is ready for the test. During the operation, when the handle is turned, the brass cup is raised and allowed to drop on a hard base. The method requires around 120 gm of oven-dried soil sample passing through the 425 μ IS sieve. The sample is then transferred to a clean dish and mixed with de-ionised water to form a uniform paste. A portion of the paste is placed in the cup and the surface is labelled and smoothened. A spatula is used for the labelling or smoothening step to a depth not exceeding 1 cm. Then, a smooth groove is cut by a standard grooving tool in one attempt along the symmetrical axis of the cup. The Casagrande tool cuts a groove of 2 mm at the bottom and 11 mm at the top with a depth of 8 mm ([Arora, 2008](#)). After the creation of the groove, the handle is turned at 2 rev/s until the two parts of the sample come into contact at the bottom part of the groove along a distance of approximately 12 mm. The soil is then again mixed and a similar step is repeated until the two consecutive experiments provide the results with the same number of blows. Once the repeated test provides a similar result, a small portion of the sample is taken (around 15 gm-20 gm) from the cup and transferred to a container with a known mass. Then, the container with the wet sample is kept inside an oven under a constant temperature of 104.5⁰ C to determine the water content.



Process of
creating the
groove



Handle

Brass cup

Groov

Flat base

Figure 3.46: Sample Casagrande test to determine LL: a) groove creation before the actual test begins, and b) different parts of the Casagrande device.

A portion of the sample is kept inside the oven, the rest of the sample is transferred to the sample dish, and another homogeneous paste is formed by adding more water than the previous sample. Then, these steps are repeated. According to this technique, the LL is the water content at which the soil exhibits the same behaviour as the liquid when the device is subject to 25 blows.

The Casagrande LL test was performed to create a database with a view to validating the experimental results of the new approach introduced in [Chapter 7](#), which involves determining the liquid limit (LL) and plastic limit (PL) of soils using the electrical conductivity method.

3.3.11 Cone Penetration Device for Liquid Limit

The cone penetration device is an alternative to the Casagrande method. As previously mentioned, the new technique to determine the LL introduced in [Chapter 7](#), requires validation with conventional techniques. As a result, both Casagrande and cone Penetration techniques were considered for identical soil samples to gain more confidence in the accuracy of the EC method.

The setup of the cone penetration method includes a 35 mm long stainless-steel cone with a top angle of $30^{\circ} \pm 1^{\circ}$. There is a sliding rod that can move up and down, and the cone is fixed at the lower end of the rod. According to the British Standard 1990, the total system has a mass of approximately $80 \text{ g} \pm 0.05 \text{ g}$.

The procedure of sample preparation is similar to that of the Casagrande. However, the homogeneous paste is transferred to a different type of cup with a diameter of 50 mm and a height of 50 mm. The cup has to be completely filled with the sample, without entrapping air. When the cup is completely filled and levelled, the rest of the samples are transferred to the sample preparing dish for the next step. The cup is then placed below the cone and

the cone is carefully lowered closer to the top surface of the cup without touching it. The height can be adjusted by pressing the circular tab, as labelled in Fig. 3.14. Once the height is fixed, leaving the circular tab free tightens the sliding rod, and after this, the graduated scale is reset to zero. Once the scale displays zero, the circular tab is pressed and the sliding rod is released leading the cone inside the soil. It is recommended to wait for 30 seconds to let the cone penetrate the soil. The penetration is then recorded and the test is repeated to observe the repeatability.

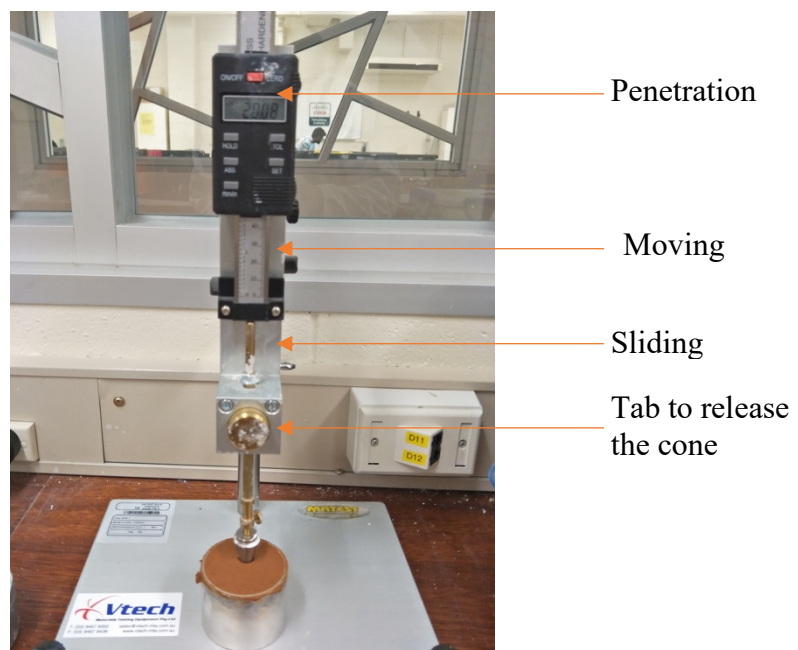


Figure 3.47: Cone penetration method for soil.

If the second values vary ± 0.5 mm, then a third reading is taken and the average is calculated. The test is then continued by adding more water in the sample and taking the penetration reading. The penetration reading may range from 12 mm to 25 mm, depending on the amount of water and the properties of the soils.

3.4 Summary

The purpose of this chapter was to briefly introduce some of the important materials and equipment used for the experiments. Other materials are utilised in different stages of this study, however, information on these will be discussed when necessary. In general, bentonite and kaolin were considered in most of the experiments due to their availability at the La Trobe University laboratory as well as in Australia. Since kaolin and bentonite are laboratory-based clays, it is easier to initiate experiments with these rather than natural soils. Natural soils were only considered in the experiments once the experimental results with kaolin and bentonite were in accord with the theoretical predictions. The devices were always used in line with the safety and professional standards specified by both the manufacturer and La Trobe University.

Chapter 4

Electrical Properties of Clay Particles

4.1 Introduction

In this chapter, the effect of temperature and pore water salinity on the electrical surface conduction of clay particles and its diffuse double layer (DDL) thickness are studied experimentally. Two new electrical surface conduction parameters that can be measured experimentally are introduced in this study. The testing soils in this study include two commercially available clays (kaolin and bentonite) and two natural soils (dermosol and chromosol). The proposed two surface conduction parameters can also be used to assess the effects of temperature and pore water salinity on the thickness of DDL indirectly. The observed results indicate that as the temperature and pore water salinity increase, the DDL thickness decreases. As the free swelling index (FSI) of the clay is a function of the DDL properties of its particles, the FSI of the tested soils was measured at different temperature and water salinity levels. The results of FSI directly confirm the observed effect of temperature and pore water salinity on DDL thickness.

4.2 Effect of Pore Water Salinity and Temperature on DDL

Fully saturated soil is considered to be a multi-phase material consisting of a solid and pore-water/fluid phase. The pore water could contain different salt concentrations (molarity) which directly influence the electrical conduction through the soil liquid phase. However, the soil electrical conduction also varies with the mineralogical properties of soils which control the fluid-particle interactions that could lead to the formation of a surface conduction layer that surrounds the solid particle surface (Klein and Santamarina, 2003; Mojid et al., 2007). This layer is called the diffuse double layer (DDL) and it plays a major role in the overall electrical conductivity of soils. The electrical properties of this layer are

controlled by pore water salinity and the surface charge properties of clay particles. However, it also evolves with temperature changes due to the temperature effect on ion mobility (Revil et al., 1998).

Several researchers (Mitchell and Soga, 2005; Mojid et al. 2007; Lu et al., 2019) have reached agreement on the effect of pore water salinity on the surface conduction and DDL thickness. As pore water salinity increases, the surface conduction effect and DDL thickness decrease. On the other hand, several studies have investigated the effect of temperature on the electrical properties of soils and showed that the electrical conductivity of soils increases as the temperature increases (Brevik et al., 2004; Robinson et al., 2004; Zhang et al., 2020). This behaviour was mainly attributed to the increase in electrical conductivity of free saline water as the temperature increases. Mitchell and Soga (2005) stated that the physico-chemical properties of DDL water change as the temperature increases due to the thermally induced changes in electro-osmotic potential. However, DDL thickness is temperature independent. According to Mitchell and Soga (2005), the temperature should have an insignificant effect on DDL thickness. However, Towhata et al. (1993), Cho et al. (1999), and Estabragh et al. (2016) suggested that at an elevated temperature, the adsorbed water may be converted into bulk pore water and DDL thickness decreases.

Based on the above discussion, it clear that more research is required to find a simple testing approach that can quantify the effect of pore water salinity and temperature on the geometric and electrical properties of the DDL of clay particles. In fact, determining these properties is crucial to better understand the electro-chemical behaviour of soils and develop an accurate electrical conductivity model of soils.

4.3 Proposed Surface Conduction Parameters

4.3.1. Phase Relationship

As discussed in the literature review, all the soil conductivity models consider solid soil particles as an insulating material and electrical conduction goes through the conductive fluid path only. To include the role of DDL in the electrical conductivity (EC) of soils, the newly proposed approach in this study considers the clay particle and its surrounding DDL as a single unit called an effective clay particle, as shown in Fig 4.1. It could be observed that insulated solid is being surrounded by DDL water, and later an equivalent conductive material/effective solid has been formed.

Following the proposed concept of an effective solid phase, the total volume of saturated clay V can be expressed as follows:

$$V = V_w^f + V_s^e \quad (4.1)$$

where V_w^f and V_s^e are the volumes of the free water and effective solid, respectively. These volumes are different from the total volume of water V_w and volume of solid V_s and is determined as follows:

$$V_w^f = V_w - V_w^{DDL} = [n - (1 - n)(\chi - 1)] V \quad (4.2)$$

$$V_s^e = V_s + V_w^{DDL} = (1 - n)\chi V \quad (4.3)$$

where:

$$\chi = \frac{V_s^e}{V_s} \quad (4.4)$$

$$n = \frac{V_v}{V} \quad (4.5)$$

$$n_e = \frac{V_w^f}{V} \quad (4.6)$$

$$\chi = \frac{1-n_e}{1-n} \quad (4.7)$$

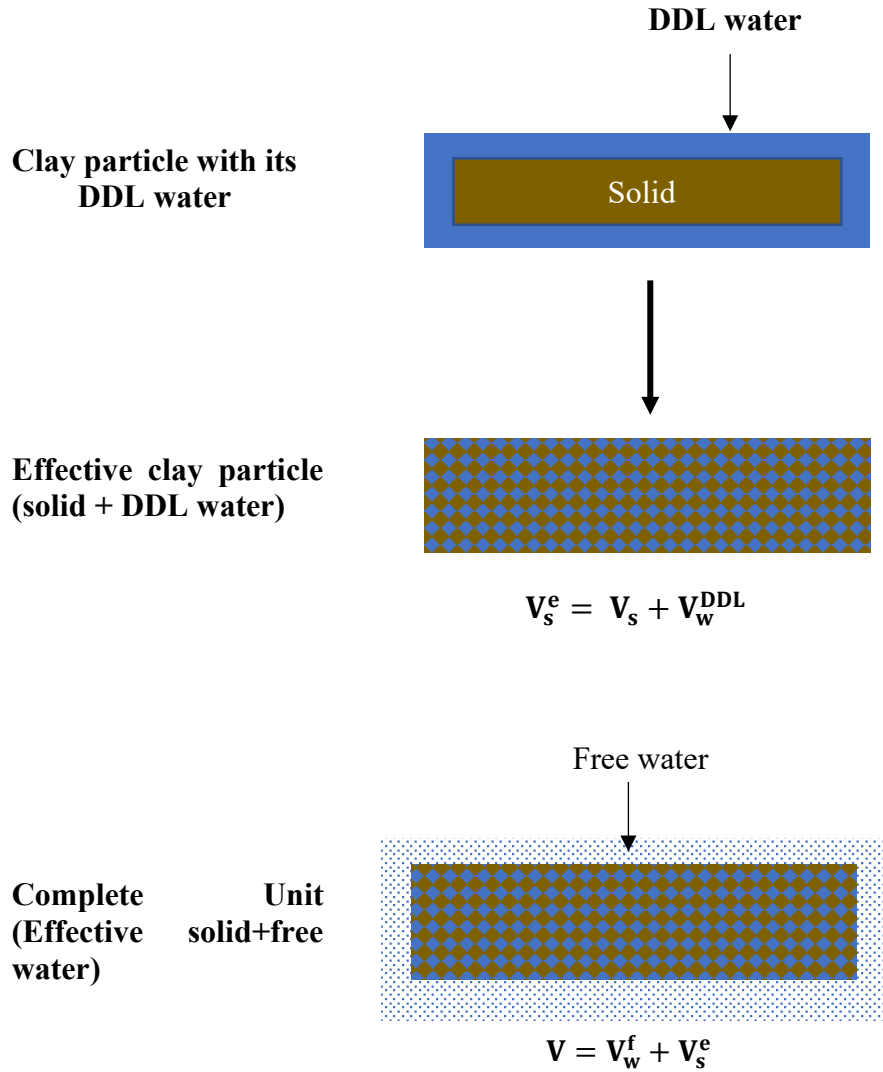


Figure 4.48: Postulation on effective clay particle/effective solid formation with DDL water.

where V_w^{DDL} and V_v are the volumes of DDL water and void, respectively; n is the porosity, and n_e is the effective porosity. Therefore, the term $\chi (\geq 1.0)$ can express the overall size of the DDL water per unit volume of soil.

As the temperature increases, the solid undergoes physical changes as its volume changes at the elevated temperatures due to the thermal expansion. The thermal expansion could be observed in terms of changes in shape, area, volume, and density as a function of temperature. In this study, the thermal expansion has been considered to change the volume

of the soil, hence referring as soil thermal expansion of volume. At the elevated temperature, the soil particles start to vibrate and become mobile. Therefore, the interparticle distance increases, leading to expansion of volume of solid. The thermal expansion coefficient of soil explains how the size of soil volume changes with temperature, particularly the fractional change in the total volume of the soil as temperature increases.

In this case, the thermal expansion coefficient of the soil solids is considered to determine the volume of the solid. This can be expressed as follows:

$$V'_s = V_s[(T' - T)\alpha + 1] \quad (4.8)$$

where V'_s is the final volume of the solid at elevated temperature T' and T is the room temperature (typically 25°C). The parameter α is known as the thermal expansion coefficient of the solid soils and has a typical value of $10^{-5} \text{ }^\circ\text{C}^{-1}$ (Abuel-Naga et al., 2006 ; Maranhã et al., 2017; Cui et al., 2018; Zhou et al., 2018).

A novel type of experimental test is proposed in this study to determine the volume and the electric properties of effective clay particles (solid + DDL water). The proposed method involves measuring the electrical conductivity of a diluted clay-water system, σ_{mix} . Assuming that the clay particles in this system do not contact each other, this system can be mathematically expressed using a series-parallel approach (Fig. 4.1) as follows (Ohm's law):

$$\sigma_{\text{mix}} = \frac{a}{\frac{d}{\sigma_s} + \frac{1-d}{\sigma_w}} + b\sigma_w \quad (4.9)$$

where σ_w is the electrical conductivity of free water and σ_s is the electrical conductivity of the effective solid. Considering that the electrical conductivity of a diluted clay-water system is isotropic ($a=d$), the parameters in Eq. 4.9 can be identified as follows:

$$ad = 1 - n_e \quad (4.10)$$

$$a = \sqrt{(1-n)\chi} \quad (4.11)$$

$$b = 1 - \sqrt{(1-n)\chi} \quad (4.12)$$

In the unit diluted clay-water system, the empirical parameters ($a=d$), and b refer to the areas of the free water, and effective solid and free water, respectively. For a better clarification, Fig.4.2 has been illustrated.

Therefore, Eq. 4.9 can be written as follows:

$$\sigma_{\text{mix}} = \frac{\frac{\sqrt{(1-n)\chi}}{\frac{\sqrt{(1-n)\chi}}{\sigma_s} + \frac{1-\sqrt{(1-n)\chi}}{\sigma_w}}}{1} + \left(1 - \sqrt{(1-n)\chi}\right)\sigma_w \quad (4.13)$$

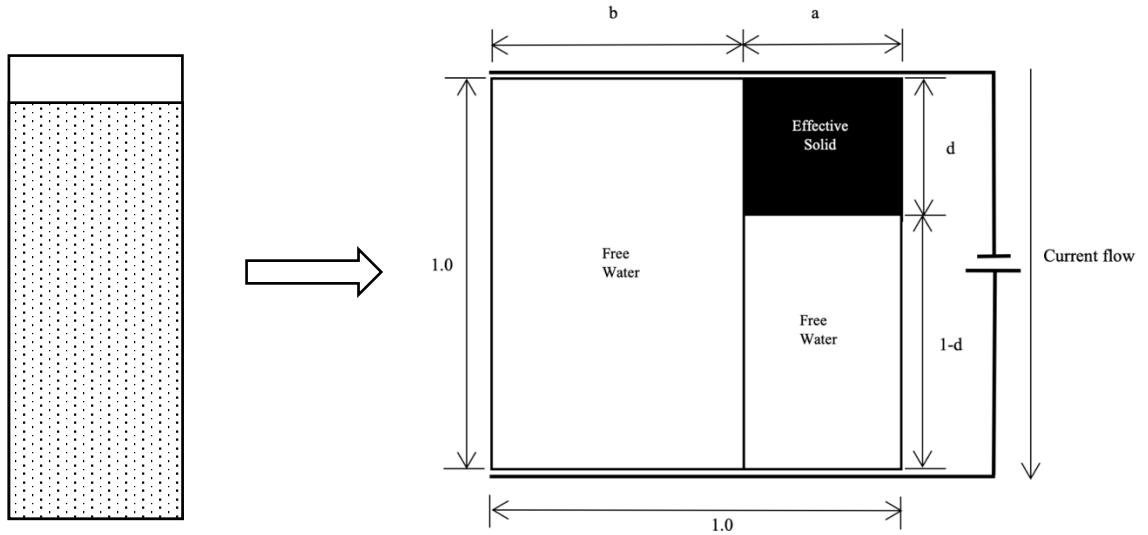


Figure 4.49: Representation of diluted clay-water system.

To find the unknown electrical surface conduction parameters χ and σ_s , the electrical conductivity of two different diluted clay-water systems in terms of their n value (n_1, n_2) should be measured experimentally. The results of the tests can be used to find χ and σ_s by back-calculation as follows (Wolfram Mathematica V11):

$$\chi = \frac{(N_2 - N_1)\sigma_{\text{mix}1w}\sigma_{\text{mix}2w}}{\sigma_w[(N_2)^2\sigma_{\text{mix}1} - (N_1)^2\sigma_{\text{mix}2} + \sigma_w\{(N_1)^2 - (N_2)^2\}]} \quad (4.14)$$

$$\sigma_s = \frac{N_1N_2(N_1 - N_2)\sigma_w\sigma_{\text{mix}1w}\sigma_{\text{mix}2w}(N_2\sigma_{\text{mix}1w} + N_1\sigma_{\text{mix}2w})}{(N_1)^2(N_2)^2\sigma_{\text{mix}1,2w}\sigma_{\text{mix}1w}\sigma_{\text{mix}2w} - N_1N_2[\sigma_{\text{mix}1w}\sigma_{\text{mix}2w}\{(N_2)^2\sigma_{\text{mix}1w} - (N_1)^2\sigma_{\text{mix}2w}\}] + \sigma_w\{(N_2)^4\sigma_{\text{mix}1w}^2 + (N_1)^4\sigma_{\text{mix}2w}^2\}} \quad (4.15)$$

Details of the notations and expressions of Eqs. (4.14-4.15) can be found in Appendix 1, and the Mathematica script is included in Appendix 2.

4.4 Experimental Programmes

The experimental programmes were conducted into two major phases. The first phase includes the experiment to determine χ and σ_s . The second and last phase includes the free swelling test at the elevated temperature to observe the changes in χ and σ_s . A flowchart outlining the experimental programmes has been provided in Fig. 4.3, for a better representation.

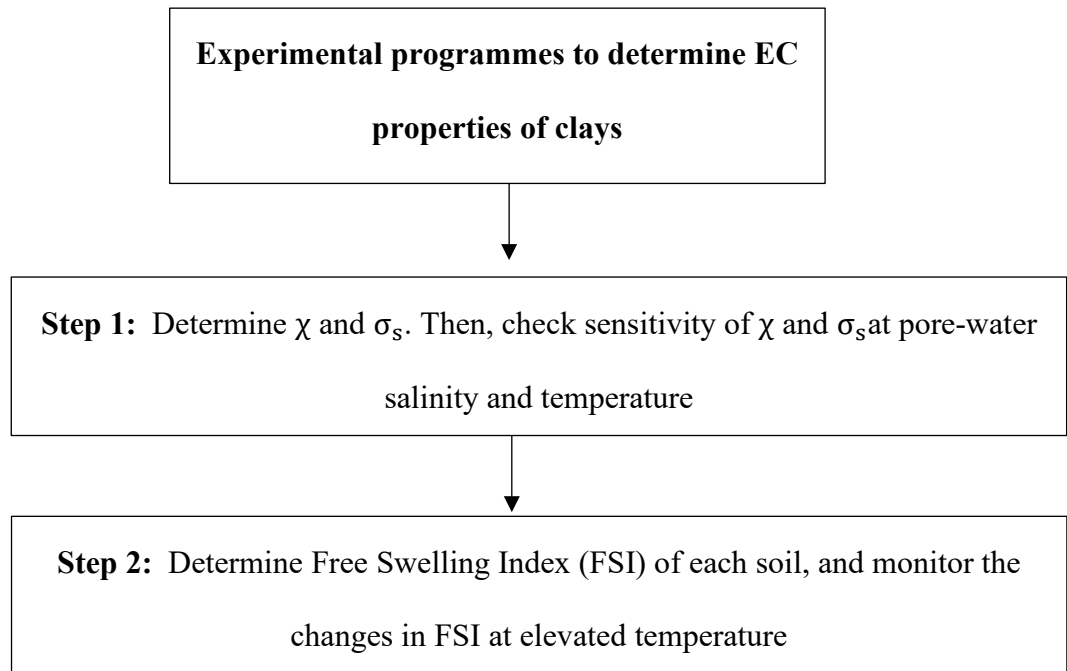


Figure 4.50: Flowchart depicting the major steps of the experimental programmes.

4.4.1 Testing soils

Four types of soils are considered in this study, namely kaolin and bentonite, and two natural soils, dermosol and chromosol. The geotechnical properties of kaolin and bentonite were discussed in Chapter 3 and the particle size distribution of dermosol and chromosol is shown in Fig. 4.4, obtained by laser diffraction method. Chromosol has a liquid limit of 58% and a plastic limit of 27.4%, whereas dermosol has a 59% liquid limit and a 28.4%

plastic limit. Chromosol and Dermosol were collected from Culcairn, NSW and Kinglake, VIC, respectively.

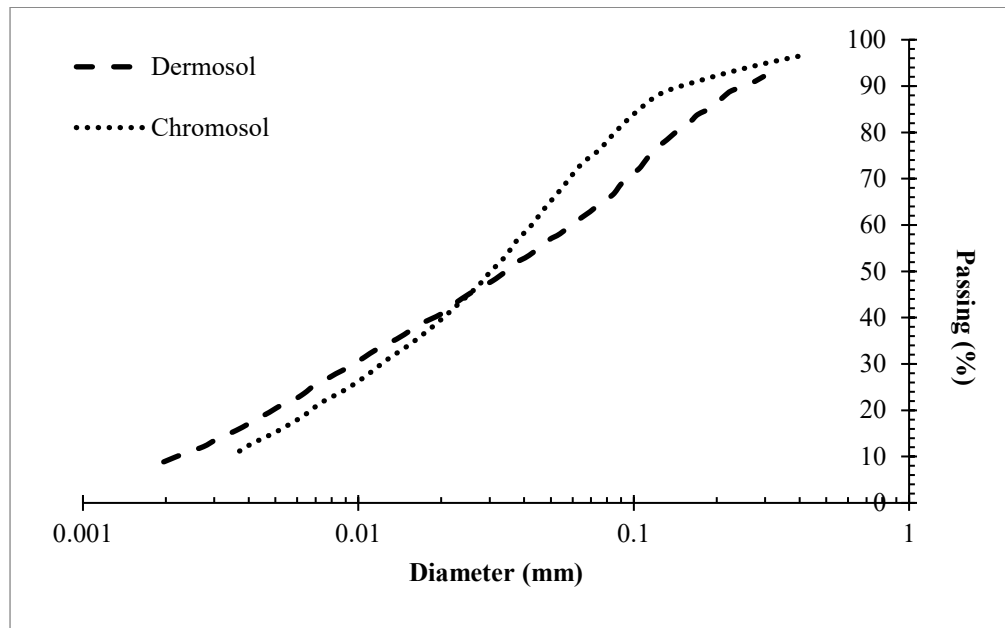


Figure 4.51: Particle size distribution of dermosol and chromosol, obtained by laser diffraction technique.

4.4.2 Determining Electrical Surface Conduction Parameters (σ_s and χ)

The experiment to determine the surface conduction parameters χ and σ_s involved some easy-to-implement experimental techniques, which are described as follows:

- I. 2L of de-aired water at the targeted salinity was prepared (in two identical 1L beakers) and kept inside the temperature bath to reach the targeted temperature of the test (25°C, 30°C, 35°C, and 40°C).
- II. Once the temperature of the beakers reached the targeted temperature, the electrical conductivity of the saline water (σ_w) was measured by the EC metre.
- III. Using the saline water, two different soil-water homogeneous suspensions were prepared at 10g/L (σ_{mix1}) and 20g/L (σ_{mix2}) by mixing it vigorously for approximately 30-40 minutes with the soil-water suspension mixer, as described illustratively in [Section 3.3.3](#) of this thesis. The MATEST suspension mixer was

used to make the homogeneous suspension. The unit has a rotary blade that spins through the suspension to ensure homogeneity. The standard container is made of aluminium and has to be adjusted and aligned properly with the black holder\, otherwise the blade won't rotate despite pressing the start button. The time-scale to mix the suspension with the mixer depends on the amount of sample present in the water, however, before re-using the unit for another sample, the metal rod and blades are washed with de-ionised water to avoid contamination. In general, the standard timescale to complete preparing homogeneous mixture was to wait for at least 30-40 minutes.

- IV. Once the mixing was completed, the suspensions were allowed a few seconds to become steady and the EC of the suspensions ($\sigma_{\text{mix}1}$ and $\sigma_{\text{mix}2}$) and temperature were measured.
- V. Finally, Eqs (4.14-4.15) were utilised to determine the surface conduction parameters σ_s and χ .

4.4.3 Modified free swelling index test

4.4.3.1 Methodology

To investigate the effect of temperature and water salinity on the electrical properties of the clay's DDL thickness, the FSI test (Gibbs and Holtz, 1956; Nagaraj et al., 2010; Zumrawi, 2013) was conducted at different temperatures ranging from 25⁰C to 40⁰C. Free swell is defined as the increase in the soil volume from a loose and dry powder form, once it is

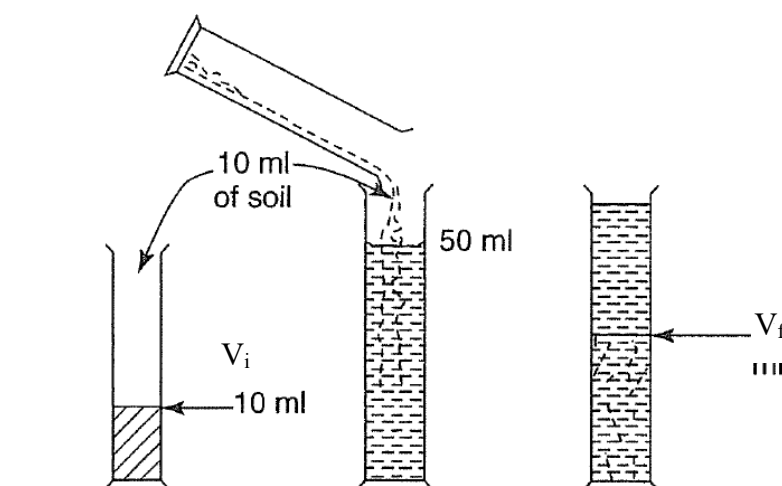


Figure 4.52: Free swelling test (Gibbs and Holtz, 1956).

poured into the water freely. The free swell is expressed as a percentage of the original volume of the dry soil. In general, the FSI test is conducted at constant room temperature (25⁰ C). The following equation is universally accepted to determine the FSI of soils:

$$FSI = \frac{\text{Final volume } (V_F) - \text{initial volume } (V_i)}{\text{initial volume } (V_i)} \times 100 \quad (4.16)$$

Figure 4.5 demonstrates an example of the free swelling test, as discussed in Gibbs and Holtz (1956). However, since the motivation of this study is to investigate the effect of temperature on the clays' DDL thickness, the temperature was varied up to 40⁰C with a view to recording the changes in the clay volume. In addition to the distilled water, two different types of saline water with different NaCl salt concentrations were considered in this study (0.5g/L and 1g/L).

4.4.3.2 Sample preparation

To conduct the FSI test at different temperatures and water salinity levels, the following procedures were followed:

- I. For each type of soil, around 20 g of oven-dried soils were passed through the sieve 40 (a 425 μm sieve) and the fraction of soils which passed through the sieve were collected in a dry container. Since different temperatures

were considered to investigate the changes in the DDL thickness, the soils were dried at the targeted temperature overnight.

- II. Clean glass beakers which were filled with water and prepared at the targeted salinity level (0.0, 0.5, 1.0 g/L) were kept inside in the temperature controlling unit overnight to ensure the targeted temperature of the water was reached. The targeted salinity refers to the salt-water solutions with different concentrations of salt. 0.0g/L means the absence of NaCl in the solution, which is directly representing the distilled water. On the other hand, 0.5g and 1.0g NaCl per litre will exhibit different electrical conductivities, which allowed to conduct further analyses at different pore water salinity.
- III. For each sample, two identical samples were prepared with a view to testing the reproducibility of the results. Two identical 100 ml cylindrical glass beakers were quickly filled with the prepared water at the targeted temperature and salinity and then placed in an oven at the targeted testing temperature. The temperature bath has a lid which needs to be closed to guarantee smooth execution.
- IV. The dry soil sample at the targeted testing temperature was poured inside the 100 ml glass beakers steadily. Then a lid was used to reduce the water evaporation effect.
- V. The soil particles were allowed to settle down at controlled temperature as shown in [Fig.4.6](#).



Figure 4.53: Soil suspensions inside the oven.

- VI. After 24 hours or more, the beakers were taken out of the oven and checked as to whether the water on the top has become transparent, as shown in [Fig.4.7](#). Although the finest particles might remain in the suspension, these can be ignored, as described by [Holtz and Gibbs \(1956\)](#).

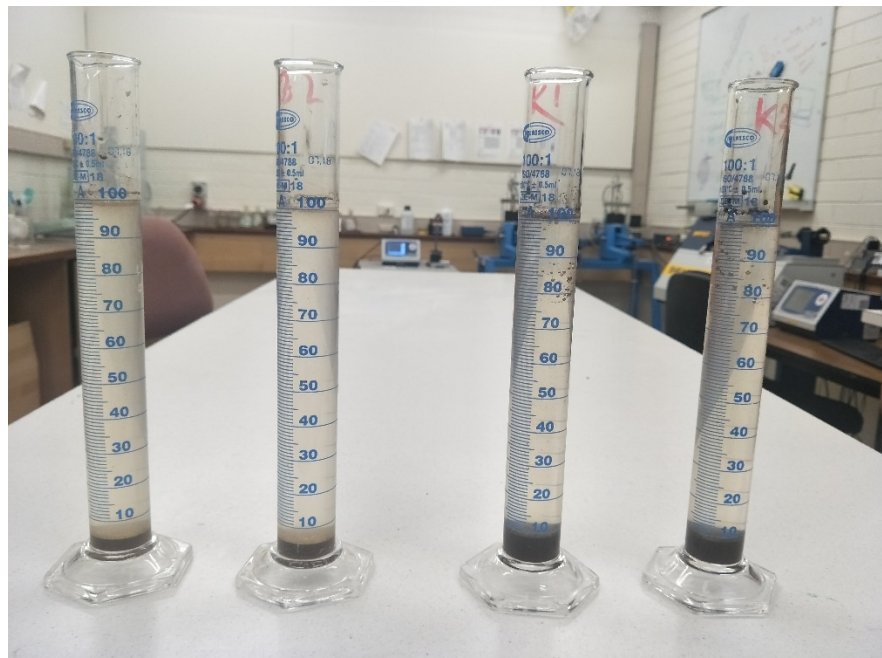


Figure 4.54: Soil samples after being subjected to a constant temperature for 24 hours.

- VII. In the final step of the experiment, the latest volume of the soil was recorded and the free swell was calculated using Eq.4.16. It should be mentioned that there was a marginal loss of water due to overnight evaporation; however, this has an insignificant impact, as recording the changes in the height of the soil was the primary objective.

4.5 Results and Discussion

The changes in the aforementioned properties and parameters were later collectively used to explain the behavioural changes in the DDL of each soil. The following section discusses on the parametric sensitivity as a function of pore water salinity.

4.5.1. Effect of Pore Water Salinity on σ_s and χ

Figures 4.8-4.9 show the changes in χ and σ_s of different clays as the salinity of the water changed. K-B mixture refers the clay mixture containing 50% Kaolin and 50% Bentonite. There is no specific guideline or standard to choose such proportion, however, making a clay mixture of 50% Kaolin and 50% Bentonite was easier to prepare inside the laboratory environment.

In general, the results show that the particles of bentonite have higher σ_s , due to its larger electro-chemical surface activity compared to the kaolin clay particles. The trendlines depicted on the points showed fit-quality/coefficient correlations R^2 between 0.92 to 0.99, which show the trend to be consistent and predictable. Furthermore, the results indicate that for different clay types, as the salinity of the free water increased, the value of σ_s increased, whereas χ decreased. In this regard, the coefficient correlation R^2 were found to be between 0.91 to 0.99, and it provides further confidence on the experimental results. Therefore, as the salinity of the free water increased, the size of the DDL decreased, whereas its electrical conductivity increased. The reduction in the size of the DDL was expected as increasing

the pore water salinity decreases the electro-osmotic potential, which was responsible for the development of DDL (Mitchell and Soga, 2005). Therefore, the observed behaviour of χ supports its proposed physical meaning.

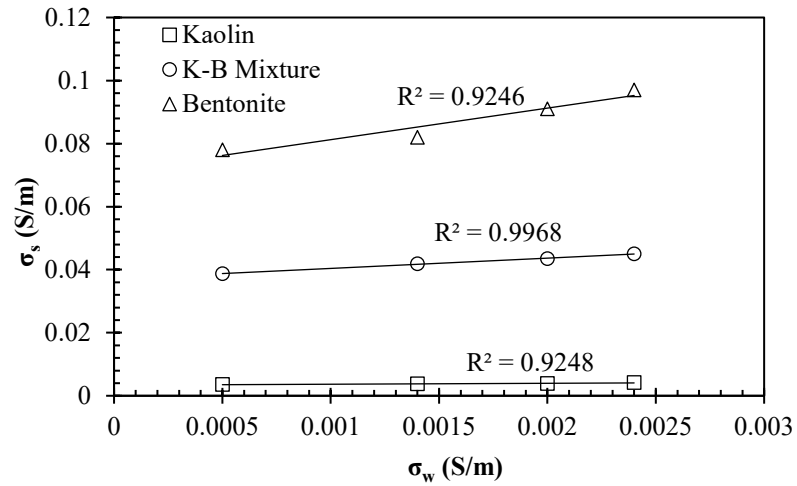


Figure 4.55: Effect of saline water on electrical conductivity for different clay particles.

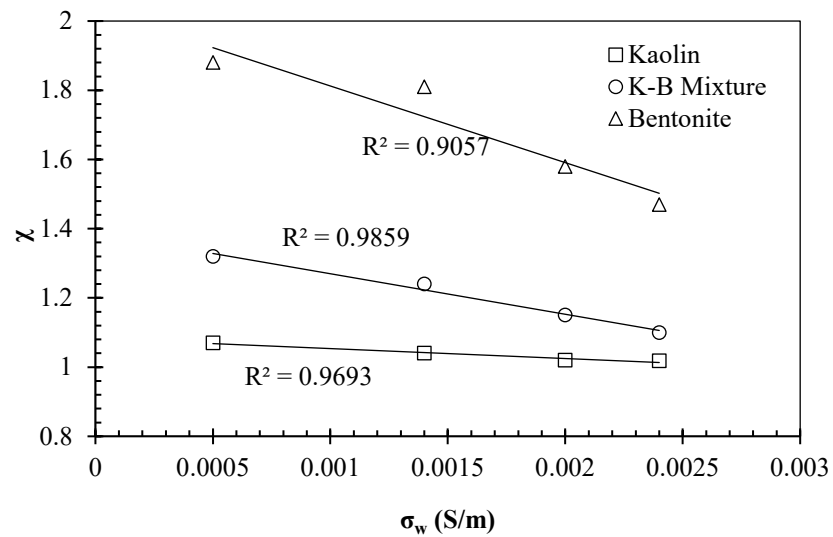


Figure 4.56: Effect of saline water on different values of χ for different clay particles.

4.5.2 Coupled Thermo-chemical Effect on σ_s and χ

Figure 4.10 illustrates the evolutions of electrical conductivity parameters σ_s as a function of σ_{FW} and T , showing that the parameter relies significantly on the changes of σ_{FW} and T . In general, the non-linear surface analyses were conducted based on the experimental results obtained from this study, and coefficient correlations (R^2) were found to be between

Table 4.16: Equations to determine σ_s of tested soils considered in this study.

Soils	Equations	R^2
Bentonite	$\sigma_s = 0.032 + (0.0003 * T) + (38 * \sigma_{FW})$	0.99
Kaolin	$\sigma_s = 0.00323 + T + (0.32 * \sigma_{FW})$	0.97
Chromosol	$\sigma_s = 0.0042 + (-0.00004 * T) + (0.8 * \sigma_{FW})$	0.94
Dermosol	$\sigma_s = 0.0035 - T + (0.9 * \sigma_{FW})$	0.88

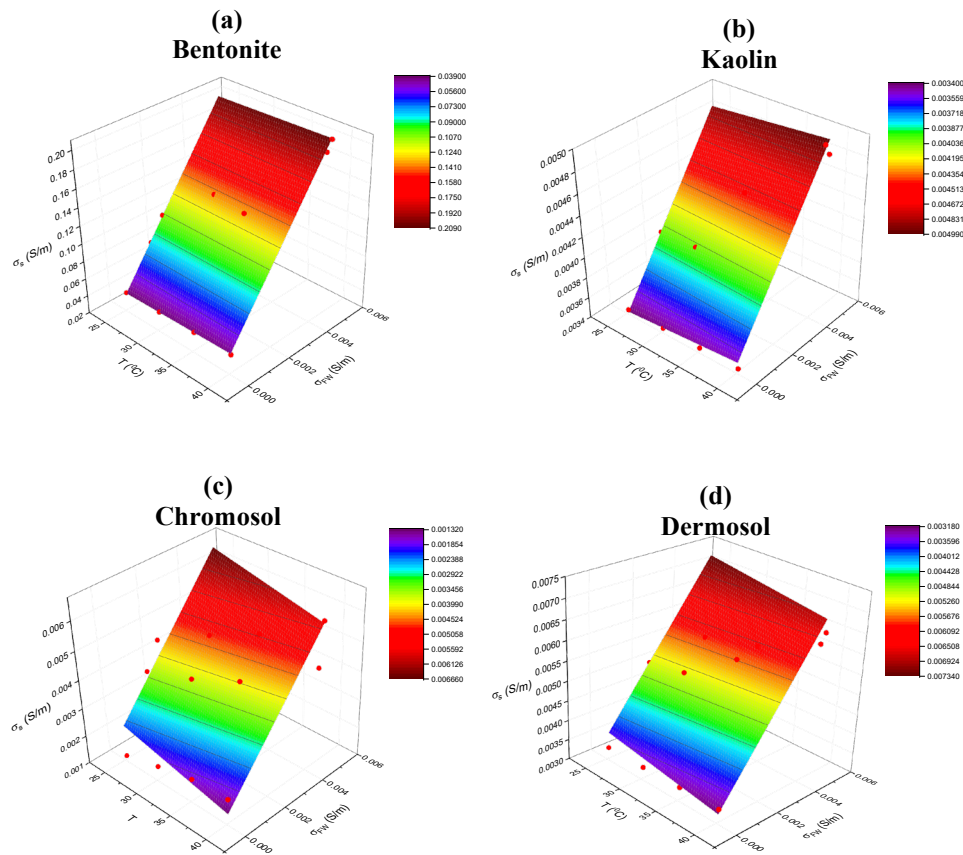
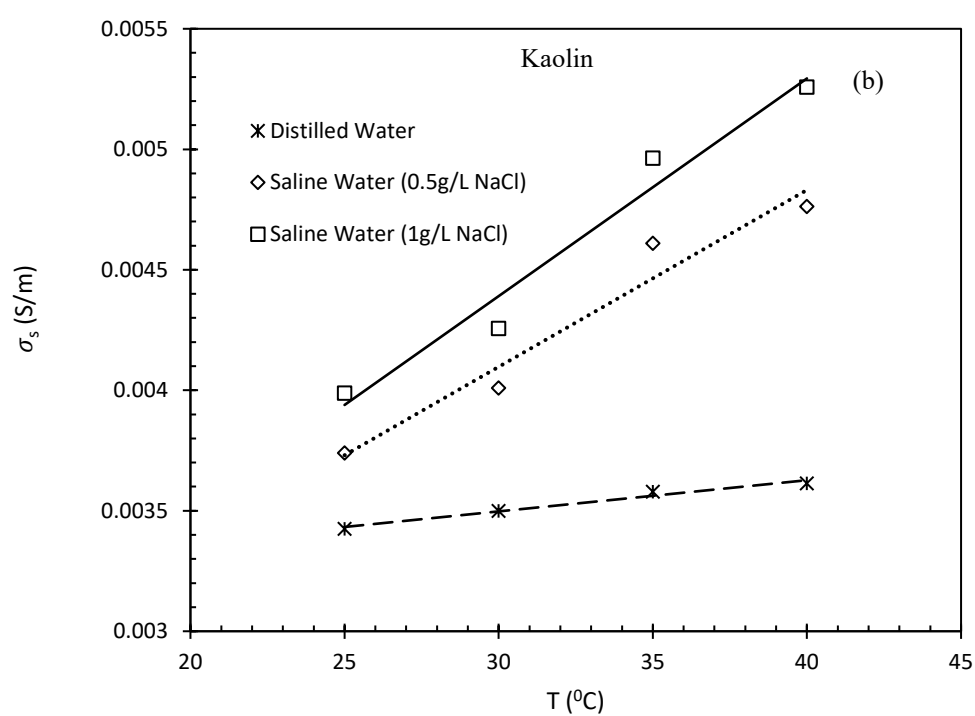
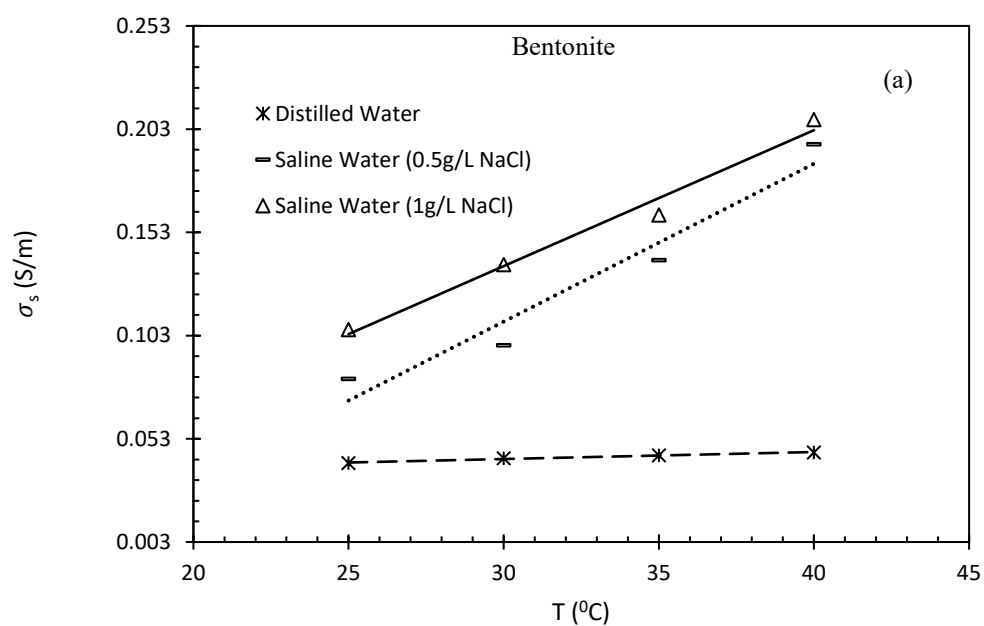


Figure 4.57: Evolution of σ_s as a function of T and σ_{FW} for a) bentonite, b) kaolin, c) chromosol, and d) dermosol.

0.85 to 0.99, which lead to unique empirical equations for each soil so that an estimation can be made at a further elevated temperature or water salinity. [Table 4.1](#) details the equations for each soil for better clarification.



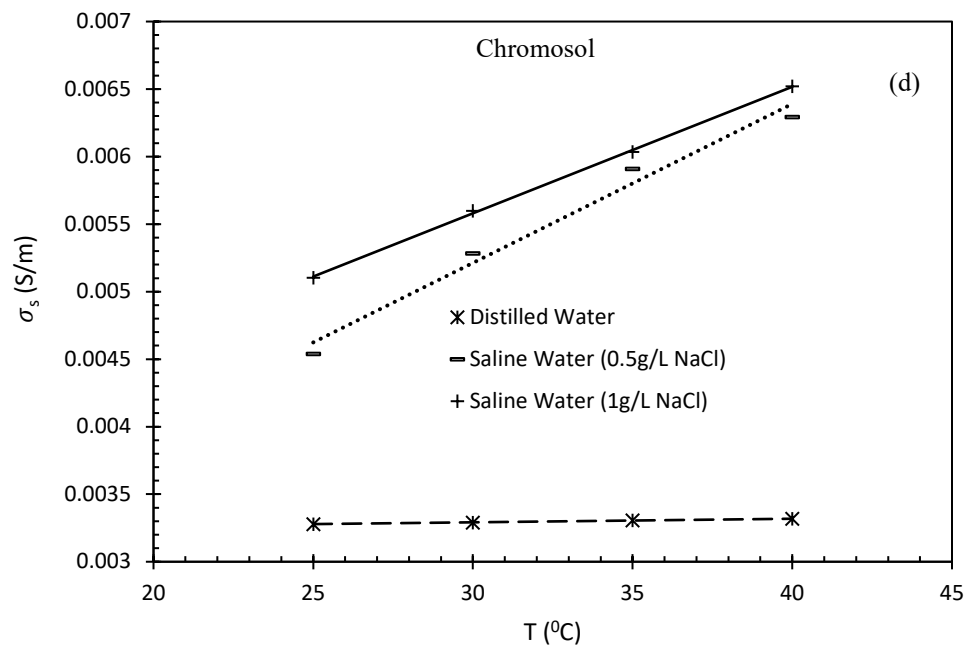
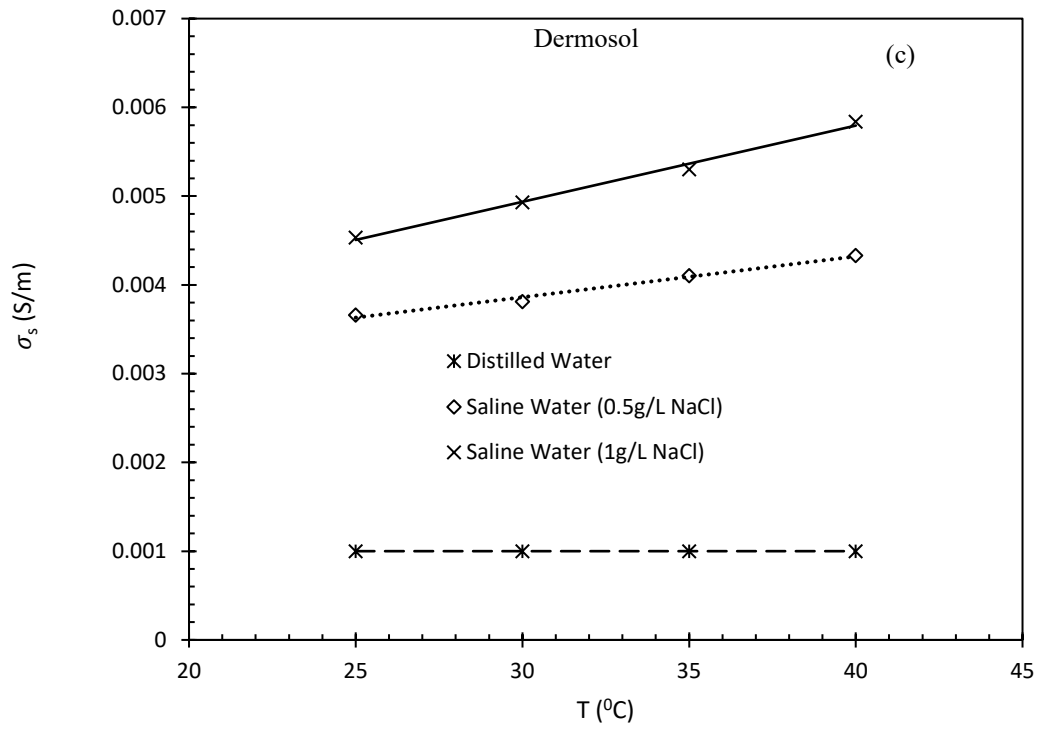


Figure 4.58: Changes in σ_s as T varies in different salt concentrations in water in (a) bentonite, (b) kaolin, (c) dermosol, and (d) chromosol.

activity (Fig.4.11). It was also seen earlier that an increase in σ_s of kaolin was quite marginal as pore water salinity increases. Furthermore, the changes in σ_s in distilled water for all types of soils were almost negligible due to the absence of salt concentration in the water, i.e., almost zero electrical conductivity of water. All the soils considered in this study exhibited similar behaviour in this regard. However, as saline waters were considered to determine σ_s , each soil demonstrated an increase in the values of σ_s as T increased, which was expected. The comprehensive results are presented in Table 4.2 for better view.

The next parameter χ , which represents the size/thickness of DDL, was also subject to study as a function T. It was found that for all soils, the size of DDL decreased as T increased. However, the rate of decrease was also less pronounced for kaolin, chromosol and dermosol compared to Bentonite. The 3D surface analyses presented in Fig.4.12 were considered to present equations to predict the χ of each soil. The equations are detailed in Table 4.3, where coefficient correlations R^2 have also been included. Pure bentonite possesses large DDL, therefore the changes are more influenced by temperature. As T increased to 40°C, χ of bentonite decreased by approximately 23.75% in saline water-1 (0.5g/L NaCl), and 24.82% in saline water-2 (1g/L NaCl), but only 4.5% in distilled water, as shown in Fig.4.13.

It should be mentioned here that there are several inconsistencies in the literature regarding the effect of T on the size of the DDL. Hammel et al. (1983) and Mitchell and Soga (2005) demonstrated that with an increase in temperature, the DDL thickness increases since the dielectric constant decreases, whereas for the constant surface charge, the surface potential increases as the dielectric constant decreases. Therefore, considering both characteristics, changes in temperature have a negligible impact on DDL thickness. The effect of

Table 4.17: Comprehensive experimental results for all types of tested soils in this study.

Soil	Water type	T (°C)	σ_{fw}^* (S/m)	V ₁ (ml)	V ₂ (ml)	V _{avg} (ml)	FSI (%)	σ_s (S/m)	χ	σ_{DDL} (S/m)
10B	Distilled	25	0.000085	69	72	70.5	605	0.0412	2.01	0.102
		30	0.000092	51	53	50	420	0.0436	2.00	0.108
		35	0.000096	44	43	43.5	335	0.045	1.99	0.113
		40	0.0001	31	30	30.5	205	0.0464	1.92	0.122
	Saline-1	25	0.0014	55	58	56.5	465	0.08201	1.81	0.23461
		30	0.00195	48	43	45.5	355	0.09829	1.66	0.32222
		35	0.0026	30	33	31.5	215	0.13951	1.51	0.55045
		40	0.00472	26	23	24.5	145	0.195723	1.38	0.97511
	Saline-2	25	0.002	47	46	46.5	365	0.10593	1.59	0.37487
		30	0.002915	39	39	39	290	0.13738	1.38	0.66824
		35	0.003616	24	26	25	150	0.16147	1.23	1.20138
		40	0.00496	22	21	21.5	115	0.20766	1.19	1.79426
10K	Distilled	25	0.000085	21	21	21	110	0.003425	1.08	0.06776
		30	0.000092	19	19	19	90	0.0035	1.077	0.0715
		35	0.000096	18	17.8	17.9	79	0.00358	1.076	0.07405
		40	0.0001	17	17	17	70	0.003614	1.075	0.0758
	Saline-1	25	0.0014	18.4	18.5	18.45	84.5	0.00374	1.042	0.1821
		30	0.00195	18.2	18	18.1	81	0.00401	1.034	0.2071
		35	0.0026	17	17	17	70	0.00461	1.029	0.20919
		40	0.00472	16	16	16	60	0.004763	1.020	0.27789
	Saline-2	25	0.002	18	17.5	17.75	77.5	0.003988	1.024	0.2455
		30	0.002915	17	17	17	70	0.004257	1.021	0.30776
		35	0.003616	15	14.5	14.75	47.5	0.004963	1.018	0.3571
		40	0.00496	13	13.5	13.25	32.5	0.005258	1.014	0.51121
	Distilled	25	0.000085	17.3	17.3	17.3	73	0.00112	1.106	0.0168
		30	0.000092	17	17	17	70	0.00147	1.082	0.02809

Dermosol		35	0.000096	16.7	16.8	16.75	67.5	0.00178	1.076	0.03672
		40	0.0001	16.4	16.5	16.45	64.5	0.00186	1.074	0.03935
	Saline-1	25	0.0014	16.5	16.7	16.6	66	0.003661	1.031	0.17532
		30	0.00195	16.3	16.3	16.3	63	0.00381	1.029	0.1958
		35	0.0026	15.9	15.9	15.9	59	0.004103	1.028	0.22103
		40	0.00472	15.6	15.6	15.6	56	0.00433	1.026	0.24776
	Saline-2	25	0.002	16	16.2	16.1	61	0.004532	1.022	0.31326
		30	0.002915	15.7	15.6	15.65	56.5	0.00493	1.020	0.36734
		35	0.003616	15.4	15.3	15.35	53.5	0.005301	1.018	0.4421
		40	0.00496	15	15	15	50	0.00584	1.014	0.62995
Chromosol	Distilled	25	0.000085	19	18.8	18.9	89	0.003279	1.055	0.092718
		30	0.000092	17.5	17.7	17.6	76	0.003291	1.054	0.094343
		35	0.000096	17	16.8	16.9	69	0.003306	1.052	0.09794
		40	0.0001	16.2	16	16.1	61	0.003318	1.050	0.102083
	Saline-1	25	0.0014	15.3	15.2	15.25	52.5	0.00454	1.025	0.27689
		30	0.00195	15	14.8	14.9	49	0.005284	1.023	0.34544
		35	0.0026	14.8	14.7	14.75	47.5	0.00591	1.022	0.40183
		40	0.00472	14.5	14.5	14.5	45	0.006294	1.020	0.47135
	Saline-2	25	0.002	15	15	15	50	0.005104	1.022	0.353099
		30	0.002915	14.7	14.5	14.6	46	0.005598	1.020	0.419265
		35	0.003616	14.3	14.2	14.25	42.5	0.006035	1.018	0.49873
		40	0.00496	14	14	14	40	0.00652	1.015	0.63699

temperature of the dielectric constant of water is shown in Table 4.4 (Mitchell and Soga, 2005):

Table 4.18: Equations to determine χ of tested soils considered in this study.

Soils	Equations	R ²
Bentonite	$\chi = 1.85 + (0.007 * T) - (158 * \sigma_{FW})$	0.91
Kaolin	$\chi = 1.032 + (0.0013 * T) - (16 * \sigma_{FW})$	0.90
Dermosol	$\chi = 1.02 + (0.0007 * T) - (8 * \sigma_{FW})$	0.89
Chromosol	$\chi = 1.01 + (0.001 * T) - (13 * \sigma_{FW})$	0.85

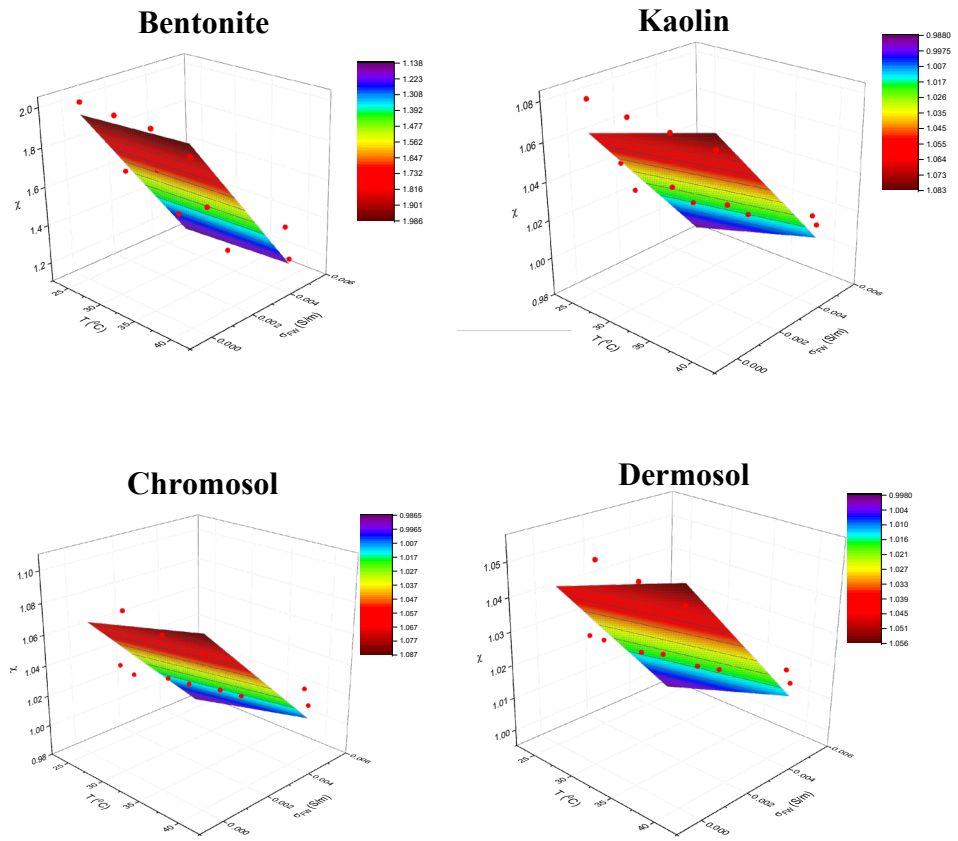
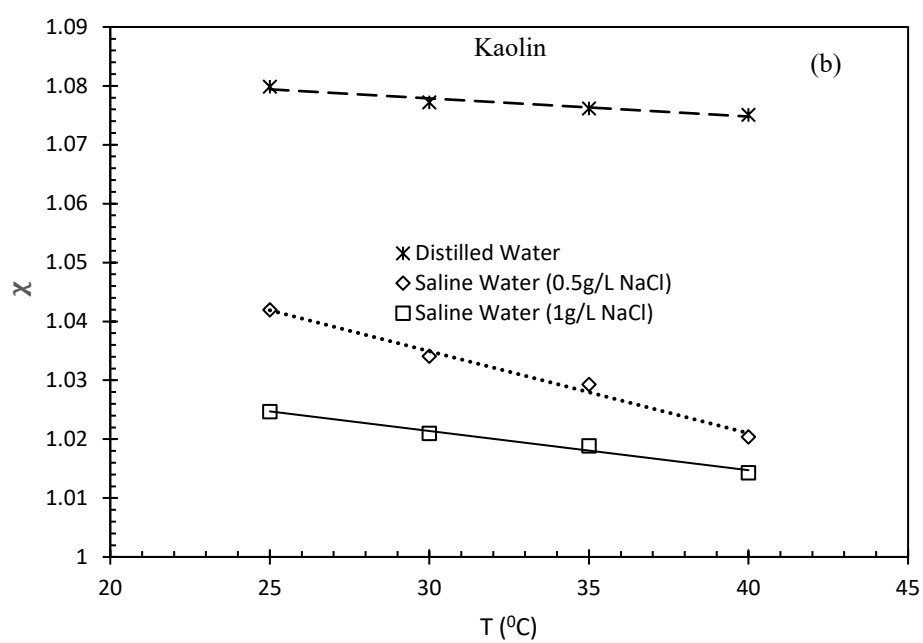
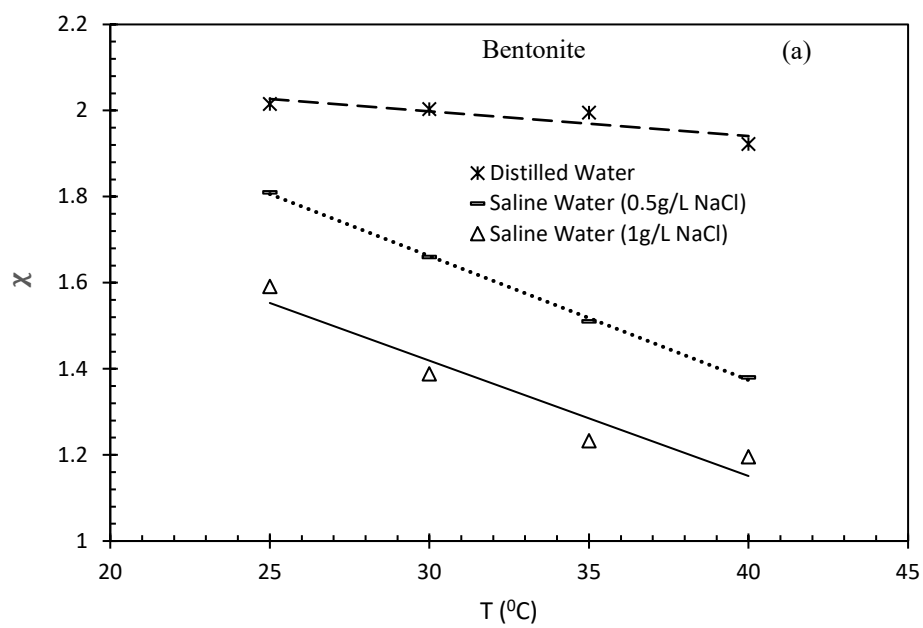


Figure 4.59: Behavioural changes in χ as T and σ_{FW} vary.

Table 4.19: Effect of temperature on the dielectric constant of water.

T (°C)	T (K)	D	DT
0	273	88	2.40×10^4
20	293	80	2.34×10^4
25	298	78.5	2.34×10^4
60	333	66	2.20×10^4

The dielectric constant is the ratio of permittivity of the substance to the permittivity in the free space, therefore D in [Table 4.4](#) doesn't have any unit ([Mitchell and Soga, 2005](#)). The small variations in DT values provide the basis of the statement by [Mitchell and Soga \(2005\)](#). [Table 4.4](#) represents D values based on some assumptions. [Sposito \(1989\)](#) showed that D of water in soil could be between 2 and 50, which casts doubt on the assumption of [Mitchell and Soga \(2005\)](#). Furthermore, it is known that the dielectric constant (D) of a substance (for example, water) decreases as the temperature increases. However, for soil, the dependency of D on the temperature is more complicated due to the existence of the surrounding or bound water. As the temperature increases, the molecular vibrations of the water and cations attracted to the soil particles can affect the dipole. In practical applications, the effect of the temperature on D is highly dependent on the type of soil.



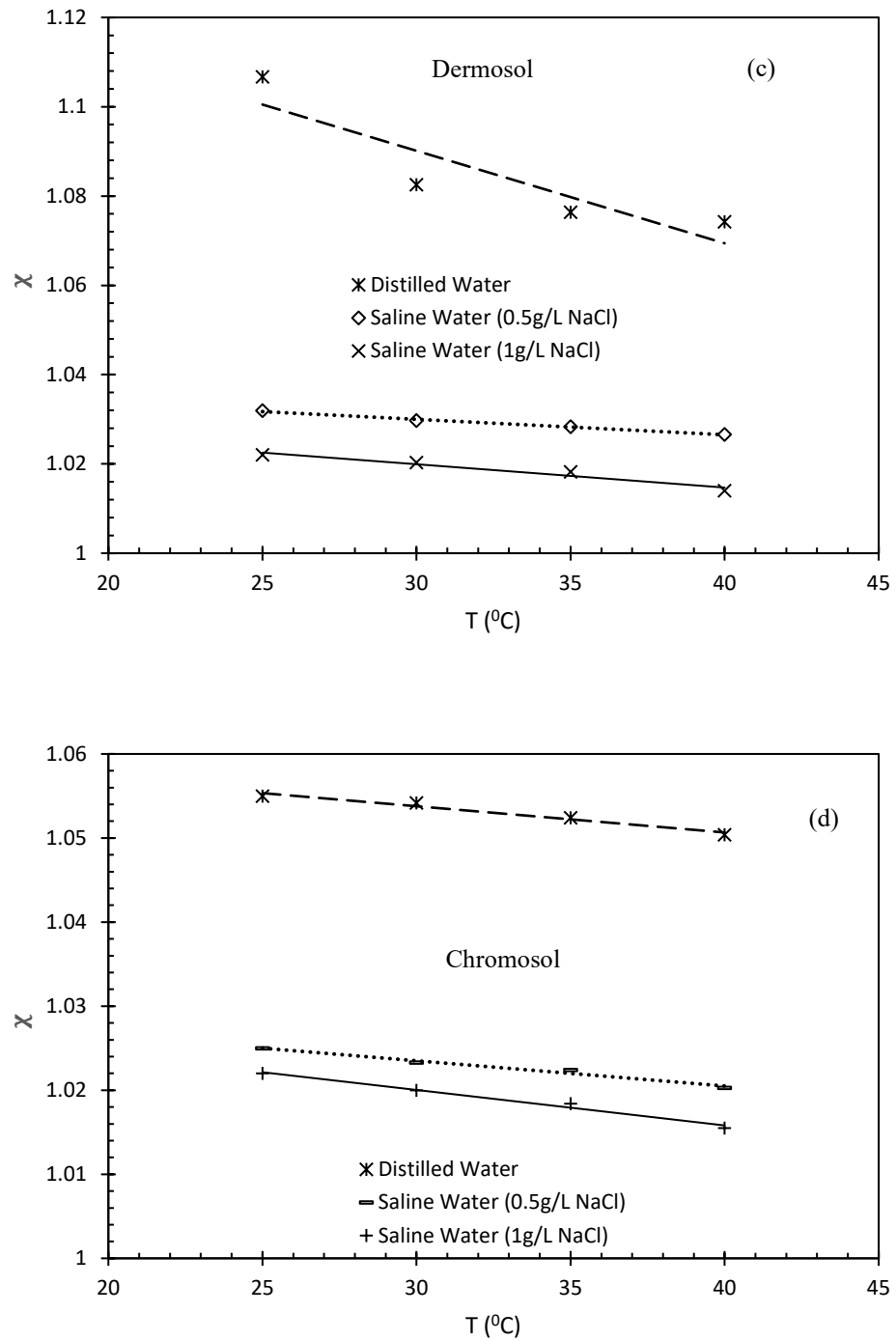


Figure 4.60: Effect of T on χ as the salinity of water changes for (a) bentonite, (b) kaolin, (c) dermosol, and (d) chromosol.

According to Seyfried and Murdock (2001) and Seyfried (2004), D can either increase or decrease significantly as temperature increases, but the impact will not be negligible. In

addition, the aforementioned statement was postulated, considering the Gouy-Chapman model for DDL (Gouy, 1910; Chapman 1913). The Gouy-Chapman theory for DDL has numerous limitations which do not consider the clay particles' interactions, electrical properties of water, hydration properties of clay, and interactive attractive forces (Sogami and Ise, 1984; Guven, 1992; Bharat et al., 2013). Furthermore, the properties of free water and DDL water are different. Therefore, the concept regarding the DDL thickness, presented with the Gouy-Chapman theory, has been subject to numerous criticisms which make the concept of the negligible impact of the temperature on DDL thickness doubtful. It should also be noted that none of these assumptions or theories was experimentally validated. Therefore, further evidence is needed which can be used as part of the validation of the effect of T on DDL.

The statement by Mitchell and Soga (2005) also contradicts the report provided by Zhang et al. (2004) who explained the changes in the thickness of DDL by linking with Atterberg limits (liquid limit and plastic limit). Zhang et al. (2004) stated that with an increase in temperature, the soil starts to dry out and goes through mechanical, physico-chemical and chemical transitions. One of the changes in the physico-chemical process involves the loss of the DDL layer, which also affects the Atterberg limits. Therefore, the thickness of DDL decreases with an increase in the temperature.

Based on the above discussion, it is clear that more evidence is required to support the observed behaviour of χ in this study which indicates that as temperature increases, DDL thickness decreases. For this purpose, a modified free swelling index test was used in this study to qualitatively validate the observed effect of temperature and water salinity on χ and DDL thickness.

4.5.3 Effect of Temperature and Water Salinity on FSI

Studying the impact of temperature on DDL thickness or changes in the size of the DDL is one of the prime objectives of this research. The theoretical assumptions and literature analyses have already been discussed. However, in order to establish confidence in the current theory, a simple experimental test (modified free swelling test) was conducted for all types of soils.

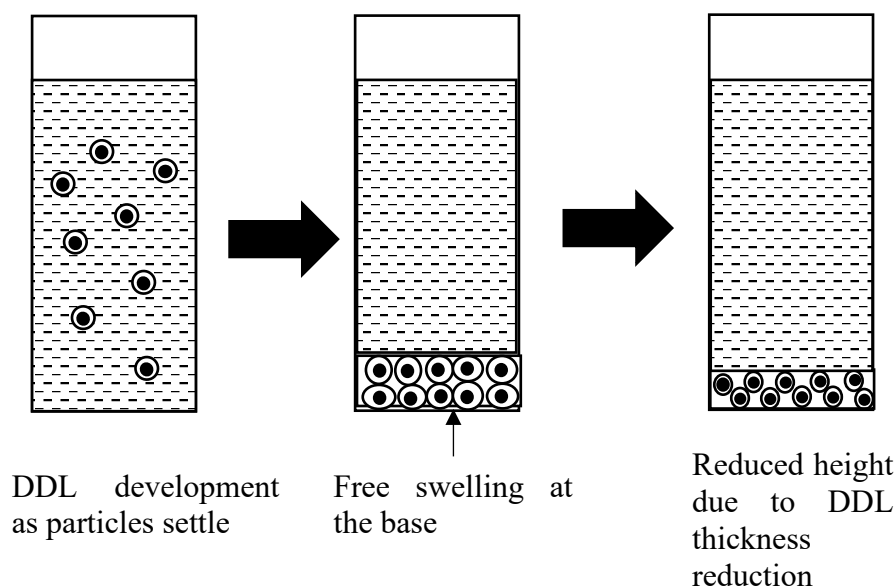


Figure 4.61: Schematic diagrams explaining DDL development and reduction in free swelling and DDL size due to temperature.

In the FSI test, when soil particles come into contact with water or fluid, the particles develop their own DDL and settle down as presented in the schematic diagrams in Fig.4.14. The volume of the settled soil comprises the volume of the solid particle, the DDL water, and the free water between the particles. By changing the temperature or/and water salinity of the FSI test, the change in the final settled volume is mainly a function of the geometric and electrical properties of the developed DDL water around the clay particles. In other words, if FSI decreases, the volume of DDL water also decreases and vice versa. Therefore,

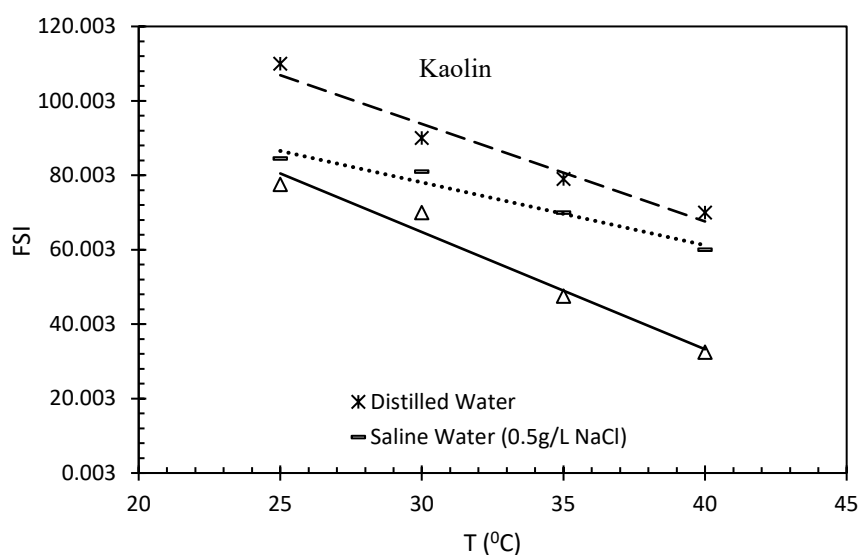
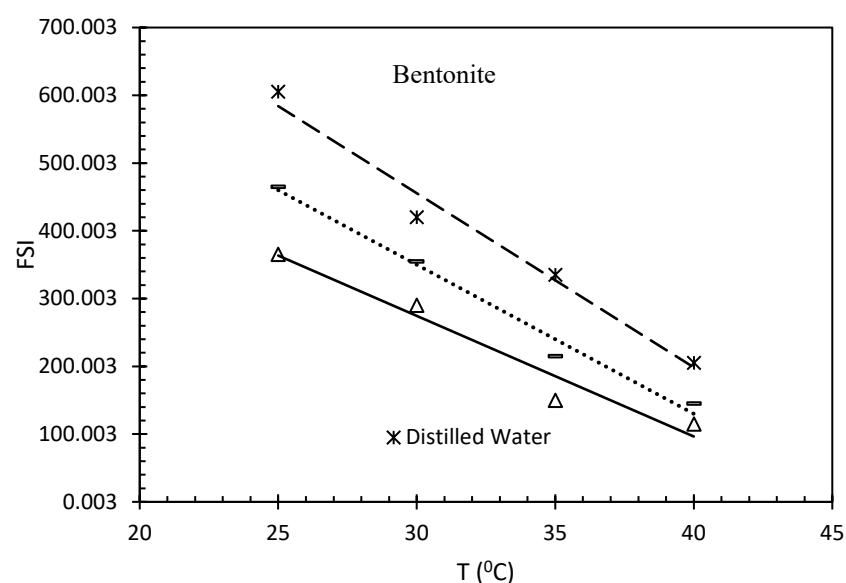
the FSI test can provide a qualitative indication of the effect of temperature and water salinity on DDL thickness.

The predominant forces, namely the attractive and repulsive forces among the clay particles play vital roles in affecting the size of the DDL. The physico-chemical interactions take place once the clay particles come in contact with the water, which leads to the formation of the adsorbed water layer. The adsorbed layer behaves similarly to a typical electrolytic solution which allows electrostatic interactions. The interactions lead to ion exchange between the negatively charged clay particles' surfaces and the pore water. Therefore, double layer repulsion is generated during the ion exchange, which is actually the electrostatic repulsion among the clay particles. An increase in the temperature significantly influences both attractive and repulsive forces, and as a consequence, the charges of the clay particles are changed. Heat also reduces the DDL thickness as well as the orientation of the soil particles (clay fabric) ([Almanza et al., 1996](#)).

The results of FS, as shown in [Table 4.2](#) and [Fig.4.15](#), indirectly indicate that as the temperature increases, the volume of DDL water (DDL thickness) decreases. However, the rate of decrement in the DDL thickness was more influenced for the saline water than the distilled water due to the cation exchange capacity and ion concentration in the water. The electrical conductivity of water also increases with an increase in temperature, therefore it was expected that surface conduction will increase. At the same time, an increase in temperature also caused the montmorillonite mineral to undergo microstructural deformation which led to the lower capacity of the adsorbed water than the initial condition. Therefore, the surface potential of clay increased as a function of the temperature and at the same time, the thickness of DDL decreased.

It should be mentioned here that while bentonite's DDL volume of water reduced from 1.81 to 1.38 from 25⁰C to 40⁰C (0.5g/L NaCl saline water), the changes were not effective for

kaolin, dermosol or chromosol. The explanation for this lies in the microstructural behaviour of the clay particles as none of the soils, apart from bentonite, have large electrical surface activities and low plasticity. Therefore, the reduction in DDL thickness was barely affected by the increasing temperature as these soils have low DDL in a room/laboratory-based temperature. This behaviour can be validated by the explanation of [de La Fuente et al. \(2000\)](#) and [Drief et al. \(2002\)](#), who explained that only bentonite undergoes significant changes in surface activities as a function of temperature ranging from 25°C to 150°C.



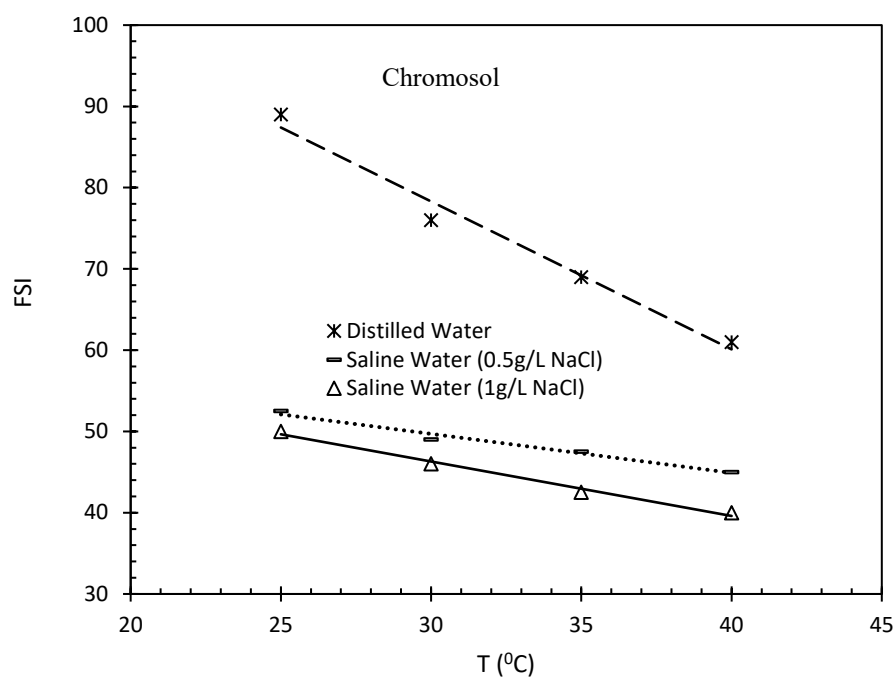
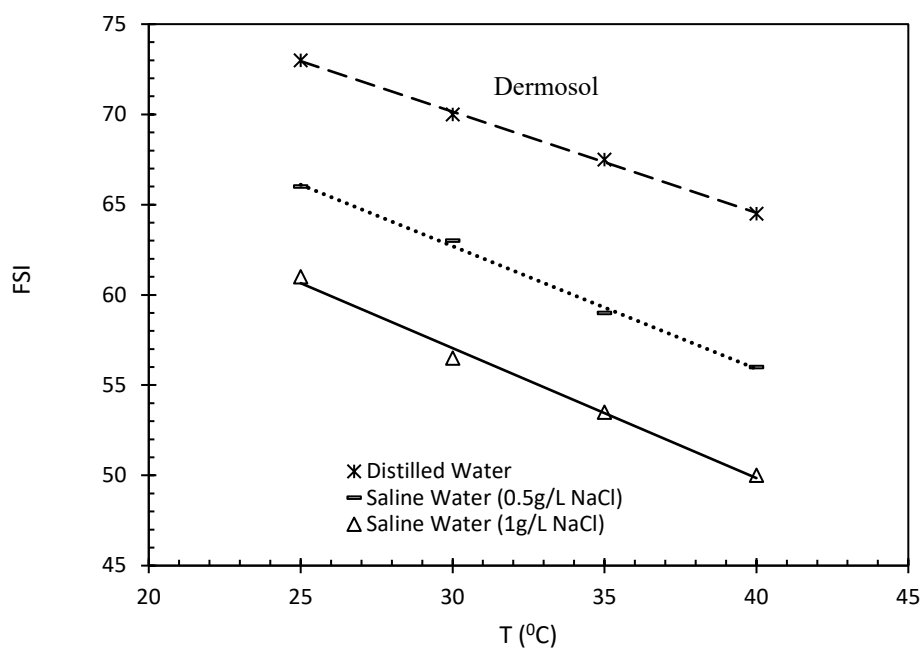


Figure 4.62: Effect of temperature on the FSI of soils.

Table 4.1 and Fig. 4.15 exhibit the experimental results achieved from this study on the effect of temperature on FSI. It was observed that bentonite demonstrated high FSI

compared to kaolin and the natural soils, namely chromosol and dermosol. Bentonite has a high liquid limit (504%) and plastic limit (53%). Bentonite consists mostly of montmorillonite or smectites and physically expands when it comes in contact with water. The other soils in this study have a liquid limit less than 100% and do not display a high swelling capacity. Kaolin is mainly composed of kaolinite mineral and has a low shrink-swell capacity, a liquid limit of 74%, a plastic limit of 32%, and low Cation Exchange Capacity (CEC) ([Al Rashid et al., 2018](#)) due to the chemical composition. Chromosol and dermosol have even lower liquid limits than kaolin, with measured values of 58% and 58.9%, respectively. Dermosol, in general, doesn't have a strong texture and is mostly siliceous, whereas chromosol is also siliceous but has a strong contrasting texture, which is due to the abrupt change in the texture of the soil between the topsoil and subsoil. In addition, none of the natural soils were strongly acidic or sodic ([Wang et al., 2015](#)). Since these soils have low liquid limits similar to kaolin, none of them demonstrated significant changes in their free swelling behaviour, regardless of the type of water used to prepare the suspension.

Furthermore, the effect of saline water on the FSI of bentonite was found to be more pronounced due to its high liquid limit and high expansion capability. The FSI of bentonite was observed to be 605% in distilled water at 25°C, however it decreased significantly to 365% at the same temperature when $\sigma_{fw}=0.002$ S/m (1g/L NaCl concentrated saline water). These significant changes are also in accord with the experimental works reported by [Shirazi et al. \(2005\)](#) and [Yukselen-Aksoy et al. \(2008\)](#), where the former showed that the liquid limit of bentonite decreased from 497% to 112% when distilled water was replaced by 0.5M of NaCl solution, and the latter demonstrated that the impact of saline water on FS is more pronounced when the soil has a liquid limit of more than 110%. Therefore, the aforementioned statements generally agree with the experimental results found in this study.

4.6 Summary

This chapter introduced two new parameters, namely the surface conduction parameter (σ_s) and the DDL volume ratio (χ). A simple experimental approach was proposed in this study to measure these new parameters. The effect of pore water salinity and temperature on these parameters was also investigated experimentally. The results show that surface conductivity (σ_s) increased with increasing salinity and DDL thickness decreased concurrently. However, as the temperature increases, the thickness of DDL decreases whereas σ_s increases.

To qualitatively validate this observation, modified free swelling index tests were conducted with the results showing that FSI decreases as the water salinity and temperature increase. The agreement between the physical meaning of the proposed surface conduction parameters and the FS experimental results give confidence in the finding of this study.

Chapter 5

Series-Parallel Structure-Oriented Electrical Conductivity Model of Saturated Clays

5.1 Introduction

A new series-parallel model for the electrical conductivity of saturated clays that considers particle structure orientation is presented in this chapter. The new model introduces a simple approach to consider the effect of the surface conductivity of clay particles on the electrical conductivity of saturated clays. The proposed approach considers a clay particle and its surrounding diffuse double layer (DDL) as a single unit called an effective clay particle, and assigns it an isotropic apparent electrical conductivity that can be determined using a simple experimental method. Therefore, the saturated clay can be considered as a two-phase material (binary mixture) namely, free pore water and effective clay particles. Considering the clay particles' structure orientation, the proposed electrical conductivity model in this study geometrically configures the components of two-phase saturated clays in a series-parallel form to determine the electrical conductivity of clay. The proposed electrical conductivity model uses one parameter that can be determined experimentally and it reflects the anisotropic condition of the clay fabric. The validity of the proposed model is verified by comparing its results with the experimental results of three different clay types reconstituted at different dry density levels and the particles' structure orientations. The comparison shows the accuracy of the proposed model in predicting the electrical conductivity of saturated clays.

Based on the theoretical assumptions of the concept of effective solid and apparent electrical conductivity, the surface conduction parameters were considered in this study, which were introduced in [Chapter 4](#). The electrical conductivity of clays was measured

from two different directions namely, vertical and horizontal and the level of anisotropy was also determined. In general, isotropic soils maintain consistency in the electrical conductivity values regardless of the direction of the measurement, whereas anisotropic soils exhibit discrepancies in horizontal and vertical electrical conductivity values in the same saturated soil samples. The experiment results in this study were in accord with the aforementioned statement, which serves as one of the validations of the proposed model. Furthermore, the inconsistency in vertical and horizontal electrical conductivity values was proved by determining the level of anisotropy of clay soils re-constituted in different compaction levels (dry density). In addition, it was also found that the electrical conductivity of soils from a vertical direction can also be predicted from the electrical conductivity of the same from a horizontal direction with one single reading, which provides more confidence in the accuracy of the findings in this study.

5.2 Background

Although there are many electrical resistivity/conductivity models in the literature, the empirical model of [Archie \(1942\)](#) is widely used for clay-free saturated porous media. For this type of soil, as the solid particles of soil are considered to be electrical insulators, the conduction of an electrical current through this saturated soil is mainly dependent on the geometrical characteristics of its voids network and the salinity of its pore water.

For saturated clays, the physico-chemical interactions between the electrically charged surface of the clay particles and the surrounding pore water create a DDL that surrounds the clay particles and possesses different electrical properties from the free water ([Mitchell and Soga, 2005](#)). This DDL creates a third phase in saturated clays that is usually considered as a two-phase material (solid particle and water). In fact, as the electrical conductivity of the solid clay particle is very low, the existence of DDL develops a surface electrical conduction on clay particles which plays an important role in the electrical conduction

behaviour of saturated clays. The surface electrical conduction of a clay particle is a function of clay mineralogy and electrolyte concentration in its pore water (Robain et al., 2003). The electrical conductivity of saturated clays shows anisotropy behaviour (Abu-Hassanein et al., 1996). Therefore, the electrical conductivity of saturated clays is a function of the clay particles' structure orientation (fabric).

Various models are available in the literature to predict the electrical conductivity of clay soils (Waxman and Smits, 1968; Rhoades et al., 1976; Rhoades et al., 1989; Revil et al., 1998; Linde et al., 2006; Mojid et al., 2007; Greve et al., 2013; Alsharari et al., 2020). To include the effect of the possible surface conduction of clay particles, most of these models use some empirical parameters that have no physical meaning and cannot be measured experimentally. Furthermore, there are very few electrical conductivity models that consider the anisotropy behaviour of electrical conductivity (Ellis et al., 2010). Therefore, there is a need to find an electrical conductivity model of saturated clays that considers the effect of surface conduction and the fabric of clays using model parameters that have physical meaning and can be determined using conventional laboratory experiments.

5.3 Proposed Model

5.3.1 Model Assumptions

The proposed electrical conductivity model of saturated clays in this study has the following assumptions:

- the proposed model is valid for organic-free clays only;
- the clay is fully saturated;
- the size and electrical properties of DDL water is clay-porosity independent;
- the voltage or electrical current applied during the electrical conductivity measurements have an insignificant effect on clay fabrics;

- increasing the density of clay has an insignificant effect on the preferred clay particle orientation (Meade, 1966; McConnachie, 1974; Martin and Ladd, 1975; Anandarajah and Kuganenthira, 1995);
- the electrical conductivity of a diluted clay-water system, where clay particles are not in contact, has an isotropic behaviour;
- the solid clay particle and its surrounding DDL water layer can be combined to form an effective solid clay particle that is assigned an apparent electrical conductivity (Tabbagh and Cosenza, 2007). Therefore, the saturated clay will consist of two phases, namely effective solid and free water.

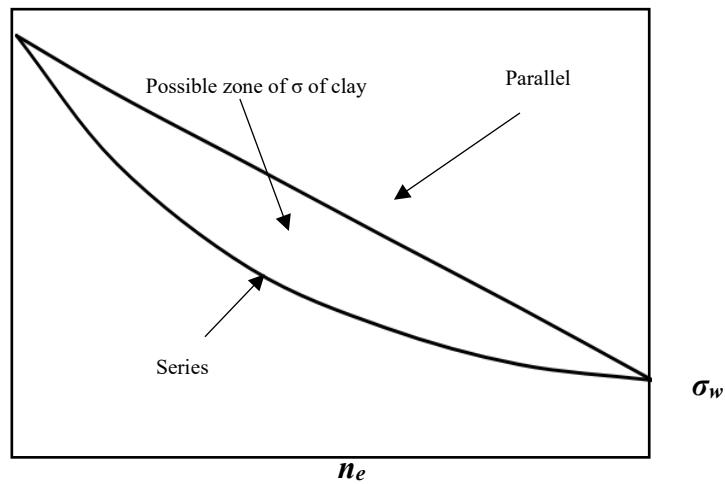
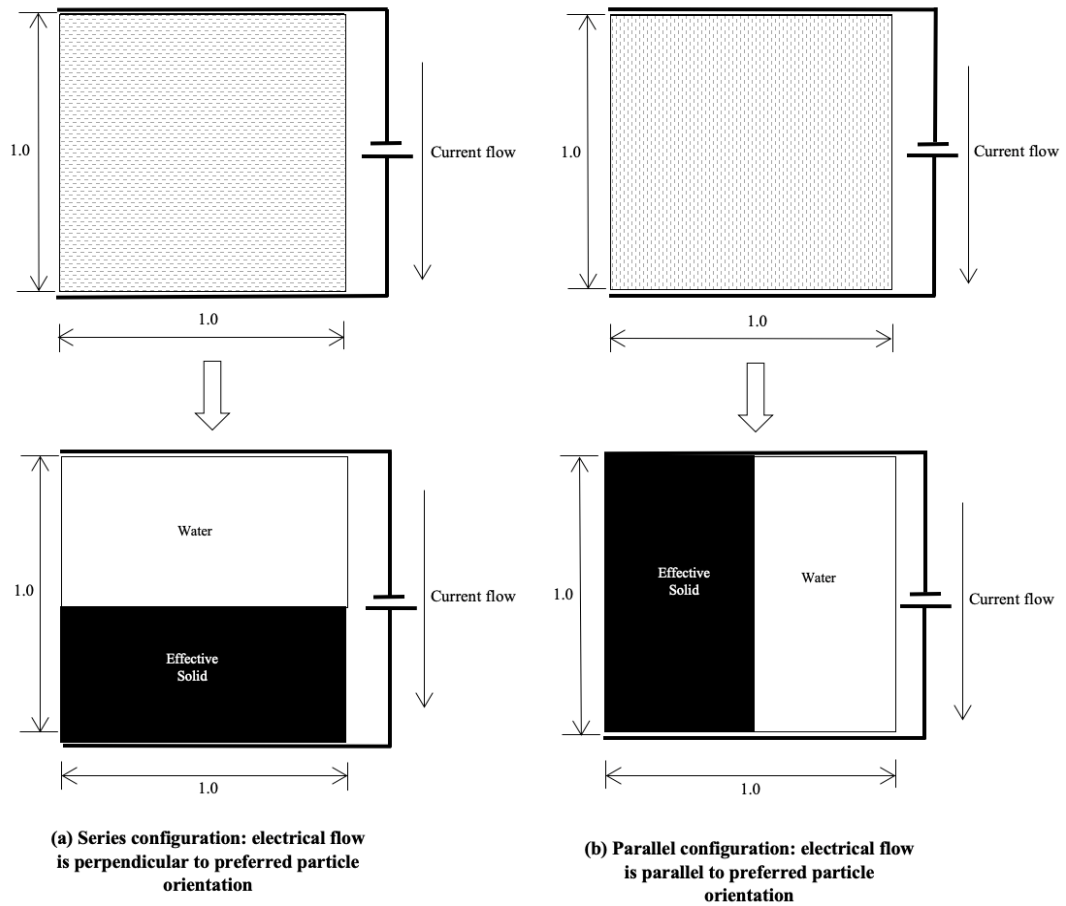
5.3.2. Model Formulation

The series and the parallel configurations express the condition where the electrical current flow is normal or parallel to the preferred particles' orientation, respectively. Using Ohm's law, the electrical conductivity for the parallel case σ_p^{vl} can be expressed as follows:

$$\sigma_p^{vl} = n_e \sigma_w + (1 - n_e) \sigma_s \quad (5.1)$$

where σ_w and σ_s are the electrical conductivities for water and effective solid particles, respectively. Following the same approach, the electrical conductivity for the series case σ_s^{vl} can be expressed as follows:

$$\sigma_s^{vl} = \frac{1}{\frac{1-n_e}{\sigma_s} + \frac{n_e}{\sigma_w}} \quad (5.2)$$



(c) Possible zone of σ of clay in $\sigma_{\text{mix}}-n_e$ plane

Figure 63: Series and parallel configurations of electrical conductivity of clay.

The two aforementioned special cases of electrical conductivity, σ_p^{vl} and σ_s^{vl} , can be considered as the upper and lower boundary limits, respectively, for the possible value of electrical conductivity of any material consisting of a binary mixture (Nielsen, 1974; McCullough, 1985), as shown in Fig. 5.1c. Therefore, the general model of clay can be

represented by a weighted combination of series and parallel configuration, as observed in Figs. 5.2a-b, where the expected possible three electrical current pathways (Figs. 5.2a-b) are included as follows:

- The first pathway is represented by the parallel effective solid phase in the parallel configuration where the solid and DDL water phases are merged together. Consequently, the volume and the electrical conductivity of DDL water are already incorporated into the model.
- The second pathway is represented by the series configuration of the effective solid phase and the free water.
- The third pathway is represented by the parallel free water in the parallel configuration.

The weightage of the contribution of both configurations (series and parallel) in the combined representative clay element can be expressed using a morphological parameter Ω which can be determined as follows:

$$\Omega = \frac{V^p}{V} \quad (5.3)$$

$$V = V^p + V^s \quad (5.4)$$

where V^p and V^s are the volumes of the clay in the parallel and series configuration, respectively. The morphological parameter Ω can also be seen as a parameter that establishes an intermediate behaviour between the two cases (series and parallel). Therefore, the vertical electrical conductivity equation of clay σ^{vl} can be expressed as follows:

$$\sigma^{vl} = (1 - \Omega)\sigma_s^{vl} + \Omega\sigma_p^{vl} \quad (5.5)$$

$$\sigma^{vl} = \frac{1-\Omega}{\frac{1-n_e}{\sigma_s} + \frac{n_e}{\sigma_w}} + \Omega[n_e\sigma_w + (1 - n_e)\sigma_s] \quad (5.6)$$

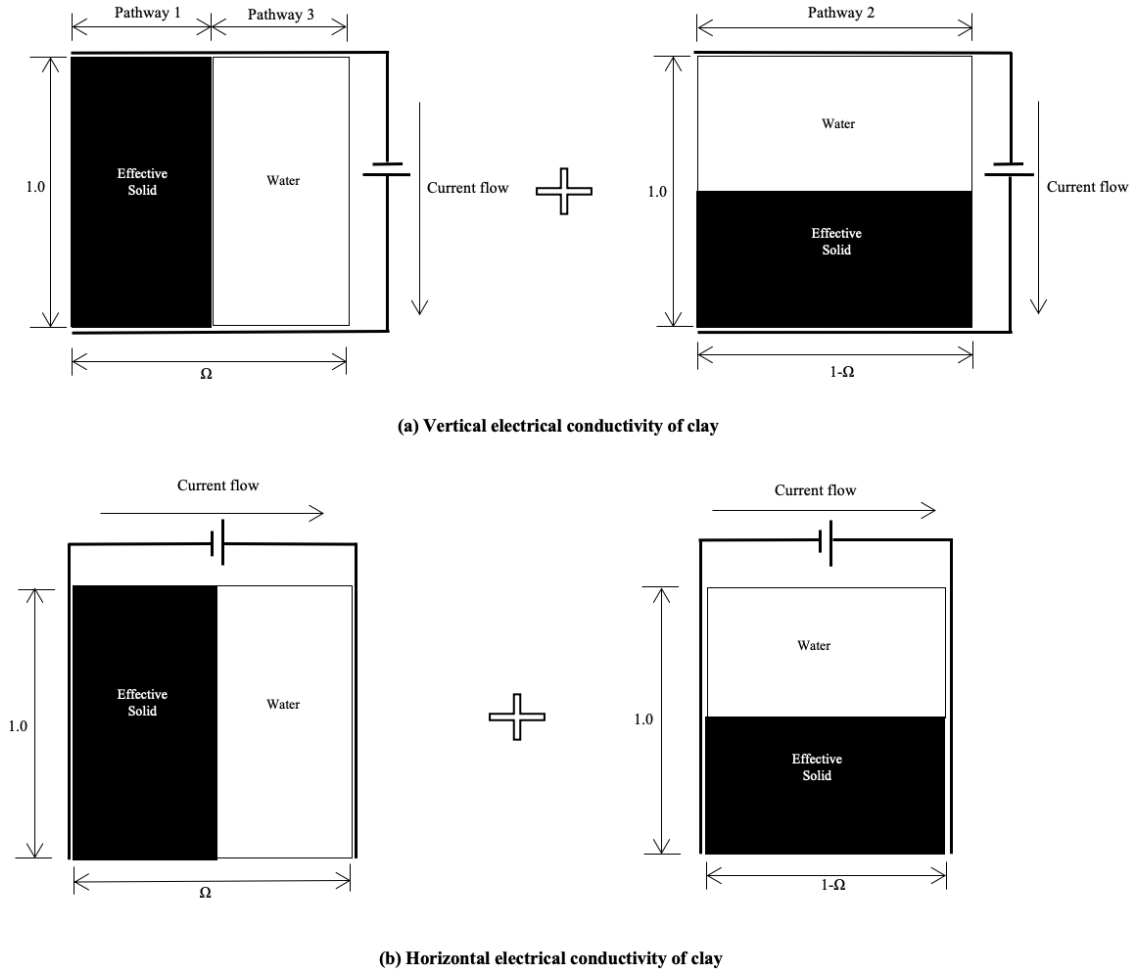


Figure 5.64: Proposed series-parallel electrical conductivity model for clays in this study.

Here, σ^{vl} is the electrical conductivity of clay in the vertical direction. It should be mentioned that for $\Omega = 1$ and $\Omega = 0$, Eq. 5.5 represents the perfect parallel and the perfect series flow models, respectively. However, the values of Ω between 0 and 1 represent the series-parallel flow condition in different combination degrees of the two extreme limits as shown in Fig. 5.1c. The space between the two extreme limits (series/parallel current flow) expresses the possible zone of the electrical conductivity value for the clay in $\sigma_{\text{mix}}-\eta_e$ plane. The morphological parameter Ω can be determined by re-arranging Eq. 5.5 as follows:

$$\Omega = \frac{\sigma^{vl} - \sigma_s^{vl}}{\sigma_p^{vl} - \sigma_s^{vl}} \quad (5.7)$$

The parts of the clay which are represented by series and parallel configurations under the vertical electrical current flow condition (Fig.5.2a) can be expected to act in parallel and series configurations, respectively, under the horizontal electrical flow condition as presented in Fig. 5.2b. Therefore, the horizontal electrical conductivity equation of clay σ^{hl} can be expressed as follows:

$$\sigma^{hl} = \Omega \sigma_s^{vl} + (1 - \Omega) \sigma_p^{vl} \quad (5.8)$$

$$\sigma^{hl} = \frac{\Omega}{\frac{1-n_e}{\sigma_s} + \frac{n_e}{\sigma_w}} + (1 - \Omega)[n_e \sigma_w + (1 - n_e) \sigma_s] \quad (5.9)$$

Therefore, for isotropic clays where $\sigma^{hl} = \sigma^{vl}$, the value of Ω should be equal to 0.5. The theoretical and experimental approach to determine surface conduction parameters σ_s and χ , as well as their influential roles in the soil conductivity model was demonstrated in section 4.2 in Chapter 4. Finally, the morphological parameter Ω can be determined using Eq. 5.9 where only one measurement of saturated electrical conductivity of clay σ^{vl} is required.

5.4 Laboratory Testing

5.4.1. Testing Materials and Experimental Programmes

Three different types of clay were used in this study to validate the proposed electrical conductivity model namely, kaolin, bentonite, and a kaolin-bentonite mixture (50% K- 50% B) by weight. The properties of kaolin and bentonite were shown in Figs. 3.1-3.2 and Table 3.1-3.6 in Chapter 3.

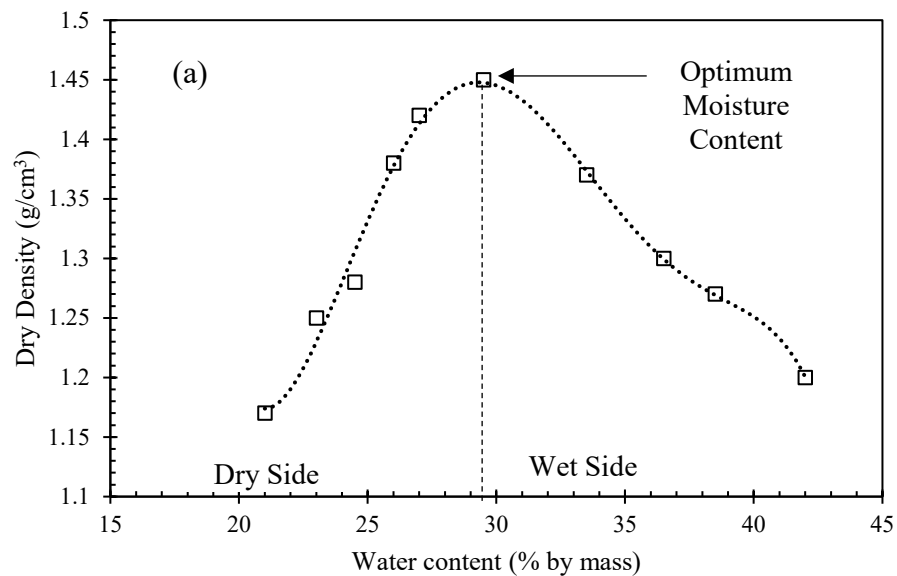
The experimental programme in this study comprise two parts. The first part determines the parameters of the proposed model χ , σ_s , and Ω whereas the second part assesses the validity of the proposed model in predicting the electrical conductivity of saturated clays.

For this purpose, a laboratory test was conducted to measure the surface conduction parameters χ and σ_s of the three tested clays in this study at four different salt concentrations in the water. The test results of this experiment are helpful in understanding the effect of clay mineralogy and pore water salinity on surface conduction. The second experiment involves the preparation of six compacted clay specimens for each clay type used in this study at different densities and clay fabrics. Then, their electrical conductivities were measured and compared with the proposed model predictions.

5.4.2. Test Setup and Procedures

To assess the effect of σ_w change on the surface conduction parameters χ and σ_s of the three tested clays (kaolin, bentonite, 50% kaolin+ 50% bentonite), four different salt concentrations in the water were used in this study.

For the validation experiment, saturated clay specimens were prepared at different dry densities (porosities) and particle orientations. The dynamic compaction approach using



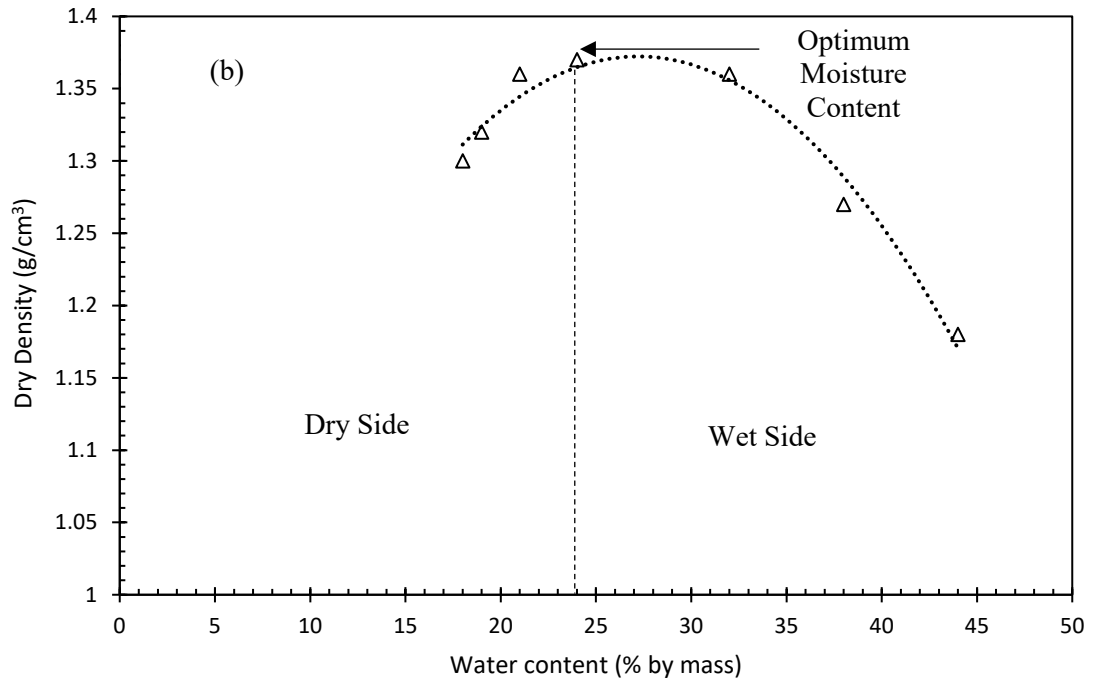


Figure 5.65: Dry density curve against different moisture contents for (a) kaolin, and (b) bentonite.

the standard proctor ([ASTM D698](#); [AS 1289.5.1.1:2017](#)) was used to prepare specimens at different dry densities by changing the compaction efforts (number of blows). Four different numbers of blows per layer (5, 10, 15, 25) were used in this study. Furthermore, the clay fabric (particle orientation) of the dynamically compacted clay specimen can be controlled by its moisture content during the orientation) is expected for a specimen with a moisture content below the compaction optimum moisture content (dry side), whereas dispersed fabric (perfect particle orientation) can be obtained for specimens compacted with moisture content larger than the compaction optimum moisture content (wet side). **Fig. 5.3** provides the curves highlighting the changes in dry density for both kaolin and bentonite at different moisture contents. Meanwhile, the assumption regarding clay particle orientation at different Ω is illustrated in **Fig. 5.4** for a better understanding.

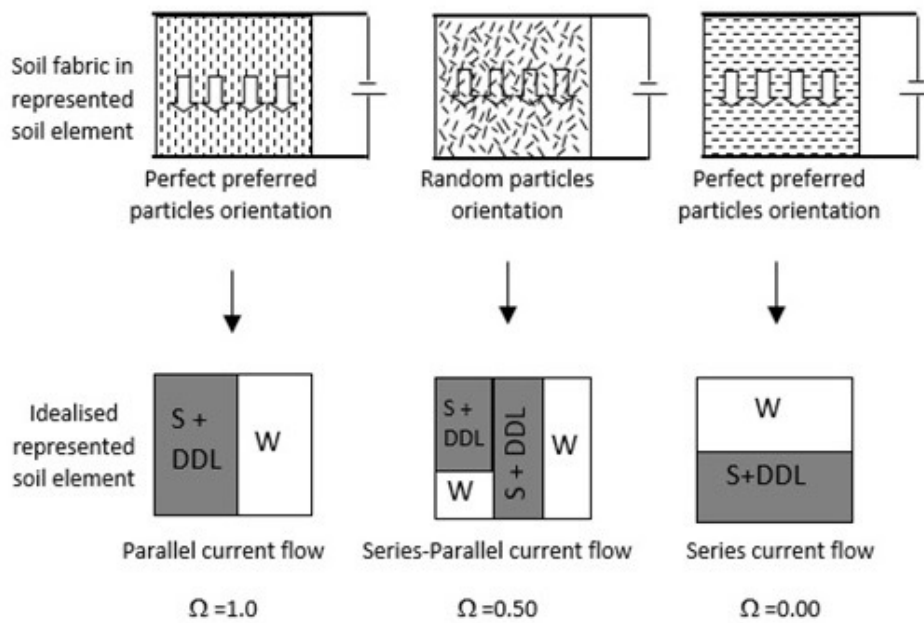


Figure 5.66: Assumption of particle orientation of clay fabric.

For each soil composition, a known mass of the dry sample was mixed with a specific amount of water to obtain the desired moisture content. In order to ensure uniform distribution of moisture, water was sprayed on each sample to reach the targeted water content (Fig. 5.5a-b). An automatic mortar mixer was used to guarantee the proper mixture of soil samples and water (Fig. 5.5c). After the mixing procedures, each sample was carefully placed inside air-tight bags at room temperature after 24 hrs for moisture equilibrium, as shown in Fig. 5.5d.



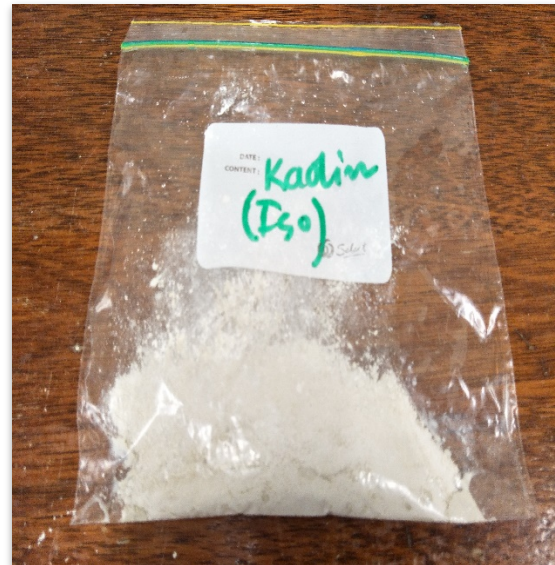
(a)



(b)



(c)



(d)

Figure 5.67: A sample procedure of mixing clay with water at a targeted moisture content: (a) spraying water to reach targeted moisture content, (b) mixing procedure of water with clay, (c) further mixing with mortar mixer, (d) some fractions of clay being transferred to sealed bag to ensure moisture equilibrium.

After the moisture equilibrium process, the compaction part was completed with the standard proctor. After the compaction process, the compacted specimens were placed in a

CBR soaking tank to fully saturate them, as shown in [Fig. 5.6](#). The electrical conductivity of the mixing and soaking water is 0.0014 Siemens per meter (S/m). The compacted moisture contents for the dry side and wet side specimens are listed in [Table 5.1](#). After this, each fully saturated compacted clay specimen was trimmed into two cylinders (3 cm in diameter and 6 cm in height) with their principal axes orientated vertical and horizontal to the compaction direction, as shown in [Fig. 5.7](#). The trimmed specimens were used to determine the vertical and horizontal electrical conductivity values σ^{vl} and σ^{hl} of each saturated compacted clay specimen using the four electrodes test setup ([Abu-Hassanein et al., 1996](#)). In this test setup, a one-dimensional electrical field was applied across the cylindrical specimen via circular plate electrodes pressed against the ends of the specimen and two inner electrodes inserted at equal spaces L along the height of the testing specimen to measure the electrical potential difference v as illustrated in [Fig. 5.7](#). The electrical conductivity σ can be expressed as follows:

$$\sigma = \frac{IL}{vA} \quad (5.10)$$

where I and A are the electrical current and the cross-sectional area of the test specimen normal to the current flow direction, respectively.

5.5 Results and Discussions

5.5.1. Model Parameters

[Table 5.1](#) reports the value of Ω for each clay type tested in this study. The values of Ω were calculated using [Eq. 5.9](#) for the clay specimen that was compacted using five blows. The results in [Table 5.1](#) demonstrate that the value of Ω for the clay specimen compacted dry of optimum was about 0.50, whereas the clay specimens compacted wet of optimum showed higher values of Ω (0.7 to 0.75). This result supported the concept of the effect of the moisture content on the fabric of compacted clay ([Lambe and Whitman, 2008](#)) as the

clay specimen compacted dry of optimum had an isotropic fabric, whereas the clay specimen compacted wet of optimum showed anisotropic fabric behaviour.



Figure 5.68: Saturation process inside a CBR soaking tank.

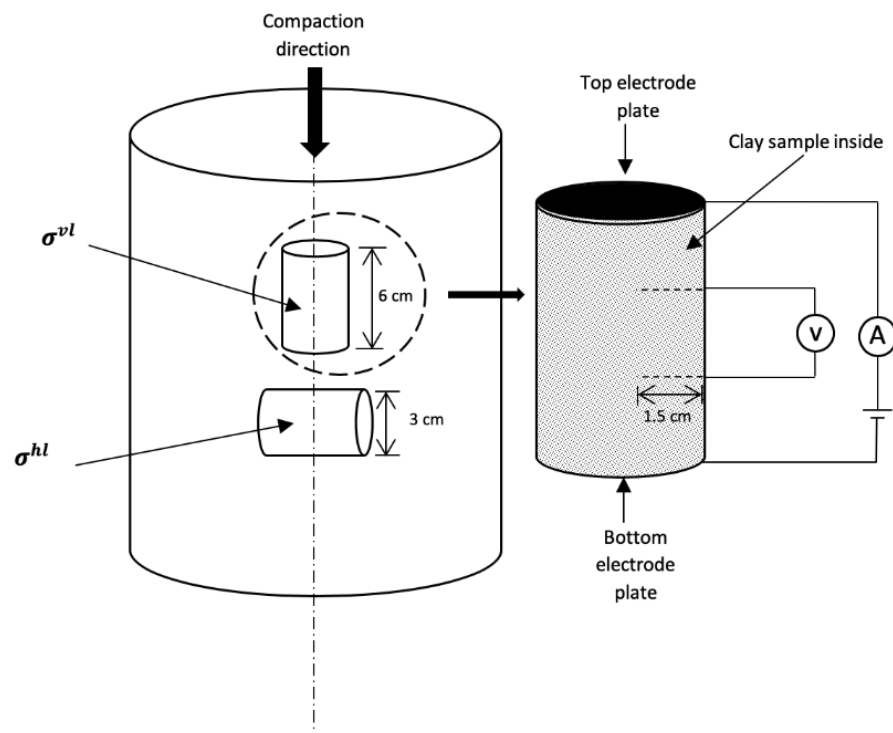


Figure 5.69: Arrangement for measuring electrical conductivity of saturated clays (σ^{vl} : principal axis orientated parallel to the compaction direction; σ^{hl} : principal axis orientated perpendicular to the compaction direction).

Table 5.20: Comparison of results for all three types of clay for both dry and wet of optimum water content tests

Testing clays		Initial W.C (%)*	χ	σ_w (S/m)	σ_s (S/m)	No of blows	Degree of Saturation, (%)**	Final W.C (%)**	n	n _e	σ^{hl} (S/m)	σ^{vl} (S/m)	σ^{vl} (% of σ^{hl})	σ_p^{vl} (S/m)	σ_s^{vl} (S/m)	Ω^{\dagger}
Kaolin	Dry	10.2	1.04	0.0014	0.00374	5	94.15	68.35	0.55	0.53	0.002471	0.002231	90.3	0.002499	0.0019832	0.48
						10	94.44	56.25	0.51	0.49	0.002500	0.002267	90.7	0.002593	0.0020561	
						15	94.47	51.75	0.48	0.46	0.002612	0.002379	91.1	0.002664	0.0021144	
						25	95.23	45.80	0.43	0.41	0.002758	0.002517	91.4	0.002781	0.0022192	
	Wet	40.1				5	94.50	60.95	0.54	0.52	0.005719	0.002362	41.3	0.002523	0.0020009	0.70
						10	95.46	54.95	0.50	0.48	0.006213	0.002448	39.4	0.002617	0.0020751	
						15	95.32	53.45	0.49	0.47	0.006432	0.002489	38.7	0.002640	0.0020946	
						25	95.67	43.72	0.41	0.38	0.007080	0.002704	38.2	0.002851	0.0022873	
Bentonite	Dry	10.3	1.81		0.082	5	97.29	80.80	0.69	0.44	0.026952	0.025146	93.3	0.046536	0.0031142	0.51
						10	97.41	67.47	0.65	0.37	0.030978	0.028748	92.8	0.052178	0.0036769	
						15	97.57	61.40	0.62	0.31	0.035936	0.032486	90.4	0.057014	0.0043508	
						25	97.94	55.33	0.56	0.20	0.044590	0.040963	91.9	0.065880	0.0065525	
	Wet	40.1				5	98.50	78.10	0.68	0.42	0.099362	0.036963	37.2	0.048148	0.0032566	0.75
						10	98.69	63.69	0.63	0.33	0.115385	0.0435001	37.7	0.055402	0.0041003	
						15	98.80	58.30	0.60	0.28	0.131268	0.0487004	37.1	0.059432	0.0047898	
						25	98.23	53.30	0.54	0.17	0.158881	0.0567668	35.7	0.068298	0.0076016	
50% K+50% B	Dry	10.3	1.24		0.0419	5	95.27	75.81	0.64	0.55	0.011597	0.010634	91.7	0.019625	0.0024777	0.48
						10	95.38	65.81	0.60	0.50	0.013129	0.011882	90.5	0.021650	0.0027094	
						15	95.63	59.60	0.57	0.47	0.014674	0.013119	89.4	0.022865	0.0028706	
						25	96.00	50.91	0.50	0.38	0.016731	0.015073	90.2	0.026510	0.0034937	
	Wet	40.1				5	96.07	73.60	0.63	0.54	0.037972	0.014940	39.4	0.02003	0.0025208	0.72
						10	96.75	62.21	0.58	0.48	0.048325	0.017542	36.3	0.02246	0.0028148	
						15	97.05	56.50	0.55	0.44	0.056517	0.019668	34.8	0.02408	0.0030520	
						25	97.25	49.54	0.49	0.34	0.070165	0.026123	34.9	0.02813	0.0038668	

W.C.= Water content by mass

* at the dynamic compaction stage

** at the end of saturation process

[†] Calculated using the test results of No. of blow

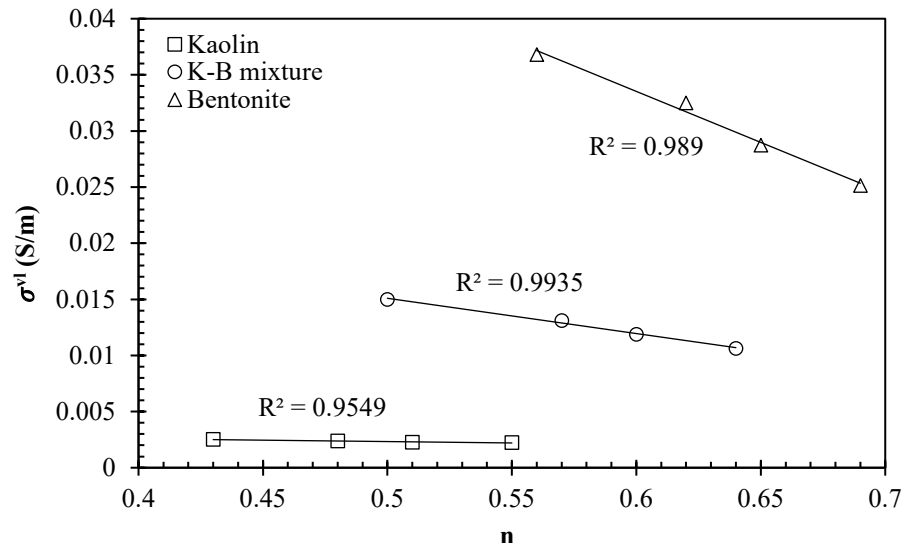
5.5.2. Electrical conductivity measurements and model validation

Table 5.1 and Figs. (5.8-5.9) present the measurements of the vertical and horizontal electrical conductivities σ^{vl} and σ^{hl} of the clay specimens compacted dry and wet of optimum. The results in Figs. 5.8 and 5.9 show that the compactability of kaolin is better than bentonite as the porosity of kaolin (0.55 to 0.41) is smaller than bentonite (0.69 to 0.54). This behaviour is attributed to the effect of clay plasticity on its compactability, which decreases as plasticity increases (Lambe and Whitman, 2008).

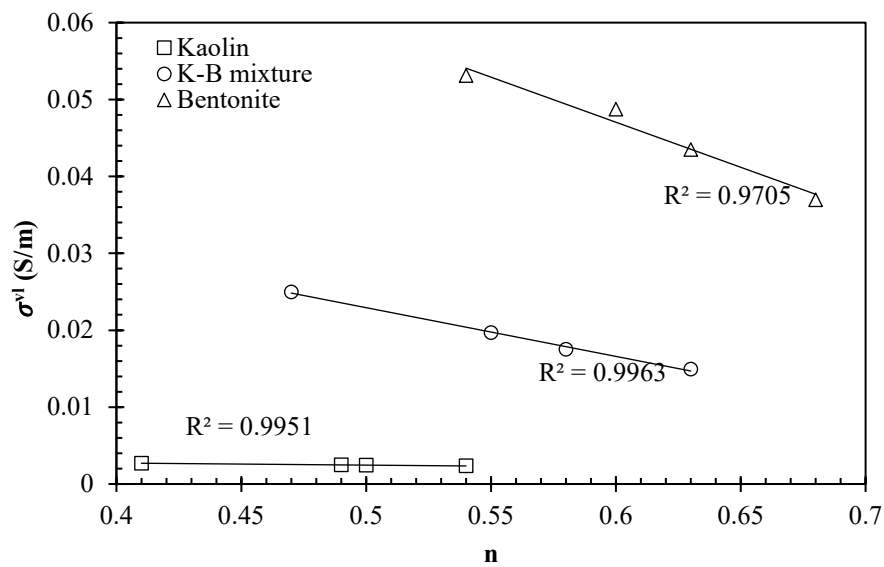
The results imply that for bentonite and the kaolin-bentonite mixture, electrical conductivity increased as porosity decreased. However, changing the porosity of kaolin has an insignificant effect on its electrical conductivity. For bentonite and the kaolin-bentonite mixture, as the electrical conductivity of their effective solid σ_s is much larger than the electrical conductivity of the free pore water σ_w , reducing the clay porosity (volume of free pore water) should increase the electrical conductivity of clay. In fact, it should be mentioned that the rate of change of the clay electrical conductivity as its porosity decreased should be a function of the ratio σ_s / σ_w . As this ratio increases, the rate of change of the clay electrical conductivity will be higher. Therefore, as bentonite had σ_s / σ_w larger than σ_s / σ_w of K-B mixture and kaolin, its rate of change should be larger as illustrated in Figs. 5.6 and 5.9. Furthermore, for the case where $\sigma_s / \sigma_w = 1.0$, changing the clay porosity will have no effect on its electrical conductivity.

The results of the ratio of $\sigma^{vl} / \sigma^{hl}$ as listed in Table 5.1 indicates that the clay specimens compacted dry of optimum had almost isotropic electrical conductivity behaviour as the values of $\sigma^{vl} / \sigma^{hl}$ were very close to 1.0. On the other hand, the clay specimen compacted wet of optimum showed anisotropic electrical conductivity behaviour. This outcome supported the physical meaning of the proposed morphological parameter Ω in this study.

Furthermore, the results in Table 5.1 show that σ^{vl}/σ^{hl} was almost independent of the number of blows. Therefore, the assumption made in the proposed model regarding the insignificant effect of clay density change on the preferred particle arrangement was reasonably correct.

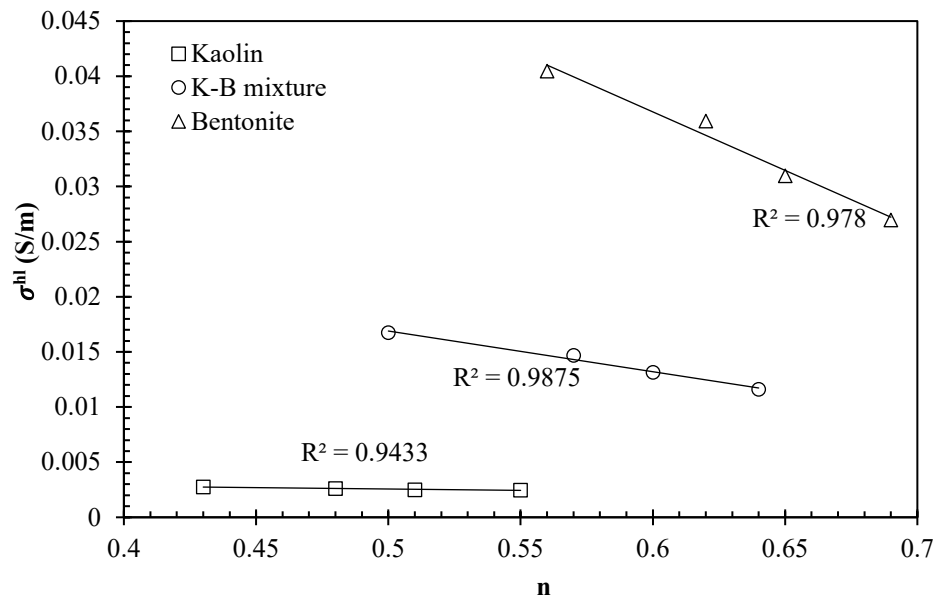


(a) Isotropic

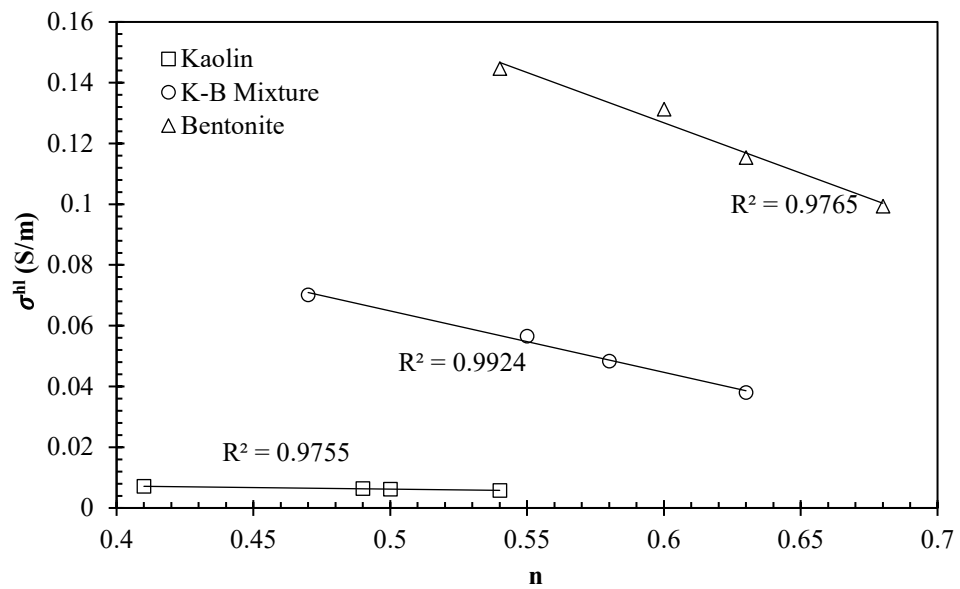


(b) Anisotropic condition

Figure 5.70: Variation of σ^{vl} at different porosities (n).



(a) Isotropic



(b) Anisotropic condition

Figure 5.71: Variation of σ^{hl} at different porosities (n) for (a) isotropic, and (b) anisotropic condition.

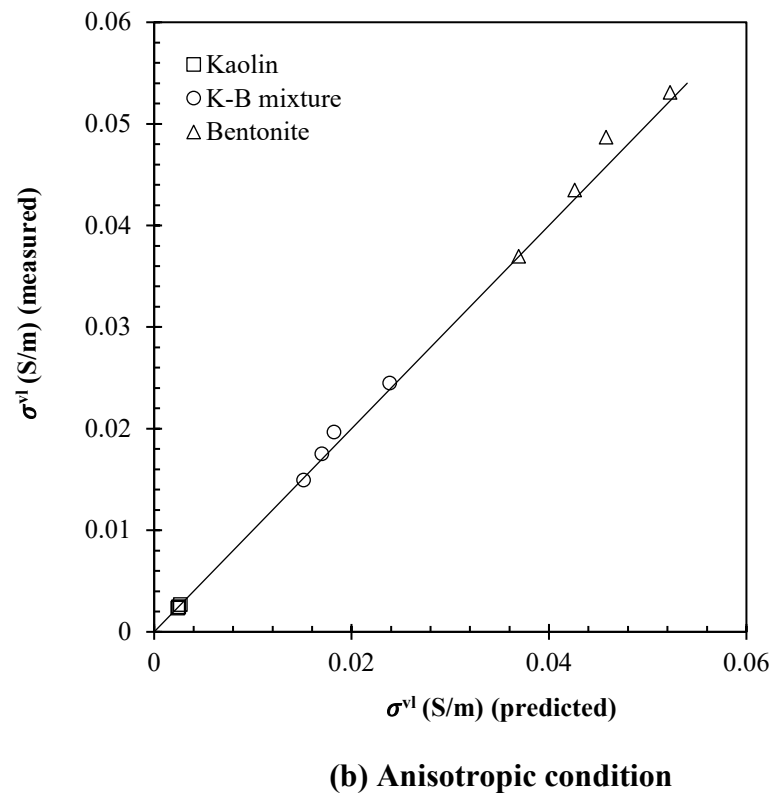
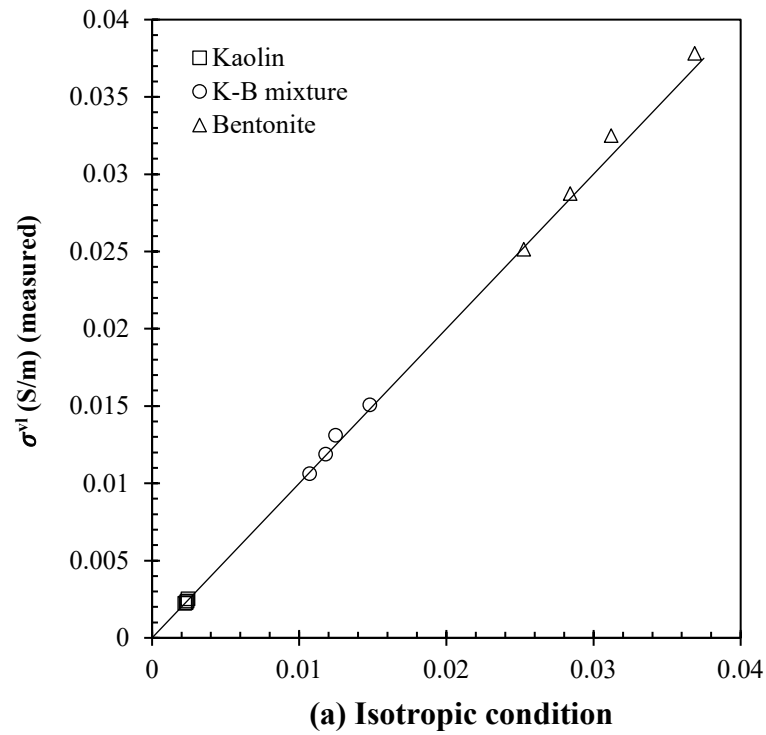
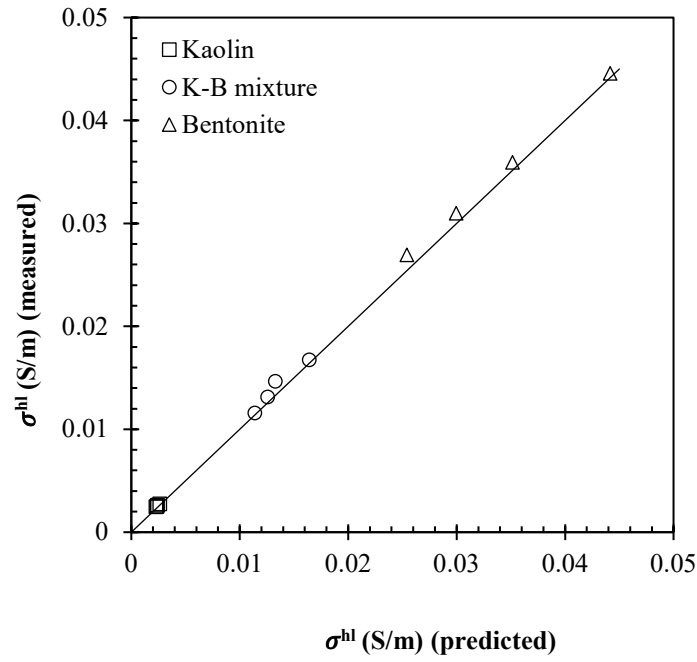
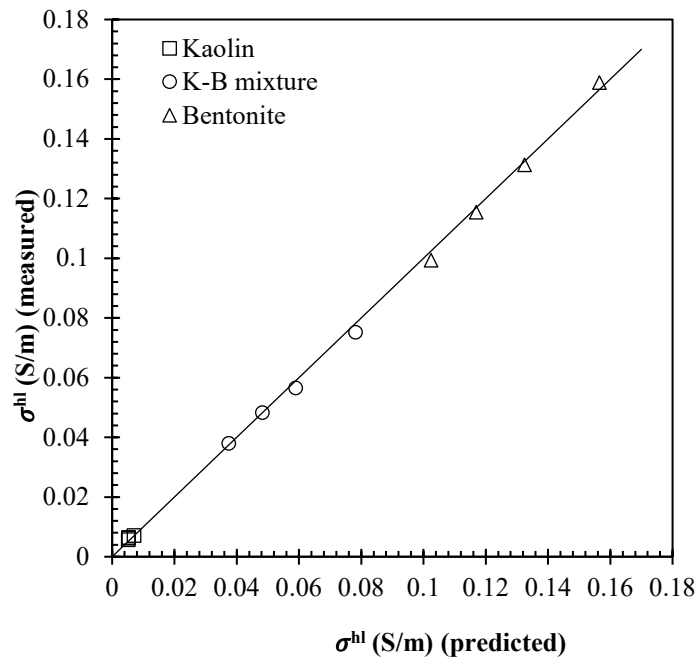


Figure 5.72: Agreement between predicted and measured values of σ^{vl} for (a) isotropic, and (b) anisotropic conditions (the straight line is the identity line).



(a) Isotropic condition



(b) Anisotropic condition

Figure 5.73: Agreement between predicted and measured values of σ^{hl} for (a) isotropic, and (b) anisotropic conditions (the straight line is the identity line).

Using the model parameters listed in [Table 5.1](#) for each clay type tested in this study, the vertical and the horizontal electrical conductivity σ^{vl} and σ^{hl} were predicted using the model proposed in this study ([Eqs. 5.6 and 5.9](#)). Good agreement between the electrical

conductivity measurements and the proposed model predictions is illustrated in Figs. 5.10 and 5.11. In fact, the ability of the proposed model to predict the horizontal electrical conductivity of the clay σ^{hl} simply by using the proposed morphological parameter Ω which was obtained from one measurement of σ^{vl} is the most important achievement of this model as it gives more confidence in the proposed physical meaning of Ω in terms of its configuration of the clay structure and its effect on the anisotropic behaviour of the electrical conductivity of clay.

5.6 Summary

A simple new electrical conductivity model for saturated clays has been presented after considering the effect of the surface conductivity of clay particles. A clay particle and its surrounding DDL were represented as an individual unit in this experiment. The electrical conductivity model was considered to have two-phase materials, free water and effective clay particles, and the model was represented in a series-parallel configuration together with mathematical expressions. The proposed model was validated by comparing the theoretical results with the experiment results for three different clays (bentonite, kaolin, and 50% bentonite+50% kaolin). The good agreement in the comparison validates the accuracy of the proposed electrical conductivity model for saturated clays. However, the model can be extended further, considering soils instead of only clays and observing the changes in electrical conductivity of soils at different temperatures.

Chapter 6

Particle Size Distribution of Soils using the Electrical Conductivity Technique

6.1 Introduction

In this study, a new method to determine the particle size distribution (PSD) of soils is introduced by considering the electrical conductivity (EC) technique. The proposed method considers the conventional sedimentation theory and Stokes' law to determine particle diameter, and at the same time, the EC of soil-water homogeneous suspensions is calculated at different densities for the purpose of calibration. The calibrated EC values are recorded for different densities of soils and later these values are utilised during the conventional sedimentation process. As the particles start to settle down at the base due to gravitational sedimentation, the EC is measured at different depths and the corresponding EC values are then matched with the calibrated EC values at different densities, therefore the density of the solid is determined. The PSD curve is then obtained using Stokes' law and the particles' passing formula is used for the hydrometer or pipette method. The PSD analysis using the EC approach is later compared with that of the hydrometer, pipette, and laser diffraction methods, and in general, good agreement was obtained for identical soil samples. The proposed approach is able to produce the PSD curve of each soil within just 2 hours, which is a major advantage over the conventional sedimentation methods.

PSD is a fundamental property of any sedimentary material. In general, the dynamic situations of transport and the properties of the constituent particles of rocks are usually determined from their size. The distribution is an essential property for analysing the behaviour of granular material under any applied fluid or gravitational forces.

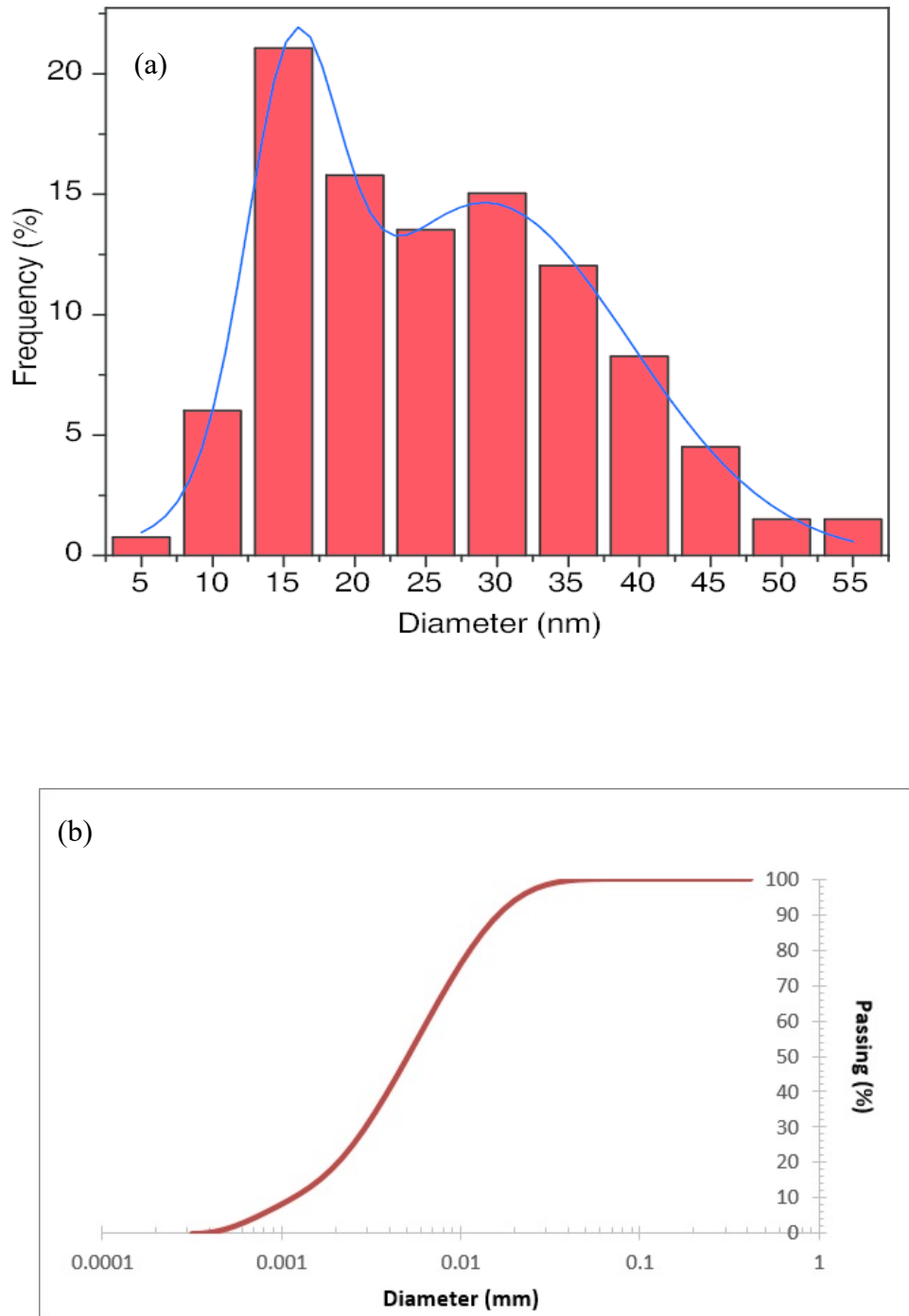


Figure 6.74: Particle size analysis by (a) Histogram of colloidal gold nanoparticles (Link and El-Sayed, 1999), and (b) Cumulative plot on log-scale (x-axis).

A conventional PSD analysis involves the determination of the mass fractions of clay, silt, and sand. These mass fractions can be presented as a histogram (Fig.6.1a) or as a cumulative plot (Fig.6.1b). For both plots, the same particle size axis can be utilised. In the

histogram plot, the area of each rectangle corresponds to the amount of soil particles and the width of the rectangle refers to the width of the size class. If there are significantly more rectangular bars in the histogram, a smooth curve can be drawn to show the PSD. On the other hand, a cumulative plot represents the amount of particulate matter belonging to particles below a specified size. The y-axis of this plot is generally expressed as a percentage, with 100% corresponding to the entire amount of the measured particles in the soil sample.

In most PSD analyses, soil particles are considered to be spheres as of all the solid bodies, only a sphere has a single characteristic linear dimension. Irregularly shaped particles may have different properties from which various distinctive linear dimensions can be acquired. The different properties include a particle's projected area, volume, settling velocity, length, and the size of the pathway through which the particle will pass ([Syvitski, 2007](#)). The dimensions of these properties are of course not counterpart to the actual PSD, but these are usually discounted. In civil engineering, engineers deal with geological samples and find the PSD of the given sample. It does not necessarily represent the whole population or properties. Geological materials generally comprise particle sizes ranging from tens of millimetres down to clay of colloidal ($<1\ \mu\text{m}$) size.

Most of the PSD test is performed in the laboratory. However, for better explanation and understanding, the PSD methods are divided into two categories, namely classical and modern techniques. The classical techniques include sieving and sedimentation. Two traditional sedimentation techniques namely, the hydrometer and pipette method are still popular among researchers as they are less expensive and readily available. On the other hand, the standard method of PSD determination involves a combination of sieving and hydrometer. The modern approach to PSD analysis involves expensive and automated devices such as laser diffraction and SediGraph, with each piece of equipment having

distinct disadvantages as discussed in [section 2.6](#) of [Chapter 2](#). Therefore, the need to identify a less expensive, easy-to-implement and accurate method of PSD determination is still open.

Although there have been numerous attempts to find alternative methods for the PSD analysis of soils, a method based on the electrical resistivity/conductivity of soils has not yet been considered. Since electrical conductivity is a function of soil mineralogy, and each soil exhibits unique electrical conductivity, this could be another option for the PSD analysis of soils. In general sedimentation theory, soil particles are allowed to fall freely due to gravity, and thus variation in the density can be recorded. A hydrometer directly provides the overall density of the suspension which varies with time due to the free fall of the soil particles' sedimentation. From the suspension's density, the density of the solid is determined. With the density of the solid, the percentage of passing of soil particles corresponding to the measured diameter can be calculated. As the particles start to fall freely, the presence of soil particles will be different at different depths. Therefore, the electrical conductivity is also different. Considering the fundamentals of sedimentation theory, it could be possible to establish a connection between the density and electrical conductivity of soil suspension.

The purpose of this chapter is to introduce a new technique to determine the PSD of soils using electrical conductivity. The method, which is based on conventional sedimentation theory, records the changes in electrical conductivity of a homogeneous suspension as a function of density for calibration purposes and aims to predict the density of solids from the calibrated, temporal electrical conductivity values of each soil at different depths. Although the method is conducted in a similar environment as the hydrometer or pipette, the sedimentation process remains uninterrupted. The procedure yields continuous readings

of the electrical conductivity of soils, but it does not require any complicated mathematical formulation or statistical analysis.

In the following, first, the theory of sedimentation is re-visited, followed by the introduction of the new approach to determine the PSD of soils, before discussing the manufacturing of the new probe, the experiments and the results.

6.2 Proposed Theory

The proposed approach is similar to the sedimentation theory, but instead of following the hydrometer or pipette method, the electrical conductivity of the suspension is included in the experiment to determine the density of the soil suspension at different times. At the beginning of the sedimentation, the soil particles are homogeneously dispersed throughout the suspension, therefore the concentration of soil particles of different sizes should remain consistent at different depths. After a certain period of time, only unsettled particles remain at a certain depth. In other words, all particles larger than a particular size D will settle below a certain depth. The following equation is utilised to find the diameter of the particle:

$$d = \sqrt{\frac{18\mu h}{g(G_s - \rho_L)t}} \quad (3.1)$$

Where, G_s is the specific gravity of the material, g is the acceleration due to gravity, h is the distance a particle travels in time t , then $v=h/t$, μ is the viscosity of the water.

The size of particle D can be calculated using Stokes' law as described in [Eq. 3.1](#) and the passing of soil particles is calculated from the following equation ([Arora, 2008](#)):

$$N = \left(\frac{G_s}{G_s - 1} \right) \cdot \frac{\rho_s - \rho_f}{M_s} \times 100 \quad (3.2)$$

where ρ_s is the density of the solid, M_s is the mass of the soil, and $G_s (= \frac{\text{unit weight of solids}}{\text{unit weight of water}})$

is the specific gravity, which is considered to be 2.58 for kaolin and 2.68 for bentonite, as confirmed by the supplier.

The proposed approach utilises this theory of sedimentation and relies on Eqs. (3.1-3.2) to find the PSD, similar to the hydrometer or pipette method. However, the proposed approach is highly dependent on the electrical properties of soils, such as soil conductivity or resistivity. It is necessary to perform the calibration by finding the electrical conductivity of the suspension at different densities. Later, these calibrated data are used to predict the density of the solid from the electrical conductivity values.

The experiments comprise three parts. The first part requires pre-treatment to prepare the soil samples for both the calibration and the experimental analysis. After the pre-treatment, the samples are calibrated at different amounts of soil samples (nearest to 0.1 g). In the final part of the experiment, the PSD is calculated and comparisons are made with other approaches.

6.3 Experiments

6.3.1 Testing Materials and Tools

The testing materials comprise soil samples, a dispersion agent, and the device to analyse the PSD. Soil samples consist of natural soils from different locations in Australia and laboratory-suited clays from industry.

The physico-chemical properties of natural soil samples are presented in Table 6.1. The geotechnical properties of kaolin and bentonite were detailed in Chapter 3. The soils characterise a wide range of textures with clay contents ranging from 15% to 37%. All are top soils and were collected within 0-25 cm depth of the ground. The natural soils were

collected from AgriBio Industry at La Trobe University and were subject to chemical pre-treatment procedures following the standard demonstrated by [Head \(1980\)](#) and [Arora \(2008\)](#).

In addition to the proposed approach, three other PSD analyses were conducted using hydrometer, pipette and laser diffraction techniques for each soil sample. The results of the other PSD approaches are considered as part of the validation of the proposed approach.

6.3.2 Role of Dispersion Agent

As Stokes' law is influential in sedimentation analysis, the individual soil or clay particles must be dispersed to ensure PSD accuracy. However, the finer grains of soil carry charges on their surface, therefore there is a chance of forming flocs. As a consequence, instead of considering the diameter of the individual grain, the grain diameter obtained will be equal to the flocs diameter, which will jeopardise the purpose of the experiment. Therefore, in sedimentation analysis, dispersion agents are added. In other words, the dispersion agent ensures the proper separation or dispersion of discrete particles of soil, especially from the silt to clay range.

Table 6.21: Physical and chemical properties of three natural soils considered in this study.

Soil name	Location	Clay content (%)	Organic C/g/kg ⁻¹	pH (0.01M CaCl ₂)
Dermosol	Kinglake, VIC	33	69.2	4.3
Vertosol	Horsham, VIC	37	15.9	7.1
Chromosol	Culcairn, NSW	15	15.8	4.6

A small quantity of soluble chemical is added before the commencement of any sedimentation test, generally in the form of a certain amount of a prepared solution. In most of the experiments, sodium hexametaphosphate (also commercially known as Calgon), is considered to be one of the most appropriate and convenient dispersants (Head, 1980; Arora, 2008; Ryżak and Bieganski, 2011). However, the choice of dispersion agent solely depends on the type of soils which are used in the test. The properties of Calgon are presented in Table 6.2.

Table 6.22: Properties of sodium hexametaphosphate.

Empirical formula	$\text{Na}_6\text{O}_{18}\text{P}_6$
Molecular weight	611.77
Appearance	White crystals
Density (g/cm^3)	2.484
pH (in water)	8.2

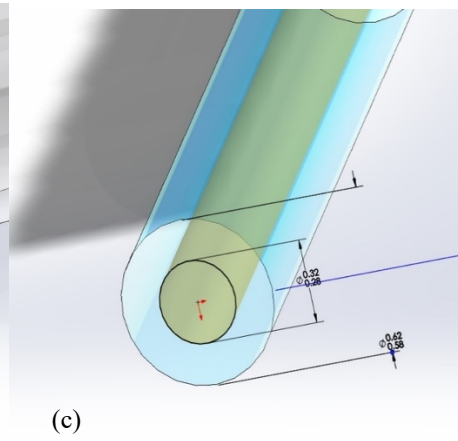
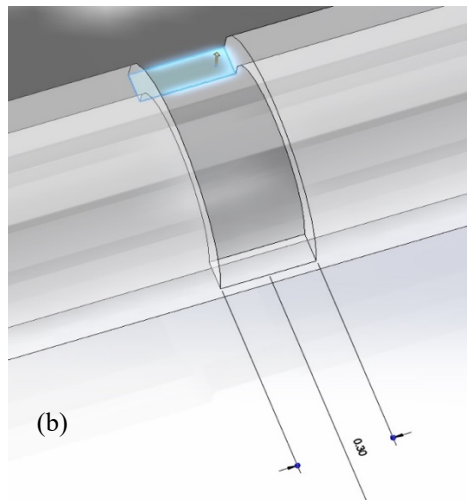
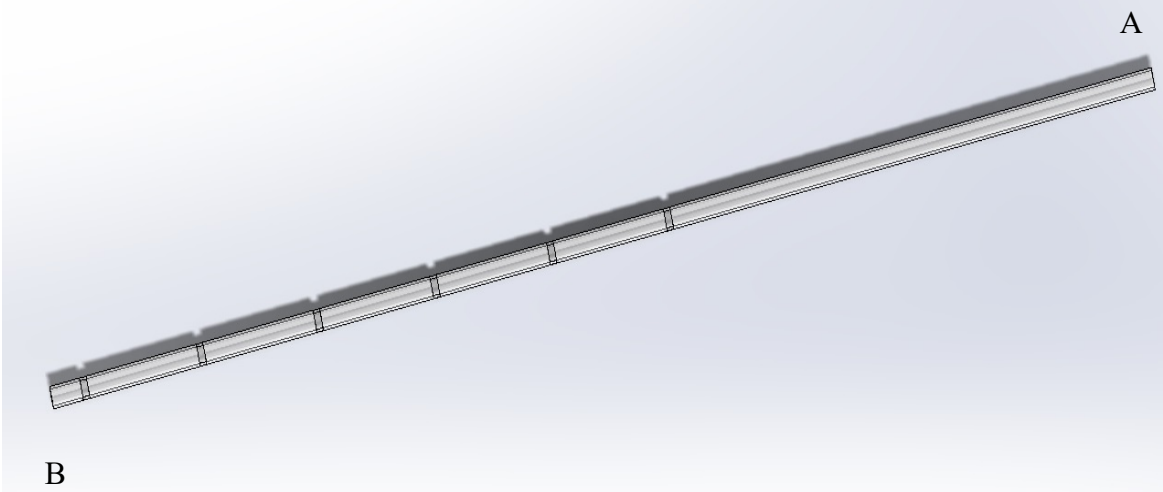
It is recommended that a fresh solution containing Calgon be prepared fortnightly or monthly as it is considered to be unstable. In the present experiment, the solution was prepared just before the commencement of the experiments. Inaccurate dispersion forms flocs of soil particles which makes the particles fall relatively rapidly through the water, leaving a transparent layer above the suspension. According to the British Standard, 2 g/L of Calgon or 50 ml of dispersant solution per litre should be considered (Head, 1980).

6.3.3 Acrylic-Brass Probe for Calibration and PSD test

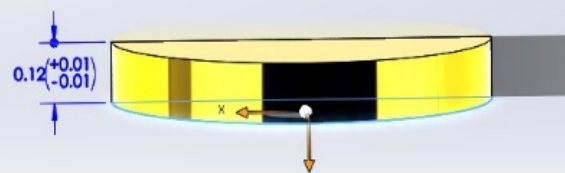
In this experiment, the probe was constructed with a 50 cm length clear acrylic tube containing six slots (Fig. 6.2a) and was customised with Tormach Inc. The tube's inner

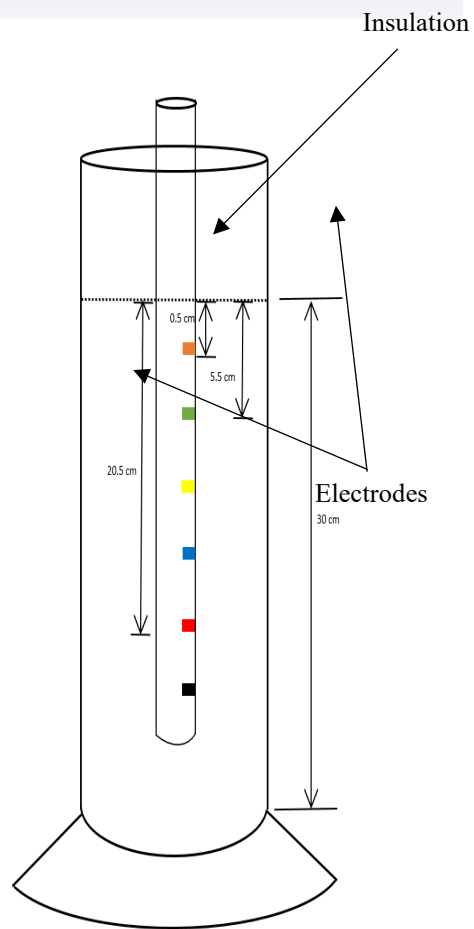
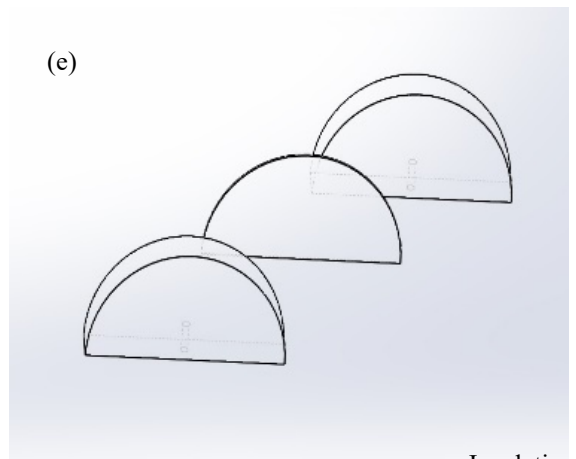
and outer diameters were 0.6 cm and 0.8 cm, respectively (Fig. 6.2b). Each slot was 0.03 cm (0.3mm) in width (Fig. 6.2c), placed at different heights of the tube. Each slot contains two half circles made of brass, each 0.12 cm thick, as shown in Fig. 6.2(d)- Fig 6.2(e). A total of 6 pairs of half-circle-shaped brass were the electrodes and were insulated from each other by a 0.1mm laser transparency film, as shown in Fig. 6.2 (f). The first slot starts at 28 cms (height) from the top of the tube (Fig. 6.2 g) and from that particular height, the tube is submerged in the soil/clay-water suspensions. The other five slots are placed 5 cm from each other. Point A in Fig. 6.2a was left open to create a pathway for the wires to go through. On the other hand, point B, which was always inside the suspension while the experiments were being conducting, was sealed completely to prevent water from going inside. Later, wires of distinct colour differences were soldered into the electrodes to create firm connections. The other side of each wire was taken outside through the channel (point A), as shown in Fig. 6.2 (h). Soldering the wires was one of the challenging tasks as during the process, excessive pressure on the tube would have caused cracks or damaged the acrylic tube. In the next step, in order to maintain a good connection and the reliability of the tool, the electrodes were affixed with waterproof epoxy adhesive to fill the void of the slots. The tube was kept in a secure place for 24 hours to allow the epoxy to dry out completely. The electrodes were connected with wires to establish a 2-pin electrical circuit configuration. The effective/optimum distance between the slots was found to be approximately 1.5 cm, as discussed in Appendix 6.

(a)



(d)





(f)

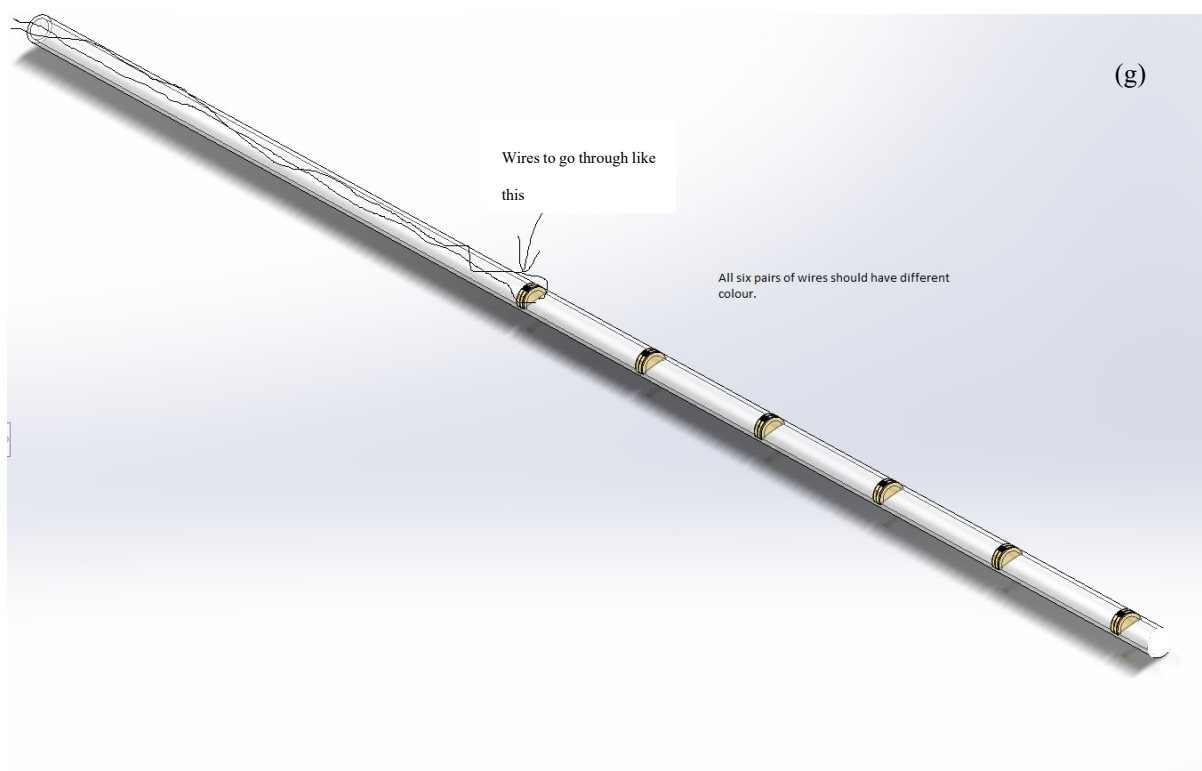


Figure 6.75: Different parts of the probe considered in this research: (a) acrylic tube with grooves, (b) width of each groove, (c) inner and outer diameter of the tube, (d) dimension of the brass electrodes, (e) assembly of electrodes and insulation, (f) approximate height (position) of each pair of electrodes submerged into the soil-water suspension, and (g) complete tool after the setup.

6.3.4 Preparation of Suspension

It is essential to prepare the suspension to ensure a more accurate prediction of the PSD. Soils may contain organic matter or calcium compounds, and without proper pre-treatment, the PSD will be erroneous. The standard steps according to [IS:2720 Part IV](#) were followed throughout the pre-treatment procedure ([Arora, 2008](#)).

i) About 25 g of oven-dried soil was weighed accurately with a balance and transferred to a glass beaker ([Fig.6.3](#)). The glass beaker was washed properly with distilled water before the commencement of the test.

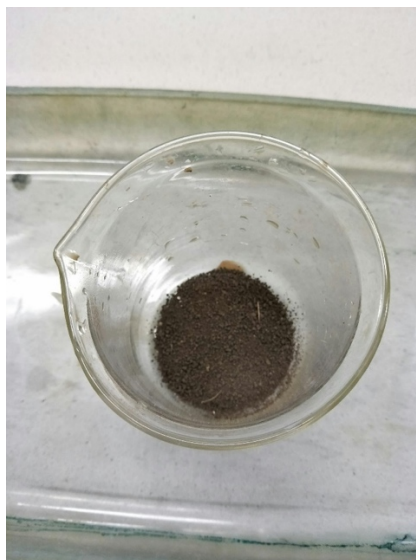


Figure 6.76: Oven-dried soil sample for PSD test.

ii) The soil was then subject to chemical pre-treatments which were performed in two stages namely, organic material removal and calcium compound elimination. First, the soil was pre-treated with a 20 volume hydrogen peroxide (H_2O_2) solution to remove the organic matter at the rate of 1ml/g of the sample, as shown in [Fig.6.4 \(a-b\)](#). Then, the mixture was kept steady to allow oxidation to take place. Hydrogen peroxide caused oxidation of the organic matter and a small amount of gas was generated. The mixture was kept steady for 10-15 minutes until no more bubbles appear. After this, the mixture was filtered with a 75 μ sieve. If less concentrated hydrogen peroxide is used, the mixture will require heating with a Bunsen burner, with a temperature not exceeding 60 $^{\circ}$ C ([Arora, 2008](#)).

iii) The soil remaining from step (ii) was transferred to another clean glass beaker. To remove the calcium compounds, 0.2M hydrochloric acid (HCl) was added to the soil at a rate of 1ml/g soil, as shown in [Fig.6.5 \(a-b\)](#). When the reaction ended, the mixture was filtered again. The filtrate was washed properly with distilled water until it was completely free from the acid. The damp soil was transferred to an evaporating dish. Both the damp and filtrate soils were oven-dried overnight and their mass was recorded.

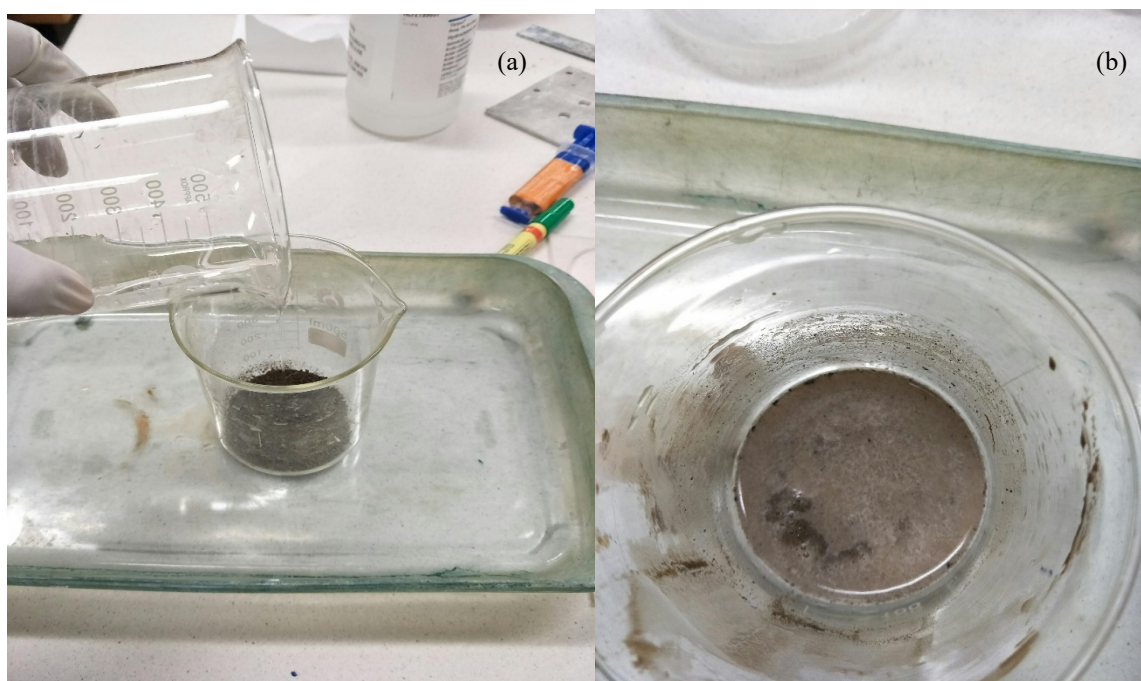


Figure 6.77: Steps of removing organic carbon from soil: (a) mixing H_2O_2 , and (b) reaction process.

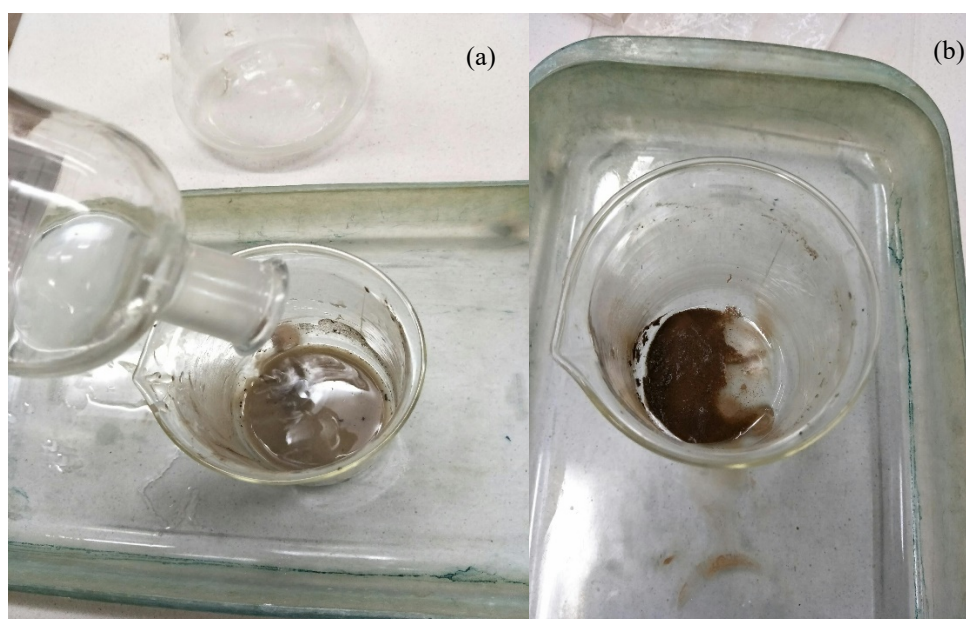


Figure 6.78: Methods of removing calcium compounds by HCl : (a) pouring HCl into the soil sample, and (b) after the reaction.

iv) The next day, the oven-dried pre-treated soils were transferred to a clean beaker. To ensure proper dispersion, around 100 ml of a dispersion solution was added in the beaker to cover the soil.

Distilled water should always be used to make the solution with the dispersing agent. The dispersing solution was then completely added to the sample. The distilled water was collected from a heating-based device, therefore the temperature of the water was still warm (roughly 60⁰ C when the experiment started). The newly prepared distilled water was allowed to cool to 25⁰C and after this, Calgon was mixed in the water.

v) The mixture was then stirred vigorously for 30 minutes using a mechanical stirrer. The contents of the mixture were then transferred to the cup of a mechanical stirrer. The cup should not be filled to more than $\frac{3}{4}$ as the turbulence created by the rotating blade may cause the mixture to spill out of the cup. Stirring time may vary based on the soil properties. For more clayey soils, the stirring period should be increased.

vi) The suspension was washed through the 75 μ sieve again using distilled water. The portion which passed through the sieve was taken for the experiment. The specimen was washed in a cylindrical 1000 ml glass jar and adequate water was added to make 1000 ml of suspension. After this, the whole suspension was mixed properly to ensure homogeneity.

vii) The cylindrical glass jar was then kept inside a water tank which has a temperature controlling motor. The whole experiment was conducted inside the water tank (Fig.6.6) so that the temperature did not affect the conductivity value. Figure 6.7 illustrates several parts of the experiment procedures.

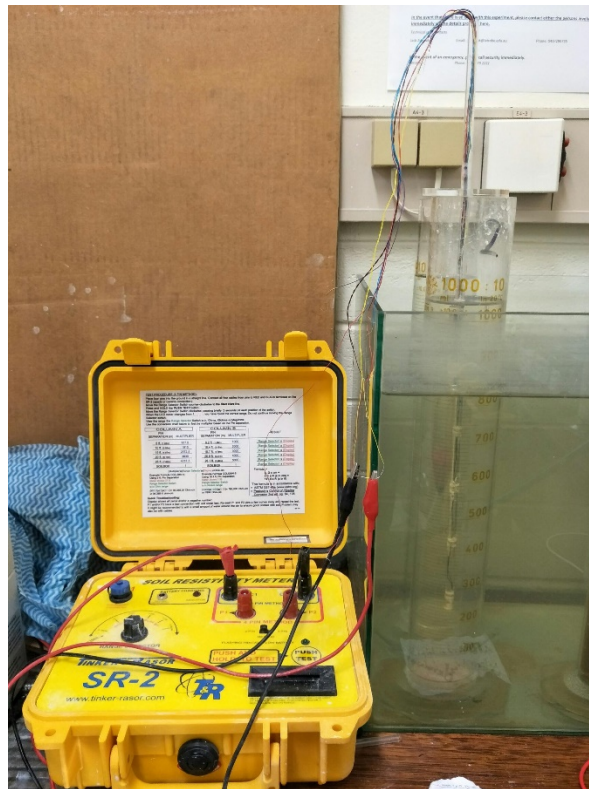


Figure 6.79: The EC setup before the commencement of the PSD test.

6.3.5 Calibration Technique

Using Stokes' law to determine particle size requires accurate knowledge of sedimentation theory. Failure to meet this requirement is one of the limitations of the hydrometer technique. In the present research, a new calibration technique has been introduced, the physical basis of which has been described in brief.

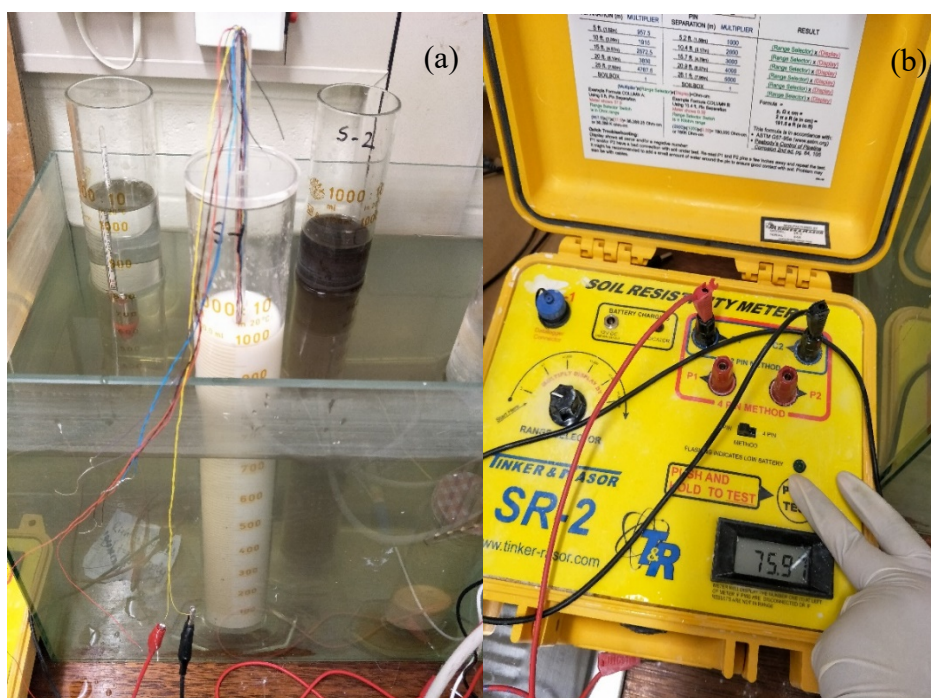


Figure 6.80: Snippets of the experimental procedures as part of the calibration and PSD analysis: (a) a sample test for kaolin, and (b) resistivity reading from the SR-2 meter.

In a particular soil/clay suspension settling under gravity, the concentration of the suspended soil/clay does not stay constant at every location inside the beaker. This means the density will be different at each brass slot. This concept led to the idea that the suspension of different densities can be calibrated with electrical resistivity values. For example, the density of the water is approximately 1 g/cm^3 . The total density will increase to 1.025 g/cm^3 if 25g of soil is added to create a suspension. The amount of dispersing agents should be deducted while recording the density values. At a particular density, electrical resistivity/conductivity can be recorded. All the available PSD techniques require calibration to some extent. It can be seen that the requirement to utilize the calibration technique in this research gave satisfactory results for all soil samples. The repetition of the technique provided more confidence in building calibration data. It should be mentioned that the amount of dispersing agent was kept the same for the actual test as well.

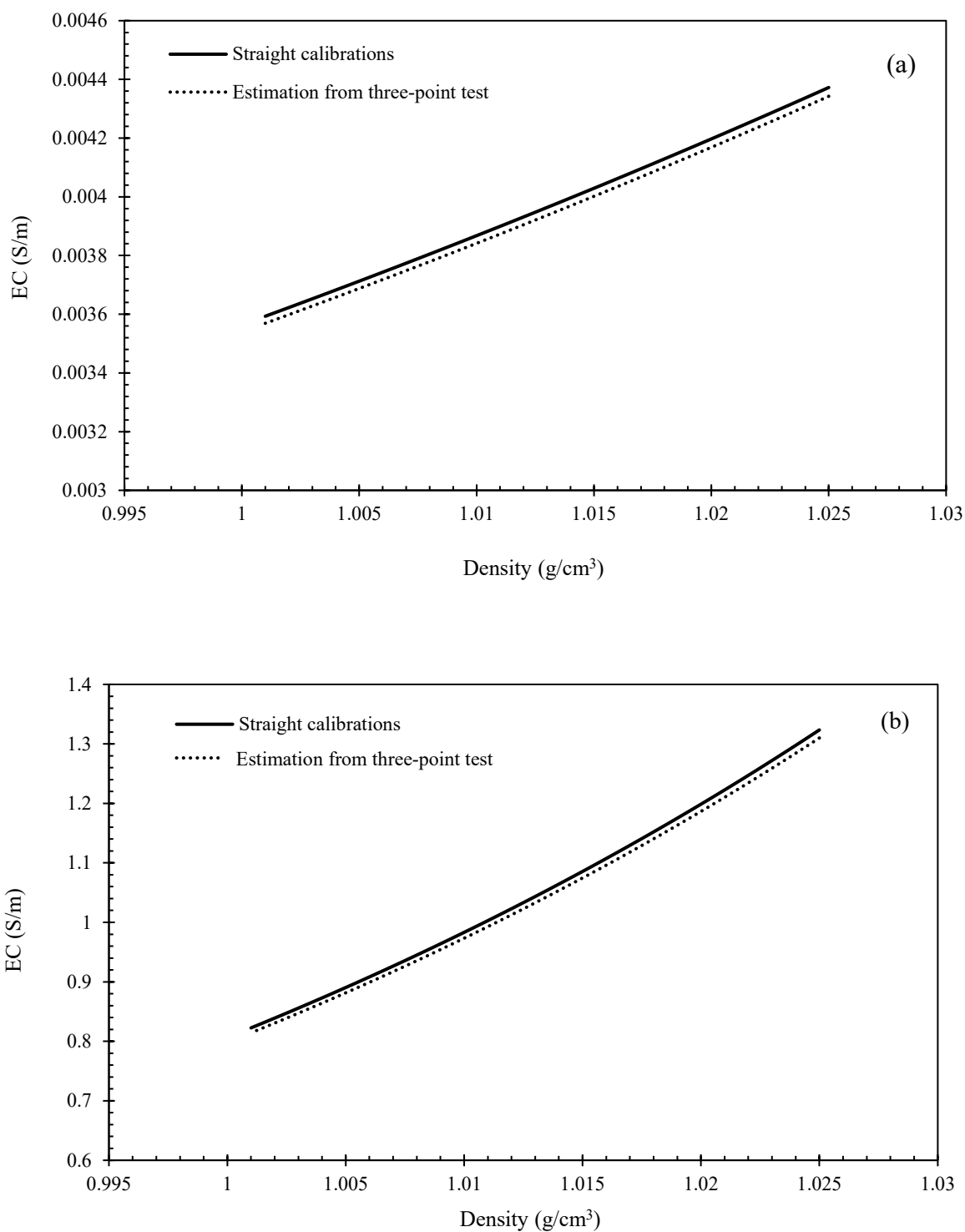


Figure 6.81: Comparison between direct calibration and 3-point calibration of (a) kaolin, and (b) vertosol.

For each type of sample, calibrations can be done in two different ways namely, (i) straight calibration at different densities, and (ii) three-point calibration and interpolations.

Technique (i) is time-consuming but more accurate. Calibrations were conducted at different densities of soils, ranging from 1.0025 g/cm³ to 1.0001 g/cm³. At different densities of suspension, different values of electrical resistivity were recorded with a two-pin SR-2 soil resistivity meter (ASTM G57-06). Each test was repeated thrice and only 0.1% - 0.5% discrepancies were noted. Meanwhile, the three-point calibration requires taking the EC readings at the lowest, mid, and the highest density range. After this, the rest of the EC values can be predicted by linear or polynomial interpolations, based on the EC behaviours of the soil samples.

It was necessary to correct the dispersing agent's density since all of the tested suspensions were a fixed amount for both calibration and the final experiment to find the PSD. This is why one dispersing agent's density correction test was conducted before starting the calibration.

Readings were taken carefully using Tinker and Raser SR-2 meter and the whole test was conducted within one hour, but this can vary depending on sample type. As the electrical interactions between one type of soil particle are not similar to another soil type, the individual calibration of each soil sample was mandatory in order to obtain precise data during the actual experiment. The calibration curves are shown in Fig. 6.8, where both kaolin and vertosol have different electrical conductivity values at different densities due to the differences in their electro-chemical properties. The overall process is presented in a schematic diagram in Fig.6.9 to provide a clear view.

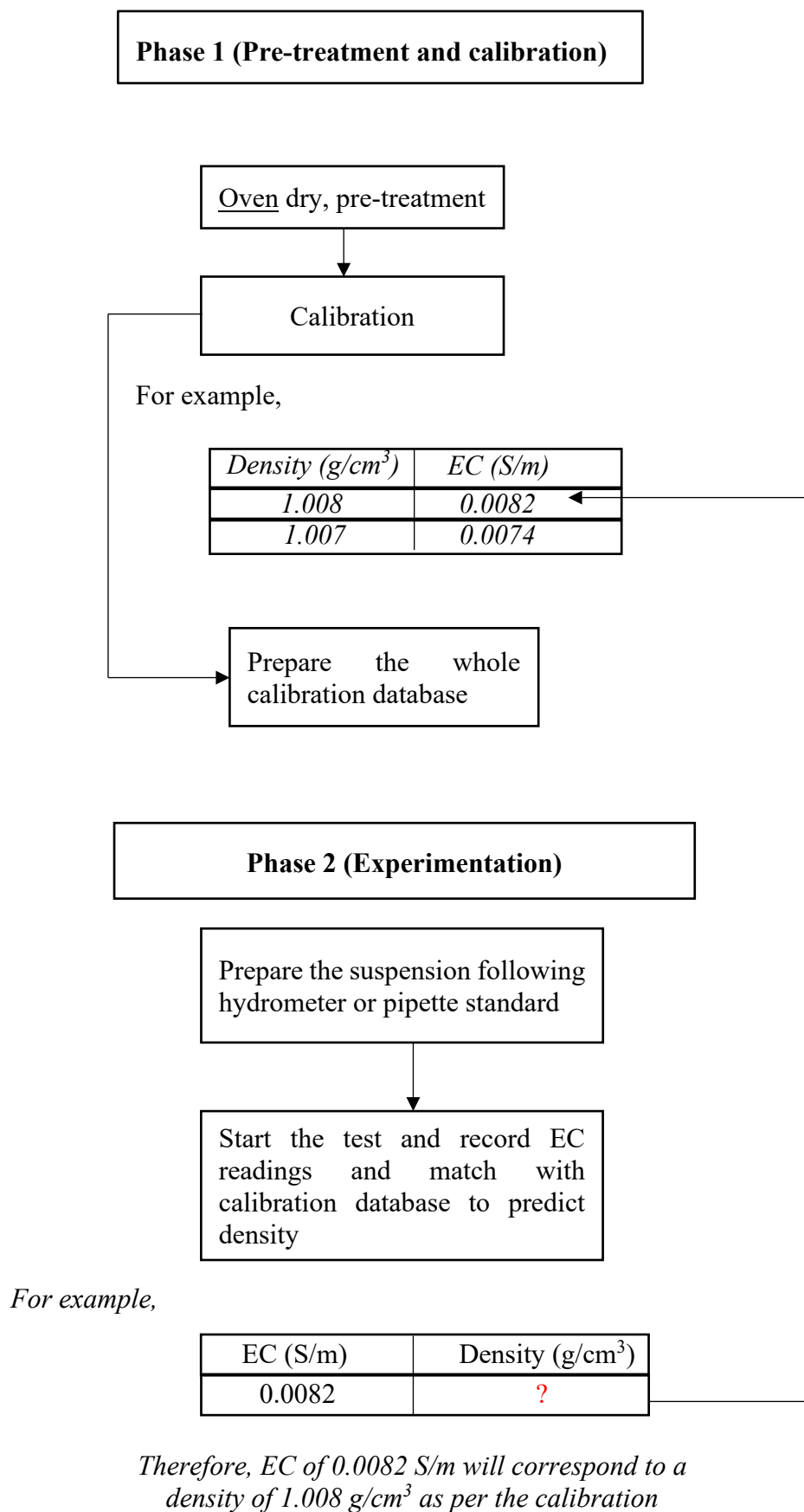


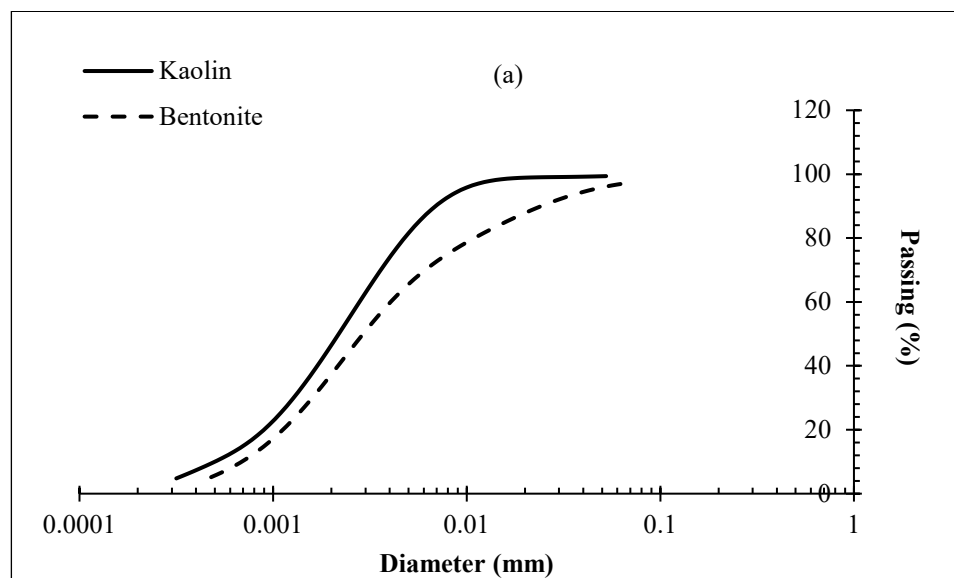
Figure 6.82: A complete overview of the PSD analysis of soils using the EC technique.

6.4 Test Results and Discussion

At the commencement of the test, the suspensions were uniformly distributed and the acrylic-brass tube was submerged inside. Although the suspensions were homogenous at the beginning, the readings were expected to be different at different slots after 2 minutes as the particles started to settle. Based on these readings, electrical conductivities were calculated. The calculated values were matched with the calibrated values which gave the densities of the solid. After this, Eq. (2.12) was utilised to calculate the diameter of the clay/soil particles and Eq. (2.13) was used to find the percentage passing on a logarithmic scale.

After the experiment with one soil/clay had been completed, the cylindrical beakers were removed from the water tank and cleaned properly with de-ionised water. Before starting the experiment with the next sample, all of the tools were cleaned and dried out appropriately in order to avoid contamination of the samples.

The PSD results of laboratory-based clays and natural soils are presented in Fig.6.10. After generating curves from the PSD data, the results were subject to accuracy and repeatability analysis. In the following section, the accuracy and repeatability are analysed.



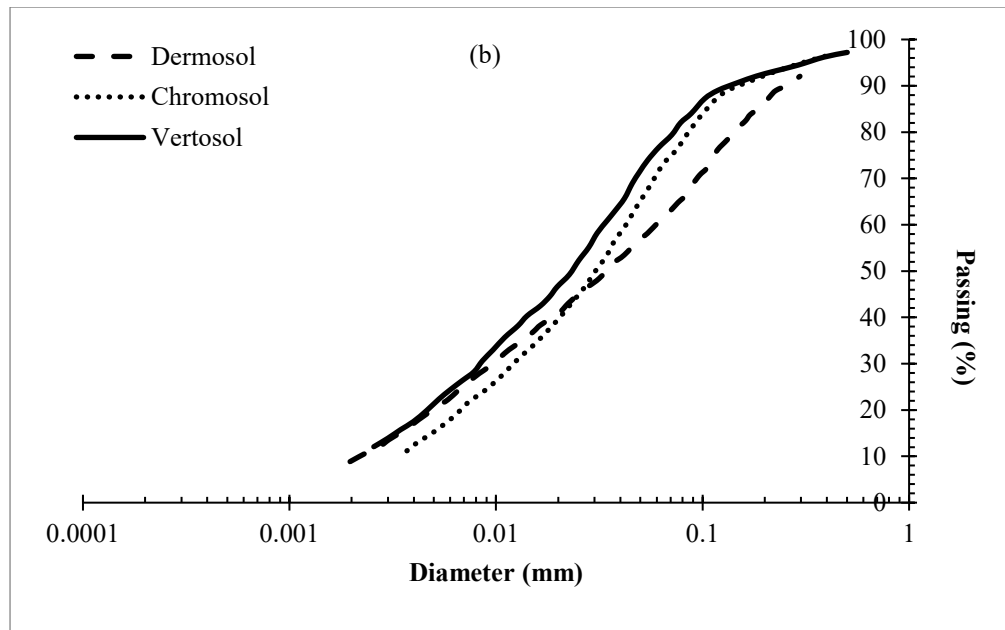


Figure 6.83: PSD curves from the EC approach of (a) laboratory clays, and (b) natural soils.

The PSD curves obtained from the proposed approach were subject to a discussion on accuracy and reproducibility. As previously mentioned, the PSD of each soil sample was also found using the hydrometer and laser diffraction technique.

6.4.1 Validation

Figure 6.11 shows that the proposed approach is able to produce the PSD curves of the corresponding soil samples, which are almost identical to the laser diffraction method. On the other hand, notable discrepancies can be observed in terms of the results obtained from the hydrometer. Several studies in the literature have also reported that the hydrometer overestimated the PSD analysis compared to the laser diffraction approach (Cheetham et al., 2008). The results demonstrate that the electrical conductivity method is an excellent alternative to finding the PSD of both laboratory clays as well as natural soils.

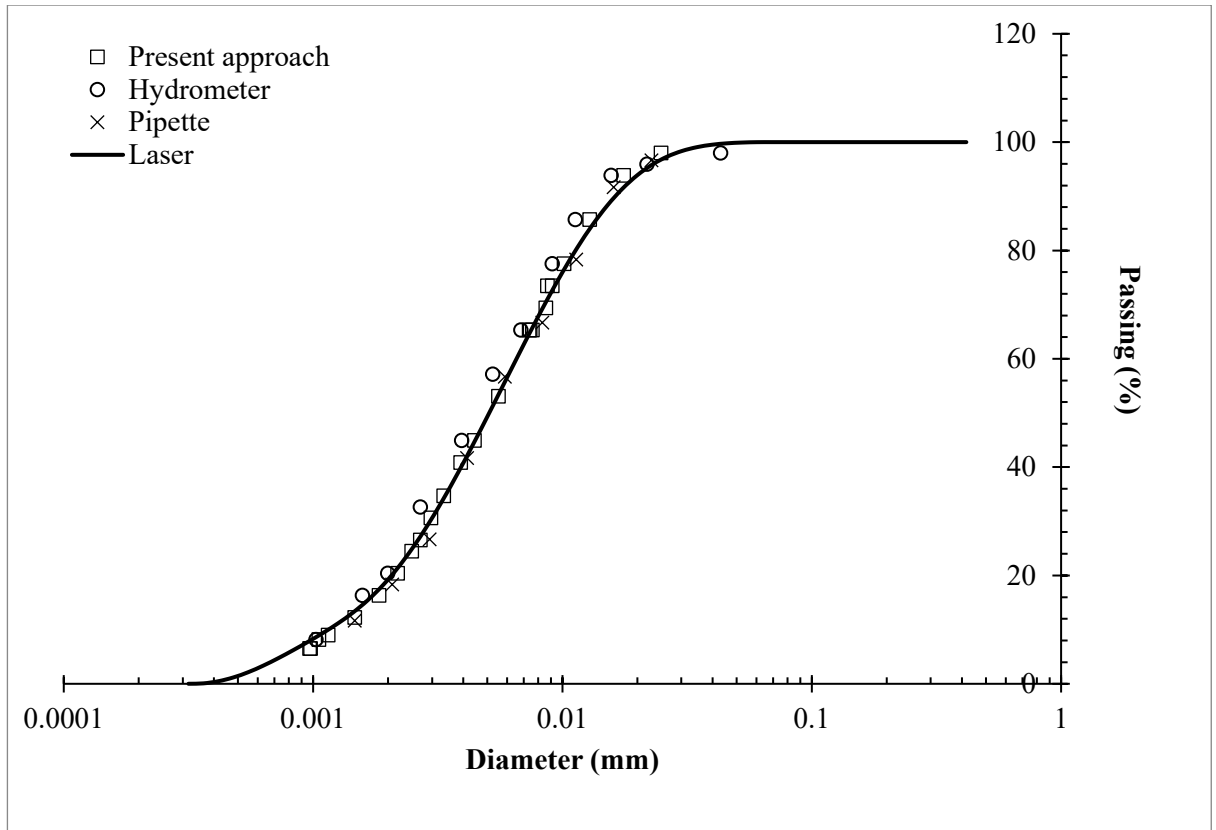


Figure 6.84: Accuracy analysis of the proposed method to find the PSD (kaolin).

As discussed in [section 2.6.7](#) in [Chapter 2](#), LD underestimates the PSD analysis compared to the pipette method for an identical sample, therefore, in this present study, the results are subjected to comparison with pipette fractions as well to establish a compelling belief in the accuracy of the proposed approach ([Fig. 6.11](#)). The limitations and elaborate discussions are in [Chapter 2](#). [Table 6.3](#) details the quantitative comparisons of the conventional methods and the proposed approach. It can be seen that the results were almost identical to each other. It should be mentioned here that for the quantitative analysis, only kaolin was considered.

Table 6.23: Quantitative comparisons between laser diffraction, hydrometer, pipette, and the proposed approach for particle size analysis of kaolin.

Diameter (mm)	Laser diffraction (%)	Hydrometer (%)	Pipette (%)	Proposed approach (%)
0.02273	95.83	95.93	96.70	97.97
0.01607	88.93	93.89	91.62	92.56
0.011366	80.54	78.83	78.33	81.24
0.008301	71.01	73.69	66.67	67.39
0.005869	54.89	57.15	56.56	53.07
0.004150	38.65	44.90	41.67	41.55
0.002935	28.32	20.41	18.33	18.89
0.001467	9.15	15.71	11.67	11.25

6.4.2 Repeatability

The reproducibility of the proposed approach was tested and the results of the laser diffraction were used as the benchmark data. As shown in [Figs 6.12](#), there is a difference of approximately 10%-12% in the results for bentonite and vertosol, whereas there is difference of approximately 1%-2% in the repeated results of the proposed test. Since the probe was always submerged in the suspension, it created less disruption in the particle settlements, and hence the results are almost identical. In addition, calibration was conducted based on the EC-density relation which does not interfere with the particle's free fall. Therefore, the results provide compelling evidence that the proposed approach is able to provide better results than the hydrometer in a time-scale of 1-2 hours.

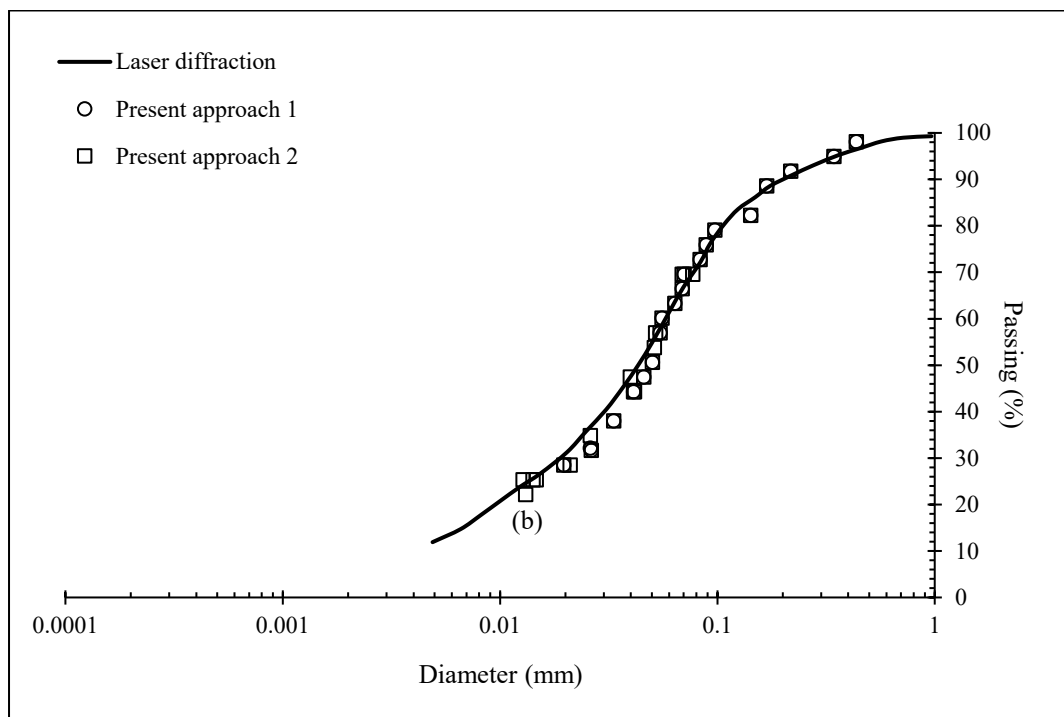
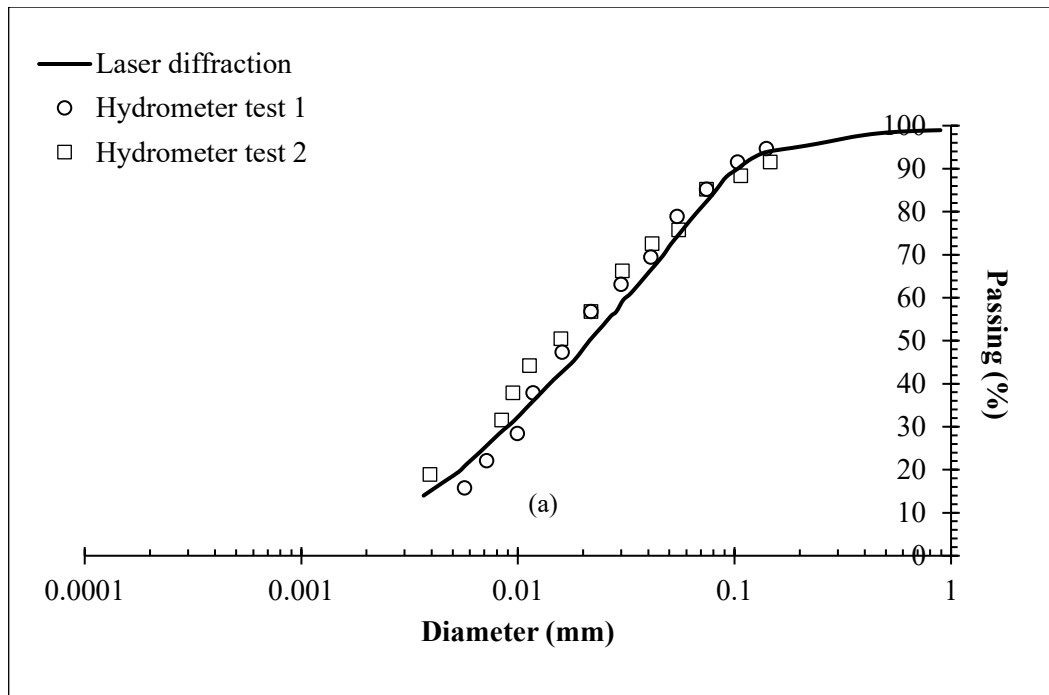


Figure 6.85: Reproducibility of (a) hydrometer, and (b) EC approach for the PSD tests for kaolin.

6.5 Summary

In this chapter, a new approach for calculating the particle size distribution of soils was presented. The acrylic-brass probe is calibrated for different soils based on the relationship between the electrical conductivity of soil particles and sample density. The concept of the approach follows the sedimentation theory and takes Stokes' law into account to find the diameter of the particles of the corresponding soil samples. The empirical results of the electrical conductivity technique using five soil samples (two laboratory-based clays and three natural soils) provide strong evidence to support its reliability for routine soil particle size analysis within just one hour. The device was also able to provide consistent results from repeated measurements on the same sample, which confirms the good precision of the results. Furthermore, the experimental approach was found to be insensitive to the mass of the soil sample analysed, provided the obscuration level was sustained within the recommended range. It is important to understand that all the available techniques to find PSD have both advantages and disadvantages. Inconsistency in the results are primarily a reflection of the differences in the physical properties of samples, the time-scale to conduct the test, and the type of operation (manual/automated). Nevertheless, the results obtained from this approach imply that these have a greater resemblance to the accuracy of the laser diffraction process and pipette.

Chapter 7

A New Electrical Approach to Predict the Liquid Limit and Plastic Limit of Soils

7.1 Introduction

In this chapter, a new method to determine the liquid limit and plastic limit of soils is introduced. The proposed method uses the non-dimensional electrical surface conduction parameters σ_n and χ to develop a robust relationship between the liquid limit and plastic limit of soils, and a volumetric water content ratio F that describes the ratio between the volume of DDL water to the volume of free water at both limits. A total of 39 different fine-grained soils were considered in this study, where F is initially calculated by back-calculation using their pre-determined liquid and plastic limit. The resampling approach was considered to predict and validate the correlations among σ_n , χ , and F . The resampling approach involves using all 39 soils by sub-categorising soils into 7 different sets, with each group having 34 soils chosen arbitrarily and the remaining 5 soils of each group for validation purposes. The predicted F values of the liquid and plastic limits using the resampling statistical approach were used to predict the liquid limits and plastic limits of the 39 soils used in this study and promising agreement was observed between the experimentally measured and the predicted values. Further study is recommended to explore the other fine soil parameters that could be included to improve the prediction accuracy of the liquid and plastic limits.

7.2 Background

Clay-rich soils need to be sensibly treated when it comes to engineering applications (civil or geotechnical) such as to support structures and embankments, or in planetary science to

study topsoil or subsoil for plant growing (Mitchell and Soga, 2005; Zbik et al., 2015). However, clay-rich soils exhibit different characteristics due to the differences in the micropore structures, mineralogy, particle size distribution, and degree of saturation (Abu-Hassanein et al., 1996; Kibria and Hossain, 2012; Rashid et al., 2018; Hasan et al., 2018; Lu et al., 2019) and these characteristics can be attributed to the unwanted damaging effect on the engineering structures. In general, these soils behave as semisolids within a particular range of water content and its physical and engineering properties are a function of its water content. The different soil states can be determined by three water contents limits (Atterberg limits); shrinkage limit (SL), plastic limit (PL), and liquid limit (LL) as shown in Fig.7.1 (Das, 2013).

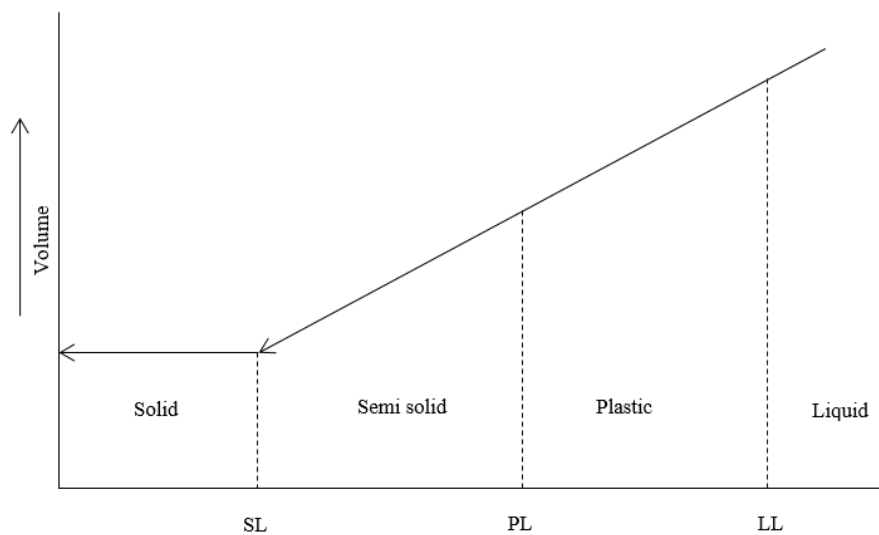


Figure 7.86: Different stages of Atterberg Limits.

Atterberg limits, first introduced by the Swedish scientist A. Atterberg in 1915, and later re-defined by Arthur Casagrande, are determined with a view to classifying and describing the characteristics of cohesive soils like clays under different water contents (Zbik et al., 2015; O'Kelly et al., 2018). The characteristics, in most of the cases, provide a basis upon which to predict soil properties like deformability, expansion ability, soil strength,

hydraulic conductivity, to name a few ([Dolinar et al., 2007](#); [Young, 2012](#)). The laboratory tests, primarily initiated by Atterberg, are still considered to be the standard testing method in modern soil mechanics.

Of the Atterberg limits, the LL and PL are defined as the upper and lower water content limits, respectively, at which a specific soil ceases to exhibit behaviour as plastic ([Coduto et al., 2011](#); [Briaud, 2013](#); [Haigh et al., 2013](#)). Both of these limits are important since they indicate how much water can be retained in a particular soil sample before it transforms from a plastic state to a liquid state. The transformation is gradual rather than a sudden change, therefore the proper definition of the transformation boundary is inherently arbitrary ([Haigh et al., 2013](#)).

The LL could vary in a wider boundary based on the physical properties of clays. For example, bentonite clay has a surface area which is almost 40 times greater than that of kaolin ([Young, 2012](#)), and therefore, a greater amount of water will be required to fill the small pores of bentonite. Other major factors which influence the LL of soils are the interparticle forces and surface area of particles ([Warkentin, 1961](#); [Nagaraj and Jayadeva, 1981](#)). In general, LL is determined by the Casagrande device ([Haigh, 2012](#); [Di Matteo, 2012](#); [Haigh and Vardanega, 2014](#)) or by the fall cone test ([Wood, 1982](#); [Feng, 2000](#); [Sharma and Bora, 2003](#)). Although both of these methods have received criticism to some extent in relation to their erratic results, their tedious nature, and the possibility of operator-made errors, they are still considered to be accurate by different standards. While the Casagrande method is preferred in the United States (defined in [ASTM D4318-10](#); [AS1289.3](#)), the cone penetrometer method has always been preferred in the United Kingdom ([BSI, 1990](#)) and Eurocode ([BSI, 2007](#)).

On the other hand, the plastic limit of a specific soil sample is defined as the specific water content at which the transition of soil from ductile to brittle behaviour takes place ([O'Kelly](#)

et al., 2018). Unlike the liquid limit, there are less variations of test methods in the plastic limit of soils are less (Prakash et al., 2009). The most commonly used method to determine the soil plastic limit is associated with the conventional thread-rolling technique. However, as discussed in Chapter 2 (section 2.7.5), the method is based purely on the operator's decision, and hence discrepancies in the results have been reported in the literature by researchers (Schofield and Wroth, 1968; Sherwood, 1970; Feng, 2004; Andrade et al., 2011).

Recent trends in soil mechanics or geotechnical engineering aim to look for alternative methods for different soil properties tests. For example, while hydrometer or pipette analysis were some of the classical methods for determining the particle size distribution of soils, researchers are developing new devices/techniques with laser diffraction analysis, sedigraph, integral suspension pressure methods, to name a few (Eshel et al., 2004, Durner et al., 2017). Therefore, the possibility of identifying a different soil classification technique to determine the LL or PL of soils remains open.

7.3 Proposed Method and its Mathematical Formulation

The water volume at LL and PL comprises volumes of DDL water V_w^{DDL} and free water V_w^{FW} , that satisfy the limit criteria.

where

$$\theta_{FW} = \frac{V_w^{FW}}{V} \quad (7.1)$$

$$\theta_{DDL} = \frac{V_w^{DDL}}{V} \quad (7.2)$$

So, a method is required to determine both volumes of water. The volume of DDL water at LL and PL are similar and can be related to the two electrical conductivity parameters of

fine soil solid particles namely, the surface conduction parameter (σ_s) and the size of the DDL (χ), as proposed in [Chapter 4 \(Hasan et al., 2018\)](#). A new parameter F is introduced in this study to present the ratio between the DDL volumetric water content and the free water as follows:

$$F = \frac{\theta_{DDL}}{\theta_{FW}} \quad (7.3)$$

Consequently, at LL and PL, the parameter F can be expressed as follows:

$$F_{LL} = \frac{\theta_{DDL}}{\theta_{FW}^{LL}} \quad (7.4)$$

$$F_{PL} = \frac{\theta_{DDL}}{\theta_{FW}^{PL}} \quad (7.5)$$

Therefore, the following expression can be written for LL:

$$W_c^{LL} = W_c^{FW} + W_c^{DDL} \quad (7.6)$$

where

$$W_c^{DDL} = \frac{(\chi - 1)V_s\gamma_w}{G_sV_s\gamma_w}$$

$$W_c^{DDL} = \frac{(\chi - 1)}{G_s} \quad (7.7)$$

Therefore, W_c^{FW} can be interpreted from [Eqs. 7.4 and 7.7](#) as follows:

$$W_c^{FW} = \frac{(\chi - 1)}{F_{LL}G_s} \quad (7.8)$$

Combining [Eqs. 7.7 and 7.8](#), the water content at LL hence can be represented as:

$$W_c^{LL} = \frac{(\chi - 1)}{F_{LL}G_s} + \frac{(\chi - 1)}{G_s}$$

$$\Rightarrow W_c^{LL} = \left(1 + \frac{1}{F_{LL}}\right) \left(\frac{\chi-1}{G_s}\right) \quad (7.9)$$

Similarly, the equation to determine the plastic limit of soils can be expressed in the light of Eq. 7.9 as follows:

$$W_c^{PL} = \left(1 + \frac{1}{F_{PL}}\right) \left(\frac{\chi-1}{G_s}\right) \quad (7.10)$$

7.4 Soil Samples

Of the soils used in this study, kaolin was the only treated clay, whereas the rest of the soils were natural soils collected from different locations in Australia. The geotechnical properties of kaolin were detailed in Chapter 3 in Table 3.4. The range of the σ_s of the soils used in this study was found to be between 0.0006 S/m to 0.0062 S/m, whereas χ varied from 1.01 to 1.25. In addition, soils possessed $29\% \leq LL \leq 96\%$, and $50\% \leq PL \leq 21\%$. For validation purposes, the cone penetration technique was considered for all the samples. In addition, the Casagrande method was also considered for some of the samples to compare the results. The normalised $\sigma_n = (\sigma_s / \sigma_w)$ was considered for the numerical analyses where σ_w is the electrical conductivity of distilled water. Conventionally, distilled water is used to determine the LL and PL of soils and a similar approach was also considered in the present approach, where $\sigma_w = 0.000082$ S/m was recorded.

To understand the range of the LL and PL of the soils considered in this study, the plasticity range for the ASTM soil classification system (ASTM D2487-93; AS1726-1993) is illustrated in Fig.7.2. The PI in Fig.7.2 refers to plasticity index, which is the difference between the LL and PL of each soil. The plasticity chart provides information on the types of soils considered in the study. U-line is not used in the classification, but it is the upper boundary of the LL -PI values and is only checked to identify the errors. A-line separates clay from silt and provides more information on the type of soils based on the values of the

PI as a function of LL. The explanation of the group symbols detailed in Fig.7.2 is given in Table 7.1 for a better understanding. The positions of A-line and U-line were determined by the following equations (ASTM D2487-93; AS1726-1993):

$$\text{A-line: Horizontal at PI}=4 \text{ to LL}=25.5, \text{ then PI}=0.73(\text{LL}-20) \quad (7.11)$$

$$\text{U-line: Vertical at LL}=16 \text{ to PI}=7, \text{ then PI}=0.9(\text{LL}-8) \quad (7.12)$$

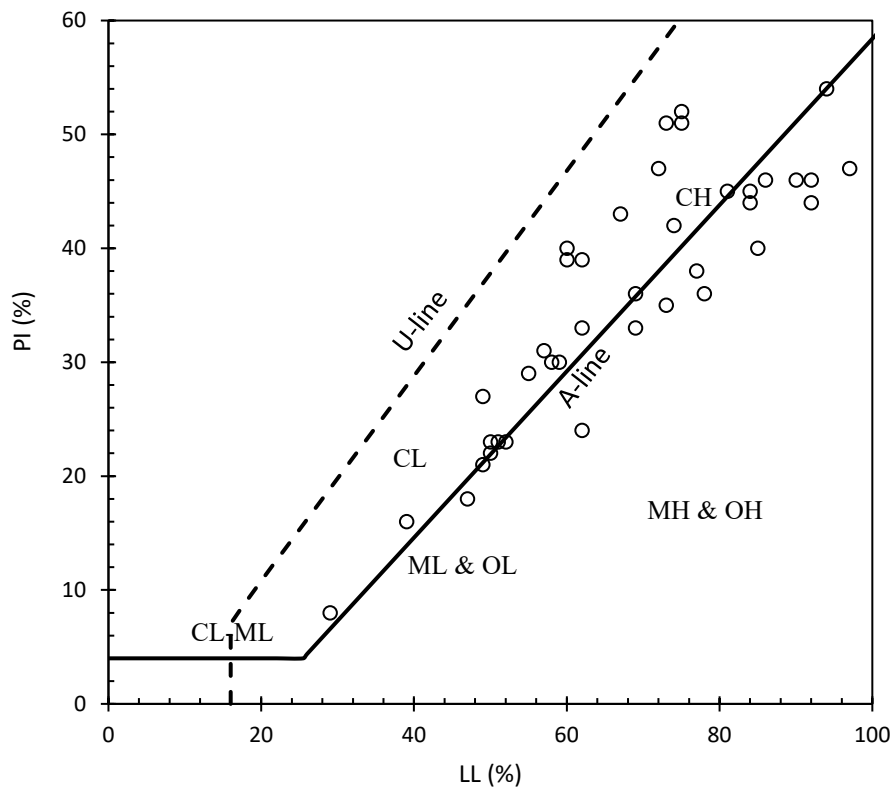


Figure 7.87: Plasticity range for the ASTM soil classification system (ASTM D2487-93; AS1726-1993).

According to the soil classification in Table 7.1, the soils considered in this study for both the resampling approach and validation consist of soils of different categories. Although most of the soils dominate the CH & MH zone, the present EC approach was able to predict the LL and PL of soils from the CL & ML groups as well.

The results in Table 7.2 show that soils with higher σ_s values were found to have lower F_{LL} and F_{PL} . This behaviour can be explained by studying the changes in the electrical surface

conduction activities. As previously discussed, the electrical conductivity of soil slurry can be affected by the soil's mineralogy, the electrical conductivity of water, temperature, to name a few (Mojid et al., 2007; Rahid et al., 2018; Hasan et al., 2018). According to Eqs. 7.4-7.5, F is a ratio of two volumetric water contents, namely, DDL and free water at the liquid limit/plastic limit. As a result, if F decreases, this means the volumetric water content at the LL or PL is increasing and $\theta_{FW}^{LL} < \theta_{DLL}$. Therefore, it is expected that lower values of F represent soil exhibiting higher LL or PL values.

Table 7.24: Soil Classification System (ASTM D2487-93; AS1726-1993). Only relevant soils are included in the chart.

Major Divisions	Typical Names	Group Symbols
Silts and clays with LL<50%	Inorganic silts and very fine sands, rock flour, silty or clayey fine sands with low plasticity	ML
	Inorganic clays of low to medium plasticity, gravelly clays, sandy clays, silty clays, lean clays	CL
	Organic silts and organic silt-clays of low plasticity	OL
Silts and clays with LL>50%	Inorganic silts, micaceous or diatomaceous fine sandy or silty soils, elastic soils	MH
	Inorganic clays of high plasticity, fat clays	CH
	Organic clays of medium to high plasticity	OH

7.5 Determination of F_{LL} & F_{PL} using the Resampling Approach

The resampling approach was considered to develop non-linear three-dimensional surface analyses to determine equations to predict F_{LL} and F_{PL} of soils as a function of σ_h and χ . For this purpose, F_{LL} and F_{PL} were determined by back-calculation, and the comprehensive database is presented in Table 7.2. The obtained results were then subject to resampling non-linear surface analyses to identify suitable equations to predict F_{LL} and F_{PL} .

numerically. This process involves using all 39 soils by sub-categorising soils into 7 different sets, with each group having 34 soils chosen arbitrarily and the remaining 5 soils of each group for validation purposes, as shown in Table 7.3 and Table 7.4. For each set of the resampling process, the coefficient correlations were found to be $0.93 \leq F_{LL} \leq 0.95$, and $0.90 \leq F_{PL} \leq 0.95$.

Based on the results found from the resampling approach, the general equations for the F_{LL} and F_{PL} are proposed as follows:

$$F_{LL} = -0.5 + \sigma_n + 0.52\chi, R^2 = 0.94 \quad (7.13)$$

$$F_{PL} = -1.498 - 0.9\sigma_n + 1.491\chi, R^2 = 0.90 \quad (7.14)$$

The performance of these two equations in predicting F_{LL} and F_{PL} for the 39 soils used in this study is shown in Fig. 7.3 and a high correlation coefficient can be observed.

7.6 Test Results and Discussions

7.6.1 Differences between the Casagrande and Cone Methods

The present method was subject to a validation test with the LL and PL of each soil sample, which was determined by cone penetration and thread-rolling techniques, respectively. However, for 10 soil samples, the cone penetration and Casagrande method were used to determine their LL as detailed in Table 7.2. The results in Fig. 7.4 show good agreement between the LL values obtained by the cone penetration and Casagrande methods.

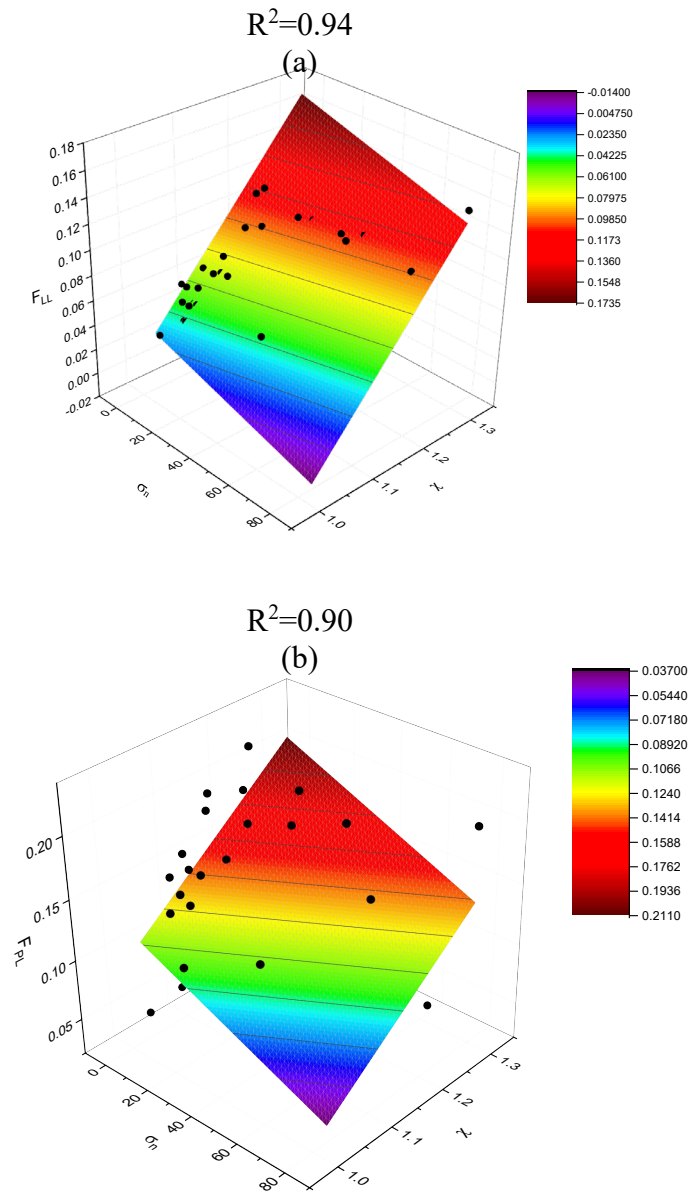


Figure 7.88: Non-linear surface analyses to observe behaviours of (a) F_{LL} and (b) F_{PL} , as functions of σ_n and χ .

Several studies have highlighted that the LL values obtained from both methods vary significantly at higher LL values, particularly $>70\%$ (Budhu, 1985; Sivapullaiah and Sridharan, 1985; Wasti and Bezirci, 1986).

The shear strength of any soil at LL consists of two types of shear resistance, namely viscous and frictional. Therefore, it is not technically possible for a device to determine

both components simultaneously (Mishra et al., 2011). Based on this conceptual understanding, LL by the Casagrande method focuses on the predominant viscous shear resistance to calculate LL (number of blows) and the cone is mainly based on frictional shear resistance. As a result, it can be said that Casagrande is well-suited for soils that have high LLs and for lower LLs, the cone is preferred (Sridharan and Prakash, 2000).

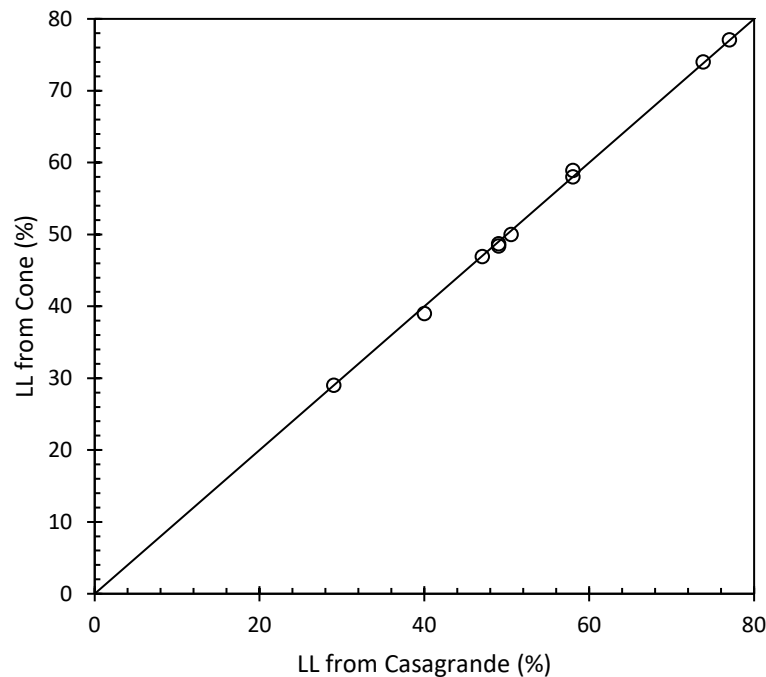


Figure 7.89: Agreement of values obtained from the Casagrande and cone technique at low LL (the straight line is the identity line).

However, Ozer (2009) showed that if a soil has $LL < 70\%$, then $< 2\%$ difference can be achieved between the LL of an identical sample. In general, most of the natural soils have an LL less than 100%. Therefore, it can be postulated that the Casagrande and cone penetration techniques produce similar LL values to identical natural soil samples ($LL < 100\%$). The results in this study (Fig. 7.4) support this statement.

7.6.2 Validation of EC Technique to Determine LL and PL

The EC approach proposed in this study to predict the LL and PL of soils involves determining σ_n and χ and using them to determine F_{LL} and F_{PL} using Eqs. 7.13-7.14, respectively. Then, LL and PL can be predicted using Eqs. 7.9-7.10, respectively. Figures 7.5-7.6 compare the LL and PL measured experimentally and predicted using the EC approach proposed in this study, respectively, and promising agreement is observed for the 39 soils tested in this study. Table 7.2 also demonstrates a comprehensive comparison of results for both LL and PL. The LL and PL values obtained by the EC method were found to be quite similar. In general, most of the predicted results were found to be within $\pm 10\%$ error lines, which provide more confidence in the accuracy of the approach. The percentage of error can be reduced with the availability of more soil databases to improve the prediction of F_{LL} and F_{PL} .

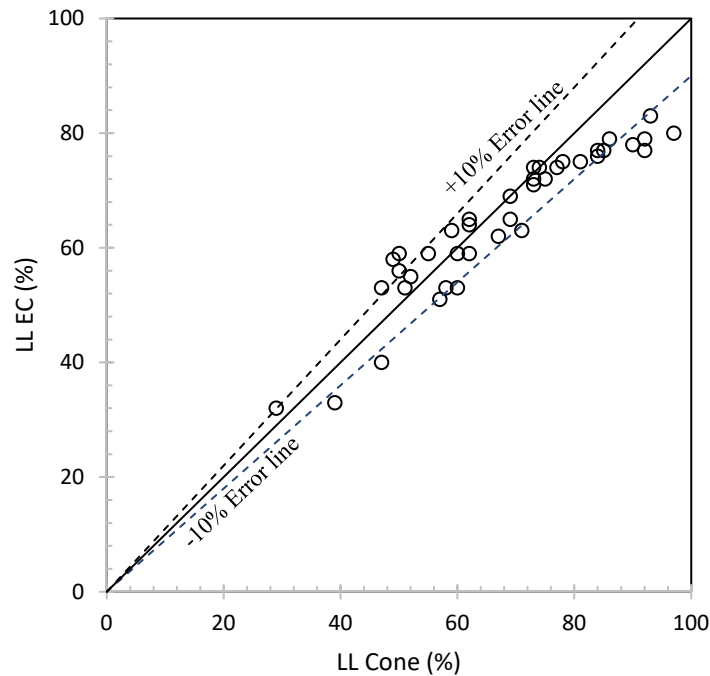


Figure 7.90: Agreement between the liquid limit values of soils obtained from the cone and EC techniques.

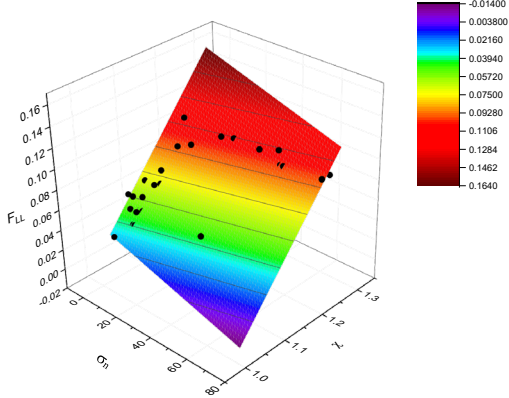
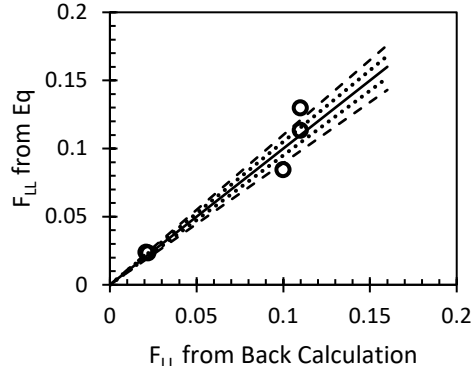
For the further validation purpose, resampling approach was considered as discussed in [Section 7.5](#). The resampling approach contains creating seven different sets with 34 soils, leaving 5 soils arbitrarily. For each set, the database was created along with 3D surface analyses and equations were proposed to numerically predict F_{LL} or F_{PL} , as shown in [Tables 7.3-7.4](#). For each set, 5 distinctive soils were left out and were later subject to validation, which includes predicting F_{LL} or F_{PL} by the equations. In general, coefficient co-relations of $R^2 > 0.90$ were obtained. For each set of resampling approach, the predicted F_{LL} or F_{PL} of the soils were found to be within the 10% error line, which provides more confidence in the accuracy of the predicted results.

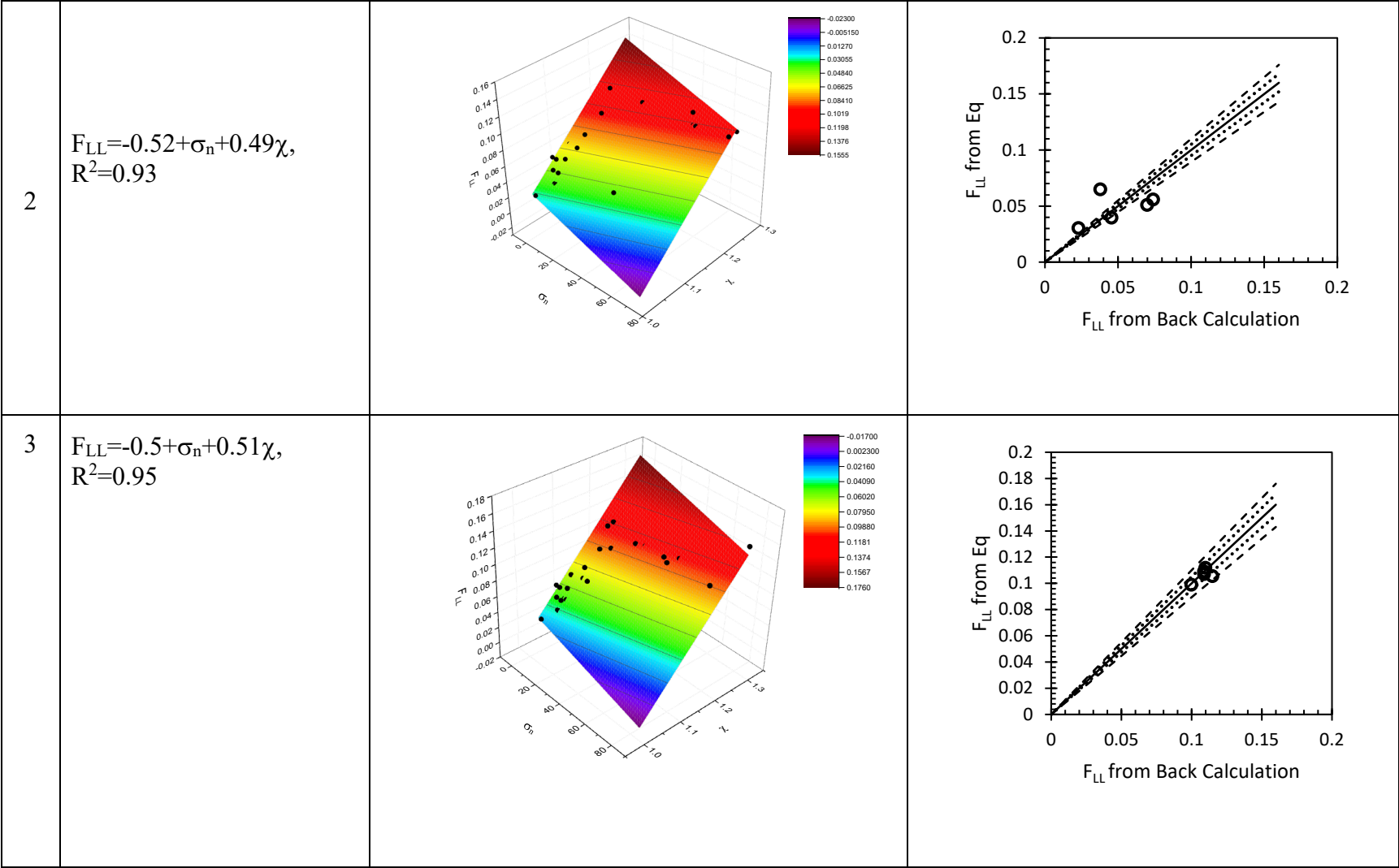
Table 7.25: Soils considered in this study for the sampling approach to predict LL and PL along with their geotechnical properties.

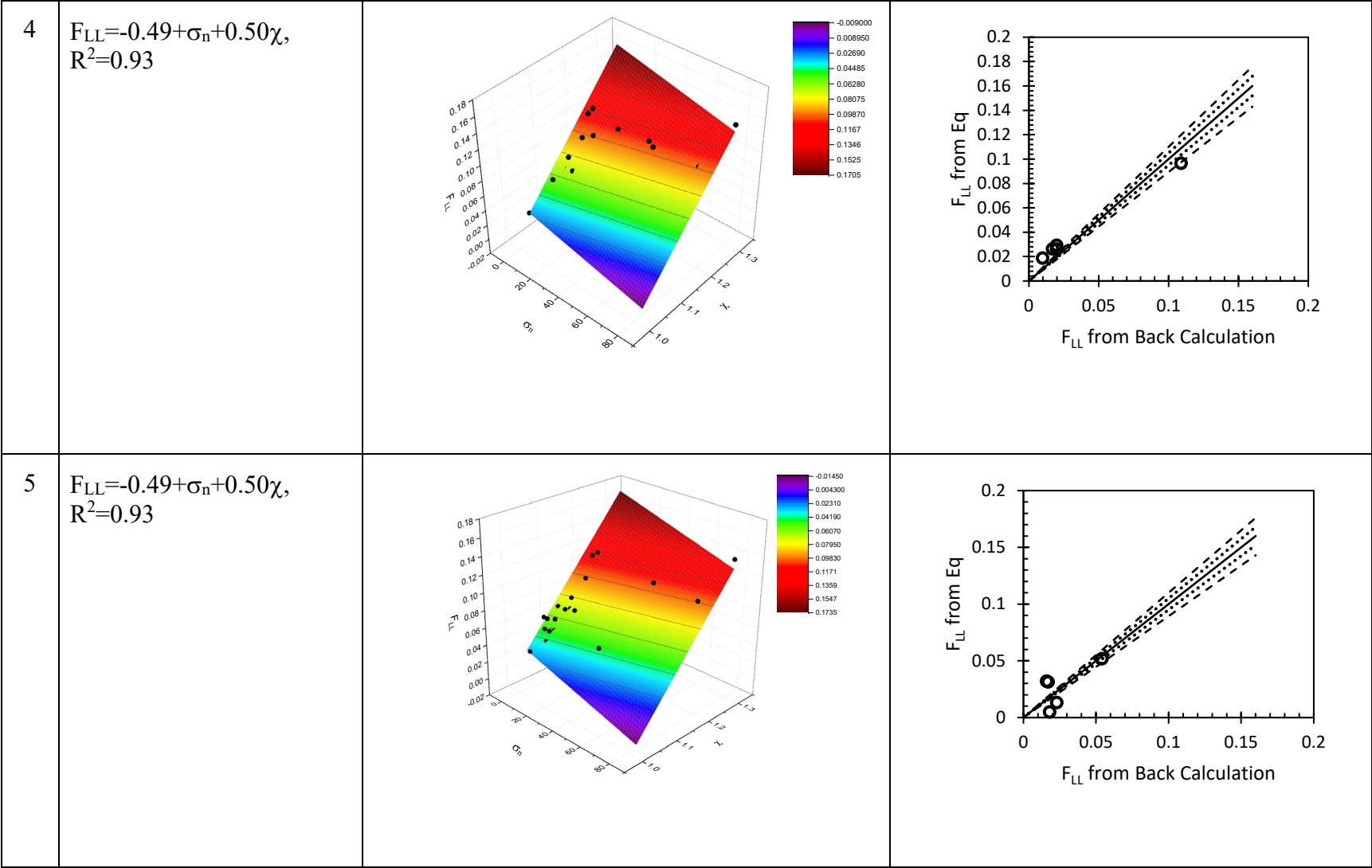
No	Soil	σ_s (S/m)	χ	F _{LL}	F _{PL}	G _s	LL (%)			PL (%)	
							EC	Cone	Casagrande	EC	Thread -rolling
1.	Kaolin	0.0034	1.07	0.12	0.11	2.58	74	74	74	32	32
2.	Dermosol	0.0011	1.1	0.06	0.16	2.6	59	59	58	28	29
3.	Chromosol	0.0032	1.05	0.04	0.08	2.59	58	58	58	28	27
4.	Vertosol	0.0009	1.07	0.06	0.11	2.58	49	49	49	28	28
5.	Red mud	0.0020	1.09	0.07	0.15	2.6	50	50	51	27	26
6.	Expansive	0.0025	1.18	0.1	0.22	2.57	77	77	77	39	39
7.	Red mud-2	0.0018	1.06	0.05	0.09	2.62	47	47	47	29	29
8.	Flowerdale	0.0007	1.02	0.03	0.11	2.56	29	29	29	21	21
9.	Coburg-2	0.0007	1.07	0.06	0.11	2.62	50	50	-	28	28
10.	Coburg-3	0.0007	1.06	0.05	0.09	2.55	51	51	-	28	28
11.	Craigieburn-1	0.0062	1.25	0.11	0.19	2.6	97	96	-	50	50
12.	Craigieburn-2	0.0008	1.12	0.08	0.12	2.65	61	61	-	29	29
13.	Wonterxina	0.0047	1.22	0.11	0.07	2.59	90	90	-	44	44
14.	Wollert-1	0.0022	1.15	0.09	0.02	2.62	70	69	-	33	33
15.	Wollert-2	0.0015	1.17	0.07	0.34	2.6	62	62	-	38	38
16.	Jae	0.0045	1.22	0.11	0.14	2.61	93	92	-	46	46
17.	Officer	0.0007	1.11	0.04	0.47	2.63	57	57	-	26	26
18.	BH1	0.0006	1.08	0.06	0.14	2.58	55	55	-	26	26

19.	S16	0.0069	1.3	0.13	0.4	2.61	94	94	-	40	40
20.	S17	0.00078	1.031	0.12	0.45	2.56	73	72	-	25	25
21.	S18	0.00079	1.03	0.11	0.445	2.56	75	74	-	24	24
22.	S1	0.0062	1.23	0.13	0.2	2.59	92	92	-	49	48
23.	S2	0.00077	1.031	0.09	0.22	2.56	73	73	-	22	22
24.	S3	0.00072	1.03	0.04	0.07	2.56	60	59	-	21	20
25.	S4	0.00088	1.038	0.11	0.3	2.61	75	75	-	22	23
26.	S5	0.00069	1.015	0.05	0.11	2.55	60	60	-	20	20
27.	S6	0.00266	1.21	0.12	0.3	2.62	81	81	-	36	36
28.	S7	0.00534	1.228	0.13	0.3	2.61	85	84	-	45	45
29.	S8	0.00225	1.2	0.12	0.3	2.6	78	78	-	42	42
30.	S9	0.00382	1.214	0.12	0.31	2.6	84	84	-	40	40
31.	S10	0.00136	1.17	0.10	0.25	2.58	73	73	-	38	38
32.	S11	0.00083	1.035	0.06	0.12	2.55	67	67	-	24	24
33.	S12	0.00149	1.22	0.16	0.4	2.6	86	86	-	40	40
34.	S13	0.00081	1.034	0.05	0.11	2.55	62	62	-	23	23
35.	S14	0.00125	1.16	0.07	0.16	2.57	69	69	-	36	36
36.	S15	0.00422	1.217	0.12	0.3	2.6	84	84	-	40	39
37.	Bendigo	0.0021	1.01	0.02	0.02	2.59	39	39	40	23	23
38.	Clyde North	0.0035	1.02	0.024	0.03	2.65	49	48	49	22	22
39.	Coburg-1	0.0008	1.07	0.05	0.16	2.64	52	52	-	29	29

Table 7.26: Statistical resampling approach to validate the accuracy of F_{LL} prediction.

Set No	Equations	3D Surface Analyses	Validations
1	$F_{LL} = -0.53 + \sigma_n + 0.50\chi,$ $R^2 = 0.93$	 <p>A 3D surface plot showing the relationship between F_{LL} (vertical axis, ranging from -0.02 to 0.16), σ_n (horizontal axis, ranging from 0 to 80), and χ (depth axis, ranging from 1.0 to 1.3). The surface is colored with a gradient from blue (low F_{LL}) to red (high F_{LL}). Data points are plotted on the surface.</p>	 <p>A scatter plot showing the relationship between F_{LL} from Eq (Y-axis, ranging from 0 to 0.2) and F_{LL} from Back Calculation (X-axis, ranging from 0 to 0.2). The data points are clustered around the 1:1 line, indicating high accuracy. Dashed lines represent the confidence interval.</p>





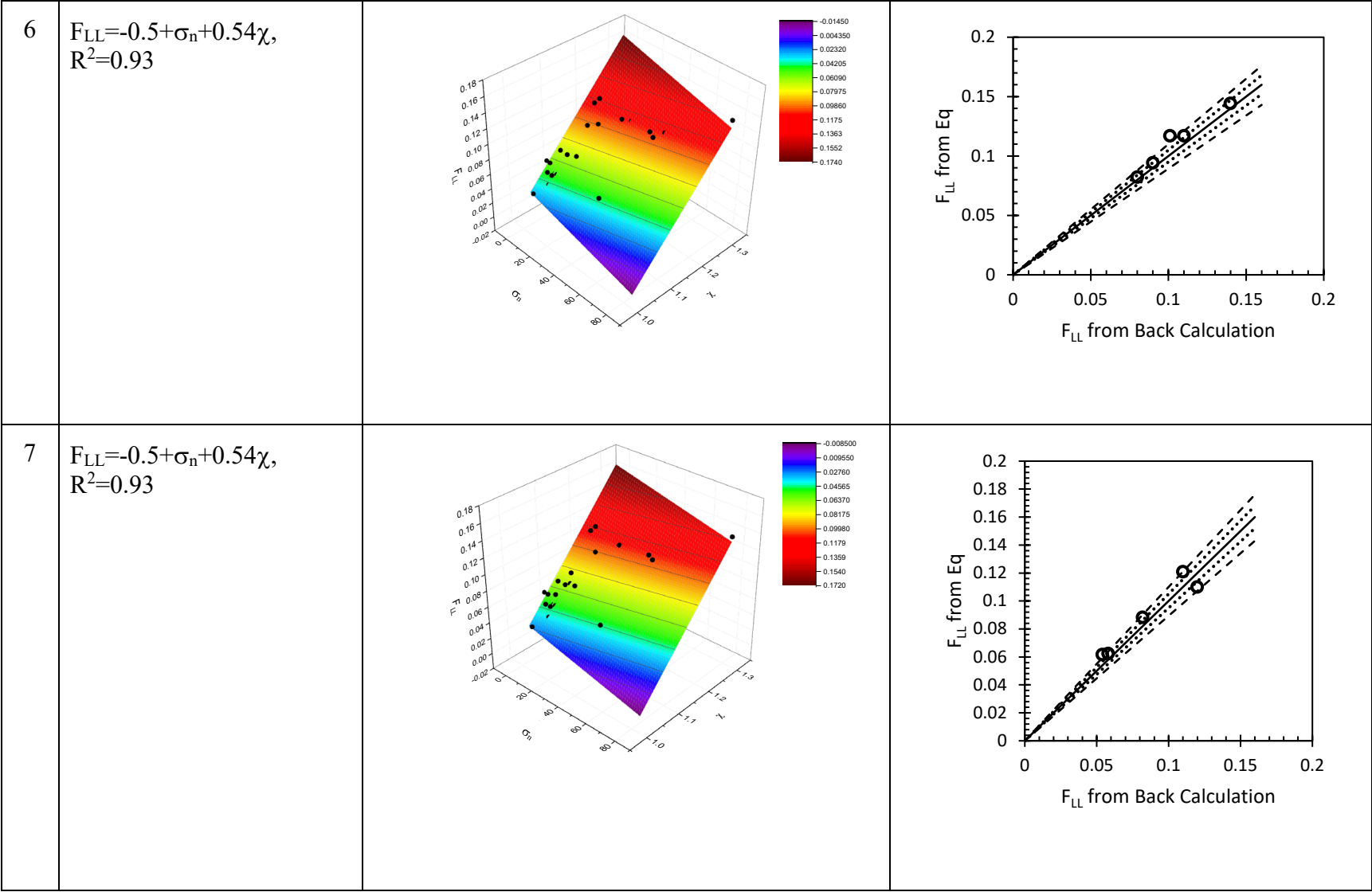
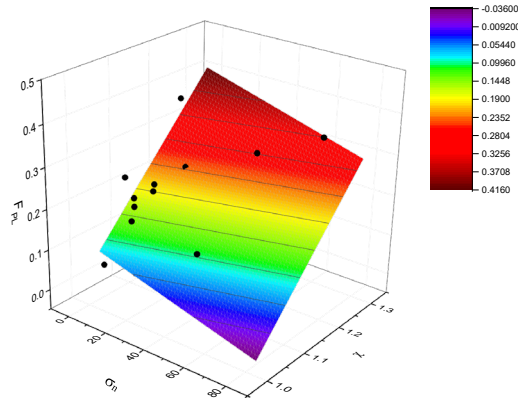
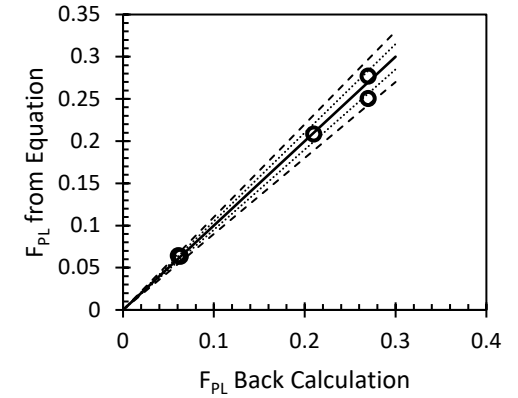
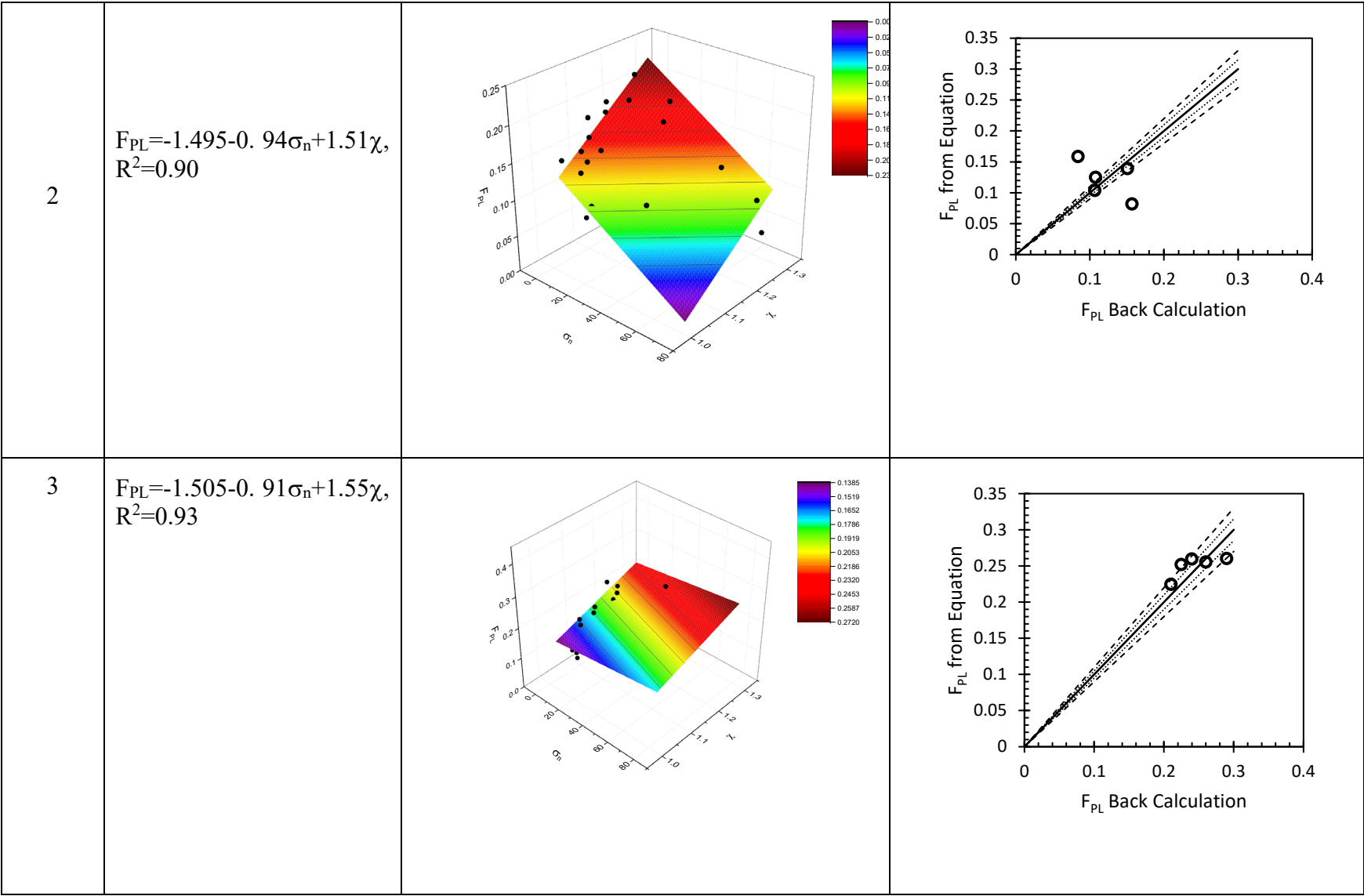
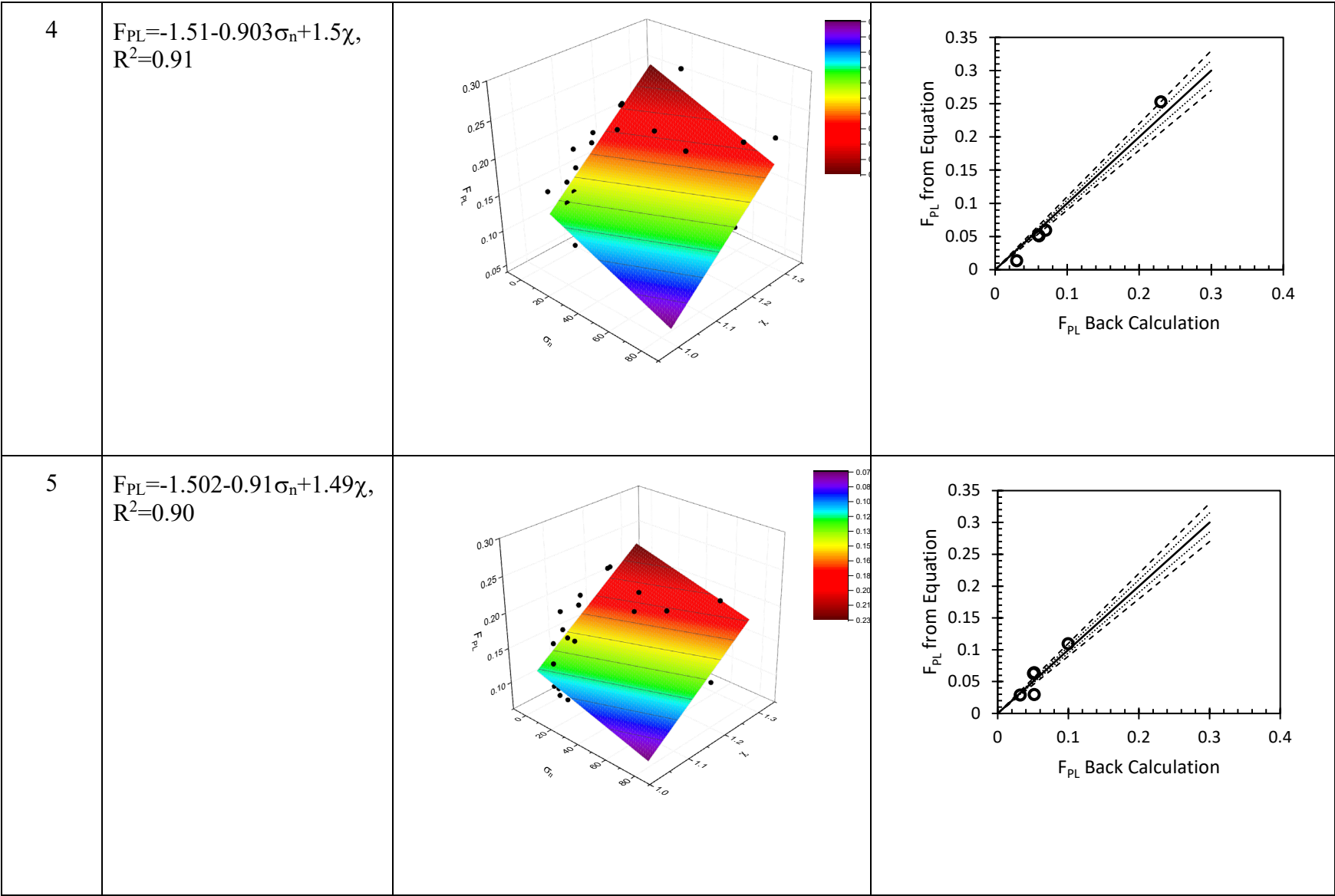
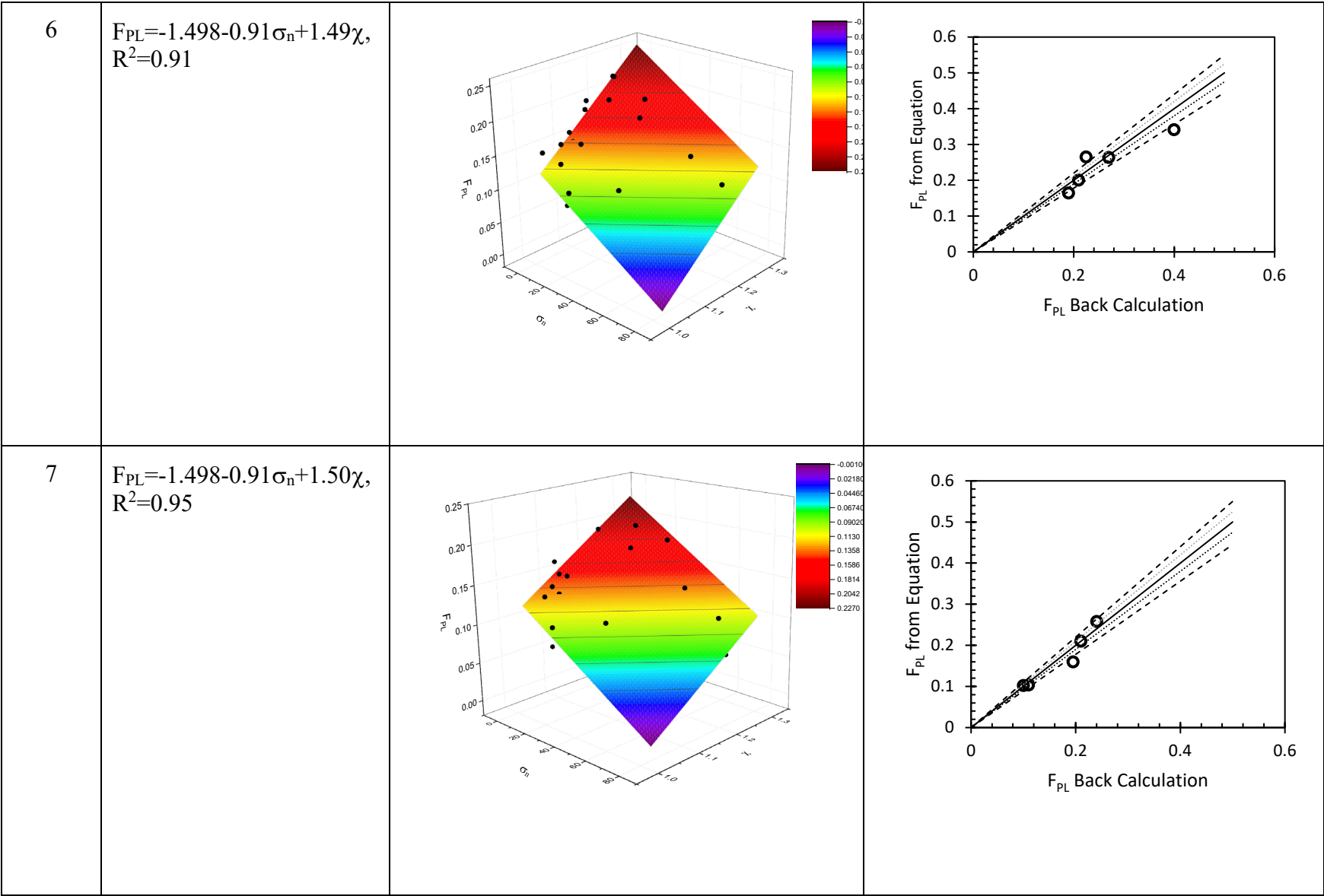


Table 7.27: Statistical resampling approach to assess the accuracy of F_{PL} prediction.

Set No	Equations	3D Surface Analyses	Validations
1	$F_{PL} = -1.49 - 0.91\sigma_n + 1.49\chi,$ $R^2 = 0.92$		







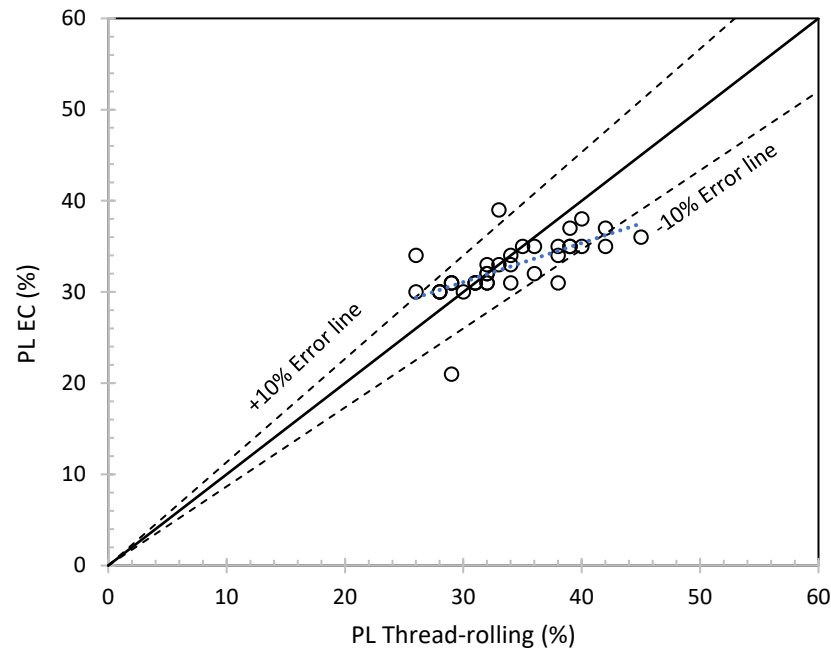


Figure 7.91: Agreement between the thread-rolling test and the EC technique to determine the plastic limit of soils.

7.7 Summary

A new technique to determine the liquid and plastic limits of soils by utilising the electrical conductivity of soils was introduced. In order to develop the numerical prediction model, the non-dimensional electrical surface conduction parameters σ_n and χ were considered to develop the relationship with volumetric water content ratio F using the resampling approach. The parameter F was initially predicted by the back-calculation approach with soils of known liquid limit and plastic limit. Later, numerical analyses were performed to determine the equations to predict F and the statistical resampling approach was performed in different sets to assess the accuracy of the prediction. A total of 39 different fine-grained soils were considered in this study. The statistical resampling approach comprised the selection of 34 soils in each group and predicting the F_{LL} and F_{PL} of 5 other soils. There were 7 sets of groups created for the statistical resampling approach to ensure all the soils fall into one set for the validation. The predicted F was later utilised to calculate the liquid

limit and plastic limit of soils and the obtained results were validated by conventional methods and showed good agreement.

Chapter 8

Conclusions and Recommendations

8.1 Summary

In this thesis, a new approach for modelling the electrical conductivity of fully saturated fine-grained soils was proposed. Furthermore, the application of electrical properties in the soil classification field was explored. At first, a simple method was proposed to determine the electrical surface conduction of the solid clay particles and its evolution as the temperature and pore water salinity change. The proposed electrical conduction parameters of the solid clay particles were used to develop a series-parallel, structure-oriented electrical conductivity model of fully saturated fine-grained soils. In the next stages, the electrical properties of soils were used to introduce new testing approaches in the soil classification field to determine particle size distribution, liquid limit (LL) and plastic limit (PL). All of the experimental results were subject to adequate validations to gain more confidence in the study. The following sections contain chapter by chapter summaries of the work, along with a short discussion on the shortcomings, if applicable.

8.1.1 Findings After Literature Review

At the initial stage, extensive literature review was conducted to identify the ongoing trends in the soil classification applications and possible inclusion of electrical conductivity technique in the same. To serve this purpose, at first, the existing electrical conductivity models were thoroughly studied, and the advantages and disadvantages of those proposed approaches were recorded in the light of the requirement of the present approach. It was found that empirical parameters would be required to propose the new series-parallel model, however, those parameters would require standard representation and definition.

Therefore, the parameters σ_s and χ were introduced. Later, the sensitivity of the parameters was studied.

In the second phase of the literature review, the existing soil classification applications, with or without the involvement of electrical conductivity (EC) technique, were studied. EC technique was identified to have the potential to replace the existing conventional methods, which are time-consuming and less accurate. The detailed literature review has been included in [Chapter 2](#).

8.1.2 Electrical Surface Conduction of Solid Clay Particles

Most of the electrical conductivity models in the literature include some empirical parameters which have no physical meaning to consider the role of the electrical surface conduction of solid clay particles in the electrical conductivity (EC) of soils. The first aim of this research was to model the EC of soils with well-defined parameters that include the effect of electrical surface conduction of solid clay particles. Therefore, [Chapter 4](#) provided more information on the definition and determination of the proposed electrical surface conduction parameters of the solid clay particles in this study (σ_s and χ). The effect of pore water salinity was investigated and the test results show that with an increase in pore water salinity (EC of water), σ_s increased and χ decreased. Later, temperature was varied to observe the effect on the EC of clay ingredients. It was found that as the temperature increased, the EC of water increased and at the same time χ also decreased due to the increase in the salinity of water. A further validation test was conducted to assess the changes in the thickness of the diffuse double layer (DDL) at elevated temperature and pore water salinity. The free swelling test showed that with an increase in temperature, the thickness of the DDL decreases as the EC of water increases.

8.1.3 Series-Parallel, Structure-oriented EC Model of Saturated Clays

A new series-parallel model was introduced to determine the EC of fully saturated, organic-free clays. The model considers the role of the electrical surface conduction parameters of clay particles by including two parameters that describe the apparent electrical conductivity of effective clay particle (σ_s) as well as the size of the DDL (χ), as presented in [Chapter 4](#).

The clay particle and the DDL were combined to form one single unit which was defined as the equivalent conductive material, assigned with isotropic apparent electrical conductivity. Therefore, saturated fine-grained soils were considered to be two-phase material comprising free water and effective clay particles. The particle orientation was denoted by one single parameter Ω , which can be determined by a simple experiment. The parameter Ω represented the anisotropy of the clay fabric, which was considered in the model for validation purposes. The model was validated by the experiment results of 10K, 10B, and 5K-5B clays, reconstituted at different compaction levels and particle orientations. The comparisons between the predicted and experimentally measured values displayed good agreement.

8.1.4 Particle Size Distribution of Soils

Although there are several ways to determine the PSD of soils, they all have advantages and disadvantages which were discussed in [Chapter 2](#).

The electrical conductivity approach proposed in this study to determine the particle size distribution (PSD) of soils provides a new basis for research which aims to reduce the limitations and expenditure of the available techniques. A new tool was developed in this study which replaces the conventional hydrometer with metal electrodes, placed at different distances from the sedimentation base. The proposed method involves the electrical conductivity calibration of the fine soil suspension at three different densities. The new

method proposed in this study considers the conventional sedimentation theory and Stokes' diameter of soil particles. With this new approach, it was possible to obtain the PSD curves of soils in only 1-2 hours and the results were validated against the results obtained by hydrometer, pipette, and laser diffraction analysis. The comparisons between the results provide strong support for the new method.

8.1.5 Liquid Limit and Plastic Limit of Soils

The electrical conductivity approach to determine the liquid limit and plastic limit required σ_s and χ and a new volume fraction parameter F which is the ratio volumetric water content of DDL and free water. A new equation was introduced which considered the effect of the aforementioned parameters along with the specific gravity (G_s) of soils. A sampling approach was considered based on the back-calculation to initially determine F using soils with a known liquid limit and plastic limit. Later, the statistical resampling approach was used to determine equations to predict F for both liquid limit and plastic limit. With the F obtained from the new equations, the liquid limit and plastic limit of each soil was predicted and compared with the results obtained from the conventional methods. In general, good agreement was observed.

8.2 Recommendations for Future Studies

This research provides a new platform from which to study the electrical properties of soils with a view to addressing the different geotechnical testing of soil. However, further research is still required to properly investigate the electrical conductivity models of soils.

The following recommendations are highlighted for future studies:

- The effect of temperature on the size of the DDL requires further investigation along with the free swelling test. Although the free swelling test has provided guidelines and information regarding the decrease in the DDL thickness at elevated

temperatures, further numerical modelling needs to be undertaken to properly understand and predict behavioural changes in the thickness of DDL.

- The series-parallel model for saturated soils can be extended further to consider the effect of coarse-grained material. In this case, a new parameter could be included to define the percentage of fines in a specific soil sample.
- The electrical conductivity model contains mere experimental works. The model is valid for fine-grained saturated clays only. The model could be further extended to predict both fine-grained and coarse-grained soils
- Determining the PSD of soils using the EC method should be computer-operated rather than relying on manual handling. A simple software program could be developed which will create a spreadsheet calculating particle diameter at different electrode locations at certain time intervals. A similar approach could be initiated in terms of calibration as well. In this way, the possibility of human-made error is lessened.
- Determining the liquid limit and plastic limit values using the EC method showed promising results in this dissertation. However, more samples are required to build a strong belief in the accuracy of the liquid limit and plastic limit. In addition, soils with different geotechnical properties such as liquid limit and plasticity index should be considered to build a better correlation between the parameters.

8.3 Concluding Remarks

The electrical conductivity of soils has been studied over the centuries, but few studies used the electrical properties of soil in the soil classification field. This thesis enhanced the understanding of the electrical surface conduction of solid clay particles and incorporated this knowledge in developing the electrical conductivity model of saturated clays. This study also makes use of the sedimentation-induced evolution of electrical conductivity of

fine soil suspension to determine the particle size distribution of fine soil. Finally, as clay mineralogy and pore water salinity control the electrical surface conduction parameters of the solid clay particles proposed in this study, these parameters could also be used to predict the LL and PL of soils. This chapter provides a summary of the thesis and re-visits the earlier discussions on the contribution of each chapter. In order to open the door for further research, some recommendations have been made which will improve both conceptual and experimental understanding.

One of the major advantages of this study is the cost effectiveness of the experimental tools presented in this study. In Chapter 6, a new PSD tool was presented. The acrylic tool itself cost \$3, and the brass metal sheet was purchased with \$10. The wires and epoxy combinedly cost less than \$8. Therefore, the total cost to purchase was the materials to make the tool was approximately \$21, and all the items were Australian made. The costs of the available devices to determine PSD range from \$100 to \$50,000 (presented in [Tables 2.3-2.7](#)). In addition, the equipment/material used in the experimental programmes were also Australian made and relatively cheaper. No equipment or tool was used in this study which was purchased from outside Australia.

The application electrical conductivity method can be further expanded to find other geotechnical properties of soils such as shrinkage limit (part of Atterberg Limit), shear strength, deformation properties of soils, to name a few. As mentioned in Chapter 7, a soil has a specific moisture content at liquid limit and plastic limit, and hence the similar database could be built to identify shrinkage limit, and hence the whole Atterberg Limit of soil could be determined by EC technique. Meanwhile, soil deformations are subject to the influence of mechanical loading or environmental changes. Deformation due to the loading is governed by the appropriate stress-strain curve of the soil, which could be calibrated by recording EC. In addition, environmental changes will lead to changes in microstructural

properties of the soil, and hence EC of the soil would be different at different stage. On the other hand, to determine shear strength of the soil, the magnitude of the shear stress that a soil can sustain needs to be determined. This characteristic can also be developed by the calibration technique, where EC would be determined at the shear strength of the soil and later by using the calibrated values of EC, shear strength of the soil can be predicted. However, further experimental analyses and validation would be required, which is under consideration for the future study.

List of References

- Abuel-Naga, H.M., Bergado, D.T., Bouazza, A., 2007. Thermally induced volume change and excess pore water pressure of soft Bangkok clay. *Engineering Geology* 89, 144–154.
- Abu-Hassanein, Z.S., Benson, C.H., Blotz, L.R., 1996. Electrical resistivity of compacted clays. *Journal of geotechnical engineering* 122, 397–406..
- Allen, T., 2013. Particle size measurement. Springer.
- Almanza, R., Castaneda, R., Silva, G., 1996. Temperature-electrolyte effects on clay soil liners, in: *Unsaturated Soils*. pp. 343–348.
- Alsharari, B., Olenko, A., Abuel-Naga, H., 2020. Modeling of electrical resistivity of soil based on geotechnical properties. *Expert Systems with Applications* 141, 112966. <https://doi.org/10.1016/j.eswa.2019.112966>
- Anandarajah, A., 2000. On influence of fabric anisotropy on the stress–strain behavior of clays. *Computers and geotechnics* 27, 1–17.
- Anandarajah, A., Chen, J., 1997. Van der Waals attractive force between clay particles in water and contaminants. *Soils and foundations* 37, 27–37.
- Anandarajah, A., Kuganenthira, N., 1995. Some aspects of fabric anisotropy of soil. *Geotechnique* 45, 69–81.
- Andrade, F.A., Al-Qureshi, H.A., Hotza, D., 2011. Measuring the plasticity of clays: a review. *Applied Clay Science* 51, 1–7.
- Andreasen, A.H., 1928. Zur Kenntnis des mahlgutes. *Fortschrittsberichte über Kolloide und Polymere* 27, 349–458.
- Ansi, B., n.d. ASTM D698-Test Methods for Moisture-Density Relations of Soils and Soil-Aggregate Mixtures. Method A (Standard Proctor).
- Archie, G.E., 1942. The electrical resistivity log as an aid in determining some reservoir characteristics. *Transactions of the AIME* 146, 54–62.
- Arora, K.R., 2008. Soil mechanics and foundation engineering (geotechnical engineering). Standard Publishers Distributors, Nai Sarak, Delhi, 953p.
- Arulanandan, K., 1969. Hydraulic and electrical flows in clays. *Clays and Clay Minerals* 17, 63–76.
- ASTM, D., 2010. Standard test methods for specific gravity of soil solids by water pycnometer.
- ASTM, D., n.d. G57-06 (2012) Standard test method for field measurement of soil resistivity using the Wenner four-electrode method. ASTM International, USA.
- ASTM. 1996c. Standard classification of soils for engineering purposes (Unified Soil Classification System), Standard D 2487-93. West Conshohocken, Pa.: American Society for Testing and Materials.
- Atkins Jr, E.R., Smith, G.H., 1961. The significance of particle shape in formation resistivity factor-porosity relationships. *Journal of Petroleum Technology* 13, 285–291.
- Atkinson, C.M.L., Wilson, R., 1983. Artefact peaks in particle size distributions measured by the electrical sensing zone (coulter counter) method. *Powder Technology* 34, 275–284.

- Bai, W., Kong, L., Guo, A., 2013. Effects of physical properties on electrical conductivity of compacted lateritic soil. *Journal of Rock Mechanics and Geotechnical Engineering* 5, 406–411.
- Baran, B., Ertürk, T., Sarıkaya, Y., Alemdaroğlu, T., 2001. Workability test method for metals applied to examine a workability measure (plastic limit) for clays. *Applied clay science* 20, 53–63.
- Bekker, P.C.F., 1981. Simple clay testing methods. *ZI INT. ZI Int.* 33, 494.
- Benbow, J., Bridgwater, J., 1993. Paste flow and extrusion.
- Benson, C.H., Daniel, D.E., 1994. Minimum thickness of compacted soil liners: I. Stochastic models. *Journal of geotechnical engineering* 120, 129–152.
- Bergaya, F., Theng, B.K.G., Lagaly, G., 2006. *Handbook of clay science*. Elsevier, Amsterdam. *Handbook of clay science*. Elsevier, Amsterdam.
- Bharat, T.V., Sivapullaiah, P.V., Allam, M.M., 2013. Novel procedure for the estimation of swelling pressures of compacted bentonites based on diffuse double layer theory. *Environmental Earth Sciences* 70, 303–314.
- Blight, G.E., 1997. Origin and formation of residual soils. *Mechanics of Residual Soil* 1, 15.
- Blott, S.J., Croft, D.J., Pye, K., Saye, S.E., Wilson, H.E., 2004. Particle size analysis by laser diffraction. *Geological Society, London, Special Publications* 232, 63–73.
- Blott, S.J., Pye, K., 2006. Particle size distribution analysis of sand-sized particles by laser diffraction: an experimental investigation of instrument sensitivity and the effects of particle shape. *Sedimentology* 53, 671–685.
- Bolt, G.H., 1956. Physico-chemical analysis of the compressibility of pure clays. *Geotechnique* 6, 86–93.
- Bouksila, F., Persson, M., Berndtsson, R. and Bahri, A., 2008. Soil water content and salinity determination using different dielectric methods in saline gypsiferous soil/Détermination de la teneur en eau et de la salinité de sols salins gypseux à l'aide de différentes méthodes diélectriques. *Hydrological Sciences Journal*, 53(1), pp.253-265.
- Brevik, E.C., Fenton, T.E., Horton, R., 2004. Effect of daily soil temperature fluctuations on soil electrical conductivity as measured with the Geonics® EM-38. *Precision Agriculture* 5, 145–152.
- Briaud, J.-L., 2013. *Geotechnical engineering: unsaturated and saturated soils*. John Wiley & Sons.
- Brillante, L., Mathieu, O., Bois, B., van Leeuwen, C., Lévêque, J., 2015. The use of soil electrical resistivity to monitor plant and soil water relationships in vineyards. *Soil* 1, 273–286.
- Brunet, P., Clément, R., Bouvier, C., 2010. Monitoring soil water content and deficit using Electrical Resistivity Tomography (ERT)—A case study in the Cevennes area, France. *Journal of Hydrology* 380, 146–153.
- Bryson, L.S., 2005. Evaluation of geotechnical parameters using electrical resistivity measurements, in: *Earthquake Engineering and Soil Dynamics*. pp. 1–12.
- Budhu, M., 1985. The effect of clay content on liquid limit from a fall cone and the British cup device. *Geotechnical Testing Journal* 8, 91–95.
- Campbell, D.J., 1976. Plastic limit determination using a drop-cone penetrometer. *Journal of Soil Science* 27, 295–300.

- Casagrande, A., 1958. Notes on the design of the liquid limit device. *Geotechnique* 8, 84–91.
- Casagrande, A., 1932. Research on the Atterberg limits of soils. *Public roads* 13, 121–136.
- Casagrande, I.L., 1949. Electro-osmosis in soils. *Geotechnique* 1, 159–177.
- Chai, J.C., Carter, J.P., Hayashi, S., 2005. Ground deformation induced by vacuum consolidation. *Journal of geotechnical and geoenvironmental engineering* 131, 1552–1561.
- Chang, W., Soto-Crespo, J.M., Ankiewicz, A., Akhmediev, N., 2009. Dissipative soliton resonances in the anomalous dispersion regime. *Physical Review A* 79, 033840.
- Chapman, D.L., 1913. LI. A contribution to the theory of electrocapillarity. *The London, Edinburgh, and Dublin philosophical magazine and journal of science* 25, 475–481.
- Cheetham, M.D., Keene, A.F., Bush, R.T., Sullivan, L.A., Erskine, W.D., 2008. A comparison of grain-size analysis methods for sand-dominated fluvial sediments. *Sedimentology* 55, 1905–1913.
- Cho, W.J., Lee, J.O., Chun, K.S., 1999. The temperature effects on hydraulic conductivity of compacted bentonite. *Applied clay science* 14, 47–58.
- Chung, C.-C., Lin, C.-P., Yang, S.-H., Lin, J.-Y., Lin, C.-H., 2019. Investigation of non-unique relationship between soil electrical conductivity and water content due to drying-wetting rate using TDR. *Engineering Geology* 252, 54–64.
- Coduto, D.P., 1999. *Geotechnical engineering: principles and practices*.
- Corwin, D.L., Lesch, S.M., 2005. Apparent soil electrical conductivity measurements in agriculture. *Computers and electronics in agriculture* 46, 11–43.
- Coulter, W.H., 1953a. Means for counting particles suspended in a fluid.
- Cui, W., Potts, D.M., Zdravković, L., Gawęcka, K.A., Taborda, D.M., 2018. An alternative coupled thermo-hydro-mechanical finite element formulation for fully saturated soils. *Computers and Geotechnics* 94, 22–30.
- Cui, Y.J., Yahia-Aissa, M., Delage, P., 2002. A model for the volume change behavior of heavily compacted swelling clays. *Engineering Geology* 64, 233–250.
- Das, B.M., 2013. *Advanced soil mechanics*. Crc Press.
- Day, P.R., 1965. Particle fractionation and particle-size analysis. American Society of Agronomy, Soil Science Society of America.
- Day, P.R., 1950. Physical basis of particle size analysis by the hydrometer method. *Soil science* 70, 363–374.
- De La Fuente, S., Cuadros, J., Fiore, S., Linares, J., 2000. Electron microscopy study of volcanic tuff alteration to illite-smectite under hydrothermal conditions. *Clays and Clay Minerals* 48, 339–350.
- De Oliveira Modesto, C., Bernardin, A.M., 2008. Determination of clay plasticity: indentation method versus Pfefferkorn method. *Applied Clay Science* 40, 15–19.
- Der Velden, V., 1979. Analysis of the Pfefferkorn test. *ZI INT. ZI Int.* 532.
- Di Matteo, L., 2012. Liquid limit of low-to medium-plasticity soils: comparison between Casagrande cup and cone penetrometer test. *Bulletin of Engineering Geology and the Environment* 71, 79–85.

- Dolinar, B., Mišić, M., Trauner, L., 2007. Correlation between surface area and Atterberg limits of fine-grained soils. *Clays and Clay Minerals* 55, 519–523.
- Doménech, V., Sánchez, E., Sanz, V., García, J., Ginés, F., 1994. Assessing the plasticity of ceramic masses by determining indentation force, in: *Qualicer 94. III World Congress On Ceramic Tile Quality. General Lectures and Open Papers II Castellon*.
- Dondi, M., 1999. Clay materials for ceramic tiles from the Sassuolo District (Northern Apennines, Italy). *Geology, composition and technological properties. Applied Clay Science* 15, 337–366.
- Drief, A., Martínez-Ruiz, F., Nieto, F., Sanchez, N.V., 2002. Transmission electron microscopy evidence for experimental illitization of smectite in K-enriched seawater solution at 50 C and basic pH. *Clays and Clay Minerals* 50, 746–756.
- Durner, W., Iden, S.C., von Unold, G., 2017. The integral suspension pressure method (ISP) for precise particle-size analysis by gravitational sedimentation. *Water Resources Research* 53, 33–48.
- Elimelech, M., Gregory, J., Jia, X., 2013. *Particle deposition and aggregation: measurement, modelling and simulation*. Butterworth-Heinemann.
- Ellis, M.H., Sinha, M.C., Minshall, T.A., Sothcott, J., Best, A.I., 2010. An anisotropic model for the electrical resistivity of two-phase geologic materials. *Geophysics* 75, E161–E170.
- EN, B., 1997. 2: 2007. “Eurocode 7-Geotechnical design-Part 2: Ground investigation and testing.” The European Union Regulation 305/2011, Directive 98/34/EC, Directive 2004/18/EC.
- Eshel, G., Levy, G.J., Mingelgrin, U., Singer, M.J., 2004. Critical evaluation of the use of laser diffraction for particle-size distribution analysis. *Soil Science Society of America Journal* 68, 736–743.
- Estabragh, A.R., Khosravi, F., Javadi, A.A., 2016. Effect of thermal history on the properties of bentonite. *Environmental Earth Sciences* 75, 657.
- Evans, J.C., 1991. *Geotechnics of hazardous waste control systems*, in: *Foundation Engineering Handbook*. Springer, pp. 750–777.
- Farzamian, M., Santos, F.A.M., Khalil, M.A., 2015. Application of EM38 and ERT methods in estimation of saturated hydraulic conductivity in unsaturated soil. *Journal of applied geophysics* 112, 175–189.
- Feng, T.-W., 2004. Using a small ring and a fall-cone to determine the plastic limit. *Journal of Geotechnical and Geoenvironmental Engineering* 130, 630–635.
- Feng, T.-W., 2000. Fall-cone penetration and water content relationship of clays. *Geotechnique* 50, 181–187.
- Flores, O.J., Andrade, F.A., Hotza, D., Al-Qureshi, H.A., 2010. Modeling of plasticity of clays submitted to compression test. *World Acad. Sci. Eng. Technol* 61, 191–196.
- Fookes, P.G., 1997. *Tropical residual soils: A Geological Society Engineering Group working party revised report*. Geological Society of London.
- Friedman, S.P., 2005. Soil properties influencing apparent electrical conductivity: a review. *Computers and electronics in agriculture* 46, 45–70.
- Fukue, M., Minato, T., Horibe, H., Taya, N., 1999. The micro-structures of clay given by resistivity measurements. *Engineering geology* 54, 43–53.

- Gabas, N., Hiquily, N., Laguérie, C., 1994. Response of laser diffraction particle sizer to anisometric particles. *Particle & particle systems characterization* 11, 121–126.
- Gee, G.W., Bauder, J.W., 1979. Particle size analysis by hydrometer: a simplified method for routine textural analysis and a sensitivity test of measurement parameters 1. *Soil Science Society of America Journal* 43, 1004–1007.
- Glover, P.W., 2010. A generalized Archie's law for n phases. *Geophysics* 75, E247–E265.
- Goldstein, J.I., Williams, D.B., Cliff, G., 1986. Quantitative X-ray analysis, in: *Principles of Analytical Electron Microscopy*. Springer, pp. 155–217.
- Gouy, M., 1910. Sur la constitution de la charge électrique à la surface d'un électrolyte. *J. Phys. Theor. Appl.* 9, 457–468.
- Goyal, V.C., Gupta, P.K., Seth, S.M., Singh, V.N., 1996. Estimation of temporal changes in soil moisture using resistivity method. *Hydrological processes* 10, 1147–1154.
- Graham, J., Oswell, J.M., Gray, M.N., 1992. The effective stress concept in saturated sand–clay buffer. *Canadian Geotechnical Journal* 29, 1033–1043.
- Greve, A.K., Roshan, H., Kelly, B.F.J., Acworth, R.I., 2013. Electrical conductivity of partially saturated porous media containing clay: an improved formulation. *Journal of Geophysical Research: Solid Earth* 118, 3297–3303.
- Gunn, D.A., Chambers, J.E., Uhlemann, S., Wilkinson, P.B., Meldrum, P.I., Dijkstra, T.A., Haslam, E., Kirkham, M., Wragg, J., Holyoake, S., 2015. Moisture monitoring in clay embankments using electrical resistivity tomography. *Construction and Building Materials* 92, 82–94.
- Guen, N., 1992. Molecular aspects of clay-water interactions. *Clay-water interface and its rheological implications* 2–79.
- Haigh, S.K., 2012. Mechanics of the Casagrande liquid limit test. *Canadian Geotechnical Journal* 49, 1015–1023.
- Haigh, S.K., Vardanega, P.J., Bolton, M.D., 2013. The plastic limit of clays. *Géotechnique* 63, 435.
- Hammel, J.E., Sumner, M.E., Burema, J., 1983. Atterberg limits as indices of external surface areas of soils. *Soil Science Society of America Journal* 47, 1054–1056.
- Hanks, A.J., 1981. Measurement of the liquid limit of soils using the cone penetration method. The Office.
- Harison, J.A., 1988. Using the BS cone penetrometer for the determination of the plastic limit of soils. *Geotechnique* 38.
- Hasan, M.F., Abuel-Naga, H., Broadbridge, P., Leong, E.-C., 2018. Series-parallel structure-oriented electrical conductivity model of saturated clays. *Applied Clay Science* 162, 239–251.
- Hashin, Z., Shtrikman, S., 1962. On some variational principles in anisotropic and nonhomogeneous elasticity. *Journal of the Mechanics and Physics of Solids* 10, 335–342.
- Head, K.H., 1980. *Manual of soil laboratory testing*. Pentech Press London.
- Head, K.H., Epps, R., 1980. *Manual of soil laboratory testing*. Pentech Press London.
- Herman, R., 2001. An introduction to electrical resistivity in geophysics. *American Journal of Physics* 69, 943–952.

- Hietala, S.L., Smith, D.M., 1989. Porosity effects on particle size determination via sedimentation. *Powder technology* 59, 141–144.
- Higgins, A.Z., Karlsson, J.O., 2008. Coincidence error during measurement of cellular osmotic properties by the electrical sensing zone method. *CryoLetters* 29, 447–461.
- Holmboe, M., Wold, S., Jonsson, M., 2012. Porosity investigation of compacted bentonite using XRD profile modeling. *Journal of Contaminant Hydrology* 128, 19–32.
- Holtz, W.G., Gibbs, H.J., 1956. Triaxial shear tests on pervious gravelly soils. *Journal of the Soil Mechanics and Foundations Division* 82, 1–22.
- Hong, C.S., Shackelford, C.D., Malusis, M.A., 2011. Consolidation and hydraulic conductivity of zeolite-amended soil-bentonite backfills. *Journal of Geotechnical and Geoenvironmental Engineering* 138, 15–25.
- Horpibulsuk, S., Chinkulkijniwat, A., Cholphatsorn, A., Suebsuk, J., Liu, M.D., 2012. Consolidation behavior of soil–cement column improved ground. *Computers and Geotechnics* 43, 37–50.
- Hueckel, T., 1992. On effective stress concepts and deformation in clays subjected to environmental loads: Discussion. *Canadian Geotechnical Journal* 29, 1120–1125.
- Jillavenkatesa, A., Dapkunas, S.J., Lum, L.-S.H., 2001. Particle size characterization. National Institute of Standards and Technology Washington, DC.
- Jones, C.J., Lamont-Black, J., Glendinning, S., 2011. Electrokinetic geosynthetics in hydraulic applications. *Geotextiles and Geomembranes* 29, 381–390.
- Jones, R.B., 1988. Rotational diffusion of a tracer colloid particle: I. Short time orientational correlations. *Physica A: Statistical Mechanics and its Applications* 150, 339–356.
- Kalinski, R.J., Kelly, W.E., 1993. Estimating water content of soils from electrical resistivity. *Geotechnical Testing Journal* 16, 323–329.
- Karuhn, R., Davies, R., Kaye, B.H., Clinch, M.J., 1975. Studies on the Coulter counter part I. Investigation into the effect of orifice geometry and flow direction on the measurement of particle volume. *Powder Technology* 11, 157–171.
- Keller, G.V., Frischknecht, F.C., 1966. Electrical methods in geophysical prospecting.
- Kibria, G., Hossain, M.S., 2015. Investigation of degree of saturation in landfill liners using electrical resistivity imaging. *Waste Management* 39, 197–204.
- Kibria, G., Hossain, S., Khan, M.S., 2018. Determination of consolidation properties using electrical resistivity. *Journal of Applied Geophysics* 152, 150–160.
- Kinsman, S., Hoff, E.V., 1979. A new coulter counter for particle size analysis in the sieve range. *Powder Technology* 24, 155–158.
- Kissa, E., 2017. *Dispersions: characterization, testing, and measurement*. Routledge.
- Klein, K.A., Santamarina, J.C., 2003. Electrical conductivity in soils: Underlying phenomena. *Journal of Environmental & Engineering Geophysics* 8, 263–273.
- Konert, M., Vandenberghe, J.E.F., 1997. Comparison of laser grain size analysis with pipette and sieve analysis: a solution for the underestimation of the clay fraction. *Sedimentology* 44, 523–535.
- Kongas, M., Saloheimo, K., Pekkarinen, H., Turunen, J., 2003. New particle size analysis system for mineral slurries. *IFAC Proceedings Volumes* 36, 309–314.

- Koumoto, T., Houlsby, G.T., 2001. Theory and practice of the fall cone test. *Géotechnique* 51, 701–712.
- Lambe, T.W., Whitman, R.V., 2008. Soil mechanics SI version. John Wiley & Sons.
- Laver, J.A., Griffiths, H., 2001. The variability of soils in earthing measurements and earthing system performance. *Rev. Energ. Ren.: Power Engineering*, School of Electrical Engineering, Cardiff University, UK 57–61.
- Lee, Y.-G., Lee, H.-W., Kim, M.-S., Choi, C.Y., Kim, J., 2008. Characteristics of particle formation events in the coastal region of Korea in 2005. *Atmospheric Environment* 42, 3729–3739.
- Leschonski, K., 1979. Sieve analysis, the Cinderella of particle size analysis methods? *Powder Technology* 24, 115–124.
- Lim, S.C., Gomes, C., Kadir, M., Abidin, M., 2013. Characterizing of bentonite with chemical, physical and electrical perspectives for improvement of electrical grounding systems. *International Journal of Electrochemical Science* 8, 11429–11447.
- Linde, N., Binley, A., Tryggvason, A., Pedersen, L.B., Revil, A., 2006. Improved hydrogeophysical characterization using joint inversion of cross-hole electrical resistance and ground-penetrating radar traveltime data. *Water Resources Research* 42.
- Link, S., El-Sayed, M.A., 1999. Spectral properties and relaxation dynamics of surface plasmon electronic oscillations in gold and silver nanodots and nanorods. ACS Publications.
- Long, M., Donohue, S., L’Heureux, J.-S., Solberg, I.-L., Rønning, J.S., Limacher, R., O’Connor, P., Sauvin, G., Rømoen, M., Lecomte, I., 2012. Relationship between electrical resistivity and basic geotechnical parameters for marine clays. *Canadian Geotechnical Journal* 49, 1158–1168.
- Lowell, S., Shields, J.E., Thomas, M.A., Thommes, M., 2012. Characterization of porous solids and powders: surface area, pore size and density. Springer Science & Business Media.
- Lu, C., Lu, J., Zhang, Y., Puckett, M.H., 2019. A convenient method to estimate soil hydraulic conductivity using electrical conductivity and soil compaction degree. *Journal of Hydrology* 575, 211–220.
- Lu, Y., Abuel-Naga, H., Al Rashid, Q., Hasan, M.F., 2019. Effect of Pore-Water Salinity on the Electrical Resistivity of Partially Saturated Compacted Clay Liners. *Advances in Materials Science and Engineering* 2019.
- Lu, Y., Abuel-Naga, H., Leong, E.-C., Bouazza, A., Lock, P., 2018. Effect of water salinity on the water retention curve of geosynthetic clay liners. *Geotextiles and Geomembranes* 46, 707–714.
- Manca, D., Ferrari, A., Laloui, L., 2015. Fabric evolution and the related swelling behaviour of a sand/bentonite mixture upon hydro-chemo-mechanical loadings. *Géotechnique* 66, 41–57.
- Maranha, J.R., Pereira, C., Vieira, A., 2017. Thermo-Viscoplastic Subloading Soil Model for Isotropic Stress and Strain Conditions, in: *Advances in Laboratory Testing and Modelling of Soils and Shales*. Springer, pp. 479–485.
- Martin, R.T., Ladd, C.C., 1975. Fabric of consolidated kaolinite. *Clays and Clay Minerals* 23, 17–25.

- Matthews, B.A., Rhodes, C.T., 1970. Studies of the coagulation kinetics of mixed suspensions. *Journal of Colloid and Interface Science* 32, 332–338.
- McCarter, W.J., Blewett, J., Chrisp, T.M., Starrs, G., 2005. Electrical property measurements using a modified hydraulic oedometer. *Canadian geotechnical journal* 42, 655–662.
- McCarter, W.J., Desmazes, P., 1997. Soil characterization using electrical measurements. *Geotechnique* 47.
- McConnachie, I., 1974. Fabric changes in consolidated kaolin. *Geotechnique* 24, 207–222.
- McCullough, R.L., 1985. Generalized combining rules for predicting transport properties of composite materials. *Composites Science and Technology* 22, 3–21.
- Meade, R.H., 1966. Factors influencing the early stages of the compaction of clays and sands—review. *Journal of Sedimentary Research* 36.
- Merkus, H.G., 2009. Particle size measurements: fundamentals, practice, quality. Springer Science & Business Media.
- Merritt, A.J., Chambers, J.E., Wilkinson, P.B., West, L.J., Murphy, W., Gunn, D., Uhlemann, S., 2016. Measurement and modelling of moisture—electrical resistivity relationship of fine-grained unsaturated soils and electrical anisotropy. *Journal of Applied Geophysics* 124, 155–165.
- Ming, F., Li, D.Q., Chen, L., 2019. Electrical resistivity of freezing clay: Experimental study and theoretical model. *Journal of Geophysical Research: Earth Surface*.
- Mishra, A.K., Ohtsubo, M., Li, L.Y., Higashi, T., 2012. Influence of various factors on the difference in the liquid limit values determined by Casagrande's and fall cone method. *Environmental Earth Sciences* 65, 21–27.
- Mitchell, J.K., Soga, K., 2005. Fundamentals of soil behavior. John Wiley & Sons Hoboken, NJ.
- Mojid, M.A., Cho, H., 2006. Estimating the fully developed diffuse double layer thickness from the bulk electrical conductivity in clay. *Applied clay science* 33, 278–286.
- Mojid, M.A., Rose, D.A., Wyseure, G.C.L., 2007. A model incorporating the diffuse double layer to predict the electrical conductivity of bulk soil. *European journal of soil science* 58, 560–572.
- Nadler, A., Frenkel, H., 1980. Determination of Soil Solution Electrical Conductivity from Bulk Soil Electrical Conductivity Measurements by the Four-Electrode Method 1. *Soil Science Society of America Journal* 44, 1216–1221.
- Nagaraj, T.S., Jayadeva, M.S., 1981. Re-examination of one-point methods of liquid limit determination. *Geotechnique* 31, 413–425.
- Nielsen, L.E., 1974. The thermal and electrical conductivity of two-phase systems. *Industrial & Engineering chemistry fundamentals* 13, 17–20.
- Norman, L.E.J., 1958. A comparison of values of liquid limit determined with apparatus having bases of different hardness. *Geotechnique* 8, 79–83.
- Norrish, K., 1954. The swelling of montmorillonite. *Discussions of the Faraday society* 18, 120–134.
- Oh, T.-M., Cho, G.-C., Lee, C., 2014. Effect of soil mineralogy and pore-water chemistry on the electrical resistivity of saturated soils. *Journal of Geotechnical and Geoenvironmental Engineering* 140, 06014012.

- O'Kelly, B.C., Vardanega, P.J., Haigh, S.K., 2018. Use of fall cones to determine Atterberg limits: a review. *Géotechnique* 68, 843–856.
- Ondruška, J., Štubňa, I., Trnovcová, V., Medved', I., Kaljuvee, T., 2015. Polarization and depolarization currents in kaolin. *Applied Clay Science* 114, 157–160.
- Ozcep, F., Yildirim, E., Tezel, O., Asci, M., Karabulut, S., 2010. Correlation between electrical resistivity and soil-water content based artificial intelligent techniques. *International Journal of Physical Sciences* 5, 47–56.
- Özer, M., 2009. Comparison of liquid limit values determined using the hard and soft base Casagrande apparatus and the cone penetrometer. *Bulletin of engineering geology and the environment* 68, 289–296.
- Pfefferkorn, K., 1924. Ein Beitrag zur Bestimmung der Plastizität in Tonen und Kaolinen. *Sprechsaal* 57, 297–299.
- Powell, J.J.M., Shields, C.H., Wallace, C.F., 2015. Liquid Limit testing—only use the Cone Penetrometer!
- Pozdnyakov, A.I., Pozdnyakova, L.A., Karpachevskii, L.O., 2006. Relationship between water tension and electrical resistivity in soils. *Eurasian Soil Science* 39, S78–S83.
- Prakash, K., Sridharan, A., Prasanna, H.S., 2009. A note on the determination of plastic limit of fine-grained soils. *Geotechnical Testing Journal* 32, 372–374.
- Rashid, Q.A., Abuel-Naga, H.M., Leong, E.-C., Lu, Y., Al Abadi, H., 2018. Experimental-artificial intelligence approach for characterizing electrical resistivity of partially saturated clay liners. *Applied Clay Science* 156, 1–10.
- Revil, A., Cathles III, L.M., Losh, S., Nunn, J.A., 1998. Electrical conductivity in shaly sands with geophysical applications. *Journal of Geophysical Research: Solid Earth* 103, 23925–23936.
- Rhoades, J.D., Manteghi, N.A., Shouse, P.J., Alves, W.J., 1989. Estimating soil salinity from saturated soil-paste electrical conductivity. *Soil Science Society of America Journal* 53, 428–433.
- Rhoades, J.D., Raats, P.A.C., Prather, R.J., 1976. Effects of liquid-phase electrical conductivity, water content, and surface conductivity on bulk soil electrical conductivity 1. *Soil Science Society of America Journal* 40, 651–655.
- Rhoades, J.D., van Schilfgaarde, J., 1976. An Electrical Conductivity Probe for Determining Soil Salinity 1. *Soil Science Society of America Journal* 40, 647–651.
- Ribeiro, M.J., Ferreira, J.M., Labrincha, J.A., 2005. Plastic behaviour of different ceramic pastes processed by extrusion. *Ceramics International* 31, 515–519.
- Richards, L.A., 1954. Diagnosis and improvement of saline and alkali soils. LWW.
- Rinaldi, V.A., Cuestas, G.A., 2002. Ohmic conductivity of a compacted silty clay. *Journal of Geotechnical and Geoenvironmental Engineering* 128, 824–835.
- Robain, H., Camerlynck, C., Bellier, G., Tabbagh, A., 2003. Laboratory measurements of electrical resistivity versus water content on small soil cores, in: EGS-AGU-EUG Joint Assembly.
- Robinson, D.A., Lebron, I., Lesch, S.M., Shouse, P., 2004. Minimizing drift in electrical conductivity measurements in high temperature environments using the EM-38. *Soil Science Society of America Journal* 68, 339–345.

- Ryżak, M., Bieganowski, A., 2011. Methodological aspects of determining soil particle-size distribution using the laser diffraction method. *Journal of Plant Nutrition and Soil Science* 174, 624–633.
- Saarenketo, T., 1998. Electrical properties of water in clay and silty soils. *Journal of applied geophysics* 40, 73–88.
- Sadek, M.S., 1993. A comparative study of the electrical and hydraulic conductivities of compacted clay. University of California, Berkeley.
- Salem, H.S., Chilingarian, G.V., 1999. The cementation factor of Archie's equation for shaly sandstone reservoirs. *Journal of Petroleum Science and Engineering* 23, 83–93.
- Samouëlian, A., Cousin, I., Tabbagh, A., Bruand, A., Richard, G., 2005. Electrical resistivity survey in soil science: a review. *Soil and Tillage research* 83, 173–193.
- Sangrey, D.A., Mitchell, R.J., 1976. Soil specimen preparation for laboratory testing, in: *Soil Specimen Preparation for Laboratory Testing, Symposium, 1975, Montreal, Canada*.
- Sauer, M.C., Southwick, P.F., Spiegler, K.S., Wyllie, M.R.J., 1955. Electrical conductance of porous plugs-ion exchange resin-solution systems. *Industrial & Engineering Chemistry* 47, 2187–2193.
- Schwartz, B.F., Schreiber, M.E., Yan, T., 2008. Quantifying field-scale soil moisture using electrical resistivity imaging. *Journal of Hydrology* 362, 234–246.
- Seyfried, M.S., Murdock, M.D., 2001. Response of a new soil water sensor to variable soil, water content, and temperature. *Soil Science Society of America Journal* 65, 28–34.
- Shah, P.H., Singh, D.N., 2005. Generalized Archie's law for estimation of soil electrical conductivity. *Journal of ASTM International* 2, 1–20.
- Shainberg, I., Rhoades, J.D., Prather, R.J., 1980. Effect of Exchangeable Sodium Percentage, Cation Exchange Capacity, and Soil Solution Concentration on Soil Electrical Conductivity 1. *Soil Science Society of America Journal* 44, 469–473.
- Sharma, B., Bora, P.K., 2003. Plastic limit, liquid limit and undrained shear strength of soil—reappraisal. *Journal of Geotechnical and Geoenvironmental engineering* 129, 774–777.
- Sharma, B., Sridharan, A., 2018. Liquid and plastic limits of clays by cone method. *International Journal of Geo-Engineering* 9, 22.
- Sherwood, P.T., Ryley, M.D., 1970. An investigation of a cone-penetrometer method for the determination of the liquid limit. *Géotechnique* 20, 203–208.
- Shevnin, V., Mousatov, A., Ryjov, A., Delgado-Rodriquez, O., 2007. Estimation of clay content in soil based on resistivity modelling and laboratory measurements. *Geophysical Prospecting* 55, 265–275.
- Shimobe, S., Spagnoli, G., 2019. A global database considering Atterberg limits with the Casagrande and fall-cone tests. *Engineering Geology* 105201.
- Shirazi, S.M., Kazama, H., Oshinbe, M., 2005. Permeability of bentonite and bentonite-sand mixtures. *Australian Geomechanics* 40, 27–36.
- Sivapullaiah, P.V., Sridharan, A., 1985. Liquid limit of soil mixtures. *Geotechnical Testing Journal* 8, 111–116.
- Sogami, I., Ise, N., 1984. On the electrostatic interaction in macroionic solutions. *The Journal of chemical physics* 81, 6320–6332.

- Soil, A.C.D.-18 on, Rock, 2006. Standard test methods for maximum index density and unit weight of soils using a vibratory table. ASTM International.
- Sowers, G., Vesić, A., Grandolfi, M., 1960. Penetration tests for liquid limit, in: *Papers on Soils 1959 Meetings*. ASTM International.
- Sperazza, M., Moore, J.N., Hendrix, M.S., 2004. High-resolution particle size analysis of naturally occurring very fine-grained sediment through laser diffractometry. *Journal of Sedimentary Research* 74, 736–743.
- Sposito, G., 1989. *The Chemistry of Soils* Oxford Univ. Press, New York, USA.
- Sridharan, A., Prakash, K., 2000. Percussion and cone methods of determining the liquid limit of soils: controlling mechanisms. *Geotechnical Testing Journal* 23, 236–244.
- Standard, A., 2010. Standard test methods for liquid limit, plastic limit, and plasticity index of soils.
- Standard, B., 1990. BS 1377-2: 1990, Methods of test for soils for civil engineering purposes- Part 2: Classification tests. London: UK: British Standard Institution.
- Syvitski, J.P., 2007. *Principles, methods and application of particle size analysis*. Cambridge University Press.
- Tabbagh, A., Cosenza, P., 2007. Effect of microstructure on the electrical conductivity of clay-rich systems. *Physics and Chemistry of the Earth, Parts A/B/C* 32, 154–160.
- Tabbagh, A., Panissod, C., Guérin, R., Cosenza, P., 2002. Numerical modeling of the role of water and clay content in soils' and rocks' bulk electrical conductivity. *Journal of Geophysical Research: Solid Earth* 107, ECV–20.
- Taubner, H., Roth, B., Tippkötter, R., 2009. Determination of soil texture: Comparison of the sedimentation method and the laser-diffraction analysis. *Journal of Plant Nutrition and Soil Science* 172, 161–171.
- Terzaghi, K., 1926. Simplified soil tests for subgrades and their physical significance. *Public Roads* 7, 153–170.
- Towhata, I., Kuntiwattanakul, P., Kobayashi, H., 1993. A preliminary study on heating of clays to examine possible effects of temperature on soil-mechanical properties. *Soils and Foundations* 33, 184–190.
- Vaillant, J.M.M., 2008. Cone de penetração adaptado para determinação da plasticidade das argilas. *Anais* 52, 1–11.
- Wang, Q., Cui, Y.-J., Tang, A.M., Delage, P., Gatmiri, B., Ye, W.-M., 2014. Long-term effect of water chemistry on the swelling pressure of a bentonite-based material. *Applied Clay Science* 87, 157–162.
- Wang, X., Tang, C., Mahony, S., Baldock, J.A., Butterly, C.R., 2015. Factors affecting the measurement of soil pH buffer capacity: approaches to optimize the methods. *European Journal of Soil Science* 66, 53–64.
- Warkentin, B.P., 1961. Interpretation of the upper plastic limit of clays. *Nature* 190, 287–288.
- Wasti, Y., Bezirci, M.H., 1986. Determination of the consistency limits of soils by the fall cone test. *Canadian Geotechnical Journal* 23, 241–246.
- Waxman, M.H., Smits, L.J.M., 1968. Electrical conductivities in oil-bearing shaly sands. *Society of Petroleum Engineers Journal* 8, 107–122.

- Wenner, F., 1915. A method for measuring earth resistivity. *Journal of the Washington Academy of Sciences* 5, 561–563.
- Wintermeyer, A.M., 1926. Adaptation of Atterberg plasticity tests for subgrade soils. *Public Roads* 7, 119–122.
- Wood, D.M., 1982. Cone penetrometer and liquid limit. *Geotechnique* 32.
- Yong, R.N., Mohamed, A.-M.O., Warkentin, B.P., 1992. *Principles of contaminant transport in soils*. Elsevier Science Publishers.
- Young, R., 2012. *Soil properties and behaviour*. Elsevier.
- Yukselen-Aksoy, Y., Kaya, A., Ören, A.H., 2008. Seawater effect on consistency limits and compressibility characteristics of clays. *Engineering Geology* 102, 54–61.
- Žbik, M.S., Williams, D.J., Song, Y.-F., Wang, C.-C., 2015. Smectite clay microstructural behaviour on the Atterberg limits transition. *Colloids and Surfaces A: Physicochemical and Engineering Aspects* 467, 89–96.
- Zhang, G., Germaine, J.T., Whittle, A.J., Ladd, C.C., 2004. Index properties of a highly weathered old alluvium. *Geotechnique* 54, 441–451.
- Zhang, Y., Daniels, J.L., Cetin, B., Baucom, I.K., 2020. Effect of Temperature on pH, Conductivity, and Strength of Lime-Stabilized Soil. *Journal of Materials in Civil Engineering* 32, 04019380.
- Zhou, H., Kong, G., Liu, H., Laloui, L., 2018. Similarity solution for cavity expansion in thermoplastic soil. *International Journal for Numerical and Analytical Methods in Geomechanics* 42, 274–294.
- Zhou, W.-H., Zhao, L.-S., 2013. One-dimensional consolidation of unsaturated soil subjected to time-dependent loading with various initial and boundary conditions. *International Journal of Geomechanics* 14, 291–301.
- Zumrawi, M., 2013. Swelling potential of compacted expansive soils. *International Journal of Engineering Research and Technology* 2, 1–6.

Appendices

Appendix 1

Derivation and Simplifications of the χ and σ_s

For two different diluted clay-water systems, The Eq. (25) from Chapter 4 can be divided in two ways as follows:

$$\sigma_{mix1} = \frac{\frac{\sqrt{(1-n_1)\chi}}{\sigma_s} + \frac{1 - \sqrt{(1-n_1)\chi}}{\sigma_w}}{1} + (1 - \sqrt{(1-n_1)\chi})\sigma_w \dots \dots \dots (A1.1)$$

$$\sigma_{mix2} = \frac{\frac{\sqrt{(1-n_2)\chi}}{\sigma_s} + \frac{1 - \sqrt{(1-n_2)\chi}}{\sigma_w}}{1} + (1 - \sqrt{(1-n_2)\chi})\sigma_w \dots \dots \dots (A1.2)$$

Eqs. (1.A1-1.A2) can be inserted to represent two expressions for χ and σ_s , and with the help of Mathematica, the following was found:

$$\chi = -\frac{(N_1 - N_2)(\sigma_{mix1} - \sigma_w)(\sigma_w - \sigma_{mix2})}{\sigma_w\{(N_2)^2\sigma_{mix1} - (N_1)^2\sigma_{mix2} + (N_1)^2\sigma_w - (N_2)^2\sigma_w\}}$$

$$\Rightarrow \chi = \frac{(N_2 - N_1)\sigma_{mix1w}\sigma_{mix2w}}{\sigma_w[(N_2)^2\sigma_{mix1} - (N_1)^2\sigma_{mix2} + \sigma_w\{(N_1)^2 - (N_2)^2\}]}$$

Where,

$$N_1 = \sqrt{(1 - n_1)}, N_2 = \sqrt{(1 - n_2)}, \sigma_{mix1w} = \sigma_{mix1} - \sigma_w, \sigma_{mix2w} = \sigma_w - \sigma_{mix2}$$

And, σ_s was found as follows (from Mathematica):

$$\sigma_s$$

$$= \frac{N_1(N_1 - N_2)N_2(\sigma_{mix1} - \sigma_w)\sigma_w(\sigma_w - \sigma_{mix2})\{N_2(\sigma_{mix1} - \sigma_w) + N_1(\sigma_w - \sigma_{mix2})\}}{-(N_1)^2(N_2)^2(\sigma_{mix1} + \sigma_{mix2})(\sigma_{mix1} - \sigma_w)(\sigma_{mix2} - \sigma_w) + N_1(N_2)^3(\sigma_{mix1} - \sigma_w)^2(\sigma_{mix2} - \sigma_w) + (N_1)^3N_2(\sigma_{mix1} - \sigma_w)(\sigma_{mix2} - \sigma_w)^2 + (N_2)^4(\sigma_{mix1} - \sigma_w)^2\sigma_w + (N_1)^4(\sigma_{mix2} - \sigma_w)^2\sigma_w}$$

$$\Rightarrow \sigma_s = \frac{N_1N_2(N_1 - N_2)\sigma_w\sigma_{mix1w}\sigma_{mix2w}(N_2\sigma_{mix1w} + N_1\sigma_{mix2w})}{(N_1)^2(N_2)^2\sigma_{mix1,2w}\sigma_{mix1w}\sigma_{mix2w} - N_1(N_2)^3\sigma_{mix1w}^2\sigma_{mix2w} + (N_1)^3N_2\sigma_{mix1w}\sigma_{mix2w}^2 + (N_2)^4\sigma_{mix1w}^2\sigma_w + (N_1)^4\sigma_{mix2w}^2\sigma_w}$$

$$\Rightarrow \sigma_s = \frac{N_1N_2(N_1 - N_2)\sigma_w\sigma_{mix1w}\sigma_{mix2w}(N_2\sigma_{mix1w} + N_1\sigma_{mix2w})}{(N_1)^2(N_2)^2\sigma_{mix1,2w}\sigma_{mix1w}\sigma_{mix2w} - N_1N_2[\sigma_{mix1w}\sigma_{mix2w}\{(N_2)^2\sigma_{mix1w} - (N_1)^2\sigma_{mix2w}\}] + \sigma_w\{(N_2)^4\sigma_{mix1w}^2 + (N_1)^4\sigma_{mix2w}^2\}}$$

Where, $\sigma_{mix1,2w} = \sigma_{mix1} + \sigma_{mix2}$

Appendix 2

Mathematica Script of Determining χ and σ_s

```

In[201]:= Simplify[Solve[ $\left\{0 = \frac{N1 X sx sw}{N1 X sw + sx (1 - N1 X)} + (1 - N1 X) sw - sm1, \right.$ 
 $\left.0 = \frac{N2 X sx sw}{N2 X sw + sx (1 - N2 X)} + (1 - N2 X) sw - sm2\right\}, \{sx, X\}]]$ 

Out[201]:=  $\left\{\left\{sx \rightarrow \frac{(N1 (N1 - N2) N2 (sm1 - sw) sw (-sm2 + sw) (N2 (sm1 - sw) + N1 (-sm2 + sw)))}{(-N1^2 N2^2 (sm1 + sm2) (sm1 - sw) (sm2 - sw) + N1 N2^3 (sm1 - sw)^2 (sm2 - sw) + N1^3 N2 (sm1 - sw) (sm2 - sw)^2 + N2^4 (sm1 - sw)^2 sw + N1^4 (sm2 - sw)^2 sw)}, X \rightarrow \frac{(N1 - N2) (sm1 - sw) (-sm2 + sw)}{sw (N1^2 (sm2 - sw) + N2^2 (-sm1 + sw))}\right\}\right\}$ 

In[188]:= Solve[ $0 = \frac{N1 X sx sw}{N1 X sw + sx (1 - N1 X)} + (1 - N1 X) sw - sm1, sx]$ 

Out[188]:=  $\left\{\left\{sx \rightarrow \frac{N1 sw X (sm1 - sw + N1 sw X)}{-sm1 + sw + N1 sm1 X - N1 sw X + N1^2 sw X^2}\right\}\right\}$ 

In[189]:= Solve[ $0 = \frac{N2 X sx sw}{N2 X sw + sx (1 - N2 X)} + (1 - N2 X) sw - sm2, sx]$ 

Out[189]:=  $\left\{\left\{sx \rightarrow \frac{N2 sw X (sm2 - sw + N2 sw X)}{-sm2 + sw + N2 sm2 X - N2 sw X + N2^2 sw X^2}\right\}\right\}$ 

In[194]:= Collect[Simplify[ $\left(\frac{N1 sw X (sm1 - sw + N1 sw X)}{-sm1 + sw + N1 sm1 X - N1 sw X + N1^2 sw X^2} - \frac{N2 sw X (sm2 - sw + N2 sw X)}{-sm2 + sw + N2 sm2 X - N2 sw X + N2^2 sw X^2}\right) * (-sm1 + sw + N1 sm1 X - N1 sw X + N1^2 sw X) * (-sm2 + sw + N2 sm2 X - N2 sw X + N2^2 sw X^2)$ ], X]

Out[194]:=  $\left(\frac{sw X (-sm1 + sw + N1 sm1 X - N1 sw X + N1^2 sw X) (N1 (sm1 - sw) (-sm2 + sw) + N1^2 sw (-sm2 + sw) X + N2 (sm1 - sw) (sm2 + sw (-1 + N2 X)))}{(-sm1 + sw + N1 sm1 X - N1 sw X + N1^2 sw X^2)}\right)$ 

In[195]:= Solve[ $\frac{N1 sw X (sm1 - sw + N1 sw X)}{-sm1 + sw + N1 sm1 X - N1 sw X + N1^2 sw X^2} - \frac{N2 sw X (sm2 - sw + N2 sw X)}{-sm2 + sw + N2 sm2 X - N2 sw X + N2^2 sw X^2} = 0, X]$ 

Out[195]:=  $\left\{\{X \rightarrow 0\}, \left\{X \rightarrow -\frac{(N1 - N2) (sm1 - sw) (-sm2 + sw)}{sw (N2^2 sm1 - N1^2 sm2 + N1^2 sw - N2^2 sw)}\right\}\right\}$ 

In[196]:= Simplify[Solve[ $0 = \frac{N1 X sx sw}{N1 X sw + sx (1 - N1 X)} + (1 - N1 X) sw - sm1 /. X \rightarrow -\frac{(N1 - N2) (sm1 - sw) (-sm2 + sw)}{sw (N2^2 sm1 - N1^2 sm2 + N1^2 sw - N2^2 sw)},$ 
 $sx]$ 
Simplify[Solve[ $0 = \frac{N2 X sx sw}{N2 X sw + sx (1 - N2 X)} + (1 - N2 X) sw - sm2 /. X \rightarrow -\frac{(N1 - N2) (sm1 - sw) (-sm2 + sw)}{sw (N2^2 sm1 - N1^2 sm2 + N1^2 sw - N2^2 sw)},$ 
 $sx]$ 

Out[196]:=  $\left\{\left\{sx \rightarrow \frac{(N1 (N1 - N2) N2 (sm1 - sw) sw (-sm2 + sw) (N2 (sm1 - sw) + N1 (-sm2 + sw)))}{(-N1^2 N2^2 (sm1 + sm2) (sm1 - sw) (sm2 - sw) + N1 N2^3 (sm1 - sw)^2 (sm2 - sw) + N1^3 N2 (sm1 - sw) (sm2 - sw)^2 + N2^4 (sm1 - sw)^2 sw + N1^4 (sm2 - sw)^2 sw)}\right\}\right\}$ 

```


Appendix 3

Stokes' Law to Find Diameter of the Soil Particles

The sedimentation analysis follows Stokes' law, which provides the terminal velocity of a small sphere-shaped particles settling in a specific fluid of infinite extent. As an individual particle reaches the base, the velocity increases due to the influence of gravity. However, due to the existence of the drag force, the free-falling particles get interrupted, and as a result, the velocity gets hindered. After an initial period of time, velocity becomes constant once the steady conditions are attained. This velocity, is, however known as terminal velocity.

Let's consider F_D be the drag force, and a particle has a radius r . The particle is settling with a velocity v through the fluid which has a viscosity μ . Hence the following expression can be established:

$$F_D = 6\pi\mu rv \quad (\text{A3.1})$$

There are two other forces acting on the particle namely, weight (W) of the sphere particle, and the buoyant force (U), which can be found by the following relations:

$$W = \frac{4}{3}\pi r^3 \gamma_s = \frac{4}{3}\pi r^3 (\rho_s g) \quad (\text{A3.2})$$

$$U = \frac{4}{3}\pi r^3 \gamma_w = \frac{4}{3}\pi r^3 (\rho_L g) \quad (\text{A3.3})$$

Here, γ_s and γ_w are the unit weight of the material of sphere, and water, respectively.

As the equilibrium of forces is attained, the following expression can be established:

$$W = U + F_D$$

$$\begin{aligned}
\Rightarrow \frac{4}{3}\pi r^3(\rho_s g) &= \frac{4}{3}\pi r^3(\rho_L g) + 6\pi\mu r v \\
\Rightarrow v &= \frac{2r^2}{9\mu}(\rho_s - \rho_L)g \\
\Rightarrow v &= \frac{1}{18} \frac{g d^2 (G_s - 1) \rho_L}{\mu}
\end{aligned} \tag{A3.4}$$

Where, d is the diameter of the spherical particle, G_s is the specific gravity of the material, g is the acceleration due to gravity.

If the particle travels a specific distance h in time t , then $v=h/t$. Therefore, Eq. (A3.4) can be written as the following:

$$d = \sqrt{\frac{18\mu h}{g(G_s - \rho_L)t}} \tag{A3.5}$$

Appendix 4

Viscosity (μ) of water at different temperature (T) ([Arora, 1992](#))

T (°C)	μ (mN-s/m ²)	T (°C)	μ (mN-s/m ²)	T (°C)	μ (mN-s/m ²)
0	1.794	11	1.274	22	0.961
1	1.732	12	1.239	23	0.938
2	1.674	13	1.206	24	0.916
3	1.619	14	1.175	25	0.895
4	1.568	15	1.145	26	0.875
5	1.519	16	1.116	27	0.855
6	1.473	17	1.088	28	0.836
7	1.429	18	1.060	29	0.818
8	1.387	19	1.034	30	0.8
9	1.348	20	1.009	31	0.783
10	1.310	21	0.984	32	0.767

Appendix 5

Derivation of Percentage Finer (passing)

Let's consider the total mass of the dry soil sample is M_s in a suspension which has a volume V , and the mass of water in the suspension be M_w . Since at the beginning of the test, the suspension is homogeneous, the mass of soil (solid)/unit volume of suspension at any depth can be considered to be M_s/V .

Therefore, the initial density, ρ_i can be expressed as the following:

$$\rho_i = \frac{M_s + M_w}{V} \quad (\text{A5.1})$$

It's also known by the definition that volume of solid, $V_s = M_s / G_s \rho_w$. Hence the volume of the solids per volume of suspension (let $\frac{V_s}{V} = V_1$) can be written as

$$V_1 = \frac{M_s}{G_s \rho_w V} \quad (\text{A5.2})$$

Considering the relation from [Eq. \(A5.2\)](#), volume of water per volume of suspension (let $\frac{V_w}{V} = V_2$) can be written as below:

$$V_2 = 1 - \frac{M_s}{G_s \rho_w V} \quad (\text{A5.3})$$

[Eq. \(A5.3\)](#) can be further transformed into the mass of water per volume of suspension ($\frac{M_w}{V} = M_w'$), and thus implies the following:

$$M_w' = \left(1 - \frac{M_s}{G_s \rho_w V}\right) \rho_w \quad (\text{A5.4})$$

Therefore, [Eq. \(A5.1\)](#) can be re-written as the following:

$$\begin{aligned}
\rho_i &= \frac{M_s}{V} + \frac{M_w}{V} \\
&= \frac{M_s}{V} + \left(1 - \frac{M_s}{G_s \rho_w V}\right) \rho_w \\
&= \rho_w + \frac{M_s}{V} \left(1 - \frac{1}{G_s}\right) \\
\Rightarrow \rho_i &= \rho_w + \frac{M_s}{V} \left(\frac{G_s - 1}{G_s}\right)
\end{aligned} \tag{A5.5}$$

However, after a specific time-scale t , the suspension will no longer be homogenous, and mass of solids will be different at different depth. Let's consider M_d be the mass of solids at a depth after time t . Therefore, the density of solids, ρ_s can be expressed as

$$\rho_s = \rho_w + \frac{M_d}{V} \left(\frac{G_s - 1}{G_s}\right) \tag{A5.6}$$

The percentage finer N than any particle size is given by the following equation ([Arora, 1992](#)):

$$N = \frac{m_d}{m_s} \times 100 \tag{A5.7}$$

In [Eq. \(A5.6\)](#), $m_d = M_d/V$, and $m_s = M_s/V$. So [Eq. \(A5.7\)](#) can be further extended as the expression below:

$$\begin{aligned}
\rho_s &= \rho_w + \frac{Nm_s}{100} \left(\frac{G_s - 1}{G_s}\right) \\
\Rightarrow \rho_s - \rho_w &= \frac{Nm_s}{100} \left(\frac{G_s - 1}{G_s}\right) \\
\Rightarrow N &= \left(\frac{G_s}{G_s - 1}\right) \frac{\rho_s - \rho_w}{m_s} \times 100
\end{aligned} \tag{A5.8}$$

Appendix 6

Determination of Effective Distance of Electrodes by Analysing Electric Field

The two electrodes, separated with thin film layer, are modelled in ANSYS Maxwell. As mentioned in the physical description of the probe, the radius of each electrode is 1.5 mm, while the thickness is 1.3 mm. The thickness of thin film layer is 0.01 mm. The electrodes are made from brass, while the thin film layer is made of insulation material. The modelled tube is made from acrylic. In order to find the effective distance, the applied voltage to the electrodes was 5V. For the ease of the analysis, only 2 sets of electrodes were taken into account. After the few iterations, the results have shown that the lines doesn't overlap at the distance of 1.4 cm, as shown in [Fig. A6.1](#). For further clarification, the distance between the pairs of electrodes was reduced to 1.3 cm, and overlapping of the electric field was observed ([Fig.A6.2](#)). It implies that a minimum distance of 1.4 cm is required in order to avoid overlapping of electric fields of the electrodes.

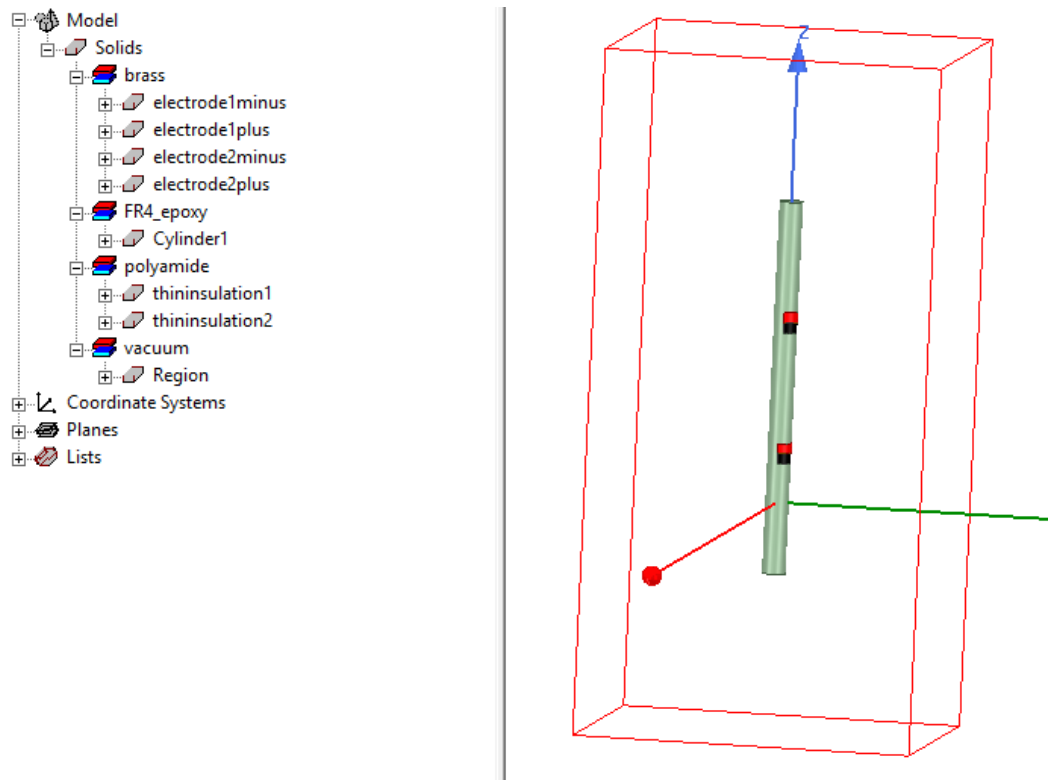


Figure A6.1: Physical model designed on Ansys.

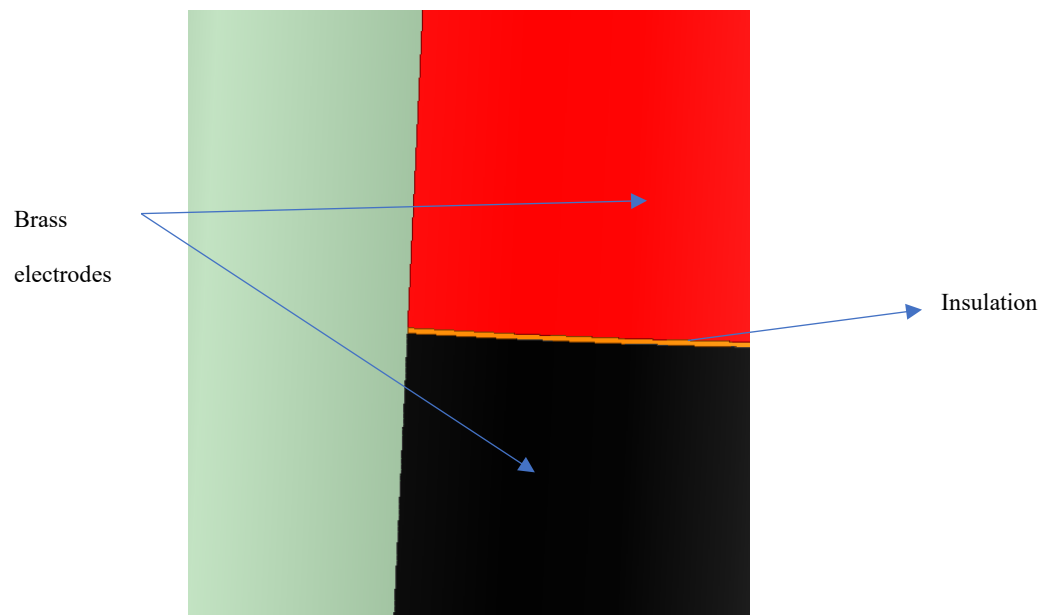


Figure A6.2: Zoomed in photo of electrodes and the insulation.

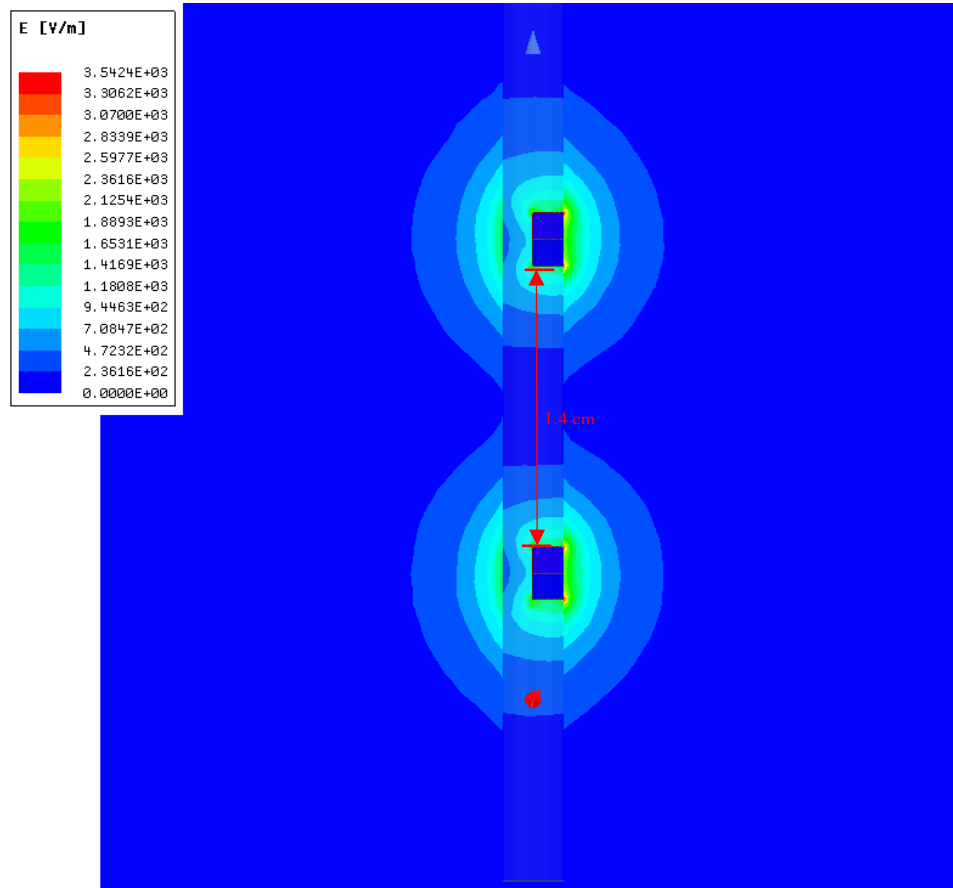


Figure: A6.3: Electric fields don't overlap at 1.4 cm of distance.

Mathematical equation used to calculate electric field is written as the following:

$$E = -\nabla\phi = -\left(\frac{\partial\phi}{\partial x}\vec{i} + \frac{\partial\phi}{\partial y}\vec{j} + \frac{\partial\phi}{\partial z}\vec{k}\right) \quad (\text{A6.1})$$

where ϕ is the voltage vector potential, and $\vec{i}, \vec{j}, \vec{k}$ are the unit vectors at x, y, and z axes, respectively.

The boundary conditions were put on the faces of the calculation area with restriction to the voltage. At $V=0$, so the lines of electric field will be zero on the face of the calculation area. In such case, the calculation area should be sufficiently large compared to the model, and therefore, it won't affect the result. It can be seen from the results that the calculation area is enough large because the value of electric field comes to zero before touching the

boundary face (Fig.2C.3). Nevertheless, at 1.3 cm of distance, at the same applied voltage, an overlapping of electric field can be seen (Fig.2C.4).

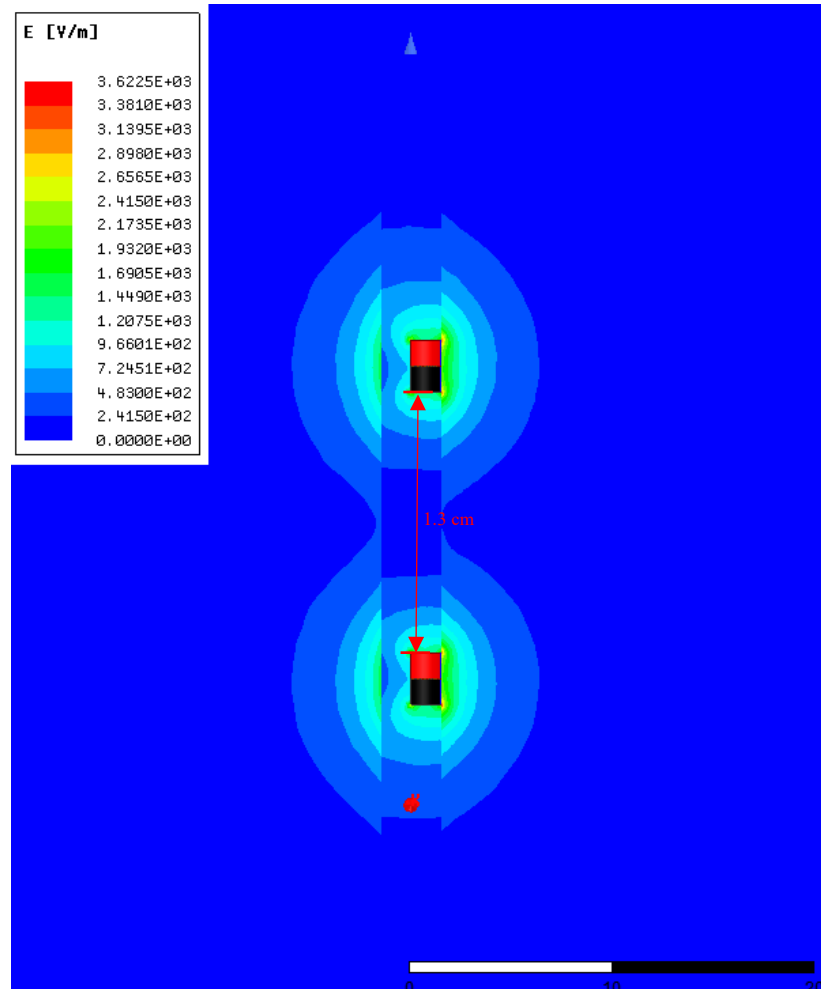


Figure A6.4: Electric fields overlap at 1.3 cm of distance.